



Durham E-Theses

Synthesis and aromatisation reactions of arene hydrates and cis-dihydrodiols

O'Mahony, Michelle J.

How to cite:

O'Mahony, Michelle J. (2009) *Synthesis and aromatisation reactions of arene hydrates and cis-dihydrodiols*, Durham theses, Durham University. Available at Durham E-Theses Online: <http://etheses.dur.ac.uk/2550/>

Use policy

The full-text may be used and/or reproduced, and given to third parties in any format or medium, without prior permission or charge, for personal research or study, educational, or not-for-profit purposes provided that:

- a full bibliographic reference is made to the original source
- a [link](#) is made to the metadata record in Durham E-Theses
- the full-text is not changed in any way

The full-text must not be sold in any format or medium without the formal permission of the copyright holders.

Please consult the [full Durham E-Theses policy](#) for further details.

Synthesis and Aromatisation Reactions of Arene Hydrates and *cis*-Dihydrodiols

A thesis submitted for the part fulfillment of the requirements for the degree of

Doctor of Philosophy

In the Faculty of Science of Durham University

By

Michelle J. O'Mahony

The copyright of this thesis rests with the author or the university to which it was submitted. No quotation from it, or information derived from it may be published without the prior written consent of the author or university, and any information derived from it should be acknowledged.

Department of Chemistry

Durham University

South Road

Durham



26 JAN 2009

For my parents

Table of Contents

Introduction	2
1.1 <i>Early History</i>	2
1.2 Substitution and solvolysis reactions	2
1.2.1 Ion Pairs	5
1.2.2 Solvent effects	8
1.3 Quantification of carbocation reactions	11
1.3.1 Kinetic relativities	11
1.3.2 Thermodynamic stabilities (pK_R Values)	12
1.4 Carbocation Intermediates in the reactions of epoxides and alcohols	17
1.4.1 Carbocation formation in the ring-opening reactions of epoxides and arene oxides	17
1.4.2 Reactions of alcohols and arene hydrates	30
1.5 Biological Relevance: Oxidative Metabolites.	35
1.5.1 Arene hydrates	36
1.5.2 Arene Oxides	37
1.5.3 Biocatalysts	37
1.5.4 Polycyclic Aromatic Hydrocarbons	39
2 Results	42
2.1 <i>Methyl benzoate Hydrate</i>	42
2.1.1 Synthesis of methyl benzoate hydrate.	42
2.1.2 Kinetic analysis of the aromatisation of methyl benzoate hydrate in dilute perchloric acid	43
2.1.3 Computational studies of methyl benzoate hydrate	49
2.2 <i>Biphenyl Hydrate</i>	51
2.2.1 Synthesis of biphenyl hydrate	51
2.2.2 First order rate constants for the aromatisation of biphenyl hydrate.	52
2.2.3 Computational studies of biphenyl hydrate	67
2.3 <i>Toluene Hydrate</i>	69
2.3.1 Synthesis of 2-methylcyclohexa-2,4-dienol (<i>ortho</i>) and 1-methylcyclohexa-2,4-dienol (<i>ipso</i>)	69
2.3.2 Kinetic analysis of the aromatisation reaction via dehydration of 2-methyl cyclohexa-2,4-dienol and 1-methylcyclohexa-2,4-dienol	70
2.3.3 Computational studies of toluene hydrates	97
2.4 <i>Ethylbenzene Hydrate</i>	103
2.4.1 Synthesis of ethylbenzene hydrate	103
2.4.2 Kinetic analysis of the aromatisation via dehydration of ethylbenzene hydrate	104
2.4.3 Computational studies of ethylbenzene hydrate	114
2.5 <i>Cumene Hydrate</i>	118
2.5.1 Synthesis of Cumene Hydrate	119
2.5.2 Kinetic analysis of the aromatisation reaction of the cumene hydrates	120
2.5.3 Computational Studies of the isopropylbenzene hydrates	145
2.6 <i>tert-butylbenzene Hydrate</i>	150
2.6.1 Synthesis of 2- <i>tert</i> -butylcyclohexa-2,4-dienol.	150
2.6.2 Kinetic analysis of the aromatisation reaction of 2- <i>tert</i> -butylcyclohexa-2,4-dienol.	151
2.6.3 Computational studies of <i>tert</i> -butylbenzene hydrates	171
2.7 <i>Computational Studies of the cis-dihydrodiols</i>	175
2.7.1 Lowest energy structures of the <i>cis</i> -dihydrodiols and corresponding carbocations	176
2.7.2 Calculated Energies of the <i>cis</i> -dihydrodiols	182

2.7.3	Relative energies of the <i>cis</i> -dihydrodiols	183
2.8	<i>Linear Free Energy Correlations</i>	183
2.8.1	Hydrates with substituents at the ' <i>ipso</i> ' and ' <i>meta</i> ' position	184
2.8.2	Hydrates with ' <i>ortho</i> ' substituents	189
2.9	<i>Indene Diol</i>	192
2.9.1	Synthesis of (1 <i>R</i> ,2 <i>S</i>)-2,3-dihydro-1 <i>H</i> -indene-1,2-diol (3.32) and ester derivative	193
2.9.2	Determination of the second-order rate constant for carbocation formation (k_{11}) from (1 <i>R</i> ,2 <i>S</i>)-2,3-dihydro-1 <i>H</i> -indene-1,2-diol	194
2.9.3	Determination of the rate constant for the reaction of the 2-hydroxyindanyl carbocation with water, k_{H_2O}	199
2.9.4	Determination of the pK_R of the 2-hydroxyindanyl carbocation	204
3	Discussion	205
3.1	<i>Synthesis of the Arene Hydrates</i>	205
3.2	<i>Aromatisation reactions of the arene hydrates</i>	213
3.2.1	Methyl benzoate Hydrate	214
3.2.2	Biphenyl hydrate	216
3.2.3	Alkyl substituted hydrates	218
3.2.4	Summary of the second-order rate constants for aromatisation	220
3.3	<i>Hammett correlations</i>	223
3.3.1	Linear Free Energy Correlations	223
3.3.2	Hammett correlations for the arene hydrates	225
3.4	<i>Computational Studies</i>	232
3.4.1	Calculated Energies of the arene hydrates, <i>cis</i> -dihydrodiols and corresponding carbocations	236
3.5	<i>pK_R of Indene dihydrodiol</i>	241
3.5.1	Synthesis of ester derivatives	242
3.5.2	Determination of k_H – Isomerisation studies	243
3.5.3	pK_R of indene dihydrodiol	244
4	Experimental	247
4.1	<i>General Procedures (GP)</i>	247
4.1.1	Birch Reduction	247
4.1.2	<i>m</i> CPBA Epoxidations	247
4.1.3	Ring-opening	248
4.2	<i>Synthetic targets</i>	248
4.2.1	7-oxa-bicyclo[4.1.0]hept-3-ene	248
4.2.2	1-Methyl-1,4-cyclohexadiene	248
4.2.3	1-Methyl-7-oxa-bicyclo[4.1.0]hept-3-ene	249
4.2.4	2-Methylcyclohexa-2,4-dienol and 1-methylcyclohexa-2,4-dienol	250
4.2.5	1-Ethyl-1,4-cyclohexadiene	250
4.2.6	1-Ethyl-7-oxa-bicyclo[4.1.0]hept-3-ene	251
4.2.7	2-Ethylcyclohexa-2,4-dienol and 1-ethylcyclohexa-2,4-dienol	252
4.2.8	1-Isopropyl-1,4-cyclohexadiene	252
4.2.9	1-Isopropyl-7-oxa-bicyclo[4.1.0]hept-3-ene	253
4.2.10	1-Isopropylcyclohexa-2,4-dienol and 2-isopropylcyclohexa-2,4-dienol	254
4.2.11	1-Tertbutylcyclohexa-1,4-diene	254
4.2.12	1-Tertbutyl-7-oxa-bicyclo[4.1.0]hept-3-ene	255
4.2.13	1-Tertbutylcyclohexa-2,4-dienol & 2-tertbutylcyclohexa-2,4-dienol	256
4.2.14	N,N-dimethylcyclohexa-1,4-dienamine	257
4.2.15	1-Methoxycyclohexa-1,4-diene	257

4.2.16	Attempted epoxidation of 1-methoxycyclohexa-1,4-diene	258
4.2.17	N-Phenylacetamide (Acetanilide)	258
4.2.18	Attempted Birch reduction of N-phenylacetamide	259
4.2.19	Trimethylsiloxy-6-methylcarboxylate-cyclohexa-1,4-diene	259
4.2.20	1-Methylcarboxylate-cyclohexa-1,4-diene	260
4.2.21	Methyl 7-oxa-bicyclo[4.1.0]hept-3-ene-3-carboxylate	261
4.2.22	Attempted synthesis of methyl 5-hydroxycyclohexa-1,3-dienecarboxylate and methyl 4-hydroxycyclohexa-1,5-diene carboxylate	261
4.2.23	(3 or 4-phenylcyclohexa-1,4-dienyloxy)trimethylsilane	262
4.2.24	(3 or 4-(Chloromethyl)cyclohexa-1,4-dienyloxy)trimethylsilane	263
4.2.25	Cyclohexa-2,5-dienecarboxylic acid	263
4.2.26	Methyl cyclohexa-2,5-dienecarboxylate	264
4.2.27	2,5-Dihydrobenzoic Acid	265
4.2.28	Methyl 7-oxa-bicyclo[4.1.0]hept-3-ene-2-carboxylate	265
4.2.29	Methyl 3-hydroxycyclohexa-1,5-dienecarboxylate (2.1)	266
4.2.30	1-(Cyclohexa-2,5-dienyl)benzene	267
4.2.31	2-Phenyl-7-oxa-bicyclo[4.1.0]hept-3-ene	268
4.2.32	3-Phenylcyclohexa-2,4-dienol (2.9)	269
4.2.33	2-Bromo-7-oxa-bicyclo[4.1.0]hept-3-ene	270
4.2.34	2,5-Dibromo-7-oxa-bicyclo[4.1.0]hept-3-ene	271
4.2.35	N,N-Dimethyl-7-oxa-bicyclo[4.1.0]hept-3-en-2-amine	272
4.2.36	2-(Ethylthio)-7-oxa-bicyclo[4.1.0]hept-3-ene	273
4.2.37	2-Methoxy-7-oxa-bicyclo[4.1.0]hept-3-ene	274
4.2.38	Attempted synthesis of dimethylaniline hydrate	274
4.2.39	Attempted synthesis of ethylphenylsulfide hydrate	275
4.2.40	(Cyclohexa-2,5-dienyl)methyl 4-methylbenzenesulfonate	275
4.2.41	3-Methylcyclohexa-1,4-diene	276
4.2.42	(1R,2S)-2,3-Dihydro-1H-indene-1,2-diol	277
4.2.43	2,3-Dihydro-2-hydroxy-1H-inden-3-yl-trifluoroacetate	278
4.2.44	Preparation of lithium trichloroacetate	279
4.3	<i>General Information</i>	281
4.3.1	Materials and preparation of solutions	281
4.3.2	pH Measurement	283
4.3.3	NMR spectroscopy	284
4.3.4	HPLC	284
4.3.5	Mass spectrometry	285
4.3.6	NMR Kinetics	285
4.3.7	UV-Vis Spectroscopy	286
4.3.8	Data Analysis	287
4.3.9	Measurements in Concentrated Acid Media	289
5	Acknowledgements	290
	References	291

Abstract

The aim of this work was to synthesis a range of substituted arene hydrates, determine their second-order rate constant for dehydration and generate a Hammett plot for comparison with other published ρ -values for similar carbocation-forming reactions.

The first hydrate presented is the methyl benzoate hydrate (see section 2.1). A number of first order rate constants for the aromatisation (dehydration) reaction were determined in dilute perchloric acid at ionic strength 0.5 maintained with sodium perchlorate. The reaction was followed by UV-Vis spectrophotometry and ^1H NMR spectroscopy. The second order rate constant was determined to be $9.32 \times 10^{-2} \text{ M}^{-1}\text{s}^{-1}$ which corresponds to a half-life of 7 seconds in 1 M HClO_4 .

The arene hydrate of biphenyl was also synthesised (see section 2.2). The solubility issues discussed in section 2.2.2 meant the aromatisation reaction could not be followed by ^1H NMR spectroscopy. The first order rate constants were determined in acetate and phosphate buffers, at ionic strength 0.5, maintained with sodium perchlorate, from pH 5 to 7. The second order rate constant was determined to be $2.11 \times 10^2 \text{ M}^{-1}\text{s}^{-1}$ which corresponds to a half-life of $3.3 \times 10^{-4} \text{ s}$ in 1M HClO_4 .

As presented in sections 2.3-2.7, the synthetic route to the alkyl substituted hydrates gave two products – the *ortho* and the *ipso* hydrates. In the case of the ethyl substituted hydrate only the *ortho* hydrate was synthesised. For $\text{R} = t\text{Bu}$, only a small proportion of the products formed was the *ipso* hydrate due to its reactivity. The *ortho* and *ipso* hydrates of toluene and cumene were both synthesised. These could not be separated and so the aromatisation kinetics were followed *in situ* and fitted to a double exponential equation. The aromatisation reactions were followed by UV-vis spectrophotometry in acetate and phosphate buffers at 25 °C and ionic strength 0.5 M, maintained with sodium perchlorate.

The second-order rate constants for aromatisation for the *ortho*-hydrates were determined to be for $\text{R} = \text{Me}$, Et, *i*Pr, *t*Bu and are 514, 538, 642 and $949 \text{ M}^{-1}\text{s}^{-1}$, respectively. The

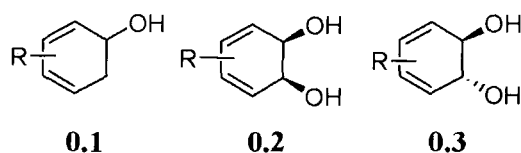
second-order rate constants for aromatisation for the *ipso*-hydrates isolated were determined to be for R = Me and *i*Pr are 9.81×10^3 and $1.47 \times 10^4 \text{ M}^{-1}\text{s}^{-1}$.

A number of linear free energy correlations were attempted and the best correlation was found with σ^+ , this is consistent with a reaction involving a planar carbocation with through-bond stabilisation. The ρ -value was determined to be -6.5 . The published ρ -value for the *cis* dihydrodiols, where a better correlation with σ_p was reported, is -8.2^1 . The magnitude of ρ suggests the hydrates have an earlier transition state to carbocation formation than the diols with less positive charge build-up.

The computational results show that the carbocation intermediate formed during the aromatisation reaction of the hydrates is planar whereas the carbocation intermediate generated from the diols is puckered. This corroborates the results from the kinetic analysis and also the magnitude and sign of the ρ -values from the Hammett correlations. When the carbocation intermediate is puckered, the through-bond stabilisation is hindered and so a poor correlation with σ^+ is observed.

The rate constant for acid-catalysed isomerisation of optically active *cis*-indene dihydrodiol was determined. This represents the rate constant for formation of the corresponding carbocation intermediate. The second-order rate constant for carbocation formation (k_H) was determined by ^1H NMR spectroscopy in concentrated perchloric acid to be $1.11 \times 10^{-6} \text{ M}^{-1}\text{s}^{-1}$. This is comparable with the second-order rate constant for carbocation formation in *tert*-butanol which is $1.4 \times 10^{-6} \text{ M}^{-1}\text{s}^{-1}$. The rate constant for reaction of the carbocation intermediate with water ($k_{\text{H}_2\text{O}}$), determined using the azide-trapping technique, is $4.99 \times 10^8 \text{ s}^{-1}$. Combining $k_{\text{H}_2\text{O}}$ with k_H allows the $\text{p}K_R$ of the indene dihydrodiol carbocation to be calculated. The $\text{p}K_R$ was determined to be -14.6 . This is greater than the $\text{p}K_R$ of the indanol carbocation. The effect of the adjacent hydroxyl group counteracts the stabilising effect of the benzylic substituent.

The present work was undertaken to develop a synthetic route to a series of substituted hydrates (0.1), to investigate their kinetics of dehydration (aromatisation) and to generate a Hammett plot for comparison with previous similar studies for the *cis*-dihydrodiols (0.2)¹. Alongside this, a brief computational study of the hydrates and *cis*-diols and their corresponding carbocations was conducted.



Earlier work on the arene hydrates and diols had found a number of interesting anomalies.

1) The rate of aromatisation of the *trans*-dihydrodiols (0.3, R = H, Cl, Br, I) is 1000-fold slower than the *cis*-dihydrodiols (0.2, R = H, Cl, Br, I). As the aromatisation mechanism was expected to proceed via a planar carbocation, the stereochemistry of the β -hydroxyl group was not predicted to greatly influence the rate of aromatisation².

2) A CF₃ substituent slowed the rate of aromatisation of the arene hydrate (0.1, R = CF₃) 5-fold when compared with benzene hydrate (R = H), however, the CF₃-substituent had a 3300-fold rate retarding effect on the *cis*-diols (0.2, R = CF₃)².

3) A Hammett correlation of the second-order rate constants for dehydration of a series of substituted *cis*-dihydrodiols against σ^p values gave a ρ -value of -8. A large, negative ρ -value was expected; however, the better correlation with σ^p rather than σ^+ was not expected in the case of the formation of a conjugated carbocation¹.

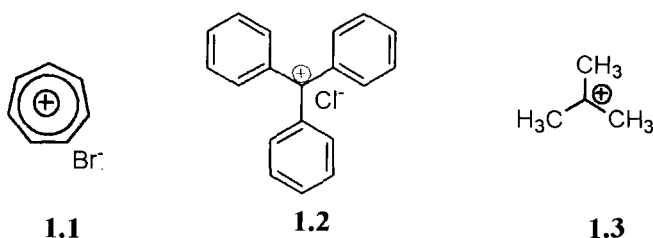
This thesis presents results on the synthesis and dehydration reactions of arene hydrates and dihydrodiols. This chapter will summarise relevant research on the reactions of arene hydrates, diols and other oxidative metabolites of aromatic hydrocarbons. As the dehydration reactions typically involve the formation of carbocation intermediates, a large focus of this chapter will be on the formation, reaction and stabilities of carbocations.



Introduction

1.1 Early History

The history of carbocations dates back to 1891 when G. Merling reported that he had added bromine to tropyliene (cycloheptatriene) and then heated the product to obtain a crystalline water soluble material, C_7H_7Br . This was later confirmed by Doering and Knox to be the tropylium ion (1.1). It was also observed that triphenylmethyl (trityl) chloride (1.2) gave conducting solutions when dissolved in liquid sulphur dioxide, a polar non-nucleophilic solvent.³ Trityl chloride also reacts with Lewis acids, such as aluminium chloride, to give coloured salt-like solids, which were subsequently used as dyes.



The existence of highly reactive carbocation intermediates was doubted amongst the chemical community until the direct observation, by Doering *et al*, of the stable hexamethylbenzenonium ion generated by the reaction of hexamethylbenzene with methylchloride and aluminium chloride. The Nobel Laureate, George Olah was the first to show the NMR spectrum of the *tert*-butyl carbocation (1.3).⁴

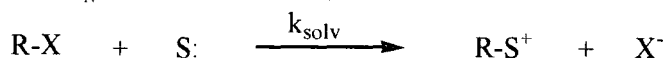
The work of Ingold, Hughes *et al* in University College London laid the foundations for the role of carbocation intermediates in organic chemistry; as discussed below (section 1.2).

1.2 Substitution and solvolysis reactions

The reaction in Scheme 1.2-1 is a classical example of a nucleophilic substitution reaction at carbon. This reaction occurs by two possible mechanisms:

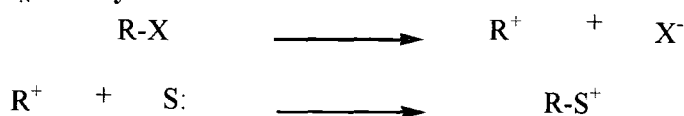
- (1) A bimolecular reaction where the rate depends on both the concentrations of substrate and solvent or nucleophile (S_N2) (Rate = $k[RX][S:]$)

Scheme 1.2-1: S_N2 Substitution Reaction



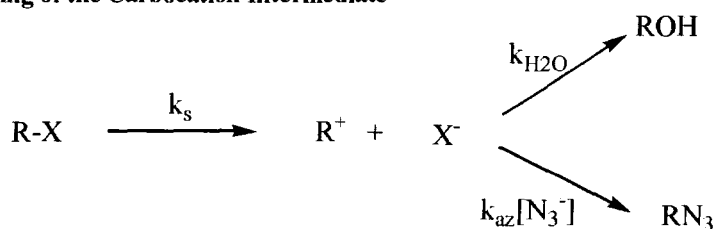
- (2) A unimolecular process (S_N1) where cleavage of the R-X bond to give a tricoordinate carbocation intermediate is rate-determining and is followed by rapid reaction with a Lewis base; the rate depends only on the substrate and is independent of the nucleophile (Rate = $k[RX]$)(see Scheme 1.2-2, below).

Scheme 1.2-2: S_N1 Solvolysis Reaction



Generally, a concerted substitution reaction will become stepwise as the covalent bond becomes progressively weaker and the carbocation becomes more stabilised relative to the substrate RX.

Scheme 1.2-3: Partitioning of the Carbocation Intermediate



Partitioning of the carbocation intermediate between reaction pathways leading to different products allows for measurement of the stability of the carbocation without direct observation. The ratio of the concentration of products formed provides a measure of the ratio of rate constants for the different reaction pathways, provided a correction is made for the relative concentrations of carbocation trapping agents (eg. N_3^- , H_2O), (see Scheme 1.2-3). This ratio is the selectivity factor, S , (Equation 1.1).

$$S = k_{\text{Nu}1}/k_{\text{Nu}2}$$

Equation 1-1

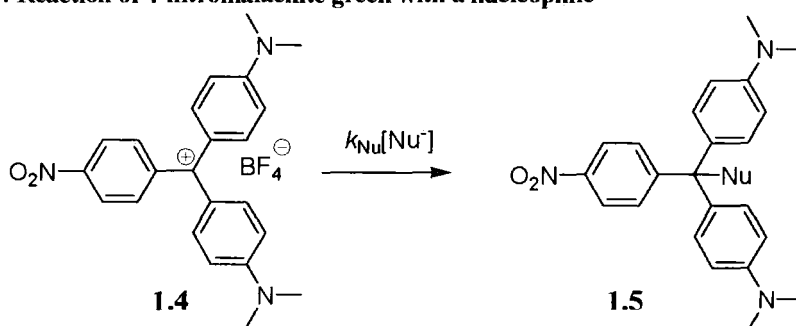
Large numbers of carbocations have been studied in this manner. Typically, the carbocation would be generated from an alkyl halide in an aqueous organic solvent, followed by competitive reaction with water and an added nucleophile such as azide ion (see Scheme 1.2-3). The stability of a carbocation intermediate can be directly related to the solvolysis rate for a series of compounds under similar reaction conditions. A large rate constant for the solvolysis reaction can indicate a relatively stable carbocation.

The relationship between k_s and S became known as the ‘reactivity-selectivity’ principle stating that an increase in reactivity results in a decrease in selectivity. Thus, stable carbocations, such as the trityl carbocation, demonstrate large selectivities, whereas more unstable carbocations show lower selectivities. This, however, is not always the case. Ritchie’s carbocations based on malachite green (see Scheme 1.2-4) show a constant selectivity. The Ritchie parameter (N^+) is defined by equation 1-2 and is characteristic of the nucleophilic system and independent of the cation.

$$\text{Log}\left(\frac{k_{\text{Nuc}}}{k_{\text{water}}}\right) = N^+$$

Equation 0-2

Scheme 1.2-4: Reaction of 4-nitromalachite green with a nucleophile



The problems with the ‘reactivity-selectivity’ principle are discussed in an excellent review by Mayr and Ofial.⁵ The decrease in selectivity is due to the fact that the reaction with azide is limited at the rate of diffusion for all carbocations that react with water at a

rate faster than 10^5 s^{-1} and the change in selectivity is caused by the variable rate constant k_w for reaction with water. The azide-clock method developed by Richard and Jencks uses this fact and this will be discussed in section 1.3.2.

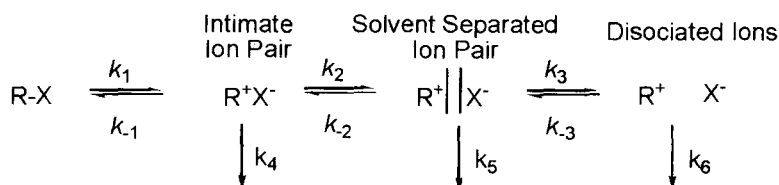
Mayr introduced the slope-parameter (s) to account for non-linearity in the correlation of his data with the Ritchie equation for the reaction of a series of π -systems with carbocations. Equation 1.3 shows the Mayr equation, where k is the second-order rate constant for reaction of a nucleophile with the relevant carbocation, E is a nucleophile independent electrophilic parameter and N is an electrophile independent nucleophilicity parameter.

$$\text{Log}(k_{20^\circ\text{C}}) = s(E + N) \qquad \text{Equation 0-3}$$

1.2.1 Ion Pairs

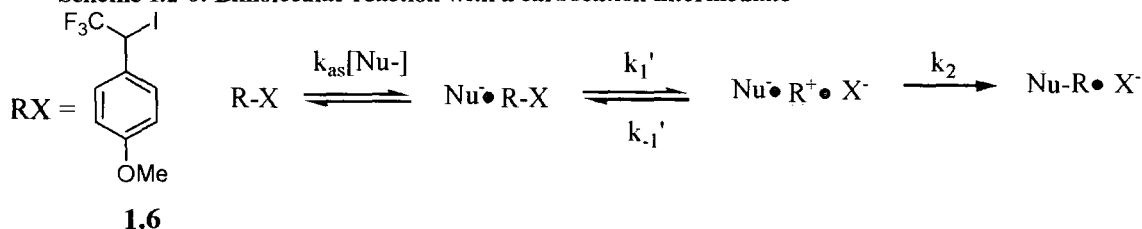
Winstein *et al* recognised that heterolytic cleavage of the R-X bond should not be considered as a single step but as the first in a sequence involving different types of ions and ion pairs. In the solvolysis reaction the first step is the formation of an intimate ion pair with a solvent cage, which then forms a solvent separated ion-pair which collapses to form dissociated ions (see Scheme 1.2-5). Only stabilised carbenium ions lead to fully dissociated carbocations, whereas, less stable carbenium ions are more likely to be intercepted earlier. The evidence for this scheme includes polarimetric rate constants (k_a) which exceed rate constants for product formation, thus indicating the presence of intimate ion pairs. When the rate constant k_{-2} is greater than k_3 , scrambling the stereochemistry of the reactant occurs. Also there is a large nonlinear 'special' salt effect at low salt concentrations, implying the formation of solvent separated ion pairs which are scavenged by salt.

Scheme 1.2-5: Solvolysis reaction with ion pair formation

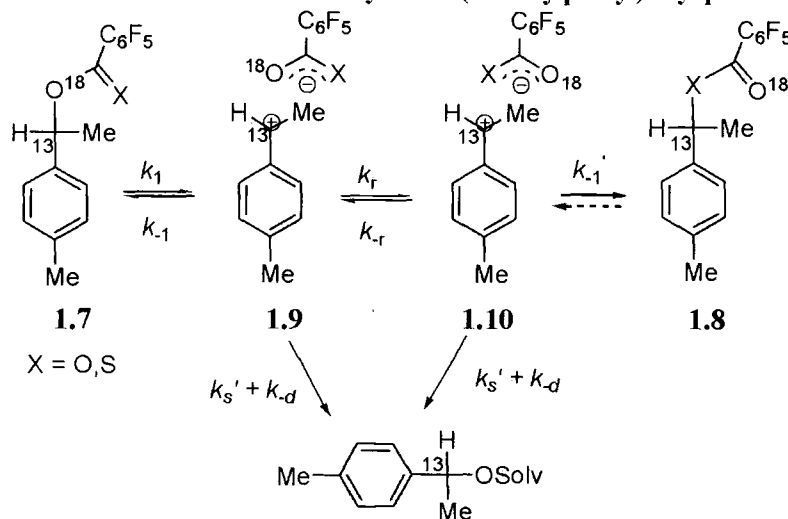


There are examples of solvolysis reactions which are kinetically bimolecular but involve a carbocation intermediate. These are unusual as there are strict conditions which must be met if the reaction of the nucleophile with an ion pair intermediate is to give a detectable increase in the rate of solvolysis by a pre-association mechanism. Richard and Yeary discuss the strict conditions for a bimolecular carbocation forming reaction and a simple protocol for determining if a second-order reaction proceeds through a carbocation intermediate using 1-(4'-methoxyphenyl)-2,2,2-trifluoroethyl iodide (1.6) as an example.⁶

Scheme 1.2-6: Bimolecular reaction with a carbocation intermediate



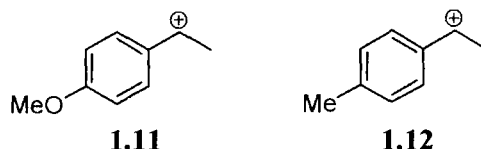
The solvolysis reactions of 1-(4-methylphenyl)ethyl pentafluorobenzoate (1.7), labelled with carbon-13 at the benzylic position and oxygen-18 at the bridging benzoate oxygen, have been studied by Tsuji *et al.*⁷ The solvolysis reaction (see Scheme 1.2-7) is known to proceed by a stepwise mechanism involving the 1-(4-methylphenyl)ethyl carbocation (1.10) as an intermediate. This carbocation has a significant lifetime in 50/50 (v/v) TFE/H₂O and has a rate of reaction with solvent (k_s') of $6 \times 10^9 \text{ s}^{-1}$.⁸ The carbocation-anion ion pair is particularly unstable in this solvent. The rate constant for isomerisation of (1.7) to (1.8) was found to be $k_{\text{iso}} = 1.6 \times 10^{-6} \text{ s}^{-1}$ by ¹³C NMR spectroscopy.

Scheme 1.2-7: Ion Pair formation in the Solvolysis of 1-(4-methylphenyl)ethyl pentafluorobenzoate⁸

The fraction of ester (1.7) that undergoes isomerisation, $k_{iso}/k_{obs} = 0.13$, is smaller than for the corresponding thiolbenzoate ester (73 % isomerisation). This reflects the greater nucleophilicity of sulphur at an ion pair⁹. The rate of exchange of the O and S atoms of the leaving group (k_r) is 6-fold faster than the diffusional separation to free ions ($k_{-d} = 1.6 \times 10^{10} \text{ s}^{-1}$). The rate constant for the overall solvolysis reaction (k_{solv}) is equal to $1.06 \times 10^{-5} \text{ s}^{-1}$. It could be shown that the ion pair intermediate undergoes significant internal return via unimolecular collapse of the ion pair, $k_{-1}' = 7 \times 10^9 \text{ s}^{-1}$. The isomerisation is slower than the solvolysis suggesting the rate of ion-pair collapse is slower than diffusional separation of the ion pair followed by reaction with solvent ($(k_s' + k_{-d}) > k_{-1}'$).

1.2.2 Solvent effects

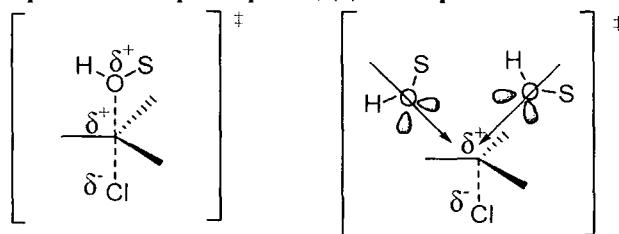
A comparison of the relative nucleophilic reactivity of solvents with a carbocation can be used to ascertain relative carbocation stabilities. Methanol is 10-fold more reactive than water and 100-fold more reactive than 2,2,2-trifluoroethanol (TFE) with the 4-(methoxy)phenylethyl cation (1.11).⁸ The sensitivity of the carbocation to the nucleophilic reactivity of alcohols and water decreases with decreasing stability of the carbocation as is seen in the 4(methyl)phenylethyl cation (1.12).¹⁰ Reactivity of solvents generally fall in the order: MeOH > EtOH > Water >> TFE >> HFIP (hexafluoroisopropanol). The viscosity of the solvent can also affect carbocation reactivity, for example, in ethylene glycol/water mixtures reactions are slower than its reaction in water.



The ionisation of *tert*-butyl chloride is endothermic by 153 kJ/mol in the gas phase. Carbocation formation is more feasible in solution due to the solvation of the ions formed. What is the nature of the nucleophilic assistance from solvent in the stabilization of the *transition state* for solvolysis of simple tertiary derivatives? There are two definitions of nucleophilic assistance as described by Richard et al¹¹. Firstly, nucleophilic solvent participation (NSP) is the interaction that accelerates solvolysis by formation of a partial covalent bond between an incoming solvent nucleophile and the developing cationic charge (see Fig 1.2-1(a)). This is an S_N2-like process, with the solvent being kinetically significant.

Nucleophilic solvation (NS) is the stabilising interaction between the dipole of nucleophilic solvents and the carbocation and the corresponding interactions in the *transition state* for their formation in a stepwise solvolysis reaction (see Fig 1.2-2(b)).

Figure 1.2-1: (a) Nucleophilic solvent participation, (b) Nucleophilic solvation¹¹



In the case of solvolysis of simple tertiary derivatives, there is no significant stabilisation of the transition structures by formation of a covalent bond to the incoming solvent nucleophile but the carbocation like transition structure is stabilised by interaction with the dipole of the nucleophilic solvent. The evidence for this is discussed by Richard *et al.*¹¹

Mayr and co-workers have identified unambiguously the rate determining step in the solvolysis reactions for a number a substituted bisaryl carbenium ions such as bis(4-methoxyphenyl)carbenium tetrafluoroborate. The carbocation was generated by stopped-flow and the rate of decay was determined and compared with the overall rate of solvolysis. In most cases, the decays of the benzhydrylium absorbances followed single exponentials from which pseudo-first-order rate constants were derived. A TFE/MeCN solvent mixture was used to prolong the lifetime of the carbocation intermediate as the ionization of a R-X bond in TFE is up to 10^5 times faster than the reaction of R^+ with TFE. Adding lithium perchlorate allowed both the rate of ionization ($5 \times 10^2 \text{ s}^{-1}$) and the overall rate of reaction with TFE ($k_{\text{TFE}} = 10.4 \text{ s}^{-1}$) in 20:80 TFE/MeCN to be determined simultaneously. Increasing the stability of the carbocation and decreasing solvent nucleophilicity transforms the generally accepted energy profiles of S_N1 reactions with carbocations as shortlived intermediates into energy profiles which imply the buildup of significant concentrations of the intermediate carbocations¹².

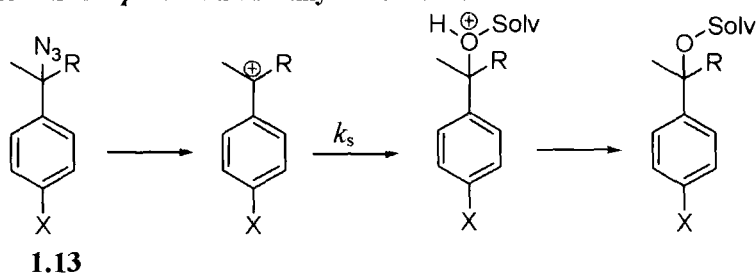
Richard *et al* have investigated the effect of changing the intrinsic barrier on reaction of a carbocation with solvent and proton transfer^{13, 14}. The Marcus equation (see Equation 1-4, below) relates the activation barriers (ΔG^\ddagger) for reactions to the overall thermodynamic driving force (ΔG°) and the intrinsic barrier (Λ), which is the value of ΔG^\ddagger when $\Delta G^\circ = 0$.

There is evidence that the Marcus intrinsic barrier for the addition of nucleophiles to ring-substituted benzyl carbocations increases with increasing carbocation stability as a result of resonance electron donation from the aromatic ring to the benzylic carbon.

$$\Delta G^\ddagger = \Lambda(1 + \Delta G^\circ/4\Lambda)^2$$

Equation 0-4

The model systems used are based on the ionisation to form *p*-substituted cumyl cations (see Scheme 1.2-8). The rate of reaction with solvent (k_s) decreased 10^8 -fold as the substituent X was changed from a *p*-methyl to a *p*-dimethylamino group i.e. k_s decreased with increasing carbocation stability. Stabilisation of the carbocation by resonance electron-donating groups results in a larger increase in the activation barrier to solvent addition than is observed for an equal stabilisation of the carbocation by polar electron-donating groups. In this case, the change in ΔG° and Λ reinforce each other resulting in an increased thermodynamic barrier.

Scheme 1.2-8: Reaction of *p*-substituted cumyl carbocation

In the solvolysis reaction of *p*-MeOArCHN₃R (1.13, X = OMe) the change from an electron donating α -substituent (R = OMe) to an electron-withdrawing substituent (R = CF₃) results in no change in the rate of solvolysis. This has been assigned to the effect of the electron-withdrawing group (CF₃), creating a destabilising charge-dipole interaction resulting in an increase in the delocalisation of the positive charge on the 4-methoxyphenyl ring. The increase in carbocation stability by charge delocalisation results in an increase in the intrinsic barrier (Λ) for the nucleophilic addition reaction. This increase in the intrinsic barrier for the reaction of the carbocation with solvent compensates for the increase in the ΔG° for the reaction thus resulting in no change in ΔG^\ddagger . As a result ΔG^\ddagger is independent of the substituent R.¹⁵

1.3 Quantification of carbocation reactions

1.3.1 Kinetic relativities

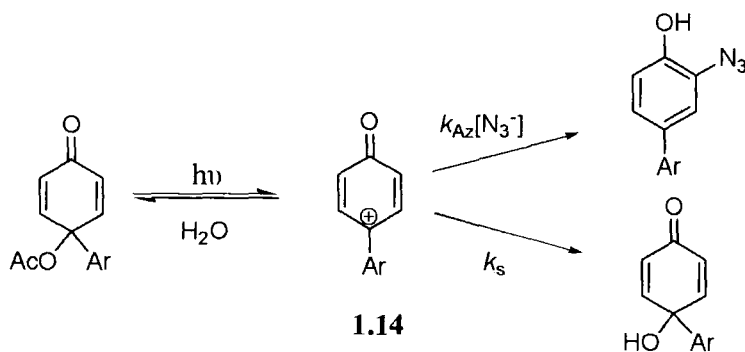
Flash photolysis offers a way of directly measuring the reactivity of cations. For the reactivity to be studied the carbocation must be observable. Usually UV-vis spectrophotometric detection is used but in some cases conductivity detection is used. The carbocation must have a sufficient lifetime, $1/k_s$, where k_s is the first order rate constant for decay in a particular solvent, which must be at least the same order of magnitude as the width of the flash or pulse of the light source employed for its generation. The general availability now of picosecond lasers allows the detection of the separation/collapse of ion pairs in a solution. Development in this regard is discussed by McClelland.¹⁶

The carbocation intermediate may be generated by photolysis of the C-X bond. In this process, radicals and triplet states can also be formed. These transient species can be distinguished by their kinetic behaviour. The presence of oxygen has no effect on the decay of carbocations intermediates but quenches radicals and triplet excited states. Triplet states also react with 1,3-cyclohexadiene. Comparing oxygen and argon saturated systems allows the presence of radicals to be investigated. A suitable choice of leaving group can favour carbocation formation in preference to radicals. Azide ion and certain other nucleophiles react with certain carbocations at the diffusional or near diffusional limit. The development of LFP techniques has allowed for the rate of reaction of azide with carbocation intermediates to be confirmed.

Recent studies^{17,18} have used laser flash photolysis to generate an aryloxonium ion. Two transient species ($\lambda = 460$ and 360 nm) were identified after LFP with a 5 ns pulse at 266 nm. The species at 360 nm was not affected by either azide or oxygen and it has not been identified to date. The species at $\lambda = 460$ nm showed increased rates of decay with added azide ion, was not affected by oxygen and was hence identified as the oxonium ion (see Scheme 1.3-1, below). For aryl equal to *para*-tolyl (1.14), the reaction with azide is diffusion limited with k_{AZ} calculated to be a $(6.6 \pm 0.2) \times 10^9 \text{ M}^{-1} \text{ s}^{-1}$. This is in line with

the expected diffusion limit of ca. $5\text{-}7 \times 10^9 \text{ M}^{-1} \text{ s}^{-1}$.¹⁰ The lifetime of the intermediate in the absence of azide is $170 \pm 10 \text{ ns}$.

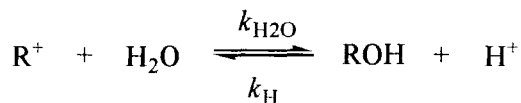
Scheme 1.3-1: Laser Flash Photolysis of 4-aryl-4-acetoxy-2,5-cyclohexadienones forming 4-aryl-4-acetoxy-2,5-cyclohexadienones



1.3.2 Thermodynamic stabilities (pK_R Values)

The equilibrium between a carbocation and alcohol can be represented by the scheme shown below (Scheme 1.3-2). The corresponding equilibrium constant, K_R (M) is represented by the equation 1-5. The equilibrium constant is a measure of the relative concentrations of carbocation and alcohol present at equilibrium in 1 M acid and so directly reflects the thermodynamic stability of the carbocation.

Scheme 1.3-2: Equilibrium between a Carbocation intermediate and alcohol

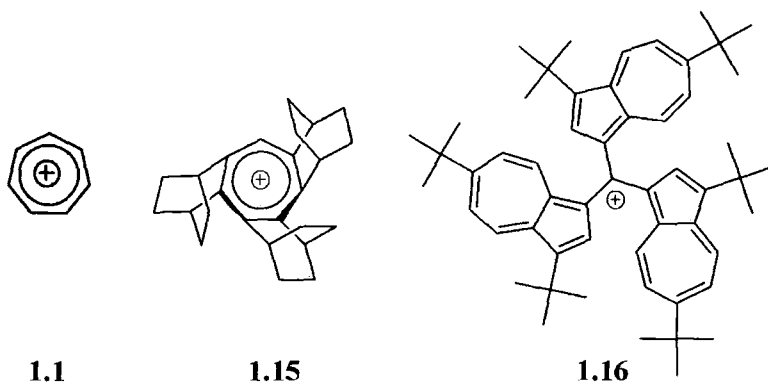


$$K_R = \frac{[\text{ROH}][\text{H}^+]}{[\text{R}^+]}$$

Equation 0-5

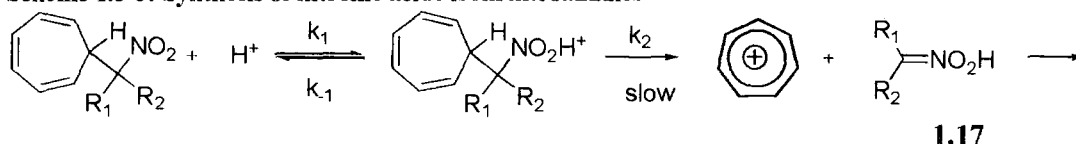
Originally, K_R was determined using traditional spectroscopy. However, this was limited as it required that the alcohols have a reasonable spectroscopic change upon ionisation to the carbocation and also, more importantly, it relied on the stability of the carbocation in

acidic solution for the timescale of the experiment and the magnitude of K_R . The technique was limited to stable carbocations, e.g., the pK_R of the aromatic tropylium ion (1.1) was determined to be + 4.7, and the measurements could be carried out in dilute acid solutions. pK_R values as high as 14 have been determined e.g. the 1,2:3,4:5,6-tris(bicyclo[2.2.2]octeno)tropylium ion (1.15) has a pK_R of +13.0¹⁹ and the tris(3,6-di-*t*-butyl-1-azulenyl)methyl carbocation (1.16) has a pK_R of + 14.2²⁰.



The stability of the tropylium cation is used to form nitronic acids (1.17) from nitroalkanes under acid catalysis^{21, 22}. The leaving group is not a proton but the highly stable tropylium (pK_R 4.7) cation (1.1) which can depart from the protonated alkane in a unimolecular fashion (see Scheme 1.3-3, below). Without using the tropylium ion as a leaving group the reaction is retarded in acid.

Scheme 1.3-3: Synthesis of nitronic acids from nitroalkanes²¹



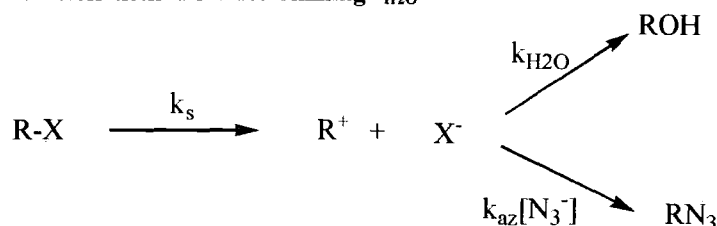
The pK_R of a triarylmethyl carbocation with at least one dimethylamino substituent can be determined in dilute acid solutions. By contrast the triphenylmethyl cation requires a strong acid media to increase the concentration of carbocation present and the excess acidity method²³ is required to determine the concentration of hydronium ion. The experimental values of the pK_R for the triphenylmethyl cation vary depending upon the mineral acid used and the method of estimation of acid concentration. The results varied from -6.12 in HCl, to -6.63 in H₂SO₄ and -6.89 in HClO₄ using, Hammett's acidity function, and -6.47 in H₂SO₄ and -5.85 in HCl using the excess acidity function²⁴.

Carbocations from aliphatic alcohols, such as the *tert-butyl* carbocation (1.3), have very short lifetimes and are thus present in equilibrium concentrations that are too small for direct monitoring. A method for measuring K_R kinetically was developed.¹¹ The rate constants for the forward and the reverse directions of scheme 1.3-2 are determined separately and the K_R is obtained as the ratio of the rate constants, k_H and k_{H_2O} (Equation 1-6), where k_H is the second-order rate constant for the hydronium ion catalyzed reaction of the alcohol to form the carbocation and k_{H_2O} is the first-order rate constant for capture of the carbocation by water.

$$pK_R = -\text{Log}K_R = \log\left(\frac{k_H}{k_{H_2O}}\right) \quad \text{Equation 0-6}$$

The primary method for determining k_{H_2O} is by the competition method, where the rate constant ratio for reaction of a carbocation with two nucleophiles is determined where one of the rate constants is at the diffusion limit. The azide 'clock' is such a method (shown below).¹¹

Scheme 1.3-4:Azide Clock method for determining k_{H_2O} ¹¹

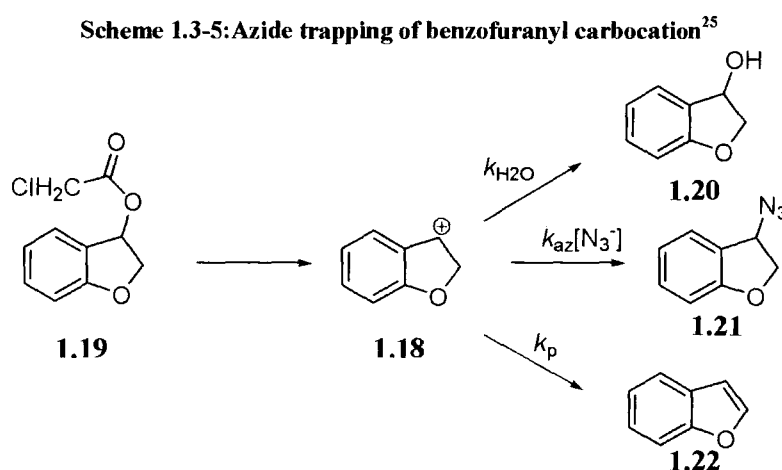


The ratio k_{az}/k_s (M^{-1}), determined by product analysis, decreases with the addition of electron-withdrawing groups due to destabilisation of the carbocation intermediate and so the proportion of solvent-adducts increases. For these unstable carbocations k_{az} is invariant as the diffusion limit, $5 \times 10^9 M^{-1} s^{-1}$ and k_s is limited by the chemical barrier to solvent addition and increases with decreasing carbocation stability. Using Equation 1-7 (below), the absolute rate constant, k_s , can be determined and this value can be then be combined with the rate constant k_H ($M^{-1}s^{-1}$) for the acid-catalysed cleavage of the corresponding alcohols to give a value for the pK_R .

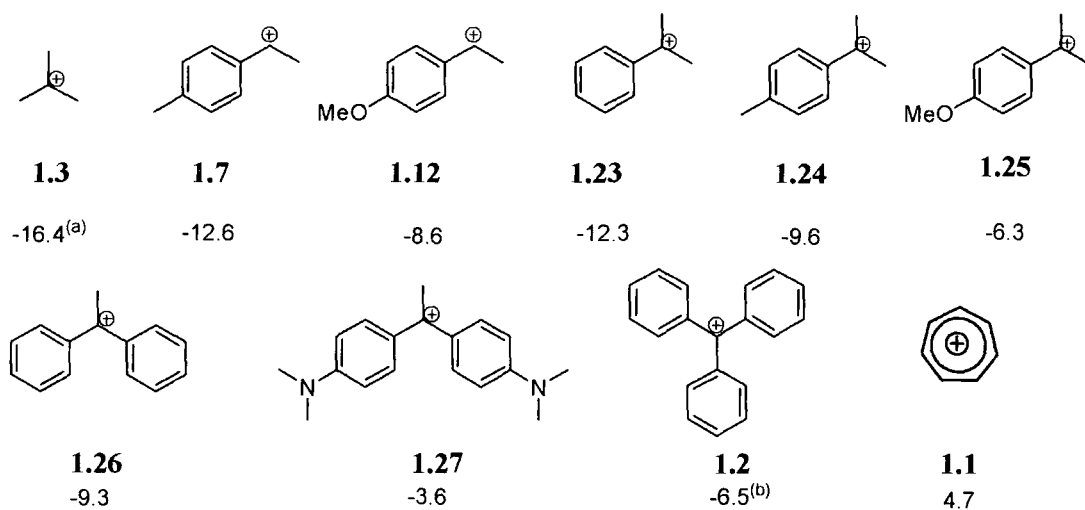
$$k_{Az}/k_s = \frac{[RN_3]}{[ROH][N_3^-]}$$

Equation 0-7

Scheme 1.3-5 (below) shows the azide trapping of the benzofuranyl carbocation (1.18)²⁵. Here, a carbocation precursor is synthesised (carboxylate ester, (1.19)) and reacted in the presence of increasing concentrations of azide. The carbocation can either react with solvent (k_{H_2O} , 1.20) and/or with azide ($k_{az}[N_3^-]$, 1.21) or can eliminate H^+ (k_p), to give benzofuran (1.22). k_{H_2O} could be determined from the ratio of product concentrations and, as mentioned above, by assuming reaction with azide is diffusion controlled ($5 \times 10^9 \text{ M}^{-1}\text{s}^{-1}$). Combining this k_{H_2O} value with the value of k_H , determined by the acid-catalysed racemisation of the hydrate, yields a value for pK_R , which is -9.3.



A series of carbocations and their pK_R values are shown below. The highly stabilized carbocations such as $(p\text{-Me}_2\text{NAryl})_2\text{MeC}^+$ (1.27) and the tropylium ion (1.1) have positive pK_R values whereas less stable carbocations that have a very short lifetime, such as the *tert*-butyl cation (1.3) have large negative pK_R values. The effect of both *p*-methoxy and *p*-methyl groups is to increase carbocation stability and corresponding pK_R values e.g. for the cumyl cation (1.23), the pK_R increases from -12.3 to -9.6 with the addition of a *p*-methyl substituent and further to -6.3 upon the introduction of a *p*-methoxy substituent (see Chart 1.3-1).

Chart 1.3-1: Series of carbocations and their pK_R values.

The “azide-clock” methodology is generally good for predicting the rate constant for the reaction of a carbocation with solvent (e.g. water), where $k_{az} = k_d$ i.e. the rate of reaction with azide is diffusion controlled. However, not all carbocations fall into that category (see Chart 1.3-1). For highly reactive carbocations, the intermediate is so reactive that it is captured before escaping the solvent cage (Fig 1.3-1 ‘reaction in pool’). The carbocation must also be sufficiently reactive to compete with azide to a sufficient extent for the solvent adduct to be detectable, corresponding to a cation with a solvent rate constant $>10^5 \text{ s}^{-1}$ (or a $k_{Az}:k_s$ ratio $<10^5 \text{ M}^{-1}$).

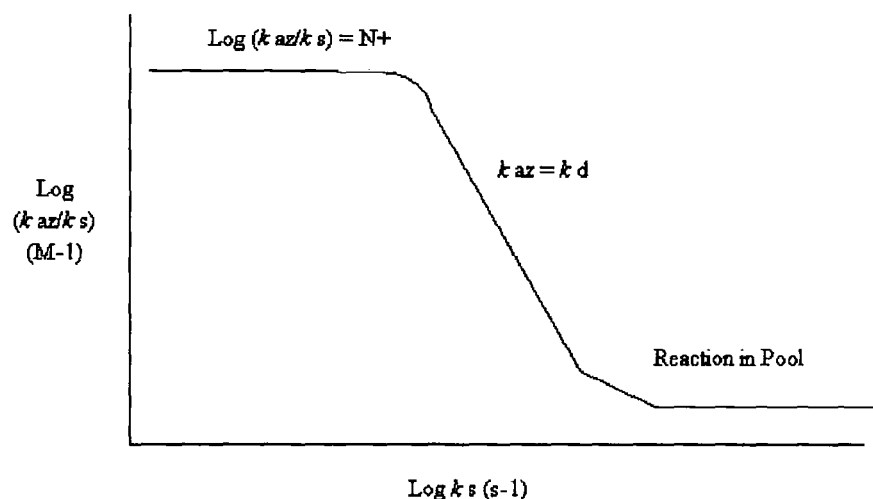
Highly stabilised cations, as investigated by Ritchie, show constant selectivity. The reactions of such cations with both N_3^- and other nucleophiles are significantly less than diffusion controlled. Ritchie expressed this in the form of equation 1-8:

$$\text{Log}\left(\frac{k}{k_0}\right) = N^+ \quad \text{Equation 0-8}$$

In this equation, k is the rate constant for reaction of the carbocation with a given nucleophile (such as azide) and k_0 is the rate constant for reaction of the cation with

water. The parameter N^+ is characteristic of the nucleophile system and independent of the cation.

Figure 1.3-1: The dependence of azide ion selectivity (k_{az}/k_s , M^{-1}) on carbocation reactivity with largely aqueous solvents.



1.4 Carbocation Intermediates in the reactions of epoxides and alcohols

This section will present some recent published literature on the reactions of carbocation intermediates generated from the reactions of epoxides towards nucleophiles, dehydration and the ionisation of alcohols.

1.4.1 Carbocation formation in the ring-opening reactions of epoxides and arene oxides

Investigation into the reactivity of the oxides of polycyclic aromatic hydrocarbons (PAHs) is a significant area of research relating to the broader area of carbocation intermediates. The biological relevance will be considered in section 1.5. The reactivity of epoxides, particularly benzylic epoxides, will be considered in this section.

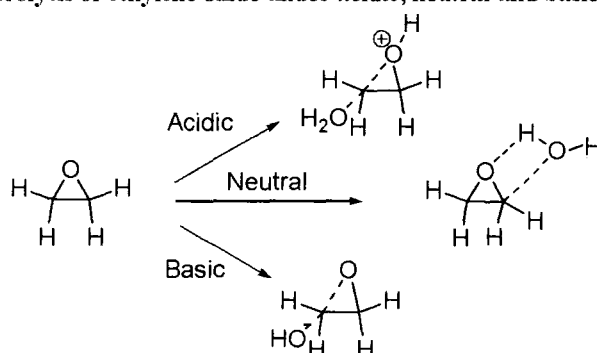
1.4.1.1 Reactions of non-aromatic epoxides

There are two possible mechanisms for epoxide hydrolysis, the A-1 (S_N1) and the A-2 (S_N2).²⁶ The A-1 mechanism involves the formation of a carbocation intermediate in a rate determining step, whereas the A-2 mechanism is concerted and the rate depends on the concentration of epoxide and nucleophile. Simple epoxides react under acid, basic and neutral conditions, to give diols. For example, the computational study of the hydrolysis of ethylene oxide shows there are two different reaction mechanisms²⁷:

(1) Under neutral conditions, the ring-opening reaction involves only one water molecule that is hydrolysed in the transition state. The activation barrier for this reaction is high (205 kJ/mol), and in agreement with the low reaction rate observed experimentally.

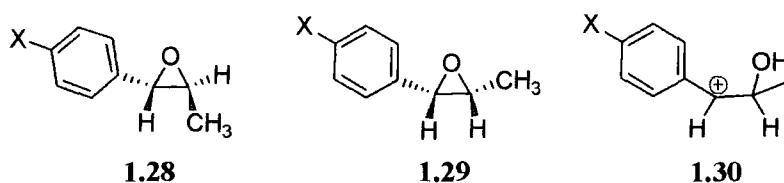
(2) Under acidic and alkaline conditions a concerted S_N2 reaction is observed with water and hydroxide ions acting as nucleophiles and oxonium ions and water acting as electrophiles. The activation enthalpies for these different reaction mechanisms are significantly lower than those for the reaction under neutral conditions (~ 80 and 60 kJ/mol).

Figure 1.4-1: Hydrolysis of ethylene oxide under acidic, neutral and basic conditions



The conjugation of an epoxide group with vinyl or aryl groups introduces additional steric and electronic effects that alter the mechanisms of acid-catalyzed addition of nucleophiles to these epoxides. In these systems, the amount of *syn* hydration increases with the ability of the aryl group to stabilize a positive charge at the benzylic carbon. The

second-order rate constant, k_H , for the acid-catalyzed hydrolysis of *trans*-(1.28) and *cis*-(1.29) anethole oxides between pH 4 and 7 was determined at ionic strength 0.1 M (NaClO_4). k_H values for the reactions of (1.28) and (1.29) ($X = \text{MeO}$) were obtained as $(1.51 \pm 0.05) \times 10^4 \text{ M}^{-1} \text{ s}^{-1}$ and $(3.17 \pm 0.21) \times 10^2 \text{ M}^{-1} \text{ s}^{-1}$. The second-order rate constants for the hydrolysis of the parent *trans*-methylstyrene oxide (1.28) ($X = \text{H}$) and *cis*-methylstyrene oxide (1.29) ($X = \text{H}$) are $12.7 \pm 0.3 \text{ M}^{-1} \text{ s}^{-1}$ and $0.27 \pm 0.03 \text{ M}^{-1} \text{ s}^{-1}$, respectively.²⁸

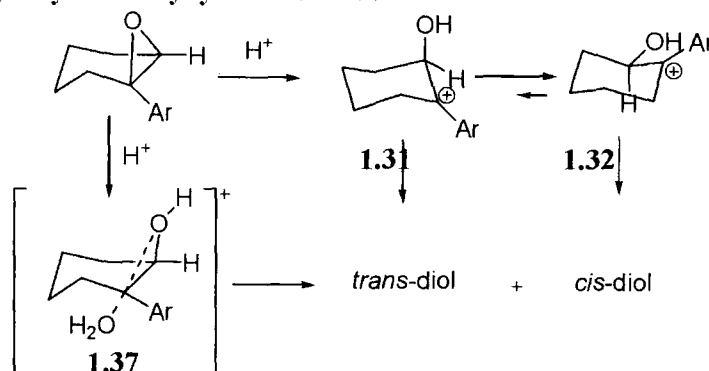


In both cases, the *trans* epoxide is 50-fold more reactive than the *cis* suggesting that the resonance interaction between the aryl group and the developing carbocation centre at the transition states for hydrolysis of (1.28) ($X = \text{OMe}$ & H) and (1.29) ($X = \text{OMe}$ & H) must be comparable, thus having a common intermediate (1.30). Azide-trapping of both methoxy-substituted methylstyrene oxides give the same first order rate constants for the reaction with solvent ($k_s = 2 \times 10^8 \text{ s}^{-1}$), assuming k_{az} is $5 \times 10^9 \text{ M}^{-1} \text{ s}^{-1}$. The life time ($1/k_s$) of this common intermediate (1.30) is estimated to be $5 \times 10^{-9} \text{ s}$, which is significantly longer than the lifetime of a bond vibration²⁸. The product distribution of the reactions of both epoxides with azide is the same. Therefore, rotation about the $\text{C}_\alpha\text{-C}_\beta$ bond in the carbocation intermediate is rapid relative to the rate at which it reacts with solvent or other nucleophiles. The products are derived mainly from the reaction with the carbocation in the most stable arrangement.

Scheme 1.4-1 (below) shows the acid-catalyzed hydrolyses of 1-arylcyclohexene oxides which yield mixtures of *cis*- and *trans*-diols resulting from *syn* and *anti* hydration of the epoxide group, respectively. The ratio of *cis* to *trans* does not depend greatly on the substituent present on the aryl ring (see Scheme 1.4-2). In fact, the product distribution is similar under conditions where the *cis* and *trans* products are stable. At $\text{pH} < 2$ there is acid-catalysed equilibration of the diol products, in which the *cis*-diol is the more stable

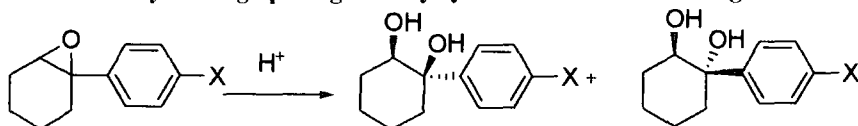
at equilibrium. Equilibration studies of the diol products show the major (thermodynamic) product to be the *cis*-diol.²⁹

Scheme 1.4-1: Hydrolysis of 1-arylcyclohexene oxides



On ring-opening of the epoxide, a carbocation intermediate is formed at the benzylic position (see Scheme 1.4-1). There are two possible conformations of the carbocation intermediate (1.31 and 1.32), axial attack on (1.31), gives the *trans*-diol and axial attack on (1.32), gives the *cis*-diol. In stabilised carbocations (Ar = anisole, (1.33), Scheme 1.4-2) the conformers are in rapid equilibrium and so the thermodynamic (*cis*) product is formed as the major product. When the carbocation intermediate is highly destabilised, for example with a nitro group in the *para*-position (1.36), the major product is the *trans*-diol, possibly resulting from a partially concerted mechanism via transition state (1.37). If conformations (1.31) and (1.32) are in rapid equilibrium, then the ratio of diol products will be independent of the equilibrium concentrations of carbocation conformations, but will instead depend only on the difference in energy between the transition states leading to *cis*- and *trans*-diol products (Curtin-Hammett Principle).³ The factors that add to the greater stability of the *cis*-diol product also contribute to the lowering of the transition state energy for attack of water on the carbocation leading to the major *cis* diol product.²⁹

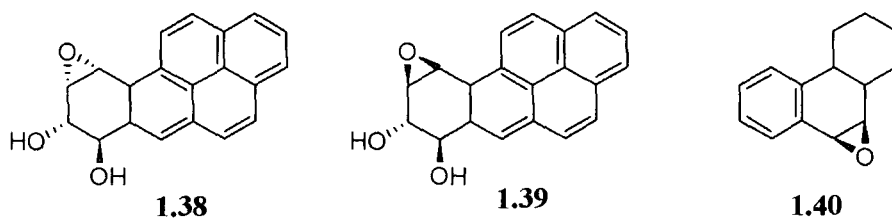
Scheme 1.4-2: Acid-catalysed ring-opening of 1-arylcyclohexene oxides forming *cis* & *trans*-diols²⁹



Epoxide	X	pH	<i>Cis</i>	<i>Trans</i>	$k_H(\text{M}^{-1}\text{s}^{-1})$
1.33	OMe	6.0	74	16	6.0×10^4
1.34	CH ₃	5.0	83	17	4.9×10^3
1.35	H	4.0	65	35	3.6×10^2
1.36	NO ₂	<1	7.5	92.5	-

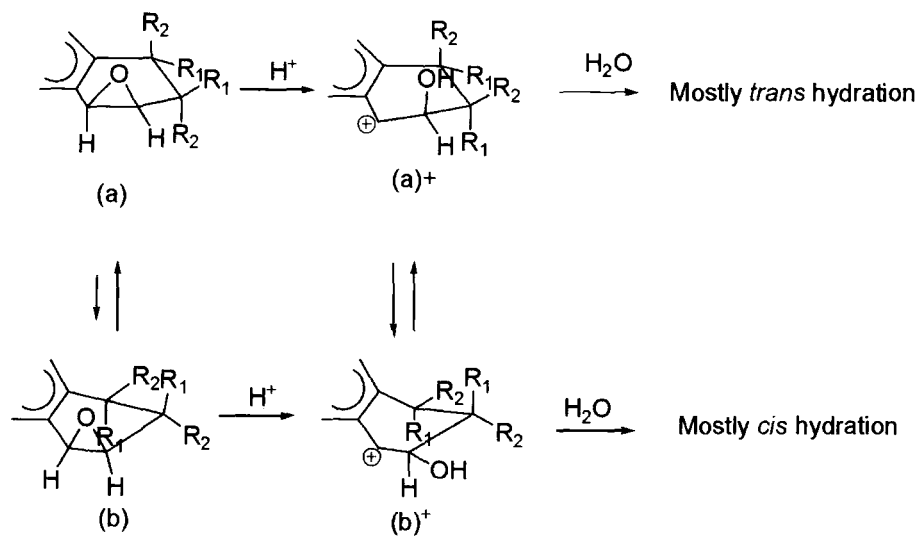
The hydrolysis reactions of the methoxy, methyl and hydrogen substituted 1-arylcyclohexene oxides (1.33 – 1.35), give a ρ -value of -2.8 from a Hammett correlation with σ^+ , whereas, a Hammett correlation for the substituted styrene oxides gives a ρ^+ of -4.2. This suggests there is less need for stabilization of the transition state by the substituent in the *para*-position as the carbocation centre is formed at a tertiary position rather than at a secondary position²⁹.

The reactivity of the diol-epoxides, such as benzo[α]pyrene 7,8-diol 9,10-epoxide (1.38), is similar to the previous two examples. Acid-catalysed ring-opening of (1.38) gives a carbocation at the benzylic position, followed by attack of solvent giving predominantly *trans*-diols (95 %), whereas, diastereomer (1.39) reacts to form predominantly *cis*-diols (90 %). This is due to favourable attack of solvent and nucleophiles at the axial position in cyclohexyl systems.³⁰ This has been confirmed in early work by Whalen *et al*; where the hydrolysis of a rigid system (1.40) forming a benzylic carbocation results in predominantly axial attack.³¹



There are two possible conformations, (a) and (b), of (1.38) and (1.39). The acid-catalysed ring-opening of the diol-epoxide yields two possible carbocation conformations – (a)⁺ and (b)⁺ (see Scheme 1.4-3, below) and these are of equal stability. Whalen suggests that the reason for the formation of the *trans* regioisomer from the reaction of diol epoxide (1.38) as the major product is that the rate of reaction of the carbocations with solvent is faster than the rate of conversion of the two carbocation conformers.³² Diol-epoxide (1.38) is found primarily as conformer (a) and (1.39) is found as conformer (b).³²

Scheme 1.4-3: Hydrolysis reaction of benzo[*a*]pyrene-7,8-diol-9,10-epoxide (1.38) and diastereomer (1.39)

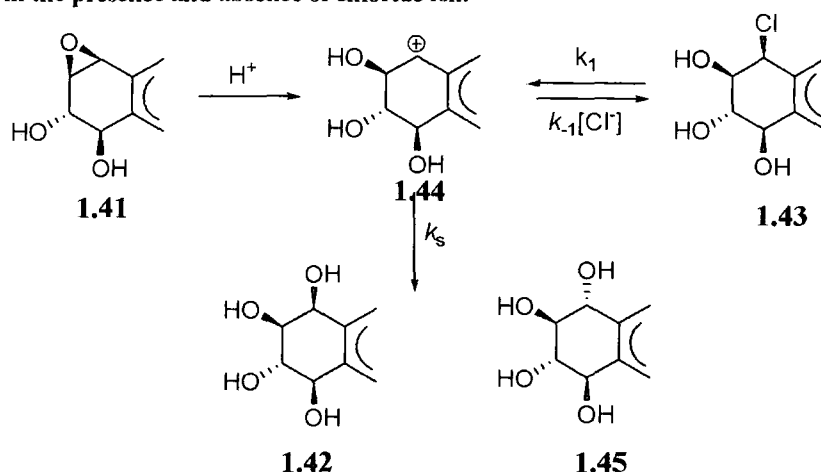


1.38 R₁ = H, R₂ = OH

1.39 R₁ = H, R₂ = OH

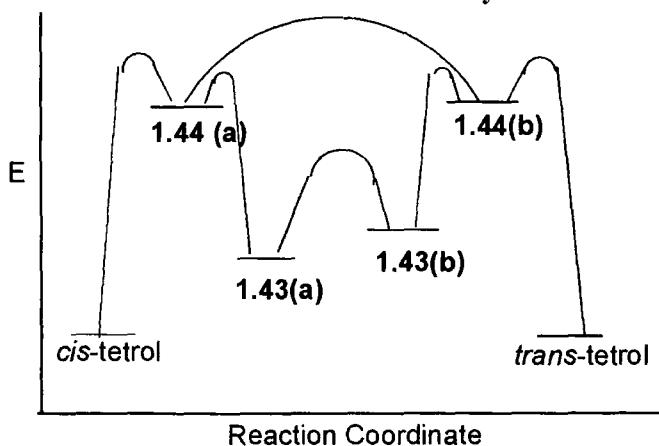
The benzylic carbocation formed as a result of the acid-catalysed ring-opening of (1.38) has a sufficient life-time to react with external nucleophiles such as azide and chloride. In particular the addition of excess chloride ion has an interesting effect. This is illustrated in Scheme 1.4-4 (below), for which diol epoxide (1.38) is represented by structure (1.41). The product analysis of the reaction of (1.37) with water in increasing chloride ion concentration shows an increase in the formation of the *cis*-tetralol (1.42). This has been attributed to formation of a chlorohydrin (1.43)^{33,34}.

Scheme 1.4-4: Solvolysis reaction of diol-epoxide (1.42) and chlorohydrin (1.44) in aqueous dioxane (50 % (v/v)) in the presence and absence of chloride ion.



The rate of reaction of the chlorohydrin in 1:1 dioxane-water was determined as a function of increasing concentration of sodium chloride at constant ionic strength maintained by the addition of sodium perchlorate; these data shows a common ion rate depression for the reaction of (1.43). This is consistent with a mechanism involving formation of a discrete carbocation intermediate (1.44) which is captured by solvent. In this mechanism carbocation formation (k_1) is rate-limiting in the absence of chloride ion; capture of the carbocation by solvent (k_s) is rate-limiting at high chloride ion concentrations. This “common ion effect” demonstrates that there is an intermediate in the reaction that is captured by chloride ion and converted back to a reactant, thus slowing the reaction. The rate of reaction of the chlorohydrin is slower in the presence of chloride ion.

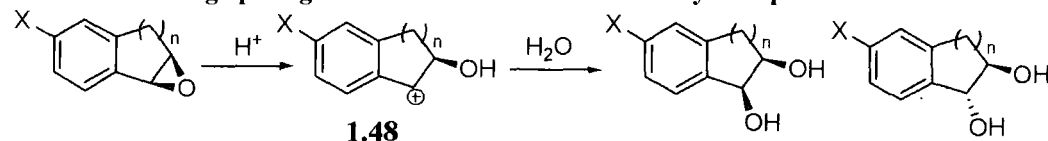
Figure 1.4-2: Reaction coordinate for the reaction of the chlorohydrin conformers with water



Similar to the reaction of the diol-epoxide (1.41) shown in Scheme 1.4-4, there are two possible chlorohydrin conformers, with the difference being the relative angle of the C-Cl bond relative to the aromatic ring (see Fig 1.4-2, 1.43 (a) and (b)). Hydrolysis of the C-Cl bond forms the corresponding carbocation intermediates (1.44) - (a) & (b), with little change in structure. The distribution of these conformers is different than that formed from the reaction of (1.41) with hydronium ion. The energy barrier to interconversion of the carbocation intermediates is higher than the reaction with water (TS⁽¹⁾ versus TS⁽²⁾, Fig 1.4-2). Axial attack of water on the carbocation intermediates (1.44(a)) or (1.44(b)) results in the formation of the *trans* and *cis* tetrol respectively. The explanation for the effect of chloride ion on the diol-epoxide (1.41), is that, in solutions containing sufficient concentrations of chloride ion, a lower energy pathway via a halohydrin exists for the interconversion of the carbocation conformations.³⁵

The acid-catalysed hydrolysis of the indene oxides (1.46) and (1.47) showed similar product ratios (see Scheme 1.4-5 (n = 1)). The methoxy substituent in the para position did not appear to affect the product distribution. The equilibration studies showed the *trans* diol to be the more stable, but the acid-catalyzed hydrolysis of these epoxides each yields the less stable *cis* diol as the major product. The difference in transition state energies for reaction of carbocation (1.48) with water does not reflect the product stabilities. Intra-molecular hydrogen-bonding in the *trans* product is not as effective as in the *cis*-diol and so cannot be the reason for the increased stability of the *trans*-product. The stability is related to there being one less gauche interaction in the *trans* product than in the *cis*. Why does the acid-catalysed ring-opening of the indene diol epoxide show formation of the *cis*-diol predominantly? The explanation given by Whalen *et al*³⁶ is that there is a relatively strong hydrogen-bonding interaction between the attacking water molecule and the hydroxyl group. Computational studies of the carbocation intermediate at the B3LYP/6-31g* level of theory show the five-membered ring to be almost planar. The rationale for this is that the Marcus intrinsic barrier to *cis* solvent attack must be lower than for the *trans* attack.

Scheme 1.4-5: Ring-opening reaction of indene oxide and tetrahydronaphthalene oxide.

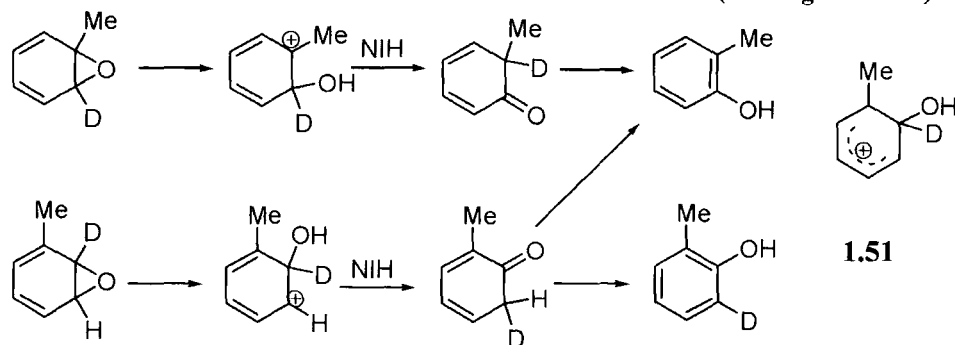


	X	N	Cis	Trans	$k_H (M^{-1}s^{-1})$
1.46	OMe	1	80	20	$(5.92 \pm 0.20) \times 10^4$
1.47	H	1	75	25	6×10^2
1.49	OMe	2	74	16	$(1.68 \pm 0.03) \times 10^5$
1.50	H	2	65	35	$(5.0 \pm 0.1) \times 10^2$

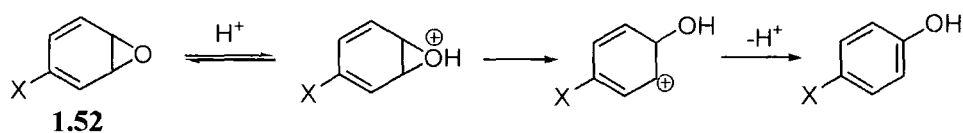
Where $n = 2$, a six-membered ring, the product distributions vary as the substituent changes from $X = H$ to $X = OMe$. The rationale for this is that unsubstituted cyclohexyl cations (1.48) are known to undergo preferential pseudo axial attack by solvent at a rate faster than conformational isomerisation of the ion³⁰, and so (1.48) ($X = H$) yields the *trans*-diol. For more stabilized ions such as those derived from (1.48) ($X = OMe$), conformational isomerisation of the initially formed ion might be expected to compete with solvent attack. Product would then be derived from the more stable conformation, which should undergo stereoselective axial attack by solvent to give preferential *cis* hydration. Therefore, as the ability of the aryl group to stabilize positive charge at the benzyl position increases, *cis* hydration will be favoured.

1.4.1.2 Arene Oxides

The rate-determining step in the aromatisation reaction of arene oxides is C-O bond cleavage. A nucleophilic intramolecular hydride (NIH) shift can occur but this is after the rate determining step and so is not kinetically significant³⁷⁻³⁹. Scheme 1.4-6 below shows the NIH shift in toluene oxide. Both selectively-deuterated oxides were synthesised and the degree of deuterium retention was monitored over time by ¹H NMR. The degree of migration and retention of deuterium was the same in both oxides, suggesting that they have a common intermediate (1.51)⁴⁰.

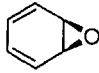
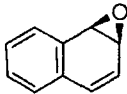
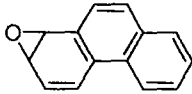
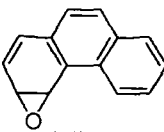
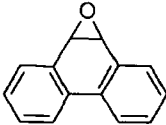
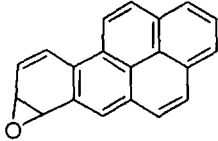
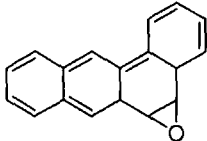
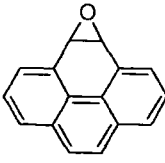
Scheme 1.4-6: Mechanism for the aromatisation of toluene oxide (showing NIH-shift).

A Hammett plot for the reaction of a series of 4-substituted 1,2 monocyclic arene oxides (1.52) gives a ρ^+ of -7.2. The correlation with σ^+ is expected as there is a carbocation intermediate with through-bond conjugation between the carbocation centre and substituent (see Scheme 1.4-7, below)⁴¹. This Hammett plot only correlates the logarithm of four second-order rate constants for the acid catalysed aromatisation; however, the rate constants span an 8140-fold change in reactivity.

Scheme 1.4-7: Aromatisation of 4-substituted-1,2-arene oxides.

The rate of reaction of the arene oxides is dependent on structure. The figure below shows a series of arene oxides and their catalysed and uncatalysed rate constants for solvolysis.

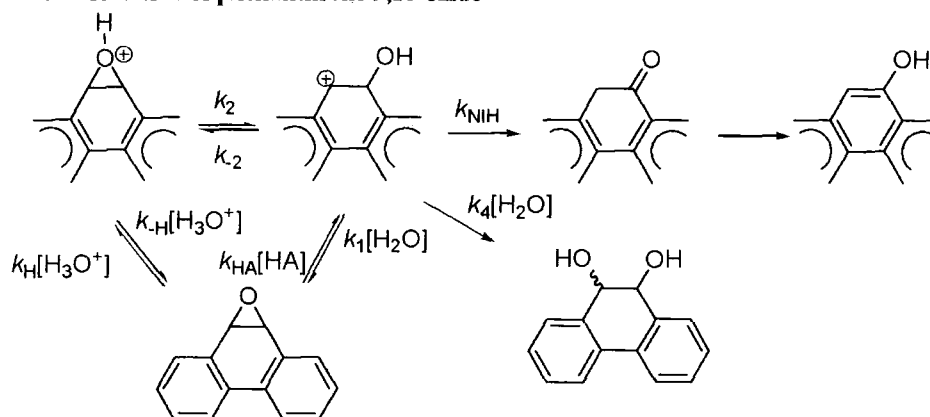
Chart 1.4-1: The acid-catalysed and uncatalysed rates of solvolysis of arene oxides in water.

				
1.53	1.54	1.55	1.56	1.57
k_H 30	140	1000	2700	100(4.6 ^(a))
k_0 1.20×10^{-3}	2.90×10^{-3}	3.10×10^{-2}	5.55×10^{-2}	2.1×10^{-4}
				
	1.58	1.59	1.60	
k_H	g ^(a)	10 ^(a)	5 ^(a)	

(a) Reaction in aqueous dioxane (50 % (v/v))

The phenanthrene oxides are known to undergo non-rate determining NIH shift. In this case the non-K region (1.55 & 1.56) and K-region (1.57) oxides react very differently. The K-region oxides are non-aromatic whereas the non-K region oxides are pro-aromatic. The K-region oxide (1.57, Scheme 1.4-8) gives both diol and phenolic products; however, the proportions of products are dependent on pH. At pH > 8, the major product is the *trans* diol; at pH < 8, the major product is the phenol, the minor diol products being formed in a 2:1 ratio of *trans*:*cis*⁴². Below pH 8 the diol product is formed as a result of carbocation trapping with solvent in an S_N1-like process. From pH 9-11 the diol is formed by nucleophilic attack by water and above pH 11, there is nucleophilic attack by hydroxide ion in an S_N2-like process.

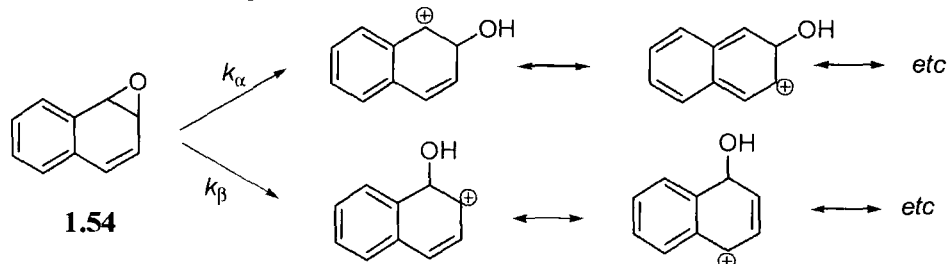
Scheme 1.4-8: Reaction of phenanthrene 9,10-oxide



The non-K region oxides (1.55 & 1.56, Chart 1.4-1) give solely a phenolic product on acid-catalysed ring-opening with the oxide opening preferably at the vinylogous benzylic carbonium ion. Opening of the epoxide ring is rate-determining and is subject to both specific and general acid catalysis. General acid catalysis is only seen above pH 6.

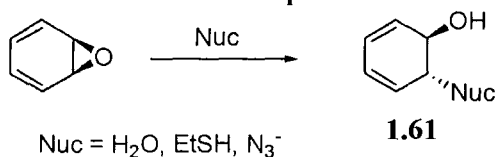
For unsymmetrical arene oxides, such as naphthalene oxide (1.55, below) appreciable reaction may occur by two pathways and rate constants must be partitioned accordingly (see Scheme 1.4-9, below). The ratio of the first order rate constants for carbocation formation, k_{α}/k_{β} , is inversely proportional to the aromatic stabilisation energy sacrificed, e.g., $k_{\alpha}/k_{\beta} = 0.30$ for 1,2-phenanthrene oxide, 0.10 for naphthalene oxide (1.54), and 0.03 for anthracene oxide. α -Benzoannellation reduces the rate constant ratios as a result of the sacrifice of aromatic resonance stabilisation in the benzene ring arising from resonance interaction between the remaining double bond and the carbocation centre (see Scheme 1.4-9, below). This analysis can equally be applied to the decreased reactivity of phenanthrene-9,10-oxide (K-region oxide (1.57)) when compared to phenanthrene-1,2-oxide (non-K region oxide (1.56)).

Scheme 1.4-9: Reaction of Naphthalene Oxide



The arene oxides of benzene, naphthalene and phenanthrene have been shown to react with a range of nucleophiles (See Scheme 1.4-9, below). As Scheme 1.4-10 shows, the nucleophiles react to form the *trans* product. Interestingly, this is not the case for the reaction with methyl lithium where only the *cis*-product is formed. In the case of azide, reaction occurs by 1,2 and 1,6 addition, shown by deuterium labelling.⁴³ In this study, no reaction with amines was seen.

Scheme 1.4-10: Reaction of Arene Oxides with Nucleophiles



The product stereochemistry suggests that the ring-opening occurs by an S_N2 type process or by formation of tight ions pairs. Spontaneous rearrangement of the arene oxide to form phenol is known to occur via a carbocation intermediate and it is this step which is rate determining in the acid-catalysed reaction. The carbocation formed can undergo H migration to form a more stable carbocation intermediate.

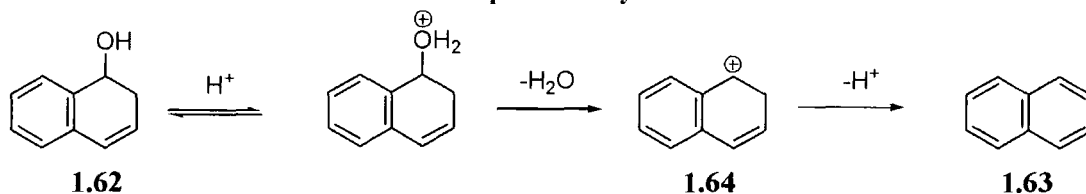
A Brønsted plot of the second-order rate constants for the reaction of oxygen nucleophiles with phenanthrene 9,10-oxide against nucleophile pK_a gave a β_{nuc} of 0.2. The corresponding β_{nuc} value for the reaction with primary and secondary amines is 0.4.⁴² The reactivity of the K-region arene oxide (1.57) is similar to ethylene oxide, as the nucleophilic substitution by both amines and hydroxide competes with the solvolysis reaction. For the non-K region oxides the ring-opening reaction and subsequent NIH shift is faster than reaction with external nucleophiles.⁴² The K-region arene oxides are

clearly more susceptible to reaction with biological external nucleophiles (such as guanine) than the non-K region oxides. The thiol nucleophiles react readily with all the oxides studied, which is relevant to their biological activity as most oxidative metabolites are isolated as glutathione derivatives.

1.4.2 Reactions of alcohols and arene hydrates

Arene hydrates are the formal water adducts of aromatic molecules and can be prepared by chemical⁴³⁻⁴⁵ or enzymatic^{46, 47} synthesis. They were first identified by Bamberger⁴⁸ from the acidification of the urine of naphthalene induced rats. They were first isolated by Boyd *et al*⁴⁷ from the microbial metabolism of the dihydroaromatic substrate (see section 1.5.1).

Scheme 1.4-11: Aromatisation reaction of Naphthalene Hydrate.



The rates of the acid-catalysed dehydration of the hydrates of benzene, naphthalene, anthracene, and phenanthrene have been reported. Naphthalene hydrate (1.62) reacts in dilute perchloric acid to form naphthalene (1.63) with rate-determining carbocation (1.64) formation (see Scheme 1.4-11)⁴⁹. The dehydration mechanism of benzene hydrate (1.65) (2,4-cyclohexadienol) has been inferred from the naphthalene hydrate studies⁵⁰. The mechanism of the acid-catalysed dehydration differs from that of simple alcohols for which deprotonation of the carbocation is rate-determining, reflecting the lower stability of an alkene than an arene product.

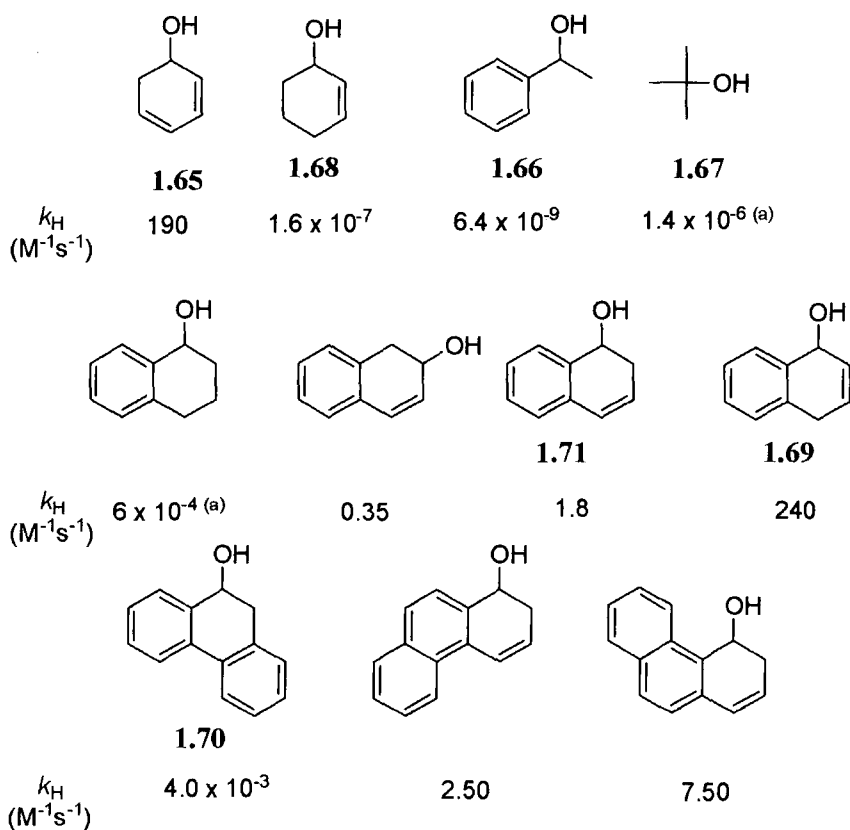
Chart 1.4-2 (below) shows the second-order rate constants for dehydration of a series of arene hydrates and alcohols. In the case of α -phenylethyl alcohol (1.66) and tertbutanol (1.67) the rate constant reflects the deprotonation of the carbocation which is the rate-limiting step for the reaction of normal alcohols. Consistent with this, the rate constant for dehydration of 1-cyclohexenol (1.68) is $1.6 \times 10^{-7} \text{ M}^{-1} \text{ s}^{-1}$, whereas the rate constant

for carbocation formation is $\sim 10^{-3} \text{ M}^{-1}\text{s}^{-1}$, thus the rate-determining deprotonation is 10^4 -fold slower than carbocation formation. Similarly, the rate constant for carbocation formation in α -phenylethyl alcohol (1.66) is $3 \times 10^{-6} \text{ M}^{-1}\text{s}^{-1}$ which is almost 500 times faster than deprotonation.

The 10^9 -fold greater reactivity of α -naphthalene hydrate (1.69) than of α -phenylethanol (1.66) towards carbocation formation derives from the cyclic nature of the naphthyl cation (1.64) and from the presence of the allylic group *ortho* to the carbocation centre. The dehydration reaction of phenanthrene hydrate (1.70) forms an aromatic product, however, the kinetics for this reaction are closer to that of a normal alcohol e.g. the rate determining step is deprotonation of the carbocation intermediate (see below).

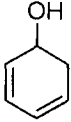
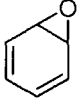
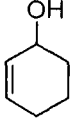
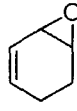
Second order rate constants for the dehydration of the hydrates are strongly influenced by benzoannulation: benzene hydrate (1.65) is 100 times more reactive than 1-hydroxy-1,2-dihydronaphthalene(1.71), and 48,000 times more reactive than 9,10-phenanthrene hydrate (1.69).⁵¹ This reactivity order reflects the effect of benzoannulation on the relative stabilities of the carbocation intermediates and hydrate reactants. Benzoannulation affects the stability not only of the carbocation step but also of the reactants and is unfavourable where it interrupts a strong resonance interaction. Ease of through conjugation in the cyclohexadienyl segment of the molecule is greatest in benzene hydrate and diminishes as the aromatic character of the double bond increases and the resonance stabilization is sacrificed⁵⁰. The net effect of benzoannulation is to decrease the stability of the carbocation relative to the parent hydrate thus decreasing the overall rate of dehydration. This effect is not seen in allylic cations.

Chart 1.4-2: Second-order rate constants for the dehydration of a series of alcohols and arene hydrates⁵⁰



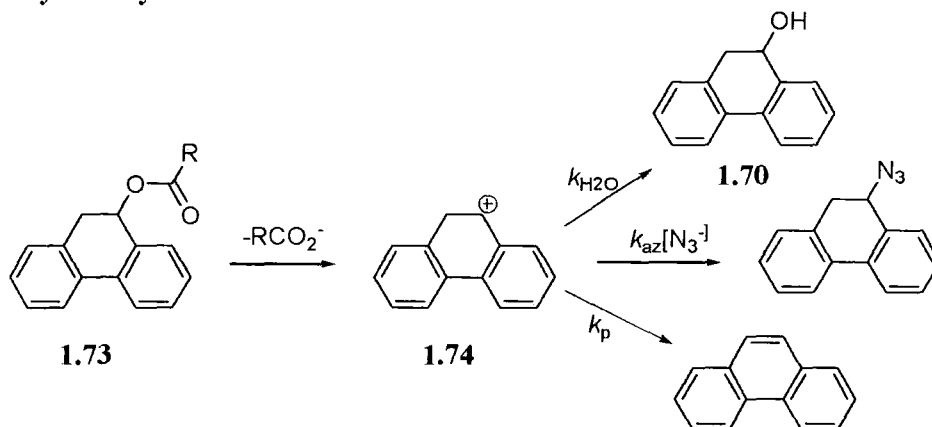
Comparison of benzene hydrate (1.65) with benzene oxide (1.53) shows (see Chart 1.4-3), surprisingly, that the hydrate is more reactive towards acid despite the fact that acid-catalyzed carbon-oxygen bond breaking in simple epoxides can occur up to 10^6 - 10^7 times more readily than in structurally related alcohols. For example the allylic epoxide (1.72) has a rate of dehydration 10-fold faster than for the analogous alcohol (1.73). For a series of arene oxides and hydrates, oxide/hydrate aromatization rate ratios are inversely related to the resonance energy of the aromatized ring. This behaviour is tentatively ascribed to homoaromatic stabilization of the arene oxides.⁵⁰

Chart 1.4-3: Rate constants for carbocation formation of a series of cyclic alcohols and epoxides.

			
1.65	1.54	1.73	1.72
k_H ($M^{-1}s^{-1}$)	190	32	$\sim 10^3$
			1.1×10^4

Aqueous solvolysis of acyl derivatives of hydrates of anthracene, phenanthrene and benzofuran yield carbocations which can undergo competitive deprotonation to form aromatic molecules and nucleophilic reaction with water to give the hydrates. Trapping experiments with azide allows the determination of the pK_R of the carbocation intermediate (see Scheme 1.4-12, below).

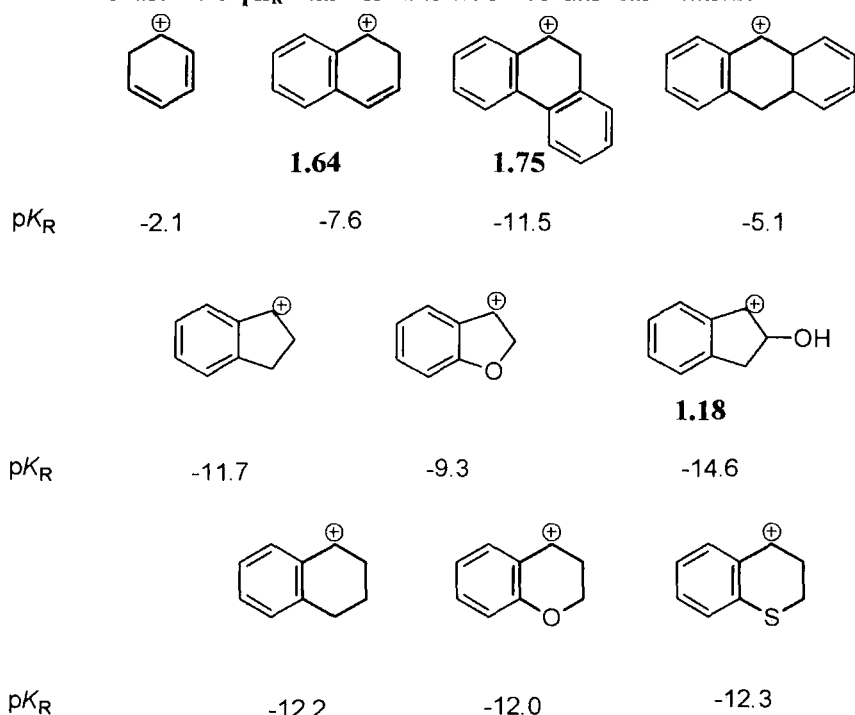
Scheme 1.4-12: Azide-trapping of the phenanthryl carbocation generated from the solvolysis of 9-phenanthryl carboxylate esters



For 9,10-phenanthrene hydrate (1.70), product studies from the solvolysis of 9-phenanthryl carboxylate esters (1.73, Scheme 1.4-12, above) show that an appreciable fraction (20%) of the 9-phenanthrenonium ion (1.74) intermediate reforms the hydrate in competition with deprotonation, indicating that deprotonation is partially rate-determining in the dehydration of (1.70) consistent with the smaller gain in resonance energy accompanying the formation of phenanthrene rather than benzene or naphthalene as products⁵⁰. Solvolysis of (1.73) in the presence of azide gives $k_p/k_{az} = 5.5$. Assuming $k_{az} 5 \times 10^9 M^{-1}s^{-1}$ leads to $k_p = 2.75 \times 10^{10} s^{-1}$, $k_{H_2O} = 1.17 \times 10^9 s^{-1}$ and $k_H = 4.1 \times 10^{-3} M^{-1}s^{-1}$ thus $pK_R = -11.46$ ⁵².

Similar methodology has allowed the pK_R of a series of protonated aromatics to be determined. Chart 1.4-4 below shows the literature values. The affect of the benzoannulation of benzene hydrate has the overall effect of decreasing the stability of the carbocation intermediate relative to the hydrate. In the case of phenanthrene (1.75), the pK_R is quite negative (-11.5) and is more negative than that for the naphthyl cation (1.64) (-7.6).

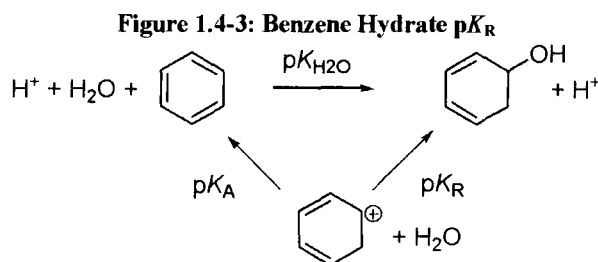
Chart 1.4-4: pK_R values for a series of aromatic carbocations



The azide-trapping experiment for naphthalene hydrate was carried out by Pirinccioglu *et al.* Only 0.03 % of naphthalene hydrate was formed ($k_{N_3}/k_{HOH} = 2.1 \times 10^4$) and the pK_R was determined to be -7.6 in 25 % aqueous acetonitrile⁵³. Understandably, the lifetime of the carbocation generated by the acid-catalysed R-OH bond cleavage of benzene hydrate is short-lived due to the rapid deprotonation step to give benzene and so cannot be trapped by external nucleophiles.

The pK_R for protonated benzene can be derived within close limits by consideration of the thermodynamic cycle shown in Figure 1.4-3. It can be assumed that the rate constant k_p for loss of a proton from the benzenonium cation lies between the corresponding

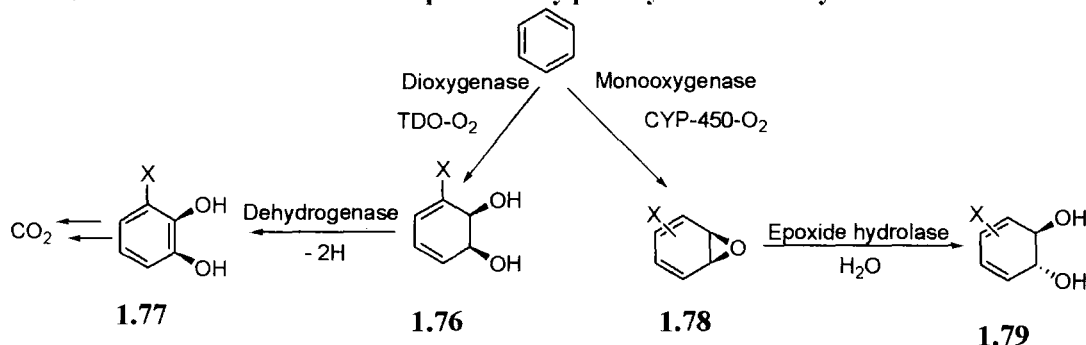
values for the naphthalenonium or phenanthrenonium ions (1.6 or $2.5 \times 10^{10} \text{ s}^{-1}$) and a limit set by the rotational relaxation of water (10^{11} s^{-1}). The estimated value for k_p may be combined with the second order rate constant for protonation of benzene to yield a pK_a value for the cyclohexadienyl cation of -24.3 . This pK_a value may be combined with a value of $pK_{H_2O} = 22.2^{54}$ for the formal hydration of benzene to yield a pK_R value of -2.1 .



1.5 Biological Relevance: Oxidative Metabolites.

Environmental pollutants such as monocyclic and polycyclic aromatic hydrocarbons are metabolised by both eukaryotes and prokaryotes. The bacterial metabolism utilises a Rieske-type non-haeme Cytochrome P450 monooxygenase enzyme giving stereospecifically the *cis*-dihydrodiol (1.76), which is normally further reacted to form catechols (1.77) and other metabolites.

Scheme 1.5-1: Metabolism of aromatic pollutants by prokaryotes and eukaryotes.



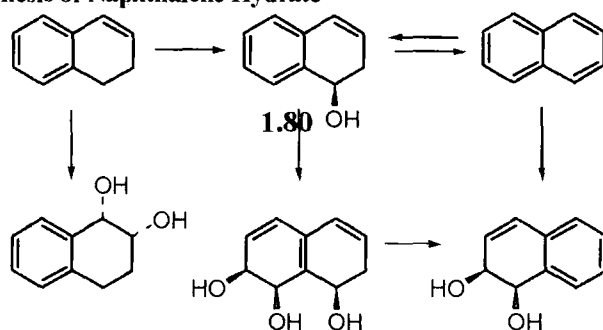
The cytochrome P450 (CYP_{450}) enzymes are also utilised in the biotransformation of hormones in animals, secondary metabolites in plants and as predator defence agents in sponges. Mammalian $\text{CYP}_{450\text{S}}$ are found in the liver microsomes and are studied in the context of drug activation. Aromatic molecules after ingestion are metabolized by the CYP_{450} *mono* and *dioxygenase* enzymes in mammalian systems (see Scheme 1.5-1) to

give a range of oxidative metabolites, including the arene oxides (1.78)³⁷, *trans* dihydrodiols (1.79)⁵⁵ and the arene hydrates (1.80, Scheme 1.5-2)⁴⁷. Further oxidation of these metabolites leads to the diol epoxides which are important metabolites with regard to carcinogenicity (see section 1.5.5, below)⁵⁶.

1.5.1 Arene hydrates

The first arene hydrate from microbial metabolism was isolated by Boyd *et al*⁴⁷. Both 1,2-dihydronaphthalene and 1,2-dihydroanthracene were hydroxylated at the benzylic or allylic position by rat liver microsomes and purified cytochrome P450 enzymes (see Scheme 1.5-2). The dehydrogenation products naphthalene and anthracene and the *trans*-1,2-dihydroxy-1,2,3,4-tetrahydronaphthalene and its anthracene analogue were also isolated. The *trans*-products are later metabolites of the classical epoxide pathway. Naphthalene and anthracene were formed enzymatically by direct dehydrogenation of the dihydro compounds rather than by dehydration of the arene hydrate metabolites. Regioselectivity (hydroxylation at benzylic or allylic positions) and stereoselectivity (hydroxylation at pro-R or pro-S hydrogen atoms) during the metabolism of dihydroarenes to yield arene hydrates were found to be dependent upon the nature of the inducing agents used during pretreatment of the rats and thus the level of particular CYP₄₅₀ enzymes.

Scheme 1.5-2: Biosynthesis of Naphthalene Hydrate



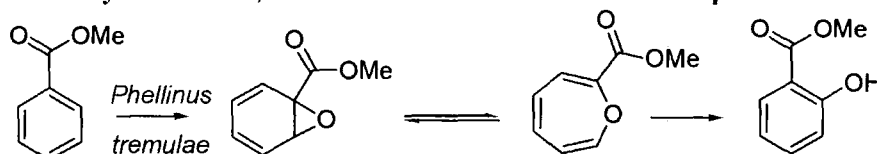
A general mechanism involving the intermediacy of benzylic and resonance-stabilized allylic carbon radicals can account for the formation of both enzyme-catalyzed hydroxylation (arene hydrate) and dehydrogenation (arene) metabolites of dihydroarene substrates⁴⁷.

1.5.2 Arene Oxides

Since it has been demonstrated that arene oxides can be formed, there has been significant interest in their chemistry and biology⁵⁷. Arene oxides can react to form phenols and dihydrodiols by non-enzymatic rearrangement and cysteine conjugates by enzyme catalysis. NIH shifts to give the most stable carbocation intermediate are also known to occur in the reactions of arene oxides (see Section 1.4.1-2)⁵⁷. The most intriguing of the biochemical studies are those which have implicated arene oxides as causative agents in mutagenesis and carcinogenesis (See section 1.5.5).

The arene oxides are derived from the incorporation of one oxygen atom from dioxygen into the aromatic ring. Generally, the arene oxides have been too unstable to isolate and their presence has been inferred from the formation of the corresponding *ortho*-, *meta*- and *para*-phenols⁵⁸. The isolation of the relatively stable 1,2-oxide metabolite of methyl benzoate (1.81) from the fungus *Phellinus tremulae* provides evidence of 1,2-epoxidation⁵⁹ (see Scheme 1.5-3).

Scheme 1.5-3: Biosynthesis of a 1,2-substituted arene via an arene oxide/oxepine⁵⁹



1.81

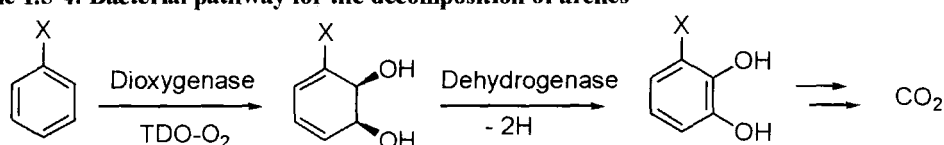
1.5.3 Biocatalysts

Naphthalene dioxygenase (NDO) has been developed as a biocatalyst by Gibson and co-workers.⁶⁰ Boyd and co-workers have worked on the toluene dioxygenase (TDO) which has been shown to have broad substrate specificity⁶¹⁻⁶³. Biphenyl dioxygenase and methyl benzoate dioxygenase have also been developed as biocatalysts. In fact, there are over 100 dioxygenase biocatalysts in the literature, showing the diversity of these microbial CYP₄₅₀ enzymes.

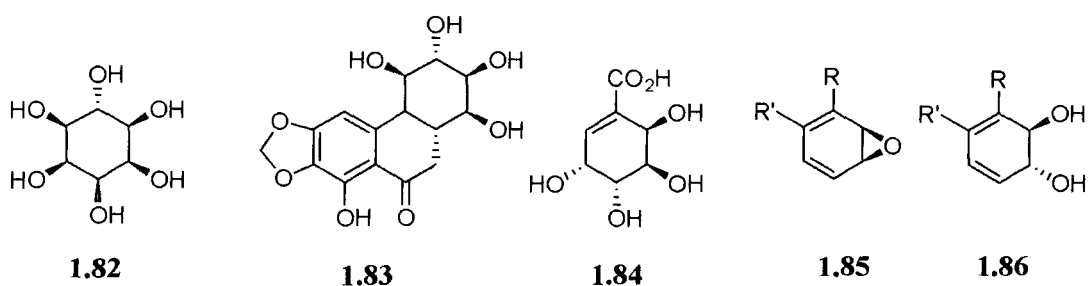
All the enzymes mentioned above catalyse the formation of *cis*-dihydrodiols from an unreactive arene substrate. Both oxygens in the *cis*-dihydrodiol are derived from

atmospheric dioxygen, whereas the biosynthesis in mammals of *trans*-dihydrodiol incorporates one atom of oxygen from dioxygen and one from water. Wild type bacterial strains capable of using arenes as a carbon source generally contain *cis*-diol dehydrogenase enzymes which catalyse the dehydrogenation of the initial *cis*-diol metabolites to yield the corresponding catechol and which in turn undergo further dioxygenase-catalysed oxidation to yield ring-opened products (see Scheme 1.5-4). The biotechnological development of strains, such as *Pseudomonas putida* (*P. putida* (UV4)), lacking the *cis*-diol dehydrogenase allows the *cis*-dihydrodiol in optically active form to accumulate. This can be isolated, thus allowing for the development of a single step biosynthetic method for synthesizing *cis*-dihydrodiols⁶⁴.

Scheme 1.5-4: Bacterial pathway for the decomposition of arenes⁶⁴



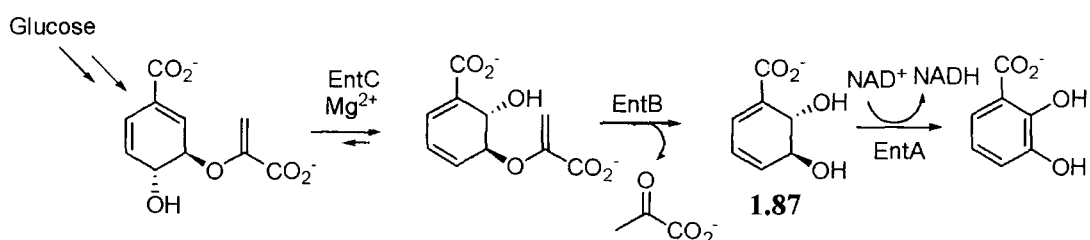
The *cis*-dihydrodiols have been utilised as chiral synthons in the synthesis of many industrially useful chemicals and natural products. A few examples are shown below, including *epi*-inositol⁶⁵ (1.82), pancratistatin⁶⁶ (1.83), 6- β -hydroxyshikimic acid (1.84) and the two oxidative metabolites associated with the mammalian system, the arene oxide (1.85) and the *trans*-dihydrodiol (1.86)⁶⁴.



Biotechnological routes to *trans*-dihydrodiol (1.87) have been developed by Müller and co-workers utilising the Shikimate pathway and metabolically deregulated, recombinant *E. coli*.⁶⁷ The *E. coli* route, using a pathway from an enterobactin with chorismate as an intermediate, is shown below, using an *E. coli* EntA- mutant, allowing the *trans* diol to accumulate. Optimisation of the conditions yielded 92 g of 2,3-*trans*-dihydrobenzoic

acid from 690 g of glucose monohydrate in a 20 L cultivation experiment with a cell density of 12 g/L. This correlated to a 12 % yield. The product was purified by ion-exchange chromatography⁶⁷.

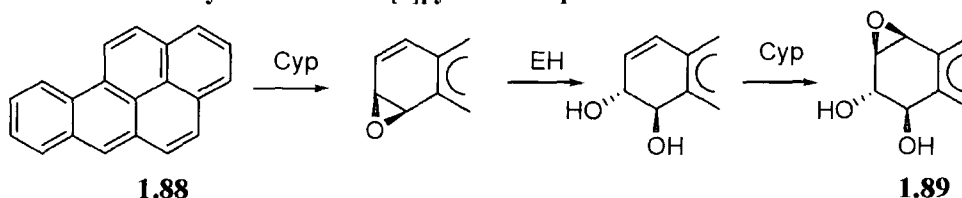
Scheme 1.5-5: Synthesis of a *trans*-dihydrodiol by *E. Coli* entA- strain AN193 with genes entB/entC⁶⁷



1.5.4 Polycyclic Aromatic Hydrocarbons

Polycyclic aromatic hydrocarbons (PAHs) (*e.g.* 1.88, Scheme 1.5-6) are in a group of over 100 different aromatic hydrocarbons that are formed during the incomplete combustion of coal, oil, gas, or other organic substances like tobacco or charbroiled meat. As environmental pollutants they are found in sea birds⁶⁸, fish⁶⁹ and soil. The PAHs and heterocyclic aromatic hydrocarbons (HACs), which contain one or more nitrogen, sulfur or oxygen, are a major class of chemical carcinogens present in the environment.

Scheme 1.5-6: Biosynthesis of benzo[*a*]pyrene diol epoxide

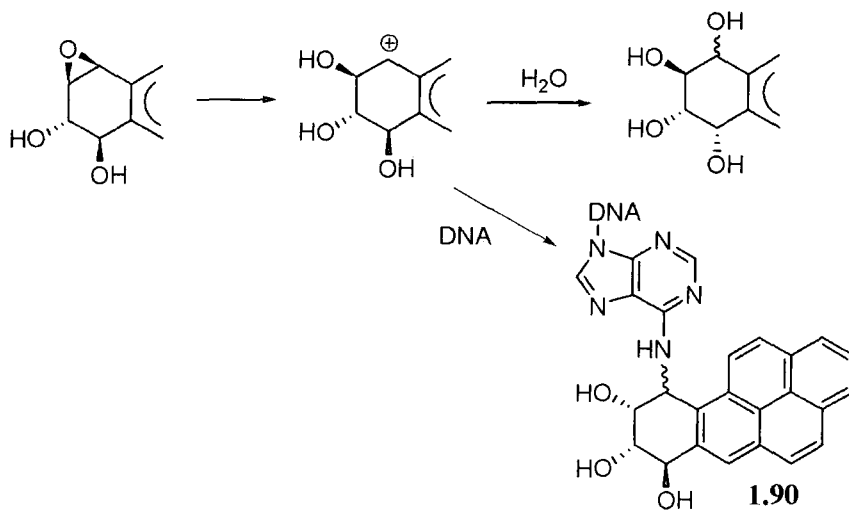


The PAHs are oxidized in the mammalian liver and lungs. Firstly molecular oxygen is incorporated into the ring using a cytochrome p450 enzyme. The epoxide is then ring-opened using an epoxide hydrolase. The diol is further oxidized forming the diol-epoxide (1.89)⁷⁰.

The PAH diol epoxides have never been isolated from the metabolic activation system due to their reactivity. They may be rapidly hydrolyzed in aqueous media to tetrols or

trapped spontaneously by nucleophiles in the system to give adducts. The deoxyribonucleic acid base guanine is nucleophilic and this can react with the carbocation intermediate formed from the ring-opening of the epoxide at the benzylic position giving the guanine adduct (1.90) which is the cause of the known mutagenicity of the diol epoxides.⁷¹⁻⁷⁴

Scheme 1.5-7: Reactions of the Diol-epoxides.



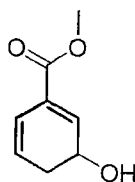
This thesis will discuss the aromatisation reaction of the monocyclic arene hydrates. The proposed mechanism for this reaction involves a carbocation intermediate similar to those discussed in this chapter. The carbocation associated with the monocyclic arene hydrate is considerably more unstable than the analogous polycyclic aromatic carbocation described in section (1.5.5) and section 1.4.2 and the benzylic carbocations described in section 1.4.1. The results for each hydrate synthesised shall be discussed in terms of their route to synthesis, kinetic studies and a computational study of the hydrate and its putative carbocation intermediate (see sections 2.1- 2.6 and 3.1). A Hammett plot of the logarithm of the second-order rate constant against a number of Hammett-type parameters shall also be presented (see section 2.8 and 3.3). A brief computational study of the *cis*-dihydrodiols synthesised by Boyd *et al* will also be presented in section 2.7 and discussed in section 3.4.

The results from dehydration reaction of indene diol will be presented and compared with the second-order rate constants for carbocation formation of similar compounds shown in Chart 1.4-2. Using the azide-trapping technique (see section 1.3.2) the pK_R of the carbocation formed in the dehydration (or isomerisation) reaction of indene diol will also be presented. This value will then be compared with the pK_R values for similar compounds shown in Chart 1.4-4 (see section 3.5).

Results

2.1 Methyl benzoate Hydrate

This section describes the synthesis and kinetic studies of the aromatisation of methyl benzoate hydrate.

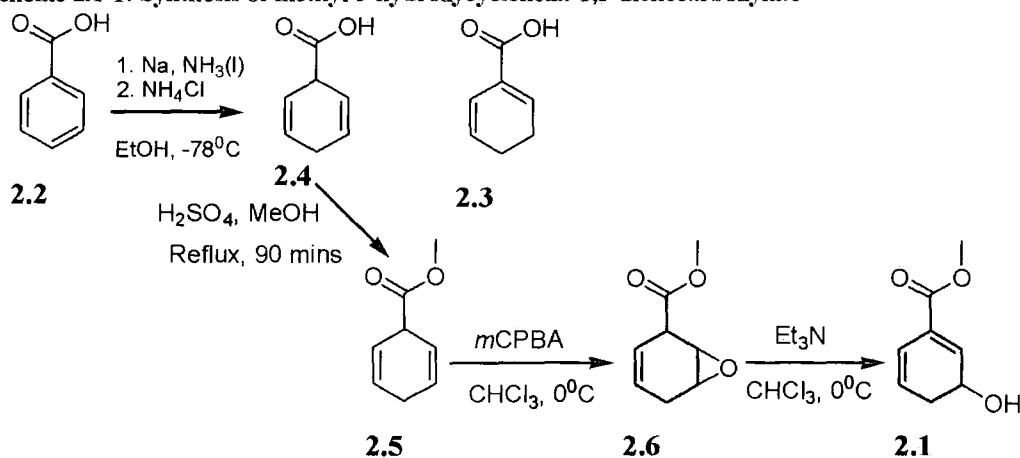


2.1

2.1.1 Synthesis of methyl benzoate hydrate.

Scheme 2.1-1 (below) outlines the synthetic route, adapted from the literature, to the methyl ester hydrate.⁷⁵ A Birch reduction was utilized to reduce the aromatic ring and this was problematic (Scheme 2.1-1). Initial attempts at reducing benzoic acid (2.2) gave the isomerised product (2.3). To prevent this, the solvent conditions and quenching procedures were changed from the generalized procedure outlined in section 4.1.1. Benzoic acid (2.2) was added in dry ethanol and no other solvent was used. Ammonia was condensed into the reaction vessel and the sodium was added to this. On disappearance of the blue colour, the reaction was quickly quenched with ammonium chloride. The ammonia was allowed to evaporate and the reduced benzoic acid was extracted after the acidification of the aqueous layer to pH 4.

Scheme 2.1-1: Synthesis of methyl 3-hydroxycyclohexa-1,5-dienecarboxylate



The reason for the isomerisation is unclear; however the use of only ethanol as a solvent and protonating agent did appear to prevent this. The rapid quenching of the reaction also appeared to help, possibly preventing a base-catalysed isomerisation.

The esterification of the dienecarboxylate (2.4) proceeded with almost quantitative yields. The epoxidation of ester (2.5) proceeded well; it was at this point the products were purified to remove any residual arene and *m*CPBA. Two diastereomers of epoxide (2.5) were formed and these could be separated by column chromatography. The subsequent ring-opening step of epoxide (2.6), using triethylamine as a base, proceeded with good yields. In this case the hydrate was reasonably stable and could be purified by column chromatography. Some decomposition of hydrate (2.1) was noticed over two months.

2.1.2 Kinetic analysis of the aromatisation of methyl benzoate hydrate in dilute perchloric acid

The aromatisation reaction of methyl 3-hydroxycyclohexa-1,5-dienecarboxylate (2.1) was followed in a range of dilute perchloric acid solutions (2 – 100 mM) (see Scheme 2.1-2 below). In an initial study, the reaction was followed by ^1H NMR spectroscopy in 2.5 mM DClO_4 . This was mainly to ensure that quantitative conversion of hydrate (2.1) to arene (2.2) was occurring.

Scheme 2.1-2: Aromatisation reaction of methylbenzoate hydrate (2.1)

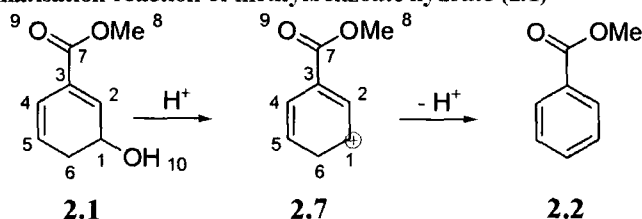


Figure 2.1-1: ^1H NMR time profile for the aromatisation reaction of methyl-3-hydroxycyclohexa-1,5-dienecarboxylate in 2.5 mM DClO_4 , $I = 0.5 \text{ M}$ (NaClO_4).

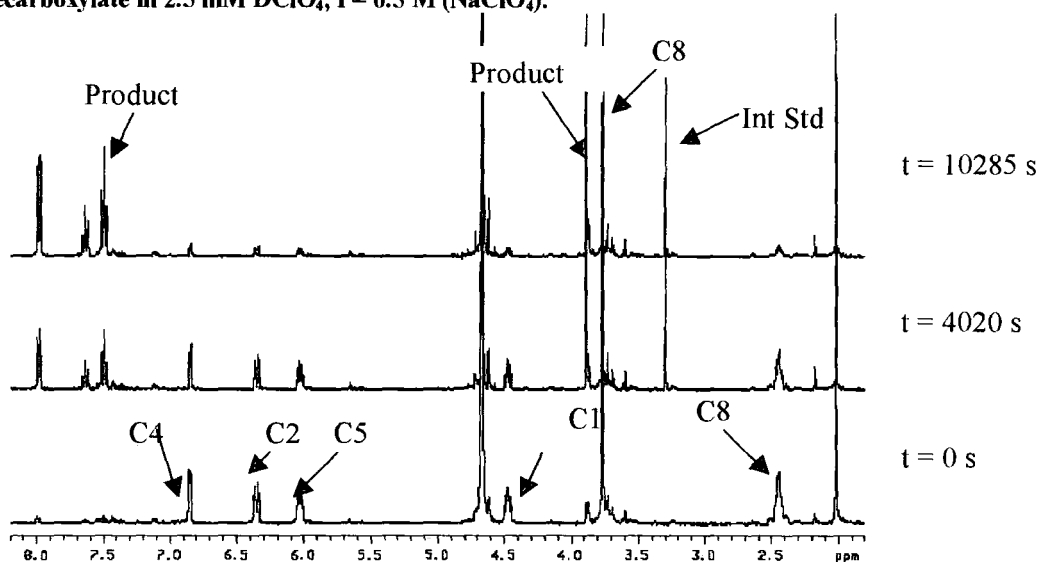


Figure 2.1-1, above, shows the ^1H NMR of the aromatisation reaction of methyl benzoate hydrate (2.1) forming methyl benzoate overtime. The spectra show the disappearance of the peaks due to the hydrate protons at 2.5, 4.4, 6.0, 6.4 and 6.9 ppm concomitant with an increase in the area of the peaks due to the aryl hydrogens of product arene between 7.5 and 8 ppm. An internal standard (methanol, 3.1 ppm) was used as a peak with constant area throughout the experiment.

The fraction of remaining substrate ($f(s)$) was calculated using equation 2.1. The term $A_{4.4}$ refers to the area of the multiplet at 4.4 ppm due to the C-1 hydrogen of the hydrate. The term A_8 refers to the area of the multiplet at 8 ppm due to the C2 and C6 hydrogens of the product arene. A correction was made to $f(s)$ to account for the presence of arene at time zero ($A_{8(t)} - A_{8(0)}$).

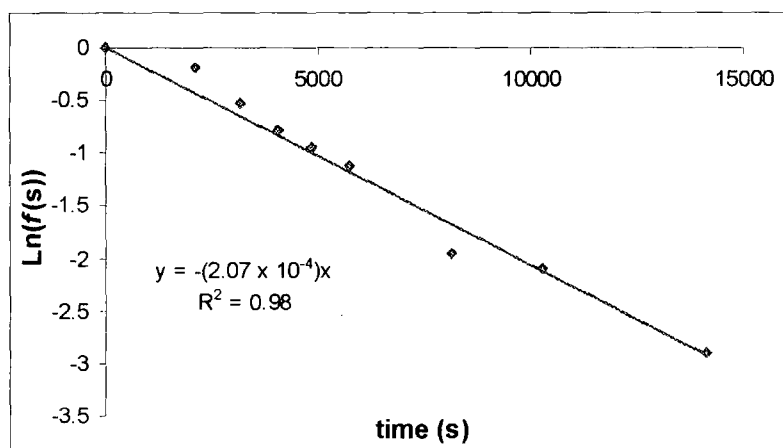
$$f(s) = \frac{A_{4.4(t)}}{A_{4.4(t)} + \left((A_{8(t)} - A_{8(0)}) / 2 \right)} \quad \text{Equation 2-1}$$

Experimental data for the change in $f(s)$ versus time are listed in Table 2.1-1. The first order rate constant, k_{obs} (s^{-1}), for aromatisation could be obtained as the slope of a $\ln(f(s))$ against time (Fig 2.1-2), and is given in Table 2.1-1.

Table 2.1-1: Aromatisation reaction of methyl benzoate hydrate in DClO_4 (2.5 mM) at $I = 0.5 \text{ M}$ (NaClO_4): Fraction of substrate over time

Time (s)	$f(s)$	$\ln(f(s))$	k_{obs} (s^{-1})
0	1.00	0.00	
2104	0.82	-0.20	
3163	0.59	-0.53	
4020	0.45	-0.79	2.07×10^{-4}
4854	0.39	-0.95	
5709	0.33	-1.12	
8138	0.14	-1.95	
10285	0.12	-2.11	
14120	0.05	-2.91	

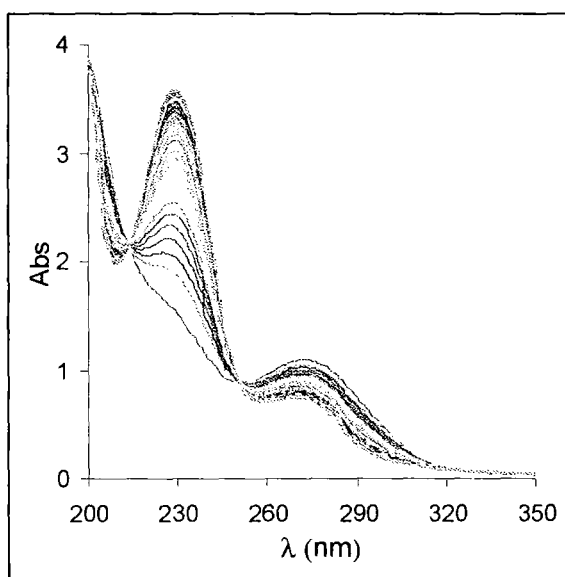
Figure 2.1-2: Aromatisation of methylbenzoate hydrate in 2.5 mM DClO_4 at $I = 0.5 \text{ M}$ (NaClO_4): Plot of $\ln f(s)$ against time



The reaction was primarily followed by UV-Vis spectroscopy, due to the greater accuracy of this technique than ^1H NMR spectroscopy. The solution of hydrate substrate was prepared in acetonitrile to a concentration of 50 mM. Typically a 1/100

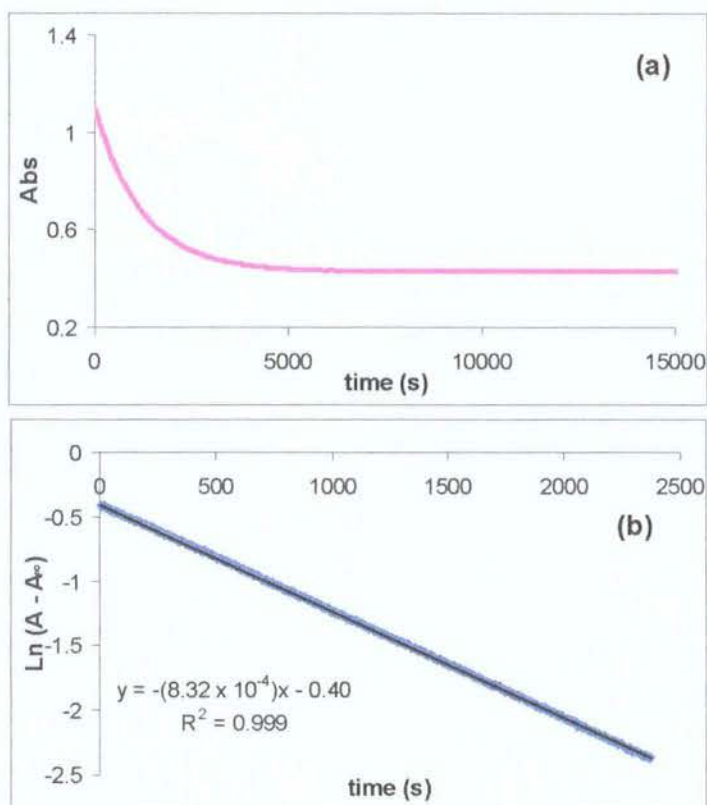
dilution of this solution into the relevant perchloric acid solution was made to initiate the reaction. A typical repetitive scan for the aromatisation reaction of methyl benzoate hydrate in dilute perchloric acid is shown below (Fig 2.1-3). As the reaction proceeds a decrease in absorbance at $\lambda_{\text{max}} = 230$ nm, due to the π - π^* transition of the conjugated diene of the hydrate is seen. An increase in absorbance due to the formation of aromatic product is seen at $\lambda = 270$ nm. Kinetic studies were performed at both of these wavelengths.

Figure 2.1-3: Representative repetitive scan of the aromatisation reaction of methyl benzoate hydrate in 6.38 mM HClO₄, I = 0.5 M (NaClO₄)



Shown below is a typical trace of the absorbance versus time data at 230 nm (Figure 2.1-4(a)). The rate constant was determined by semi-logarithmic analysis. An example is shown below (Fig 2.1-4(b)). The first order rate constant for the aromatisation, k_{obs} (s^{-1}), could be obtained as the slope of a semilogarithmic plot of $\Delta A = A_t - A_{\infty}$ against time, and was determined as $8.32 \times 10^{-4} \text{ s}^{-1}$.

Figure 2.1-4: Aromatisation reaction of methyl benzoate hydrate in 10 mM HClO₄ at I = 0.5 M (NaClO₄) and 25 °C (a) Plot of absorbance at 230 nm versus time. (b) Semi-logarithmic plot of ΔA versus time.



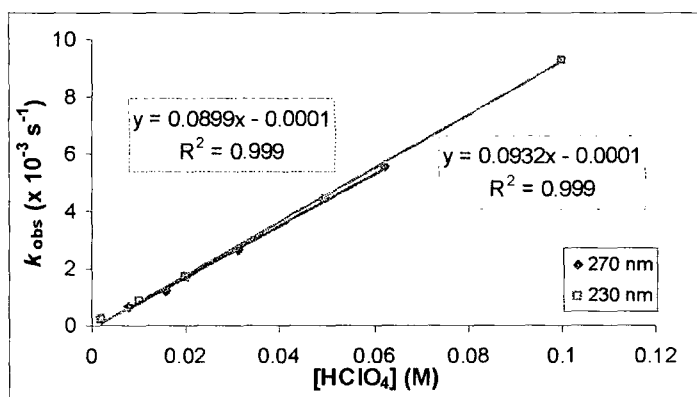
The table below summarizes the kinetic data of the aromatisation reaction of methyl benzoate hydrate in dilute perchloric acid.

Table 2.1-2: Summary of the kinetic data of the aromatisation reactions of methyl benzoate hydrate in dilute perchloric acid solution followed at 230 and 270 nm^(a).

[HClO ₄] ^(b) (mM)	$\lambda = 230$ nm		$\lambda = 270$ nm		R ²
	k_{obs} ^(c) Mean (n=2)	R ²	[HClO ₄] ^(b) (mM)	k_{obs} ^(c) Mean (n=2)	
2.00	$1.90 (\pm 0.05) \times 10^{-4}$	0.99	7.81	$6.43 (\pm 0.01) \times 10^{-4}$	0.99
10.0	$8.23 (\pm 0.09) \times 10^{-4}$	0.99	15.6	$1.28 (\pm 0.01) \times 10^{-3}$	0.99
20.0	$1.70 (\pm 0.02) \times 10^{-3}$	0.99	31.3	$2.70 (\pm 0.02) \times 10^{-3}$	0.99
50.0	$4.40 (\pm 0.03) \times 10^{-3}$	0.99	62.5	$5.87 (\pm 0.01) \times 10^{-3}$	0.99
100	$9.29 (\pm 0.04) \times 10^{-3}$	0.99			

(a) Measurements were made at a substrate concentration of 0.5 mM and 1 % acetonitrile (b) [H⁺] determined by titration against sodium hydroxide standard. (c) k_{obs} determined from the slope of the plot of Ln(ΔA) versus time (e.g. Fig 2.1-4(b)).

The second-order rate constants for acid catalysed aromatisation could be obtained as the slope of a plot of the k_{obs} values against acid concentration (Figure 2.1-5)

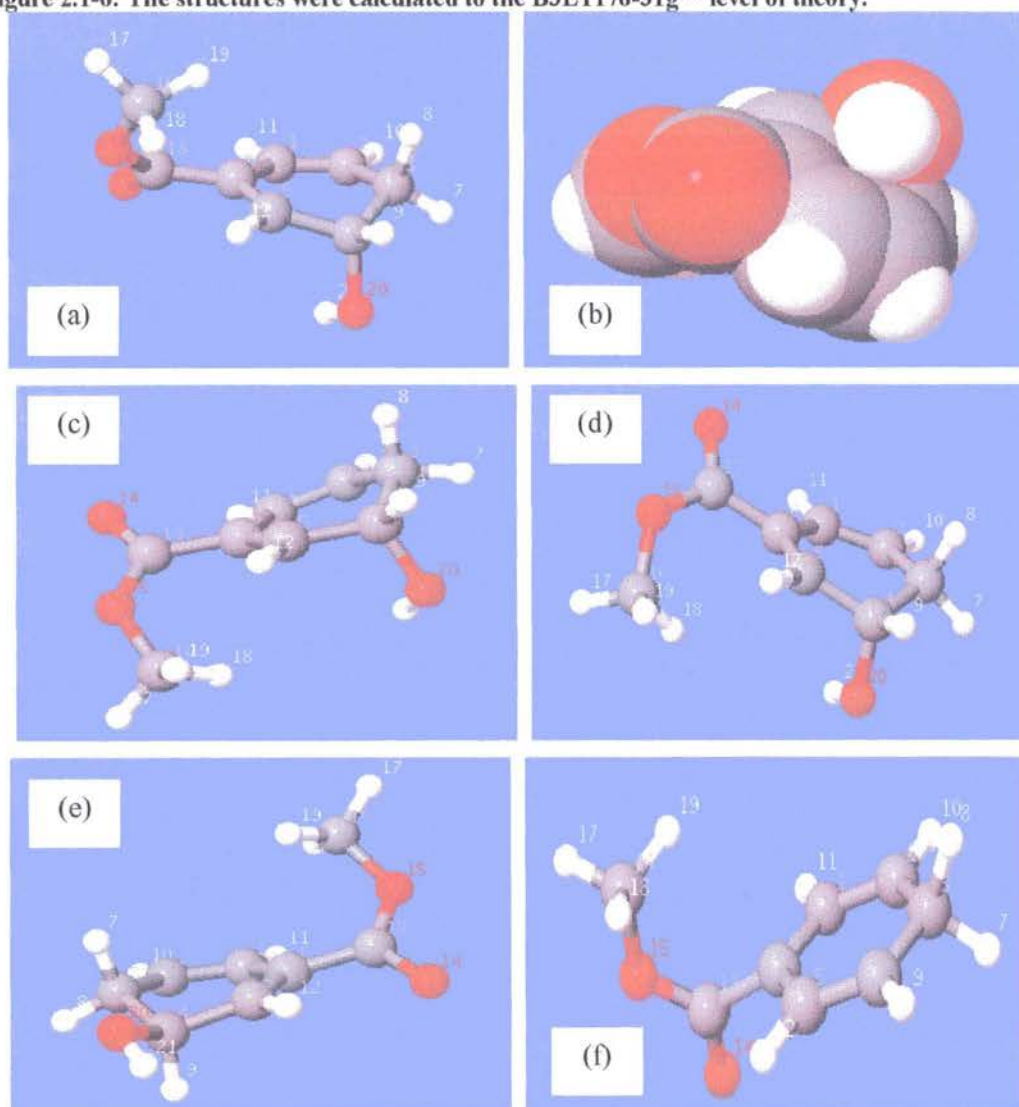
Figure 2.1-5: Second-order rate constants for the aromatisation of methyl benzoate hydrate followed at 270 and 230 nm.

The second-order rate constant for the aromatisation of methylbenzoate hydrate was obtained as $9.32 \times 10^{-2} \text{ M}^{-1}\text{s}^{-1}$ which corresponds to a half-life of 7 seconds in 1 M HClO₄.

2.1.3 Computational studies of methyl benzoate hydrate

The structures below in Figure 2.1-6 are the lowest energy conformers of the methyl benzoate hydrate (2.1), and the putative carbocation intermediate (2.7) (see p 40) formed during aromatisation reaction, calculated to the B3LYP/6-31g** level of theory using Gaussian 03.⁷⁶ The starting points for the calculations were generated from Monte Carlo calculations (MM3* level of theory) using the Maestro program.

Figure 2.1-6: The structures were calculated to the B3LYP/6-31g** level of theory.



The lowest energy structure (Fig 2.1-6(a)) shows the hydroxyl group in the axial position, the ester substituent is coplanar with the C-H bonds of the cyclohexadiene and rotated 30° relative to the ring structure. The space-filling model of conformer (a), Fig 2.1-6 (b), does not show any hydrogen-bonding between the hydroxyl H and the C=O of the ester. The hydroxyl substituent sits facing the conjugated diene of the ring-structure. The next lowest energy hydrate conformer (Fig 2.1-6(c)) shows a 15° rotation of the ester group relative to the ring. The conformer shown in Figure 2.1-6(d) shows the hydroxyl group in the axial position; the ester substituent is rotated 45° relative to the ring. The fourth lowest conformer (Fig 2.1-6(e)) shows the hydroxyl group in the equatorial position, a ring-flip of structure (a). The lowest energy calculated structure for the carbocation (Fig 2.1-6(f)) reveals the ester substituent at a 45° angle relative to a planar ring.

The calculated energies of the structures illustrated in Figure 2.1-6 (a – f) are summarized in Table 2.1-3.

Table 2.1-3: Energies of methyl benzoate hydrate conformers and putative carbocation intermediate calculated to the B3LYP/6-31g level of theory.**

Hydrate	Gas phase		With water sphere		
	kJ/mol	$\Delta^{(a)}$	kJ/mol	$\Delta^{(a)}$	$\Delta^{(b)}$
Fig 2.1-6(a)	-1408606.66	0.00	-1408658.04	0.00	-51.38
Fig 2.1-6 (c)	-1408603.42	3.24	-1408655.85	2.19	-52.43
Fig 2.1-6 (d)	-1408598.41	8.25	-1408654.38	3.66	-55.97
Fig 2.1-6 (e)	-1408595.69	10.97	-1408652.28	5.76	-56.59
carbocation Fig 2.1-6 (f)	-1208841.49	199765.17	-1209082.48	199575.56	-240.99

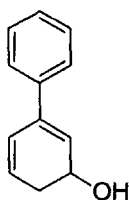
(a) Change in energy relative to the lowest energy structure (b) change in energy on going from the gas phase to a water sphere.

Of the hydrate structures, the highest energy structure in both the gas phase and calculated polarised continuous model, using water as the solvent, is structure (e) above with the hydroxyl group in the equatorial position. The effect of the water sphere is stabilisation in the order of 50 kJ/mol. The calculated energy of the carbocation is

almost 200,000 kJ/mol less stable than the lowest energy hydrate in the gas phase. The water sphere has a 240 kJ/mol stabilising effect on the energy of the carbocation.

2.2 Biphenyl Hydrate

This section describes the synthesis and kinetic studies of the aromatisation of biphenyl hydrate.



2.8

2.2.1 Synthesis of biphenyl hydrate

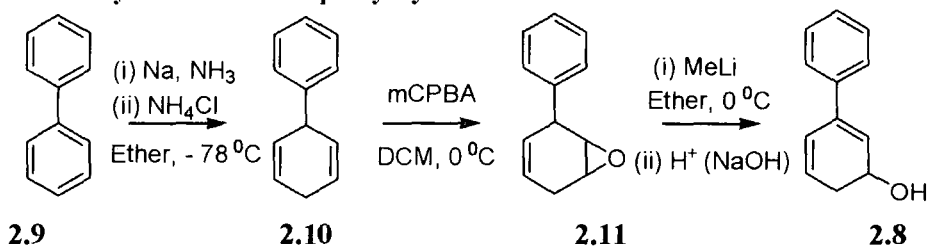
Scheme 2.2-1 (below) outlines the synthetic route to biphenyl hydrate. The Birch reduction was problematic and showed low conversion to the diene. No other regioisomers of the diene were formed. The low conversion to the diene is assigned to rearomatisation of the diene as noted by Hückel and Schwen⁷⁷.

On adding the sodium metal to the biphenyl solution in ammonia, the reaction mixture turned dark red. After further stirring for 20 minutes, solid ammonium chloride was added to quench the sodium and to minimise reduction of the second aromatic ring. The ammonia was allowed to evaporate overnight and the diene was extracted using diethyl ether. The diene was characterised quickly by NMR spectroscopy, however, it was not detectable by mass spectroscopy. As soon as possible, the diene (2.10) was further reacted to yield epoxide (2.11) which is more stable than the diene. The epoxide was purified by column chromatography (silica gel, petroleum ether/ diethyl ether).

The deprotonation and ring-opening of epoxide (2.11) using methyllithium gave only one product (2.8) after quenching with water. It was possible to purify this hydrate by

flash column chromatography (silica gel, ether) although some product was lost due to aromatisation on the column.

Scheme 2.2-1: Synthetic route to biphenyl hydrate

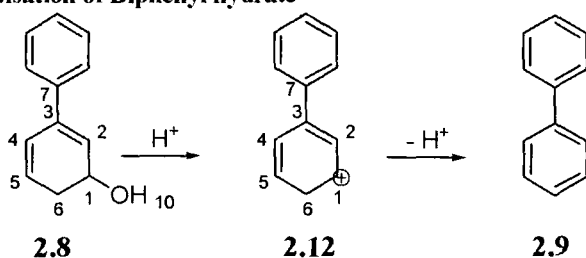


The major issue with the kinetics of the aromatisation reaction of biphenyl hydrate was the poor solubility of the hydrate and the aromatic product. Accurate NMR kinetics were not possible due to the insolubility of the product and hydrate at the concentrations required to achieve NMR spectra in a reasonable timeframe. The solubility of biphenyl in water is reported to be between 35 and 45 μM ^{78, 79}.

2.2.2 First order rate constants for the aromatisation of biphenyl hydrate.

The aromatisation reactions of hydrate (2.8) were followed in a range of acetic acid and phosphate buffers (pH 4.9 – 7.1). The substrate solution was prepared in acetonitrile to a concentration of 5 mM. Typically a 1/100 dilution of this solution into the relevant buffer solution was made to initiate the reaction. The total substrate concentration that could be used was limited by product arene solubility.

Scheme 2.2-2: Aromatisation of Biphenyl hydrate



The repetitive scan for the aromatisation of 3-phenylcyclohexa-2,4-dienol (biphenyl hydrate, 2.8) is shown in Fig 2.2-1. As can be seen the aromatisation reaction can be monitored either by following the disappearance of substrate ($\lambda = 249\text{ nm}$) or by following the appearance of the biphenyl (2.9) product ($\lambda = 230\text{ nm}$).

Figure 2.2-1: Representative repetitive scan of biphenyl hydrate in acetate buffer (90 % FB, pH 5) at 25 °C and I = 0.5 M (NaClO₄) recorded over 6 minutes .

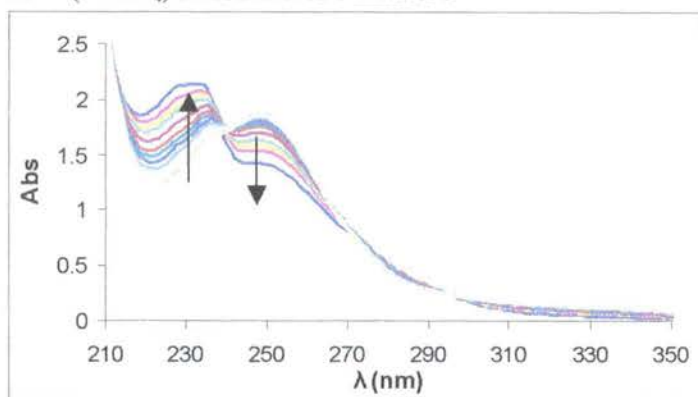
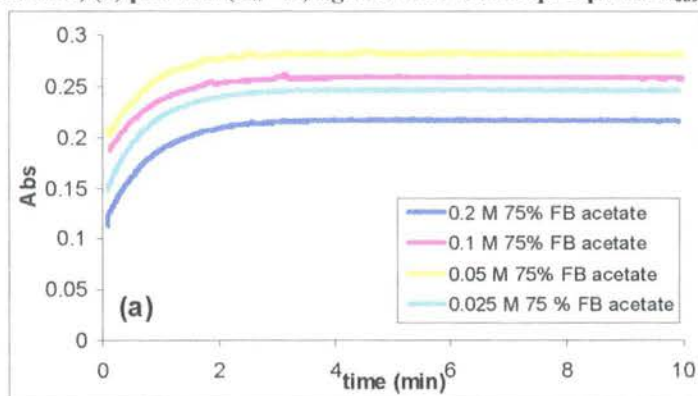
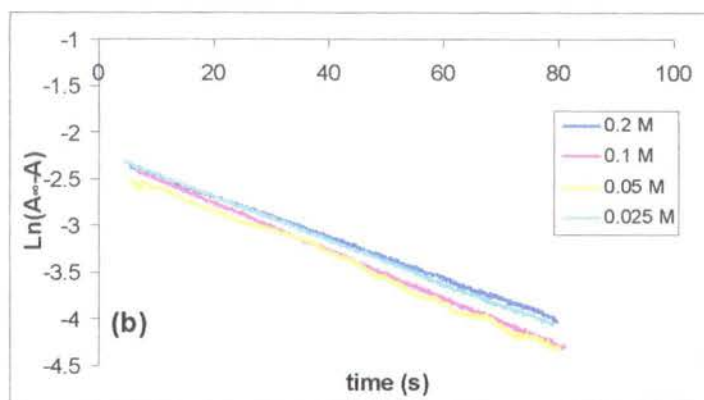


Figure 2.2-2(a) shows the change in absorbance against time at 230 nm as a result of the reaction of biphenyl hydrate in acetate buffer (75 % Free base (FB), pH 4.9). A corresponding semi-logarithmic plot of $\Delta A = A_{\infty} - A$ against time is shown in Figure 2.2-2 (b) where A_{∞} refers to the absorbance at the end of the reaction.

Figure 2.2-2: Aromatisation of biphenyl hydrate in 75 % FB acetate at pH 4.9 (a) Plot of absorbance versus time; (b) plot of $\ln(A_{\infty} - A)$ against time with slope equal to k_{obs}





The least squares analysis of the data in Figure 2.2-2(a) showed a very good fit. The error of the estimate was in the order of 5×10^{-4} and the t-values for the regression were over 1000, with the p-values all less than 1×10^{-4} . The mean of the results from the least squares analysis is $k_{\text{obs}} = 2.37 \pm 0.1 \times 10^{-2} \text{ s}^{-1}$. The semi-logarithmic analysis (see Fig 2.2-2(b)) also showed a very good fit of the results with the error for the fit in the third decimal. The mean of the results from the semi-logarithmic analysis is $k_{\text{obs}} = 2.38 \pm 0.1 \times 10^{-2} \text{ s}^{-1}$. Table 2.2-1 (below) summarises the data obtained from the aromatisation of biphenyl hydrate (2.8) in 75 % FB acetate at pH 4.9.

Table 2.2-1: First-order rate constants for aromatisation of biphenyl hydrate (2.8) in 75% FB acetate buffers (0.2 – 0.025 M) at 25 °C and $I = 0.5 \text{ M}$ (NaClO_4)^(a).

[Buffer] (M)	pH ^(b)	$[\text{H}^+]^{(c)}$ $\times 10^{-5}$ M	Semi-log Plot			Least Squares Plot		
			$k_{\text{obs}}^{(d)}$ ($\times 10^{-2}$) s^{-1}	R^2	$k_{\text{int}}^{(e)}$ ($\times 10^{-2}$) s^{-1}	$k_{\text{obs}}^{(f)}$ ($\times 10^{-2}$) s^{-1}	R^2	$k_{\text{int}}^{(g)}$ ($\times 10^{-2}$) s^{-1}
0.20	4.93	3.11	2.19	0.999		2.17	0.999	
0.10	4.93	3.10	2.54	0.998	2.47	2.52	0.999	2.37
0.05	4.94	3.03	2.45	0.997	(2.38 ^(g))	2.45	0.998	(2.37 ^(g))
0.025	4.95	3.00	2.32	0.999		2.34	0.999	

(a) Measurements were made at a substrate concentration of 0.05 mM and 1 % acetonitrile (b) pH was determined using a MeterLabTM PHM 290 pH-Stat Controller equipped with a radiometer (pH 4 - 7 - 10 @ 25 °C) combination electrode (type pHC4006) with a saturated LiTCA filling solution. (c) $[\text{H}^+]$ was calculated using $[\text{H}^+] = 10^{-(\text{pH} / \gamma_{\text{H}})}$ where $\gamma_{\text{H}} = 1$ is the activity coefficient of the hydronium ion under the experimental conditions. (d) The value of the first-order rate constant (k_{obs}), was obtained from the slope of the plot of $\ln(A_{\infty} - A)$ against time in Figure 2.2-2(b). (e) k_{int} is defined as the intercept of the plot of k_{obs} against buffer concentration Figure 2.2-3. (f) The value of the first-order rate constant (k_{obs}), was obtained from the least squares analysis of Figure 2.2-2(a) (g) Mean of k_{obs} for 0.2- 0.05 M solutions at constant pH.

Both buffer catalysis plots (see Fig 2.2-3) have negative slopes in the order of $-1 \times 10^{-3} \text{ M}^{-1}\text{s}^{-1}$ which indicates a potential salt or medium effect. However it clear that there is negligible buffer catalysis as the overall change in the first order rate constants for aromatisation with buffer concentration is small in comparison with the change in rate with increasing pH (see later results). The mean first order rate constant of aromatisation of biphenyl hydrate at pH 4.95 is $2.38 \times 10^{-2} \text{ s}^{-1}$ corresponding to a half-life of 29 seconds.

Figure 2.2-3: Aromatisation of biphenyl hydrate in 75 % FB acetate at pH 4.9: Plot of k_{obs} against buffer concentration

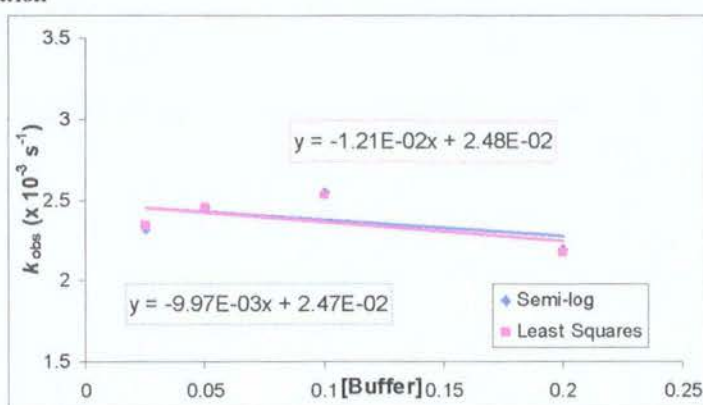
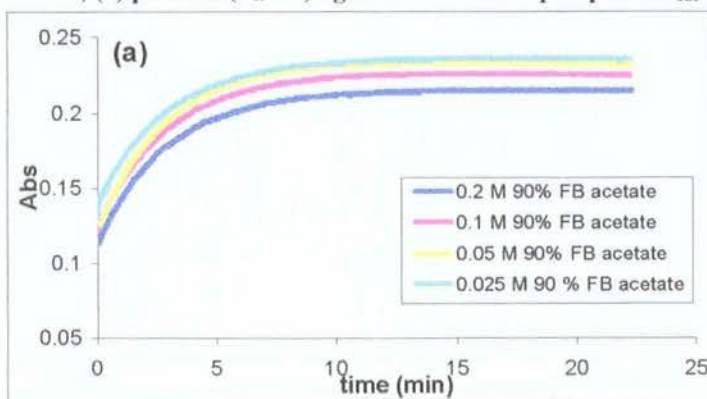


Figure 2.2-4(a) shows the change in absorbance against time at 230 nm as a result of the reaction of biphenyl hydrate in acetate buffer (90 % FB, pH 5.6). A corresponding semi-logarithmic plot of $\Delta A = A_{\infty} - A$ against time is shown in Figure 2.2-4(b) where A_{∞} refers to the absorbance at the end of the reaction.

Figure 2.2-4: Aromatisation of biphenyl hydrate in 90% FB acetate at pH 5.6 (a) Plot of absorbance versus time; (b) plot of $\ln(A_{\infty} - A)$ against time with slope equal to k_{obs}



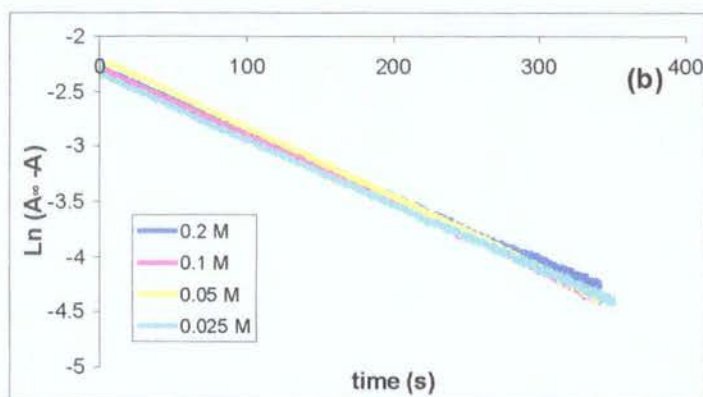


Table 2.2-2 (below) summarises the data obtained from the aromatisation of biphenyl hydrate (2.8) in 90 % FB acetate buffers at pH 5.6. The least squares analysis of figure 2.2-4(a) shows a very good fit of the regression line with the error of the estimate in the order of 4×10^{-4} and t-values for the regression over 1000. The mean of the results from the least squares analysis is $k_{\text{obs}} = 5.92 \pm 0.1 \times 10^{-3} \text{ s}^{-1}$. The results from the semi-logarithmic analysis (see Fig 2.2-4 (b)) gave a mean rate constant of aromatisation, $k_{\text{obs}} = 6.00 \pm 0.1 \times 10^{-3} \text{ s}^{-1}$.

Table 2.2-2: First-order rate constants for aromatisation of biphenyl hydrate (2.8) in 90 % FB acetate buffers (0.2 – 0.025 M) at 25 °C and I = 0.5 M (NaClO₄)^(a)

[Buffer] (M)	pH ^(b)	$[\text{H}^+]^{(c)}$ $\times 10^{-6}$ M	Semi-log Plot			Least Squares Plot		
			$k_{\text{obs}}^{(d)}$ ($\times 10^{-2}$) s^{-1}	R ²	$k_{\text{int}}^{(e)}$ ($\times 10^{-2}$) s^{-1}	$k_{\text{obs}}^{(f)}$ ($\times 10^{-2}$) s^{-1}	R ²	$k_{\text{int}}^{(e)}$ ($\times 10^{-2}$) s^{-1}
0.20	5.55	2.84	5.78	0.999		5.79	0.999	
0.10	5.55	2.85	6.08	0.999	6.13	5.91	0.999	6.01
0.05	5.54	2.88	6.31	0.999	(6.00 ^(g))	6.13	0.999	(5.92 ^(g))
0.025	5.56	2.74	5.84	0.999		5.85	0.999	

(a) Measurements were made at a substrate concentration of 0.05 mM and 1 % acetonitrile (b) pH was determined using a MeterLab™ PHM 290 pH-Stat Controller equipped with a radiometer (pH 4 - 7 - 10 @ 25 °C) combination electrode (type pHC4006) with a saturated LiTCA filling solution. (c) $[\text{H}^+]$ was calculated using $[\text{H}^+] = 10^{-(\text{pH}/\gamma_{\text{H}})}$ where $\gamma_{\text{H}} = 1$ is the activity coefficient of the hydronium ion under our experimental conditions. (d) The value of the first-order rate constant (k_{obs}), was obtained from the slope of the plot of $\ln(A_0 - A)$ against time in Figure 2.2-4(a). (e) k_{int} is defined as the intercept of the plot of k_{obs} against buffer concentration Figure 2.2-5. (f) The value of the first-order rate constant (k_{obs}), was obtained from the least squares analysis of Figure 2.2-4(a) (g) Mean of k_{obs} for 0.2- 0.05 M solutions at constant pH.

Both methods of analysis gave similar results; a paired t-test gave a p-value of 0.23 and an unpaired t-test gave a p-value of 0.58. The buffer catalysis (Fig 2.2-5) plots show only a negative slope in the order of $-1 \times 10^{-3} \text{ M}^{-1} \text{ s}^{-1}$. The medium effects in this case seem to be less apparent. The mean first order rate constant of aromatisation at pH 5.6 is $5.95 \times 10^{-3} \text{ s}^{-1}$ corresponding to a half-life of 116 seconds.

Figure 2.2-5: Aromatisation of biphenyl hydrate in 90 % FB acetate: Plot of k_{obs} against buffer concentration

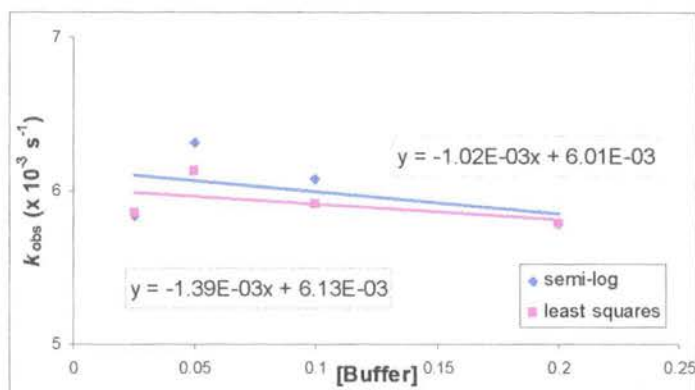
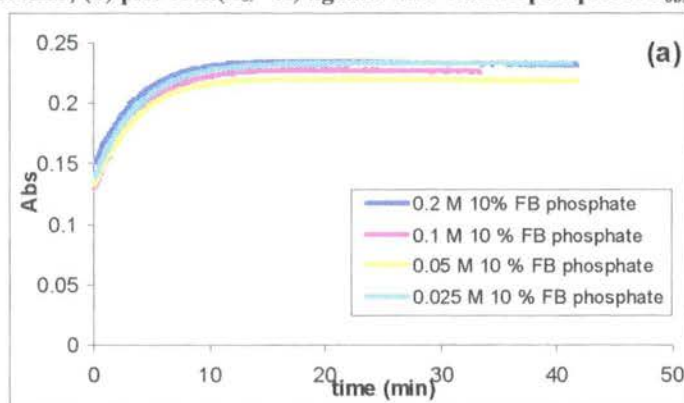


Figure 2.2-6(a) shows the change in absorbance against time at 230 nm as a result of the reaction of biphenyl hydrate in phosphate buffer (10 % FB, pH 5.7). A corresponding semi-logarithmic plot of $\Delta A = A_{\infty} - A$ against time is shown in Figure 2.2-6(b) where A_{∞} refers to the absorbance at the end of the reaction.

Figure 2.2-6: Aromatisation of biphenyl hydrate in 10% FB phosphate at pH 5.7 (a) Plot of absorbance versus time; (b) plot of $\ln(A_{\infty} - A)$ against time with slope equal to k_{obs}



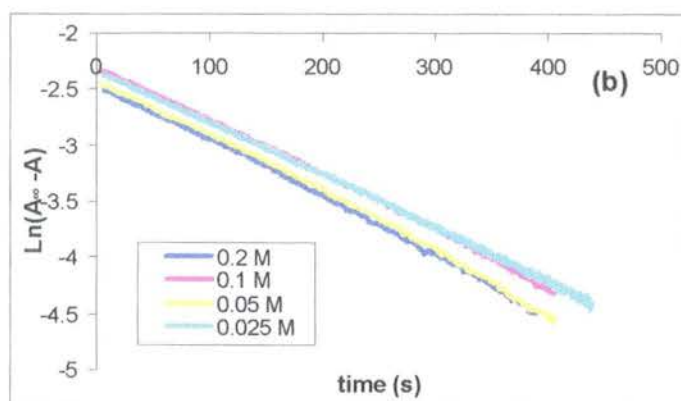


Table 2.2-3 (below) summarises the data obtained from the aromatisation of biphenyl hydrate (2.8) in 10 % FB phosphate buffer at pH 5.7. The results above show a good consistency between the two methods of analysis. The mean first order rate constant from the least squares analysis of the data in Figure 2.2-6(a) is $k_{\text{obs}} = 4.94 \pm 0.1 \times 10^{-3} \text{ s}^{-1}$. The results from the semi-logarithmic analysis (see Fig 2.2-6(b)) gave a mean of $k_{\text{obs}} = 4.98 \pm 0.1 \times 10^{-3} \text{ s}^{-1}$. Comparing the two sets of analysis, an unpaired t-test gave a p-value of 0.82 and a paired t-test gave a p-value of 0.40.

Table 2.2-3: First-order rate constants for aromatisation of biphenyl hydrate (2.8) in 10% FB phosphate buffers (0.2 – 0.025 M) at 25 °C and I = 0.5 M (NaClO₄)^(a)

[Buffer] (M)	pH ^(b)	[H ⁺] ^(c) ($\times 10^{-6}$ M)	Semi-Log Plot			Least Squares Fit		
			$k_{\text{obs}}^{(d)}$ ($\times 10^{-3}$ s^{-1})	R ²	$k_{\text{int}}^{(e)}$ ($\times 10^{-3}$ s^{-1})	$k_{\text{obs}}^{(f)}$ ($\times 10^{-3}$ s^{-1})	R ²	$k_{\text{int}}^{(e)}$ ($\times 10^{-3}$ s^{-1})
0.20	5.59	2.59	5.13	0.999		5.14	0.999	
0.10	5.60	2.51	4.91	0.999	4.84	4.96	0.999	4.73
0.05	5.61	2.46	5.20	0.998	(4.98 ^(g))	5.07	0.999	(4.94 ^(g))
0.025	5.62	2.38	4.68	0.999		4.59	0.999	

(a) Measurements were made at a substrate concentration of 0.05 mM and 1 % acetonitrile (b) pH was determined using a MeterLabTM PHM 290 pH-Stat Controller equipped with a radiometer (pH 4 - 7 - 10 @ 25 °C) combination electrode (type pHC4006) with a saturated LiTCA filling solution. (c) [H⁺] was calculated using $[\text{H}^+] = 10^{-(\text{pH} / \gamma_{\text{H}^+})}$ where $\gamma_{\text{H}^+} = 1$ is the activity coefficient of the hydronium ion under our experimental conditions. (d) The value of the first-order rate constant (k_{obs}), was obtained from the slope of the plot of $\ln(A_{\infty} - A)$ against time in Figure 2.2-6(b). (e) k_{int} is defined as the intercept of the plot of k_{obs} against buffer concentration Figure 2.2-7. (f) The value of the first-order rate constant (k_{obs}), was obtained from the least squares analysis of Figure 2.2-6(a) (g) Mean of k_{obs} for 0.2- 0.05 M solutions at constant pH.

In this case, the buffer catalysis plot (Fig 2.2-7) shows a positive slope of $2 \times 10^{-2} \text{ M}^{-1}\text{s}^{-1}$. The overall change in first order rate constants of aromatisation between the lowest and highest buffer concentrations is 0.4×10^{-3} , which is a change of 9%. This is negligible when compared to the rate constant changes over the pH range. The mean first order rate constant for aromatisation at pH 5.6 is $4.96 \times 10^{-3} \text{ s}^{-1}$ with a half-life of 140 seconds.

Figure 2.2-7: Aromatisation of biphenyl hydrate in 10% FB phosphate at pH 5.7: Plot of k_{obs} against buffer concentration

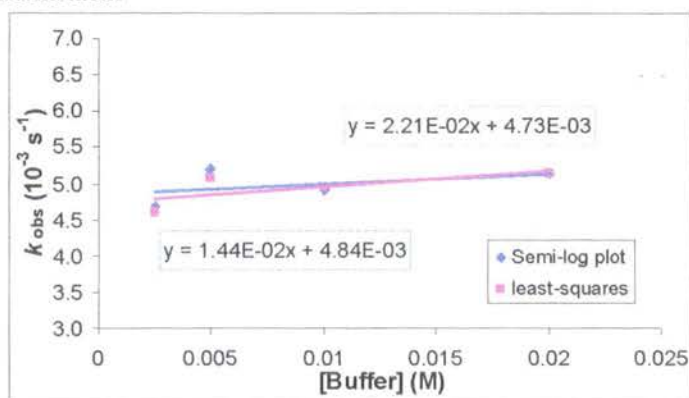
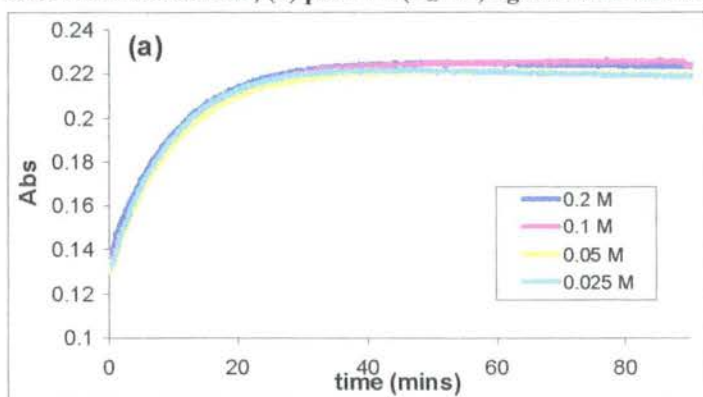


Figure 2.2-8(a) shows the change in absorbance against time at 230 nm as a result of the reaction of biphenyl hydrate in phosphate buffer (25 % FB, pH 6.1). A corresponding semi-logarithmic plot of $\Delta A = A_{\infty} - A$ against time is shown in Figure 2.2-8 (b) where A_{∞} refers to the absorbance at the end of the reaction.

Figure 2.2-8: Aromatisation of biphenyl hydrate in 25% FB phosphate at pH 5.7 (a) Plot of absorbance versus time; (b) plot of $\ln(A_{\infty} - A)$ against time with slope equal to $k_{\text{obs}} (\text{s}^{-1})$.



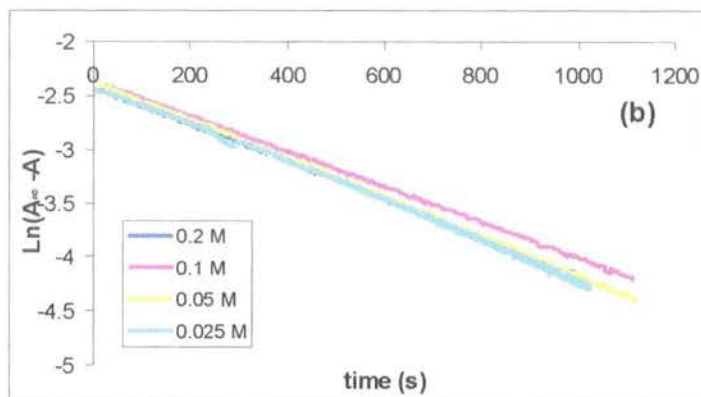


Table 2.2-4 (below) summarises the data obtained from the aromatisation of biphenyl hydrate (2.8) in 25 % FB phosphate buffers at pH 6.1. The least squares analysis of figure 2.2-8(a) was good. The regression line showed a good correlation with the recorded data to 11 half-lives (72 minutes). The error of the estimate was in the order of 9×10^{-4} and the t-values for the estimate of k_{obs} were greater than 150. The mean first order rate constant calculated is $k_{\text{obs}} = 1.72 \pm 0.0 \times 10^{-3} \text{ s}^{-1}$.

The results from the semi-logarithmic analysis (see Fig 2.2-8(b)) were fit to 3 half-lives and show a good correlation with the error of the regression line in the fourth decimal. The mean first order rate constant is $k_{\text{obs}} = 1.74 \pm 0.0 \times 10^{-3} \text{ s}^{-1}$. Both methods of analysis gave similar results, a paired t-test gave a p-value of 0.11 and an unpaired t-test gave a p-value of 0.65.

Table 2.2-4: First-order rate constants for aromatisation of biphenyl hydrate (2.8) in 25 % FB phosphate buffers (0.2 – 0.025 M) at 25 °C and I = 0.5 M (NaClO₄)^(a)

[Buffer] (M)	pH ^(b)	$[H^+]^{(c)}$ $\times 10^{-5}$ M	Semi-log Plot			Least Squares Plot		
			$k_{obs}^{(d)}$ ($\times 10^{-2}$) s^{-1}	R^2	$k_{int}^{(e)}$ ($\times 10^{-2}$) s^{-1}	$k_{obs}^{(f)}$ ($\times 10^{-2}$) s^{-1}	R^2	$k_{int}^{(e)}$ ($\times 10^{-2}$) s^{-1}
0.20	6.09	8.22	1.74	0.998		1.71	0.9997	
0.10	6.08	8.28	1.64	0.999	1.77	1.63	0.9999	1.74
0.05	6.08	8.34	1.79	0.998	(1.74 ^(g))	1.74	0.9998	(1.72 ^(g))
0.025	6.07	8.45	1.79	0.999		1.78	0.9991	

(a) Measurements were made at a substrate concentration of 0.05 mM and 1 % acetonitrile (b) pH was determined using a MeterLab™ PHM 290 pH-Stat Controller equipped with a radiometer (pH 4 - 7 - 10 @ 25 °C) combination electrode (type pHC4006) with a saturated LiTCA filling solution. (c) $[H^+]$ was calculated using $[H^+] = 10^{-(pH/\gamma_H)}$ where $\gamma_H = 1$ is the activity coefficient of the hydronium ion under our experimental conditions. (d) The value of the first-order rate constant (k_{obs}), was obtained from the slope of the plot of $\ln(A_\infty - A)$ against time in Figure 2.2-8(a). (e) k_{int} is defined as the intercept of the plot of k_{obs} against buffer concentration Figure 2.2-9. (f) The value of the first-order rate constant (k_{obs}), was obtained from the least squares analysis of Figure 2.2-8(a) (g) Mean of k_{obs} for 0.2- 0.05 M solutions at constant pH.

The buffer catalysis plot (see Fig 2.2-9) shows no evidence of any buffer catalysis, in fact the slope is negative ($-3 \times 10^{-4} M^{-1}s^{-1}$). Again, the overall change in rate constant with changing buffer concentration is small. The mean first order rate constant for aromatisation of biphenyl hydrate at pH 6.1 is $1.73 \times 10^{-3} s^{-1}$ corresponding to a half-life of 400 seconds.

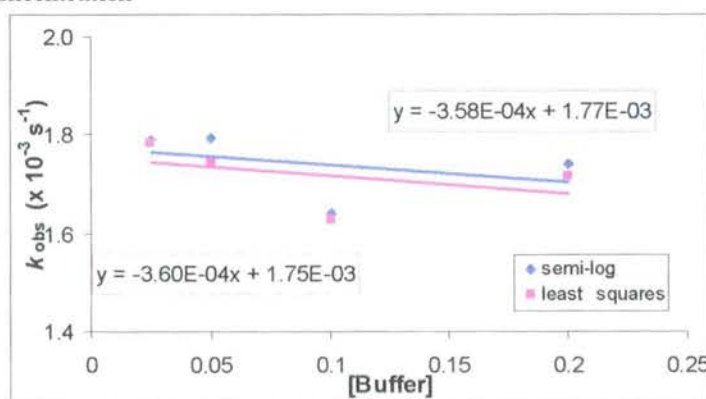
Figure 2.2-9: Aromatisation of biphenyl hydrate (2.8) in 25% FB phosphate at pH 5.7: Plot of k_{obs} against buffer concentration

Figure 2.2-10(a) shows the change in absorbance against time at 230 nm as a result of the reaction of biphenyl hydrate in phosphate buffer (50 % FB, pH 6.6). A

corresponding semi-logarithmic plot of $\Delta A = A_{\infty} - A$ against time is shown in Figure 2.2-10(b) where A_{∞} refers to the absorbance at the end of the reaction.

Figure 2.2-10: Aromatisation of biphenyl hydrate in 50 % FB phosphate at pH 6.6 (a) Plot of absorbance versus time; (b) plot of $\ln(A_{\infty} - A)$ against time with slope equal to k_{obs}

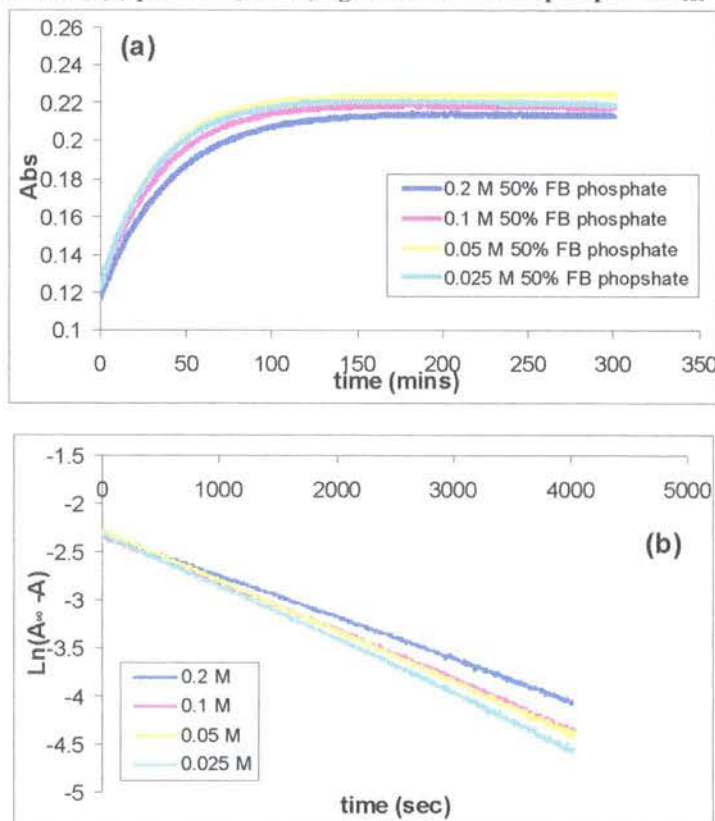


Table 2.2-5 (below) summarises the data obtained from the aromatisation of biphenyl hydrate (2.8) in 50 % FB phosphate at pH 6.6. The data in figure 2.2-10(a) was fitted to 10 half-lives, except in the case of the 0.2 M buffer, this was fit to 15 half-lives. The mean of the results from the least squares analysis is $k_{\text{obs}} = 4.93 \pm 0.2 \times 10^{-4} \text{ s}^{-1}$. The semi-logarithmic analysis (see Fig 2.2-10(b) above) gave a mean of $k_{\text{obs}} = 5.04 \pm 0.2 \times 10^{-4} \text{ s}^{-1}$.

Table 2.2-5: First-order rate constants for aromatisation of biphenyl hydrate (2.8) in 50 % FB phosphate buffers (0.2 – 0.025 M) at 25 °C and I = 0.5 M (NaClO₄)^(a)

[Buffer] (M)	pH ^(b)	[H ⁺] ^(c) (x 10 ⁻⁷) M	Semi-log Plot			Least Squares Plot		
			k_{obs} ^(d) (x 10 ⁻⁴) s ⁻¹	R ²	k_{int} ^(e) (x 10 ⁻⁴) s ⁻¹	k_{obs} ^(f) (x 10 ⁻⁴) s ⁻¹	R ²	k_{int} ^(e) (x 10 ⁻⁴) s ⁻¹
0.20	6.65	8.41	4.42	0.9993		4.39	0.9995	
0.10	6.62	8.97	4.99	0.9992	5.45	4.82	0.9998	5.61
0.05	6.59	9.40	5.23	0.9997	(5.04 ^(g))	5.18	0.9999	(4.93 ^(g))
0.025	6.59	9.48	5.54	0.9993		5.35	0.9997	

(a) Measurements were made at a substrate concentration of 0.05 mM and 1 % acetonitrile (b) pH was determined using a MeterLab™ PHM 290 pH-Stat Controller equipped with a radiometer (pH 4 - 7 - 10 @ 25 °C) combination electrode (type pHC4006) with a saturated LiTCA filling solution. (c) [H⁺] was calculated using $[H^+] = 10^{-(\text{pH} / \gamma_{\text{H}})}$ where $\gamma_{\text{H}} = 1$ is the activity coefficient of the hydronium ion under our experimental conditions. (d) The value of the first-order rate constant (k_{obs}), was obtained from the slope of the plot of $\ln(A_{\infty} - A)$ against time in Figure 2.2-10(a). (e) k_{int} is defined as the intercept of the plot of k_{obs} against buffer concentration Figure 2.2-11. (f) The value of the first-order rate constant (k_{obs}), was obtained from the least squares analysis of Figure 2.2-10(a) (g) Mean of k_{obs} for 0.2 - 0.05 M solutions at constant pH.

The buffer catalysis plots (Fig 2.2-11) show negative slopes in the order of $-6 \times 10^{-4} \text{ M}^{-1} \text{ s}^{-1}$. This could simply be a pH effect or a medium effect as discussed previously. The mean first order rate constant of aromatisation at pH 6.6 is $4.97 \times 10^{-4} \text{ s}^{-1}$ corresponding to a half life of 1394 seconds.

Figure 2.2-11: Aromatisation of biphenyl hydrate (2.8) in 25% FB phosphate at pH 6.6: Plot of k_{obs} against buffer concentration

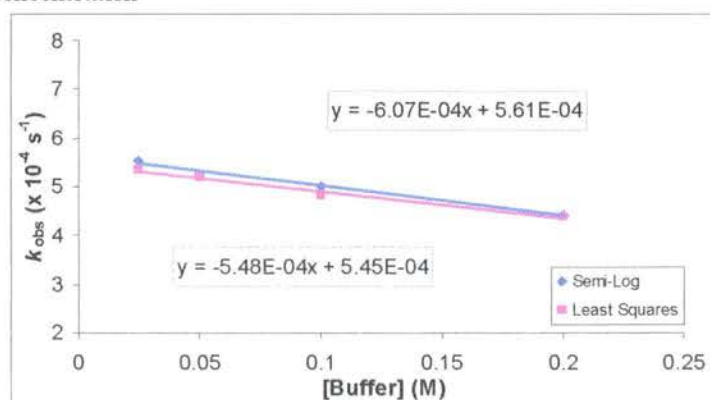


Figure 2.2-12(a) shows the change in absorbance against time at 230 nm as a result of the reaction of biphenyl hydrate in phosphate buffer (75 % FB, pH 7.1). A

corresponding semi-logarithmic plot of $\Delta A = A_{\infty} - A$ against time is shown in Figure 2.2-12 (b) where A_{∞} refers to the absorbance at the end of the reaction.

Figure 2.2-12: Aromatisation of biphenyl hydrate in 75% FB phosphate at pH 7.1 (a) Plot of absorbance versus time; (b) plot of $\ln(A_{\infty} - A)$ against time with slope equal to k_{obs}

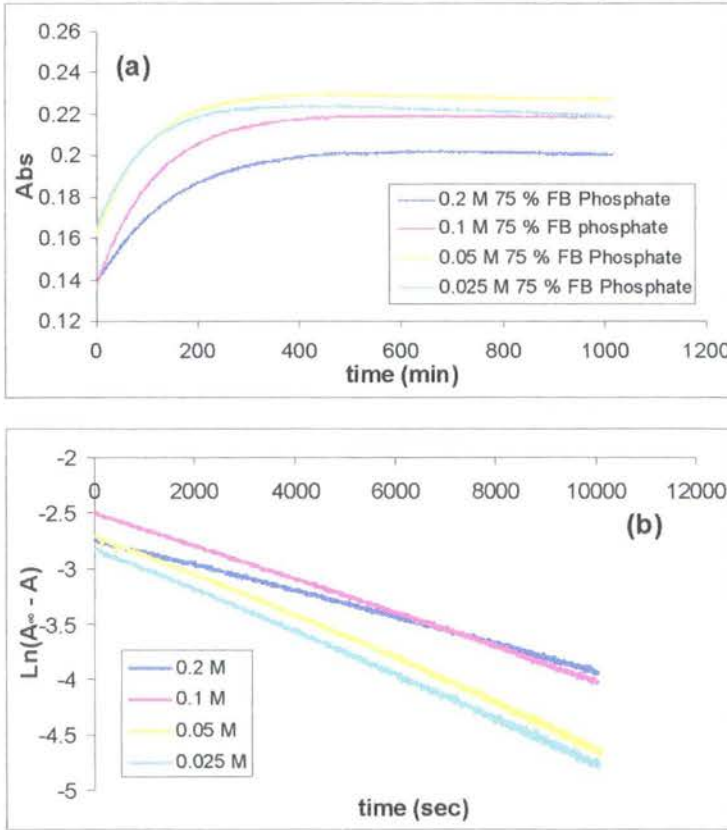


Table 2.2-6 (below) summarises the data obtained from the aromatisation of biphenyl hydrate (2.8) in 75 % FB phosphate at pH 7. The results above show a reasonable correlation between the least squares and semi-logarithmic analysis. The least squares analysis (see Fig 2.2-12(a)) gave a mean of $k_{\text{obs}} = 1.60 \pm 0.2 \times 10^{-4} \text{ s}^{-1}$. The semi-logarithmic analysis (see Fig 2.2-12(b)) gave a mean of $k_{\text{obs}} = 1.68 \pm 0.2 \times 10^{-4}$. Overall the intercepts and means are very similar. An unpaired t-test gave a p-value of 0.73 whereas a paired t-test gave a p-value of just 0.02.

Table 2.2-6: First-order rate constants for aromatisation of biphenyl hydrate (2.8) in 75 % FB phosphate buffers (0.2 – 0.025 M) at 25 °C and I = 0.5 M (NaOCl₄)^(a)

[Buffer] (M)	pH ^(b)	[H ⁺] ^(c) x 10 ⁻⁷ M	Semi-log Plot			Least Squares Plot		
			<i>k</i> _{obs} ^(d) (x 10 ⁻⁴) s ⁻¹	R ²	<i>k</i> _{int} ^(e) (x 10 ⁻⁴) s ⁻¹	<i>k</i> _{obs} ^(f) (x 10 ⁻⁴) s ⁻¹	R ²	<i>k</i> _{int} ^(e) (x 10 ⁻⁴) s ⁻¹
0.20	7.16	2.84	1.32	0.998		1.22	0.9993	
0.10	7.11	3.19	1.54	0.999	2.04	1.50	0.9998	1.97
0.05	7.08	3.39	1.93	0.998	(1.68 ^(g))	1.82	0.9988	(1.60 ^(g))
0.025	7.06	3.50	1.94	0.999		1.88	0.9997	

(a) Measurements were made at a substrate concentration of 0.05 mM and 1 % acetonitrile (b) pH was determined using a MeterLab™ PHM 290 pH-Stat Controller equipped with a radiometer (pH 4 - 7 - 10 @ 25 °C) combination electrode (type pHC4006) with a saturated LiTCA filling solution. (c) [H⁺] was calculated using $[H^+] = 10^{-(pH/\gamma_H)}$ where $\gamma_H = 1$ is the activity coefficient of the hydronium ion under our experimental conditions. (d) The value of the first-order rate constant (*k*_{obs}), was obtained from the slope of the plot of ln (A_∞ - A) against time in Figure 2.2-12(a). (e) *k*_{int} is defined as the intercept of the plot of *k*_{obs} against buffer concentration Figure 2.2-13. (f) The value of the first-order rate constant (*k*_{obs}), was obtained from the least squares analysis of Figure 2.2-12(a) (g) Mean of *k*_{obs} for 0.2 - 0.05 M solutions at constant pH.

The buffer catalysis plots (Fig 2.2-13) show negative slopes on the order of $-3.8 \times 10^{-4} \text{ M}^{-1} \text{ s}^{-1}$. The total change in rate constants over the four buffer concentrations is on the order of 51 %. The mean first order rate constant of aromatisation at pH 7.1 is $1.60 \times 10^{-4} \text{ s}^{-1}$ corresponding to a half-life of 4332 seconds.

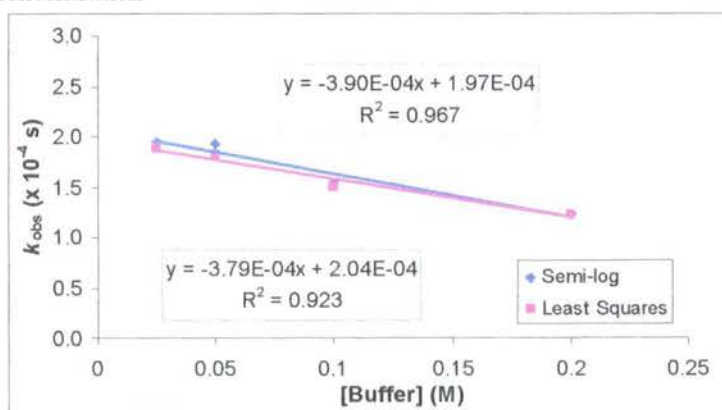
Figure 2.2-13: Aromatisation of biphenyl hydrate (2.8) in 75% FB phosphate at pH 7.1: Plot of *k*_{obs} against buffer concentration

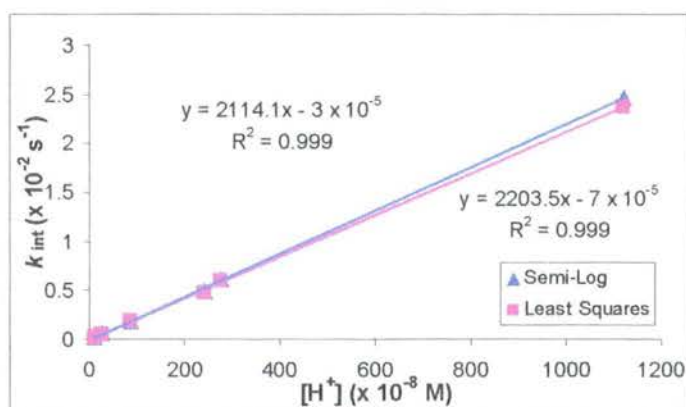
Table 2.2-7 (below) summarises the first order rate constants for the aromatisation reactions of biphenyl hydrate (2.8) in acetate and phosphate buffers (pH 4.2 – 7.1).

Table 2.2-7: Second-order rate constant for the aromatisation of biphenyl hydrate in aqueous acetate and phosphate buffers with I = 0.5 M (NaClO₄)

pH ^(a)	[H ⁺] ^(b) M	k_{obs}		Log (k_{obs})	
		k_{int} s ⁻¹	k_{H} ^(c) M ⁻¹ s ⁻¹	Log (k_{int}) ^(d) s ⁻¹	Log k_{H} ^(e) M ⁻¹ s ⁻¹
4.95	1.12 x 10 ⁻⁵	2.37 x 10 ⁻²		-1.63	
5.56	2.75 x 10 ⁻⁶	6.01 x 10 ⁻³		-2.22	
5.62	2.40 x 10 ⁻⁶	4.73 x 10 ⁻³	2114.1	-2.31	3.24
6.07	8.51 x 10 ⁻⁷	1.81 x 10 ⁻³	(2203.5) ^(f)	-2.74	(3.22) ^(g)
6.59	2.57 x 10 ⁻⁷	5.14 x 10 ⁻⁴		-3.29	
7.06	8.71 x 10 ⁻⁸	1.97 x 10 ⁻⁴		-3.71	

(a) pH was determined using a MeterLabTM PHM 290 pH-Stat Controller equipped with a radiometer (pH 4 - 7 - 10 @ 25 °C) combination electrode (type pHC4006) with a saturated LiTCA filling solution. (b) [H⁺] was calculated using $[H^+] = 10^{-(\text{pH}/\gamma_{\text{H}})}$ where $\gamma_{\text{H}} = 1$ is the activity coefficient of the hydronium ion under our experimental conditions. (c) Slope of the plot of k_{int} against acid concentration Fig 2.2-14 below. (d) k_{H} from semi-logarithmic analysis. (e) Log(k_{H}) from semi-logarithmic analysis.

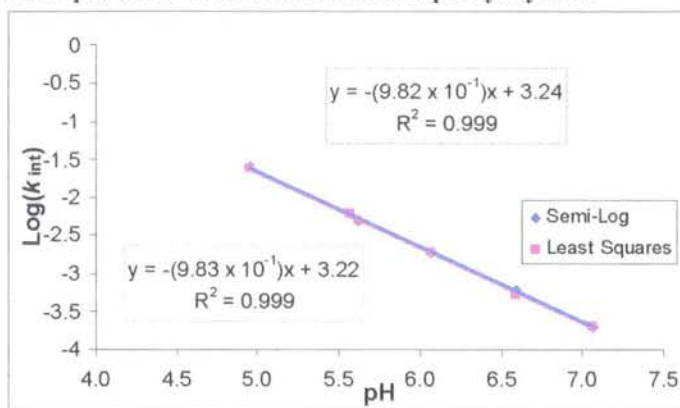
As with the previous hydrate, the second-order rate constant for acid-catalysed aromatisation, k_{H} , could be obtained as the slope of a plot of k_{obs} (or k_{int}) values against acid concentration (see Fig. 2.2-14). The second-order rate constant for the acid-catalysed aromatisation of biphenyl hydrate was determined as $k_{\text{H}} = 2114 \text{ M}^{-1}\text{s}^{-1}$.

Figure 2.2-14: Plot of k_{int} versus concentration of hydronium ion for the aromatisation of biphenyl hydrate (2.8)

The least squares and semi-logarithmic methods of analysis both gave a good fit of the data as is shown in Figure 2.2-14. The pH-rate profile (see Fig 2.2-15) also gives a

very good extrapolation to $\log k_H$ (3.22 & 3.24) which corresponds to a second-order rate constant for the acid-catalysed aromatisation (k_H) of $1660 \text{ M}^{-1}\text{s}^{-1}$.

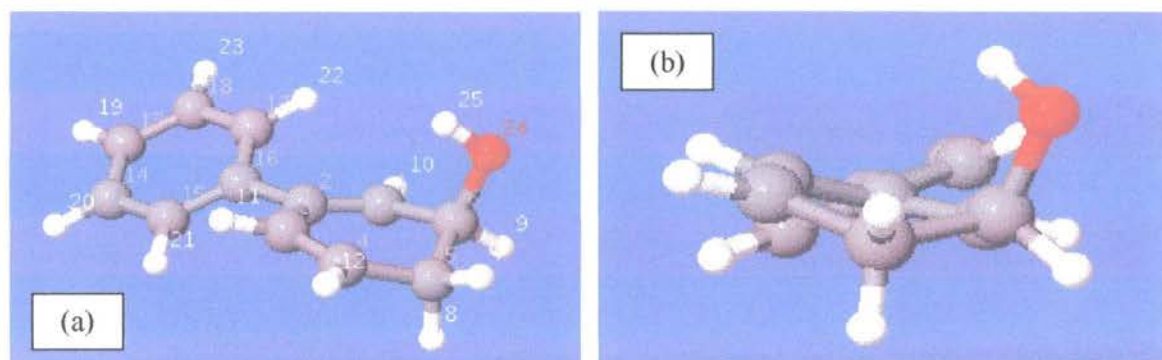
Figure 2.2-15: pH- rate profile for the aromatisation of biphenyl hydrate



2.2.3 Computational studies of biphenyl hydrate

The possible structures and energies of biphenyl hydrate and the putative carbocation intermediate (2.12) for aromatisation were calculated using Gaussian '03. The level of theory used was B3LYP/6-31g** using Gaussian 03⁷⁶. The starting point for the calculation were generated from Monte Carlo calculations (MM3* level of theory) using the Maestro program. The structures below are the lowest energy structures calculated (see Fig 2.2-16).

Figure 2.2-16: Lowest energy structures of biphenyl hydrate and the putative carbocation intermediate calculated to B3LYP/6-31g** level of theory



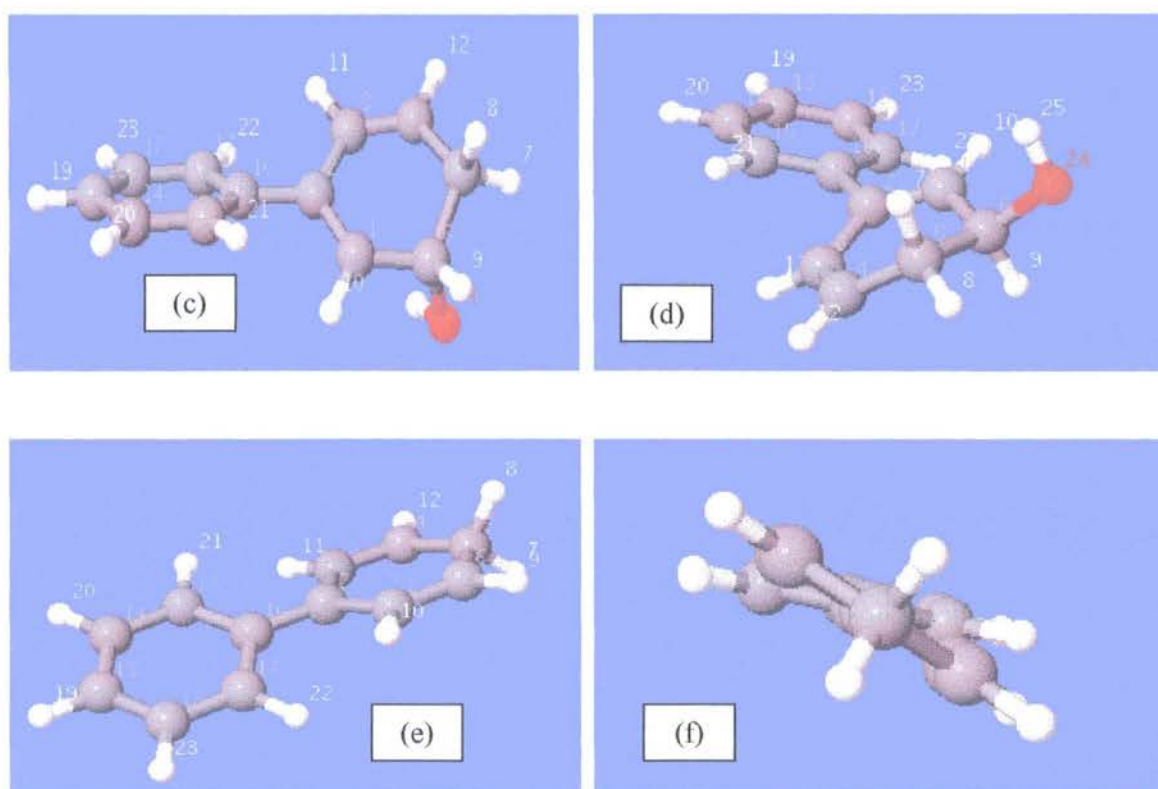


Figure 2.2-16 (a – d) above shows the lowest energy structures of biphenyl hydrate. Figure 2.2-16 (a) illustrates the lowest energy structure which has the hydroxyl substituent in an pseudo-axial position; and the phenyl ring in an pseudoequatorial position. The phenyl substituent is twisted approximately 15° relative to the cyclohexadienol ring (Fig 2.2-16(b)). Hydrate structure (c) is the next lowest in energy; in this case the hydroxyl group is also in the axial position, and the major difference in the structure is the angle of the phenyl group relative to the primary ring (30°). The next lowest energy hydrate structure is shown in Fig 2.2-16(d); this is a partial ring-flip of structure (a), and so the hydroxyl group is now in the equatorial position. The angle between the phenyl ring and the primary ring structure is larger (35°). Figures 2.2-16(e) and (f) show the calculated structure of the same carbocation intermediate shown from different angles. The cyclohexadiene ring is planar and the phenyl substituent is tilted slightly relative to the primary ring structure (5°).

Table 2.2-8 (below) shows the energies of the structures shown in Fig 2.2-16(a) – (f) calculated to the B3LYP/6-31g** level of theory using Gaussian 03.⁷⁶

Table 2.2-8: Energies of biphenyl hydrate structures calculated to the B3LYP/6-31g level of theory.**

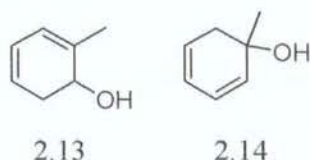
Hydrate	Gas phase		With water sphere		
	kJ/mol	$\Delta^{(a)}$	kJ/mol	$\Delta^{(a)}$	$\Delta^{(b)}$
Fig 2.16-1(a)	-1417008.69	0.00	-1417047.55	0.00	38.31
Fig 2.16-1(c)	-1417006.96	1.73	-1417046.43	1.12	39.47
Fig 2.16-1(d)	-1417004.19	4.50	-1417045.32	2.23	41.12
Fig 2.16-1(e) carbocation	-1217330.44	199678.25	-1217531.11	199516.44	200.67

(a) Change in energy relative to the lowest energy structure (b) change in energy on going from the gas phase to a water sphere.

Table 2.2-8 shows that the energy differences between the different conformers are very small. The stabilization by the water sphere is approximately 40 kJ/mol for the hydrate conformers. In the case of the carbocation the stabilization is much larger (200 kJ/mol).

2.3 Toluene Hydrate

This section gives the results of the synthesis and kinetic studies of aromatisation of *ortho* (2.13) and *ipso* (2.14) toluene hydrate.

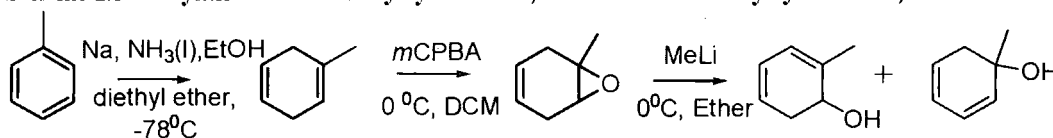


2.3.1 Synthesis of 2-methylcyclohexa-2,4-dienol (*ortho*) and 1-methylcyclohexa-2,4-dienol (*ipso*)

Scheme 2.3-1 (below) shows the synthesis of the toluene hydrates (2.13) and (2.14). The Birch reduction proceeded with a reasonable yield of cyclohexadiene (45 %). The epoxidation proceeded with a poor yield (18 %), as most of the product was lost through purification and removing the solvent *in vacuo*. The final ring-opening step also proceeded in low yields. The mixture of hydrate products was not stable to any

purification techniques attempted, for example column chromatography and distillation. As the major by-product was the parent arene, it was decided to continue with the kinetics. The hydrate products decomposed over approximately two weeks, as indicated by NMR spectra taken in chloroform over time.

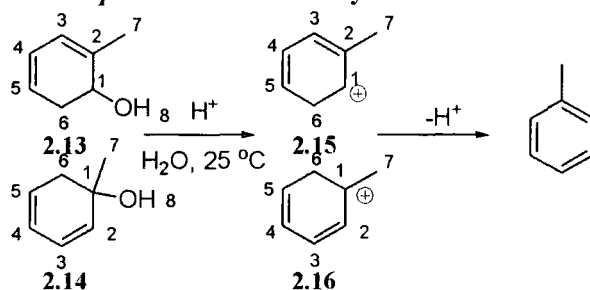
Scheme 2.3-1: Synthesis of 2-methylcyclohexa-2,4-dienol and 1-methylcyclohexa-2,4-dienol



2.3.2 Kinetic analysis of the aromatisation reaction via dehydration of 2-methylcyclohexa-2,4-dienol and 1-methylcyclohexa-2,4-dienol

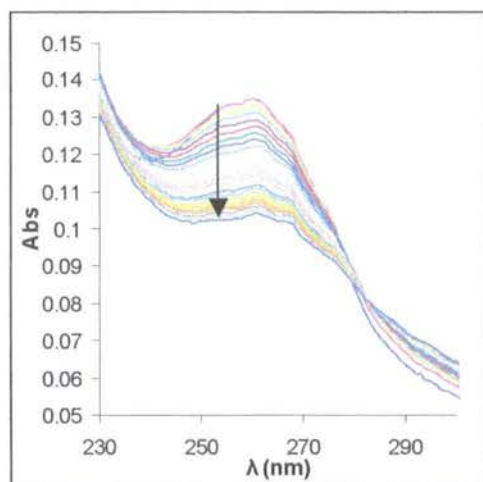
The aromatisation reactions of 2-methylcyclohexa-2,4-dienol (2.13) and 1-methylcyclohexa-2,4-dienol (2.14) were followed in acetate and phosphate buffers (pH 4.2 – 7) at ionic strength 0.5 M, maintained with sodium perchlorate. The substrate solution was prepared in acetonitrile to a concentration of 5 mM. Typically a 1/100 dilution of this solution into the relevant buffer solution was made to initiate the reaction. The total substrate concentration (0.05 mM) was limited due to the solubility of the reactant and product. The reported solubility of toluene in water is $6.03 \times 10^{-4} \text{ M}^{80}$.

Scheme 2.3-2: Dehydration of *ipso* and *ortho* toluene hydrates



A representative repetitive scan is shown below (Fig 2.3-1) for the aromatisation reaction. The scan shows the disappearance of the hydrates at $\lambda = 254 \text{ nm}$ and the appearance of the dehydration product toluene at 290 nm. The analytical wavelength chosen is 254 nm.

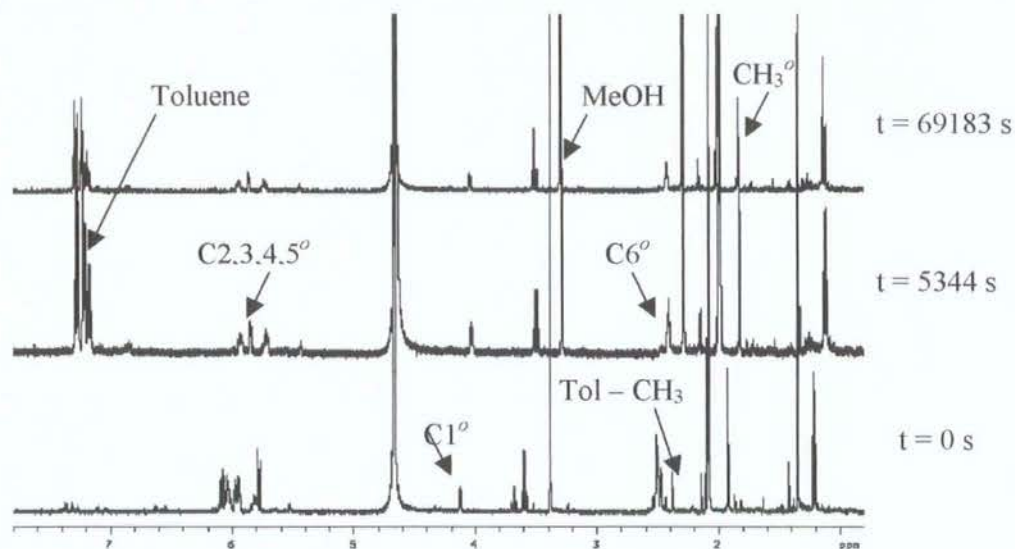
Figure 2.3-1: Repetitive scan for the aromatisation of toluene hydrate in 50 % FB phosphate buffer at pH 6.6



The reaction of the 2-methylcyclohexa-2,4-dienol (*ortho* hydrate, 2.13) was slower than that of the corresponding 1-methylcyclohexa-2,4-dienol (*ipso* hydrate, 2.14) as determined by NMR spectroscopy (see Fig 2.3-2). The repetitive scan (Fig 2.3-1) shows the reaction of both hydrates.

The aromatisation of the mixture of '*ortho*' and '*ipso*' hydrates was also followed by ^1H NMR and this reaction is shown below (Fig 2.3-2 & 3). The reactions were run in phosphate buffers (0.1 M, 50 % & 90 % FB) at pD 7.20 and 8.12 with the ionic strength maintained at 0.5 with sodium perchlorate. The NMR-time profiles clearly show the rapid reaction of the '*ipso*' hydrate. Figure 2.3-2 shows that the reaction of the *ipso* hydrate is almost complete before the spectrum is taken. The zero time spectra were recorded in 5 mM sodium deuterioxide due to the reactivity of the hydrates at pH 7. The relevant peaks in the $t=0$ spectra are shifted slightly upfield due to the shift in chemical shift of the water peak at high pH.

Figure 2.3-2: ^1H NMR time profile of 2-methylcyclohexa-2,4-dienol and 1-methylcyclohexa-2,4-dienol in phosphate buffer (0.2 M 50 % FB) at pD = 7.30 (pH = 6.90), I = 0.5 M (NaClO_4) and 25 $^\circ\text{C}$.



A group of 3 multiplets are observed at 6.1, 5.9 and 5.8 ppm due to the conjugated double bond hydrogens (C-3, 4 & 5) of the *ortho* hydrate. Overlapping these peaks in the time zero spectra are the conjugated double bond hydrogens (C-2, 3, 4 & 5) of the *ipso* hydrate. The multiplet at 4.1 ppm is due to the C-1 hydrogen of the '*ortho*' hydrate which decreases over time (see Figure 2.3-2). The disappearance of this peak is concomitant with an increase of the area of the aromatic hydrogens of the arene product between 7.2 and 7.4 ppm. The internal standard used in this case is methanol (3.3 ppm). The rate constant for aromatisation of the *ortho* hydrate could only be estimated as on the order of $1 \times 10^{-5} \text{ s}^{-1}$ at 25 $^\circ\text{C}$ due to the insolubility of the hydrate and the product arene at this buffer concentration. The spectra do, however, show the rapid reaction of the *ipso* hydrate compared to the *ortho* hydrate.

The NMR-time profile shows the insolubility of the arene product. The appearance of the arene product in the second spectrum ($t = 5344 \text{ s}$) can clearly be seen, however the area of the aromatic region changes little over the time course of the reaction and in fact, the final time-point ($t = 69183 \text{ s}$) shows a decrease in the area of the arene peaks. This is attributed to either desolvation of the arene at the relatively high concentrations necessary for NMR analysis (10 mM, 10 % acetonitrile co-solvent), or else it could be the volatilization of the arene from the surface of the reaction mixture

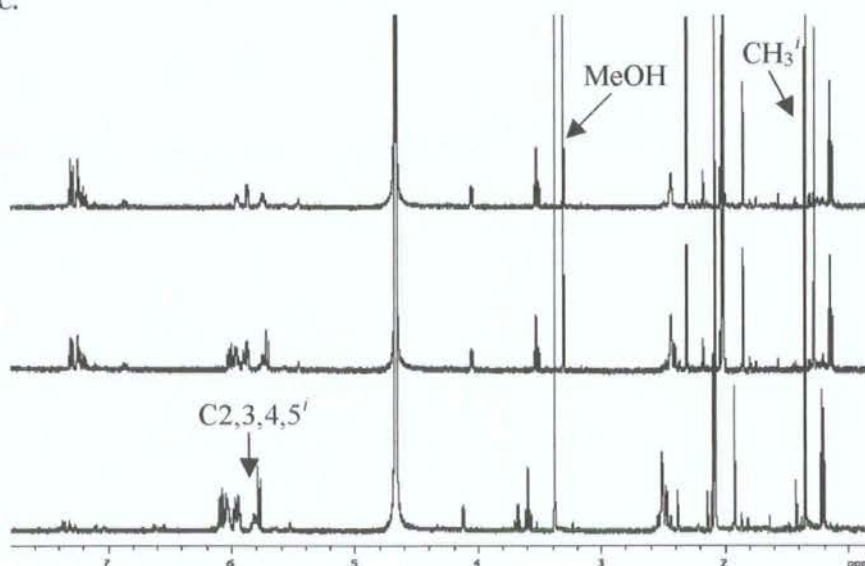
which is known to occur via a first order process in lakes and rivers at a rate of $1.7 \times 10^{-4} \text{ s}^{-1}$ corresponding to a half-life of 68 minutes⁸¹. This behaviour was also observed when a solution of arene only was prepared and analysed by NMR over time.

The ^1H NMR-time profile for the same reaction in 90 % FB phosphate buffer (pD 8.1) shows the rate of reaction of the *ipso* hydrate (see Figure 2.3-3, below). The *ortho* hydrate reacts very slowly at this pD and its concentration is assumed to be constant over the time of the experiment. The fraction of substrate ($f(s)$) for the '*ipso*' hydrate could be determined using Equation 2-2 (below), where $A^{Me/3}$ is the area of the singlet at approximately 1.8 ppm associated with the methyl substituent of the '*ipso*' hydrate and A^o is the area of the C-1 H peak of the *ortho* hydrate.

$$f(s) = \frac{\left(\frac{A^{Me/3}}{A^o}\right)_t}{\left(\frac{A^{Me/3}}{A^o}\right)_0} \quad \text{Equation 2-2}$$

The first order rate constant was determined as the slope of the semi-logarithmic plot of $f(s)$ against time and was found to be $8.8 \times 10^{-3} \text{ s}^{-1}$ at 25 °C.

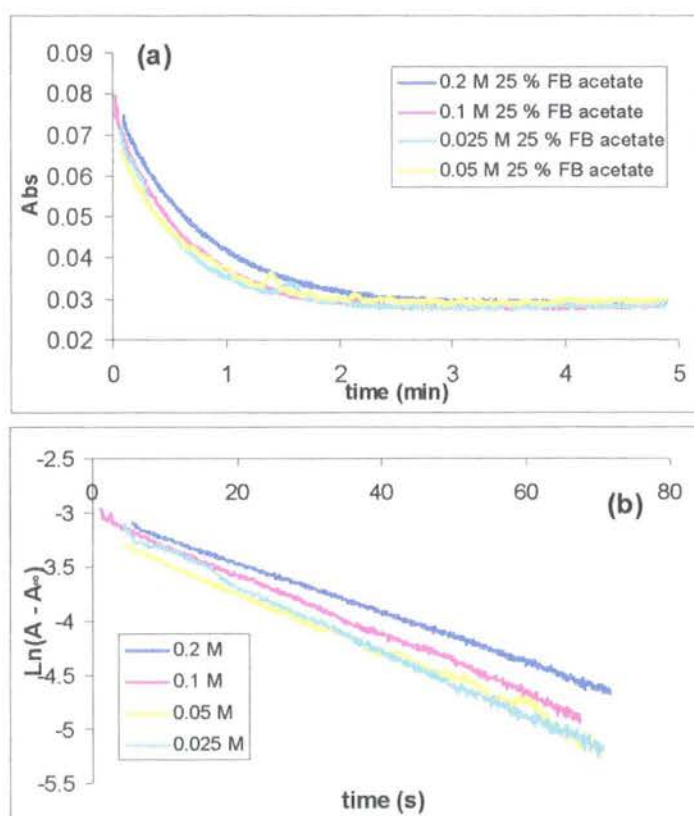
Figure 2.3-3: ^1H NMR time profile of the reaction of 2-methylcyclohexa-2,4-dienol and 1-methylcyclohexa-2,4-dienol in 90 % FB phosphate (pD = 7.30 (pH = 6.90)) at I = 0.5 M (NaClO_4) and 25 °C.



For the UV-vis kinetics the concentration of the hydrate reactant used was below the reported solubility of the product arene in water⁸⁰.

Figure 2.3-4(a) shows the change in absorbance against time at 254 nm as a result of the reaction of 2-methylcyclohexa-2,4-dienol in acetate buffer (25 % FB, pH 4.2). A corresponding semi-logarithmic plot of $\Delta A = A - A_\infty$ against time is shown in Figure 2.3-4 (b) where A_∞ refers to the absorbance at the end of the reaction. Table 2.3-1 shows summarises the first order rate constants for the aromatisation of *ortho* toluene hydrate (k_{obs}). At this pH the reaction of the *ipso* hydrate was too fast to be monitored by standard UV-vis spectroscopy.

Figure 2.3-4: Aromatisation of 2-methylcyclohexa-2,4-dienol in 25 % FB acetate at pH 4.2 and 25 °C. (a) Plot of absorbance versus time; (b) plot of $\ln(A - A_\infty)$ against time with slope equal to k_{obs}



At this pH the reaction of 1-methylcyclohexa-2,4-dienol (2.14) is too fast to monitor by standard UV-vis spectrophotometric methods.

Table 2.3-1: First-order rate constants for aromatisation of toluene hydrate (2.13) in 25% FB acetate buffers (0.2 – 0.025 M) at 25 °C and I = 0.5 M (NaClO₄)^(a)

[Buffer] (M)	pH ^(b)	[H ⁺] ^(c) x 10 ⁻⁵ M	Semi-log Plot			Least Squares Plot		
			k_{obs}° ^(d) (x 10 ⁻²) s ⁻¹	R ²	k_{int}° ^(e) (x 10 ⁻²) s ⁻¹	k_{obs}° ^(f) (x 10 ⁻²) s ⁻¹	R ²	k_{int}° ^(e) (x 10 ⁻²) s ⁻¹
0.20	4.21	6.14	2.38	0.998		2.51	0.995	
0.10	4.21	6.12	2.76	0.999	3.08	2.89	0.998	3.10
0.05	4.22	6.08	2.81	0.992	(2.75 ^(g))	2.81	0.998	(2.83 ^(g))
0.025	4.22	6.07	3.05	0.998		3.10	0.997	

(a) Measurements were made at a substrate concentration of 0.05 mM and 1 % acetonitrile (b) pH was determined using a MeterLabTM PHM 290 pH-Stat Controller equipped with a radiometer (pH 4 - 7 - 10 @ 25 °C) combination electrode (type pHC4006) with a saturated LiTCA filling solution. (c) [H⁺] was calculated using $[H^+] = 10^{-(\text{pH}/\gamma_H)}$ where $\gamma_H = 1$ is the activity coefficient of the hydronium ion under our experimental conditions. (d) The value of the first-order rate constant (k_{obs}°), was obtained from the slope of the plot of $\ln(A - A_{\infty})$ against time in Figure 2.3-3(b). (e) k_{int}° is defined as the intercept of the plot of k_{obs}° against buffer concentration Figure 2.3-4. (f) The value of the first-order rate constant (k_{obs}°), was obtained from the least squares analysis of Figure 2.3-3(a). (g) mean of k_{obs}°

The data above show a very good correlation between the two analytical methods. The error of the estimate of the least squares analysis of figure 2.3-3(a) is in the order of 6×10^{-4} and the t-values for the estimate of k_{obs}° are greater than 300. The mean first order rate constant for aromatisation is $2.83 \pm 0.1 \times 10^{-2} \text{ s}^{-1}$. The semi-logarithmic analysis (see Fig 2.3-3(b)) gave a good fit also with the error in the third decimal; the mean first order rate constant of aromatisation is $2.75 \pm 0.14 \times 10^{-2} \text{ s}^{-1}$.

There is no buffer catalysis (see Fig 2.3-5); however there is an increase in rate with decreasing buffer concentration on the order of 25 %. The mean first order rate constant of aromatisation of 2-methylcyclohexa-2,4-dienol at pH 4.2 is $2.94 \pm 0.09 \times 10^{-4} \text{ s}^{-1}$ with a corresponding half-life of 24 seconds.

Figure 2.3-5: Aromatisation of 2-methylcyclohexa-2,4-dienol in 25 % FB acetate at pH 4.2: Plot of k_{obs}^o against buffer concentration

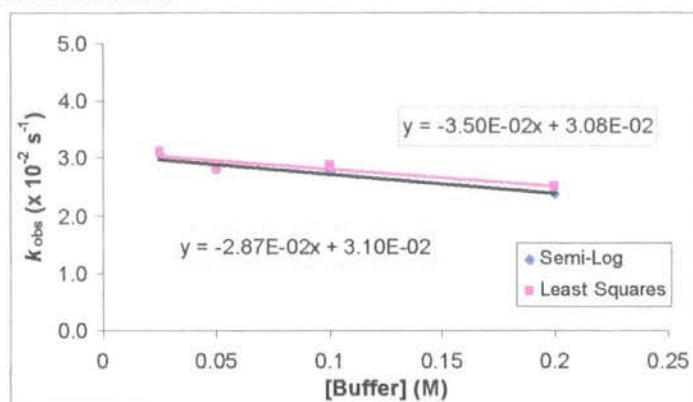
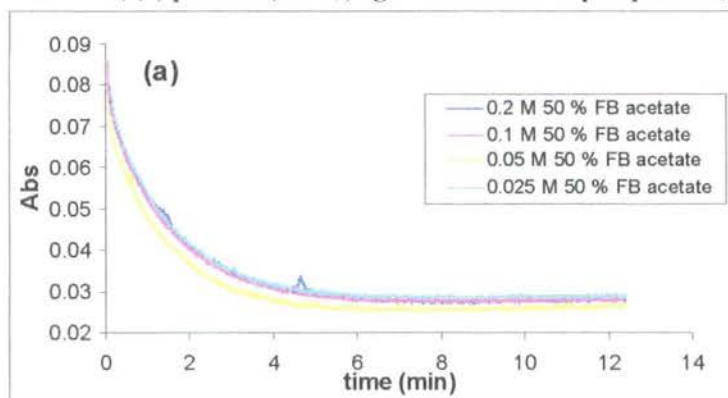
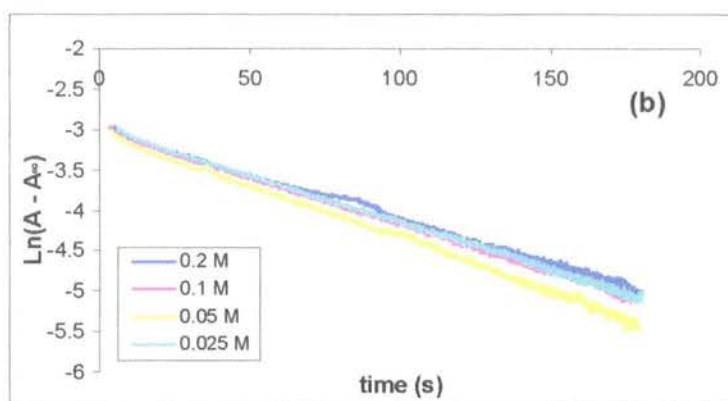


Figure 2.3-6(a) shows the change in absorbance against time at 254 nm as a result of the reaction of 2-methylcyclohexa-2,4-dienol in acetate buffer (50 % FB, pH 4.6). A corresponding semi-logarithmic plot of $\Delta A = A - A_{\infty}$ against time is shown in Figure 2.3-6 (b) where A_{∞} refers to the absorbance at the end of the reaction.

Figure 2.3-6: Aromatisation of 2-methylcyclohexa-2,4-dienol in 50 % FB acetate at pH 4.2. (a) Plot of absorbance versus time; (b) plot of $\ln(A - A_{\infty})$ against time with slope equal to k_{obs}^o





The table below summarises the first order rate constants of aromatisation of 2-methylcyclohexa-2,4-dienol in 50 % FB acetate at pH 4.6. At this pH the dehydration reaction of 1-methylcyclohexa-2,4-dienol is too fast to be monitored by standard UV-vis methods.

Table 2.3-2: Summary of first order rate constants for the aromatisation of 2-methylcyclohexa-2,4-dienol (2.13) in 50 % FB acetate at pH 4.6.

[Buffer] (M)	pH ^(b)	[H ⁺] ^(c) x 10 ⁻⁶ M	Semi-log Plot			Least Squares Plot		
			$k_{\text{obs}}^{\text{o(d)}}$ (x 10 ⁻²) s ⁻¹	R ²	$k_{\text{int}}^{\text{o(e)}}$ (x 10 ⁻²) s ⁻¹	$k_{\text{obs}}^{\text{o(f)}}$ (x 10 ⁻²) s ⁻¹	R ²	$k_{\text{int}}^{\text{o(e)}}$ (x 10 ⁻²) s ⁻¹
0.20	4.58	2.63	1.12	0.998		1.10	0.998	
0.10	4.54	2.88	1.17	0.998	1.23	1.18	0.999	1.24
0.05	4.56	2.75	1.28	0.998	(1.18 ^(g))	1.24	0.999	(1.18 ^(g))
0.025	4.56	2.75	1.16	0.999		1.19	0.998	

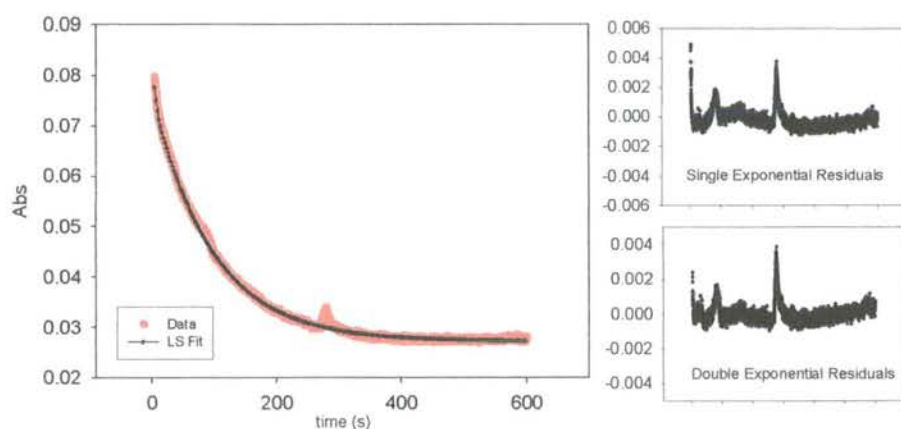
(a) Measurements were made at a substrate concentration of 0.05 mM and 1 % acetonitrile (b) pH was determined using a MeterLab™ PHM 290 pH-Stat Controller equipped with a radiometer (pH 4 - 7 - 10 @ 25 °C) combination electrode (type pHC4006) with a saturated LiTCA filling solution. (c) [H⁺] was calculated using $[H^+] = 10^{-(\text{pH}/\gamma_{\text{H}})}$ where $\gamma_{\text{H}} = 1$ is the activity coefficient of the hydronium ion under our experimental conditions. (d) The value of the first-order rate constant (k_{obs}), was obtained from the slope of the plot of $\ln(A - A_{\infty})$ against time in Figure 2.3-5(b). (e) k_{int} is defined as the intercept of the plot of k_{obs} against buffer concentration Figure 2.3-7. (f) The value of the first-order rate constant (k_{obs}), was obtained from the least squares analysis of Figure 2.3-5(a). (g) Mean of $k_{\text{obs}}^{\text{o}}$

The least squares regression of data in Figure 2.3-6(a) shows an excellent fit with t-values for the estimate of a k_{obs} value greater than 800 and the error of the estimate in the order of 5×10^{-4} . The mean first order rate constant of aromatisation from the least squares data is $1.18 \pm 0.03 \times 10^{-2} \text{ s}^{-1}$.

The semi-logarithmic plots (Fig 2.3-6(b)) show a reasonable fit with the error in the third decimal. The beginning of the plot shows non-linearity which could be the very fast aromatisation reaction of 1-methylcyclohexa-2,4-dienol. The mean first order rate constant of aromatisation from the semi-logarithmic analysis is $1.18 \pm 0.04 \times 10^{-2} \text{ s}^{-1}$.

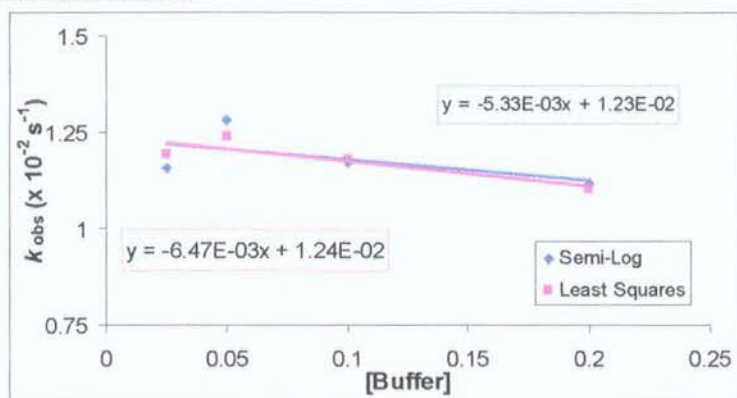
The only buffer concentration at pH 4.6 where both reactions could be followed is at 0.20 M and this yields a first order rate constant for the dehydration of 1-methylcyclohexa-2,4-dienol of 0.2 s^{-1} , corresponding to a half-life of 3 seconds. However, the t-value for the estimate of this rate constant is only 14. The double exponential.l regression is shown below (Fig 2.3-7). The residuals (inset Fig 2.3-7) show that the double exponential equation better fits the initial stages of the reaction. As the half-life of the reaction of 1-methylcyclohexa-2,4-dienol at pH 4.6 are in general too short, the results for 2-methylcyclohexa-2,4-dienol are only shown.

Figure 2.3-7: Double exponential fit of data from 0.2 M 50 % FB acetate (pH = 4.58) showing the fast dehydration reaction of 1-methylcyclohexa-2,4-dienol. (Inset: single and double exponential residuals).



The buffer catalysis plot (Fig 2.3-8) shows no buffer catalysis. There are negative slopes on the order of $-6 \times 10^{-3} \text{ M}^{-1}\text{s}^{-1}$, with a change in the first order rate constants with decreasing buffer concentration on the order of 8 %. The mean first order rate constant of aromatisation of 2-methylcyclohexa-2,4-dienol at pH 4.6 is $1.21 \pm 0.02 \times 10^{-2} \text{ s}^{-1}$.

Figure 2.3-8: Aromatisation of 2-methylcyclohexa-2,4-dienol in 50 % FB acetate at pH 4.2: Plot of k_{obs} against buffer concentration

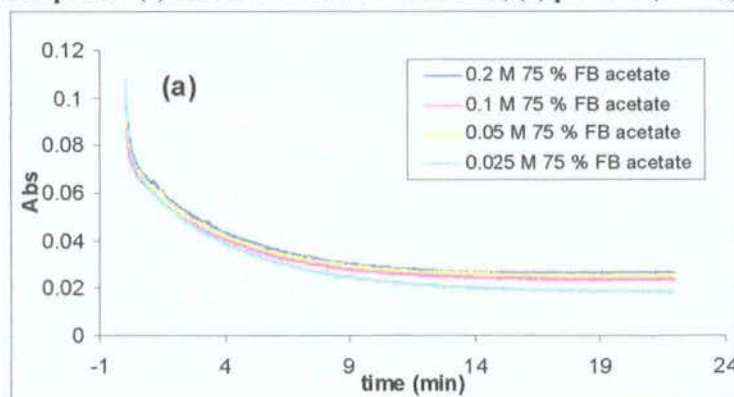


At pH values above ~ 4.9 , the contribution of the faster reaction of the *ipso*-hydrate became significant. This could be deduced on the basis of whether the data was fitted better by a double exponential least squares analysis rather than a single exponential analysis. To extract the two first order rate constants a double exponential least squares fit of the experimental data for absorbance versus time is used (eqn 2.3).

$$y = y_0 + Ae^{-bx} + Ce^{-dx} \quad \text{Equation 2-3}$$

Figure 2.3-9(a)(below) shows the experimental data from the aromatisation of 2-methylcyclohexa-2,4-dienol and 1-methylcyclohexa-2,4-dienol in acetate buffer (75 % FB, pH 4.9). A corresponding semi-logarithmic plot of $\Delta A = A - A_{\infty}$ against time is shown in Figure 2.3-9(b) where A_{∞} refers to the absorbance at the end of the reaction.

Figure 2.3-9: Aromatisation of 2-methylcyclohexa-2,4-dienol and 1-methylcyclohexa-2,4-dienol in 75 % FB acetate at pH 4.9 (a) Plot of absorbance versus time; (b) plot of $\ln(A - A_{\infty})$ against time



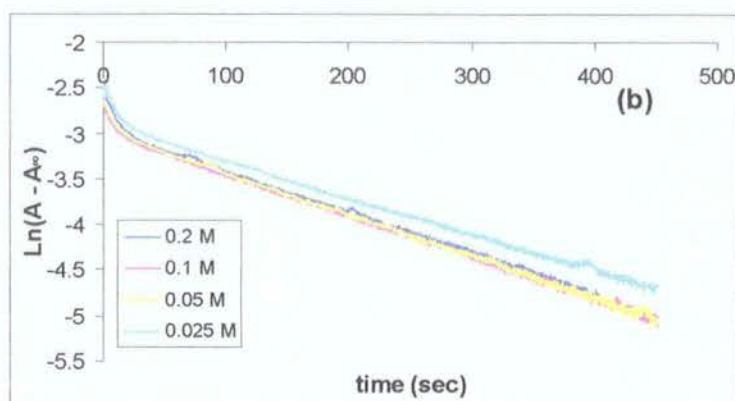


Figure 2.3-10 below shows an example of a double exponential regression. The red line is the recorded data and the black line is the regression line. The residuals (Fig 2.3-9 (inset)) clearly show the error in the fit of the initial data using a single exponential equation. The double exponential residuals show the error of the regression line is ± 0.002 whereas in the single exponential case the error is ± 0.006 .

Figure 2.3-10: Double exponential fit of the 0.2 M 75 % FB acetate at pH 4.93 data. (Inset: single and double exponential residuals).

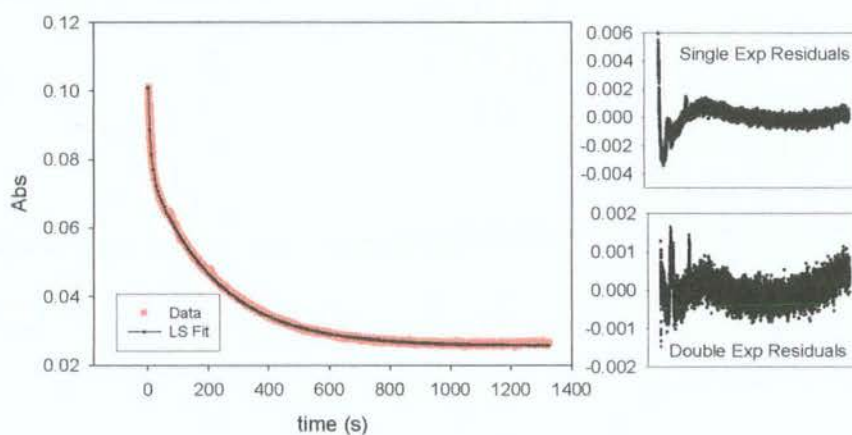


Table 2.3-3 (below) summarises the first order rate constants for aromatisation of 2-methylcyclohexa-2,4-dienol and 1-methylcyclohexa-2,4-dienol in 75 % FB acetate at pH 4.9. The single and double exponential fits are compared.

Table 2.3-3: First-order rate constants for aromatisation of *ipso* and *ortho* toluene hydrate in 75% FB acetate buffers (0.2 – 0.025 M) at 25 °C and I = 0.5 M (NaClO₄)^(a)

[Buffer] (M)	pH ^(b)	[H ⁺] ^(c) (x 10 ⁻⁵) M	Single Exponential ^(d)		Double Exponential ^(e)		
			k_{obs}^o (x 10 ⁻⁴) s ⁻¹	R ²	k_{obs}^i (x 10 ⁻²) s ⁻¹	k_{obs}^o (x 10 ⁻⁴) s ⁻¹	R ²
0.2	4.93	3.11	4.92	0.9954	1.19	4.49	0.9997
0.1	4.93	3.10	4.79	0.9972	1.24	4.46	0.9998
0.05	4.94	3.03	4.93	0.9965	1.07	4.53	0.9998
0.025	4.95	3.00	4.50	0.9937	1.10	4.06	0.9997

(a) Measurements were made at a substrate concentration of 0.05 mM and 1 % acetonitrile (b) pH was determined using a MeterLabTM PHM 290 pH-Stat Controller equipped with a radiometer (pH 4 - 7 - 10 @ 25 °C) combination electrode (type pHC4006) with a saturated LiTCA filling solution. (c) [H⁺] was calculated using $[H^+] = 10^{-(pH/\gamma_H)}$ where $\gamma_H = 1$ is the activity coefficient of the hydronium ion under our experimental conditions. (d) The value of the first-order rate constant (k_{obs}), was obtained from the slope of the plot of $\ln(A - A_\infty)$ against time in Figure 2.3-9(b). (e) The value of the first-order rate constant (k_{obs}^o), was obtained from the least squares analysis of Figure 2.3-9(a) using equation 2.3.

The data above clearly show that a double exponential equation fits the data more accurately. The t-values for the estimation of the first rate constant are smaller (>300) than for the second (> 1500). The t-values for the estimate of k_{obs} from the single exponential fit are in the order of 600; however, the error of the estimate is 5-fold higher for the single exponential fit than for the double, 1.4×10^{-3} and 2.8×10^{-4} respectively.

Table 2.3-4 (below) compares the semi-logarithmic and the double exponential least squares analyses of the data from the dehydration in reaction of 2-methylcyclohexa-2,4-dienol (k_{obs}^o) and 1-methylcyclohexa-2,4-dienol (k_{obs}^i) in 75 % FB acetate at pH 4.9.

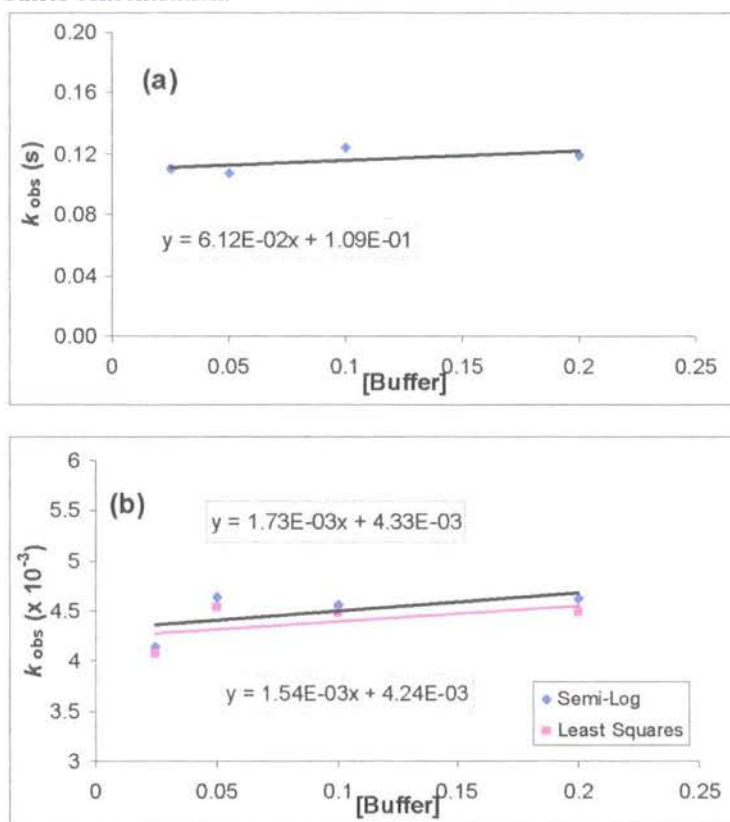
Table 2.3-4: First-order rate constants for aromatisation of toluene hydrate (2.13 & 2.14) using both semi-log and least squares analysis in 75 % FB acetate buffers (0.2 – 0.025 M) at 25 °C and I= 0.5 M (NaClO₄)^(a)

[Buffer] (M)	pH ^(b)	Semi-log Plot			Least Squares Plot			
		$k_{\text{obs}}^{(c)}$ ($\times 10^{-4}$) s ⁻¹	R ²	$k_{\text{int}}^{(d)}$ ($\times 10^{-4}$) s ⁻¹	$k_{\text{obs}}^{i(e)}$ ($\times 10^{-2}$) s ⁻¹	$k_{\text{obs}}^{o(e)}$ ($\times 10^{-4}$) s ⁻¹	R ²	$k_{\text{int}}^{(d)}$ (s ⁻¹)
0.2	4.93	4.61	0.9935		1.19	4.49	0.9997	4.24×10^{-3}
0.1	4.93	4.57	0.9966	4.33	1.24	4.46	0.9998	(4.39×10^{-3})
0.05	4.94	4.64	0.9959	(4.49)	1.07	4.53	0.9998	1.09×10^{-2}
0.025	4.95	4.14	0.9900		1.10	4.06	0.9997	(1.15×10^{-2})

(a) Measurements were made at a substrate concentration of 0.05 mM and 1 % acetonitrile (b) pH was determined using a MeterLabTM PHM 290 pH-Stat Controller equipped with a radiometer (pH 4 - 7 - 10 @ 25 °C) combination electrode (type pHC4006) with a saturated LiTCA filling solution. (c) The value of the first-order rate constant (k_{obs}), was obtained from the semi-logarithmic analysis of Figure 2.3-9(a). (d) k_{int} is defined as the intercept of the plot of k_{obs} against buffer concentration Figure 2.3-11(a & b). (e) The value of the first-order rate constant (k_{obs}), was obtained from the least squares analysis of Figure 2.3-9(a) using equation 2.3

The least squares analysis of the data in Figure 2.3-9(a) gives an accurate fit and predicts the two rate constants accurately as discussed above. As with the single exponential analysed data above, the semi-logarithmic analysis (Fig 2.3-9(b)) fails to take account of the two reactions occurring simultaneously. Figure 2.3-9(b) clearly shows non-linearity confirming the presence of a second reaction. The slope of the line only predicts the rate of the slower reaction. There is no evidence of any buffer catalysis (Fig 2.3-10(a & b)) for the reactions of both hydrates. In both cases the slope is negative and the change in first order rate constant with decreasing buffer concentration is negligible at this pH.

Figure 2.3-11: Aromatisation of 2-methylcyclohexa-2,4-dienol and 1-methylcyclohexa-2,4-dienol in 90 % FB acetate at pH 5.6: (a) plot of k_{obs}^i (*ipso*) against buffer concentration (b) plot of k_{obs}^o (*ortho*) against buffer concentration.



The mean first order rate constant of aromatisation of 1-methylcyclohexa-2,4-dienol at pH 4.9 is $0.12 \pm 0.004 \text{ s}^{-1}$. This corresponds to a half-life of 6 seconds. The mean first order rate constant of aromatisation of 2-methylcyclohexa-2,4-dienol is $4.39 \pm 0.11 \times 10^{-3} \text{ s}^{-1}$. This corresponds to a half-life of 158 seconds.

An example of the double exponential least squares analysis of the data from 90 % FB acetate (pH = 5.55) is shown below in Figure 2.3-12. The red line shows the collected data and the black line shows the double exponential regression line. The single and double exponential residuals are also shown (Fig 2.3-12(inset)). The single exponential equation clearly does not fit the initial data. The double exponential residuals show the error of the regression line is ± 0.002 whereas in the single exponential case the error is ± 0.02 .

Figure 2.3-12: Double exponential fit of the aromatisation of 2-methylcyclohexa-2,4-dienol and 1-methylcyclohexa-2,4-dienol in 0.2 M 90 % FB acetate at pH 5.55 data. (Inset: single and double exponential residuals).

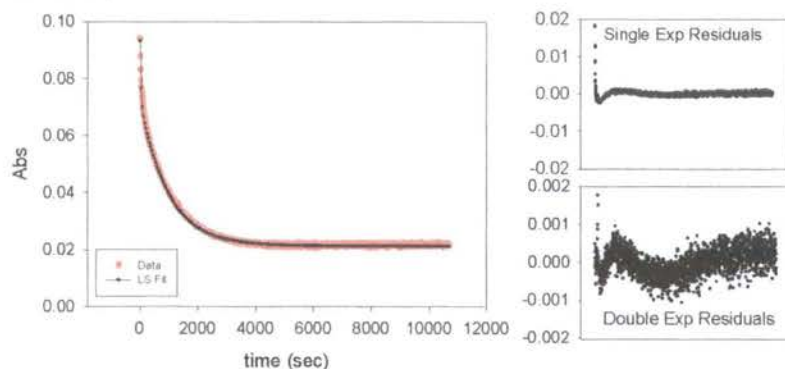


Figure 2.3-13 (below) shows the experimental data from the aromatisation of 2-methylcyclohexa-2,4-dienol and 1-methylcyclohexa-2,4-dienol in acetate buffer (90 % FB, pH 5.6). A corresponding semi-logarithmic plot of $\Delta A = A - A_{\infty}$ against time is shown in Figure 2.3-6 (b) where A_{∞} refers to the absorbance at the end of the reaction.

Figure 2.3-13: Aromatisation of 2-methylcyclohexa-2,4-dienol and 1-methylcyclohexa-2,4-dienol in acetate buffer (90 % FB, pH 5.6) at 25 °C and I = 0.5 M (NaClO_4) (a) Plot of absorbance versus time; (b) plot of $\ln(A - A_{\infty})$ against time

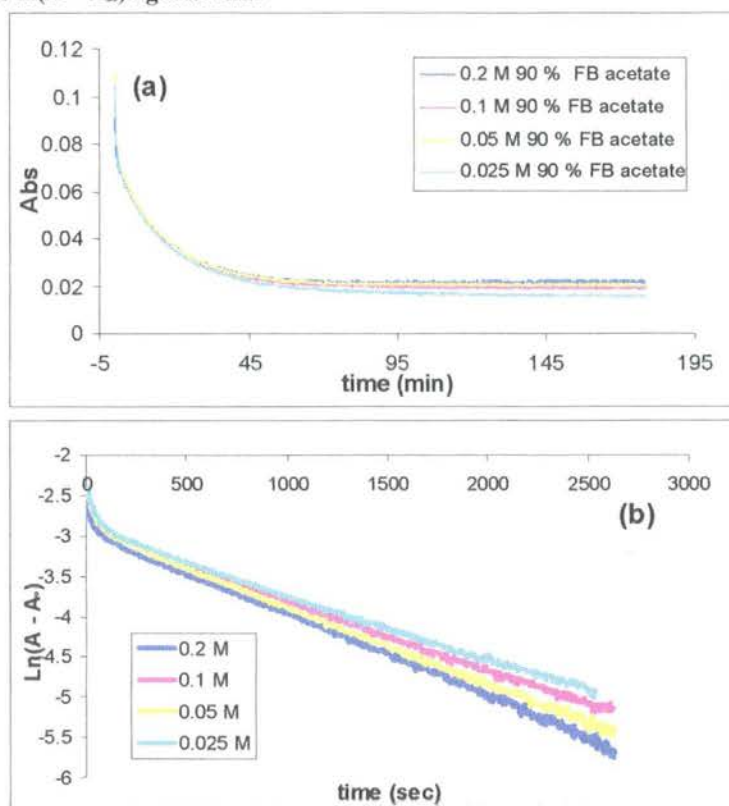


Table 2.3-5 (below) summarises the first order rate constants of aromatisation of 2-methylcyclohexa-2,4-dienol and 1-methylcyclohexa-2,4-dienol in 90 % FB acetate at pH 5.6.

Table 2.3-5: First-order rate constants for aromatisation of toluene hydrate in 90 % FB acetate buffers (0.2 – 0.025 M) at 25 °C and I = 0.5 M (NaClO₄)^(a)

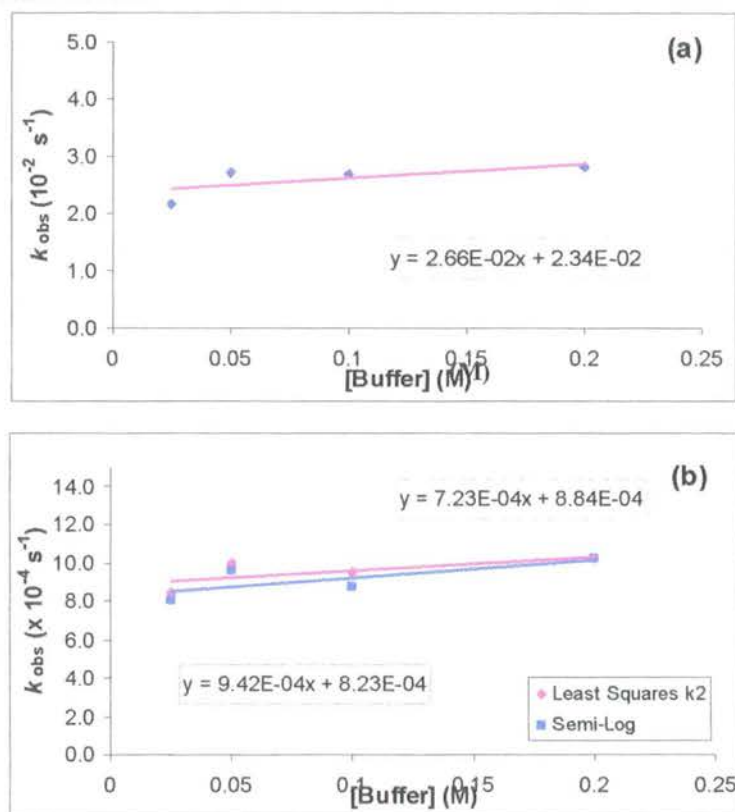
[Buffer] (M)	pH ^(b)	[H ⁺] ^(c) (x 10 ⁻⁶)	k_{obs}^i ^(d) (x 10 ⁻²) s ⁻¹	k_{obs}^o ^(d) (x 10 ⁻⁴) s ⁻¹	R ²	k_{int}^i ^(e) (s ⁻¹)	k_{int}^o ^(e) (s ⁻¹)
0.2	5.55	2.82	2.81	10.20	0.9994		
2.1	5.55	2.82	2.68	9.51	0.9997	8.23 x 10 ⁻⁴	2.34 x 10 ⁻²
0.05	5.54	2.88	2.72	9.98	0.9997	(9.52 x 10 ^{-4(f)})	(2.59 x 10 ^{-2(f)})
0.025	5.56	2.75	2.16	8.38	0.9994		

(a) Measurements were made at a substrate concentration of 0.05 mM and 1 % acetonitrile (b) pH was determined using a MeterLabTM PHM 290 pH-Stat Controller equipped with a radiometer (pH 4 - 7 - 10 @ 25 °C) combination electrode (type pHC4006) with a saturated LiTCA filling solution. (c) [H⁺] was calculated using $[H^+] = 10^{-(\text{pH} / \gamma_H)}$ where $\gamma_H = 1$ is the activity coefficient of the hydronium ion under the experimental conditions. (d) The value of the first-order rate constant (k_{obs}), was obtained from the least squares analysis of Figure 2.3-13 (a). (e) k_{int} is defined as the intercept of the plot of k_{obs} against buffer concentration Figure 2.3-14(a & b). (f) Mean of k_{obs}

As discussed above there are two reactions occurring simultaneously at this pH and so the single exponential regression and semi-logarithmic plots are unable to take account of this. The double exponential least squares analysis, using equation 2.3, of the data in Figure 2.3-13(a) shows an excellent fit with t-values for the estimate of the first rate constant in the order of 90 and 600 for the second rate constant. The error of the estimate for the double exponential fit is 3×10^{-4} , whereas for the single exponential fit the error was on the order of 1.2×10^{-3} .

The semi-logarithmic plot (Fig 2.3-13(b)) shows non-linearity, further evidence for the presence of a second reaction. The buffer catalysis plots in Figure 2.3-14 (a & b) show a slightly positive slope, however, this slope is negligible when compared with the change in first order rate constants over the pH-range.

Figure 2.3-14: Aromatisation of 2-methylcyclohexa-2,4-dienol and 1-methylcyclohexa-2,4-dienol in 90 % FB acetate at pH 5.6: (a) plot of k_{obs} (*ipso*) against buffer concentration; (d) plot of k_{obs} (*ortho*) against buffer concentration



The mean first order rate constant for the aromatisation of 1-methylcyclohexa-2,4-dienol at pH 5.6 is $2.59 \pm 0.15 \times 10^{-2} \text{ s}^{-1}$. The mean first order rate constant for the aromatisation of 2-methylcyclohexa-2,4-dienol is $9.52 \pm 0.40 \times 10^{-4} \text{ s}^{-1}$. These correspond to half-lives of 27 and 728 seconds respectively.

An example of the double exponential least squares analysis of the data from 10 % FB phosphate (pH = 5.60) is shown below in figure 2.3-15. The green line shows the collected data and the black line shows the double exponential regression line. The single and double exponential residuals are also shown (Fig 2.3-15 (inset)). The single exponential equation clearly does not fit the initial data. The double exponential residuals show the error of the regression line is ± 0.002 whereas in the single exponential case the error is ± 0.02 .

Figure 2.3-15: Double exponential fit of the aromatisation reaction of 2-methylcyclohexa-2,4-dienol and 1-methylcyclohexa-2,4-dienol in 0.1 M 10 % FB phosphate at pH 5.60. (Inset: single and double exponential residuals).

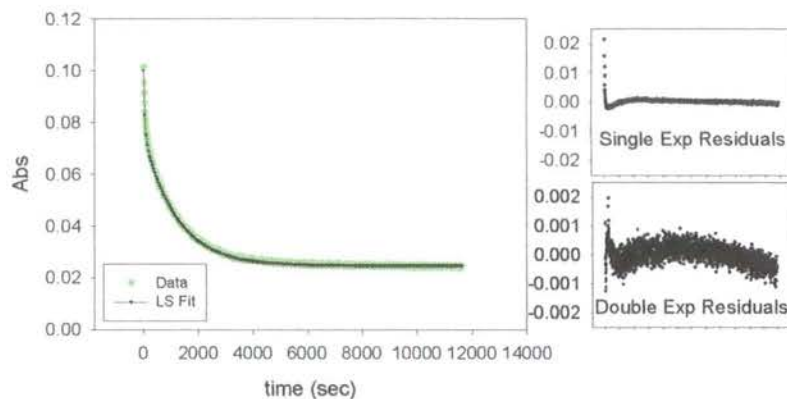
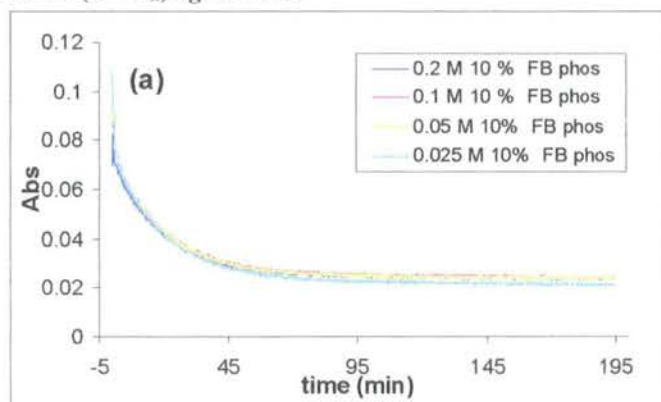


Figure 2.3-16 (a) (below) shows the experimental data from the aromatisation reactions of 2-methylcyclohexa-2,4-dienol and 1-methylcyclohexa-2,4-dienol in phosphate buffer (10 % FB, pH 5.6) at 25 °C. A corresponding semi-logarithmic plot of $\Delta A = A - A_{\infty}$ against time is shown in Figure 2.3-16(b) where A_{∞} refers to the absorbance at the end of the reaction.

Figure 2.3-16: Aromatisation of 2-methylcyclohexa-2,4-dienol and 1-methylcyclohexa-2,4-dienol in phosphate buffer (10% FB, pH 5.6) at 25 °C and $I = 0.5 \text{ M M} (\text{NaClO}_4)$ (a) Plot of absorbance versus time; (b) plot of $\ln(A - A_{\infty})$ against time



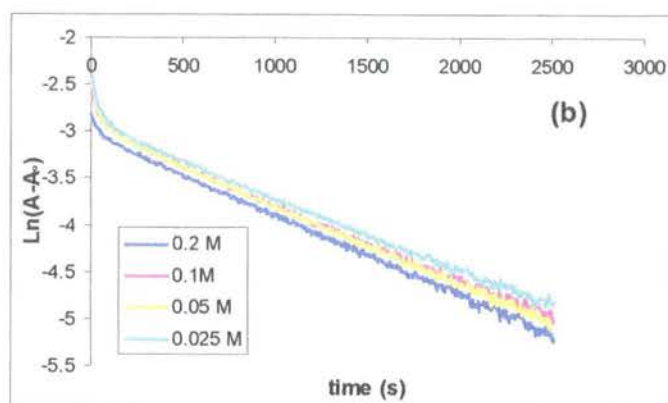


Table 2.3-6 (below) summarises the first order rate constants for the aromatisation of 2-methylcyclohexa-2,4-dienol and 1-methylcyclohexa-2,4-dienol in 10 % FB phosphate at pH 5.6.

Table 2.3-6: First-order rate constants for aromatisation of *ipso* and *ortho* toluene hydrate using least squares analysis in 10 % FB phosphate buffers (0.2 – 0.025 M) at 25 °C and I = 0.5 M (NaClO₄)^(a).

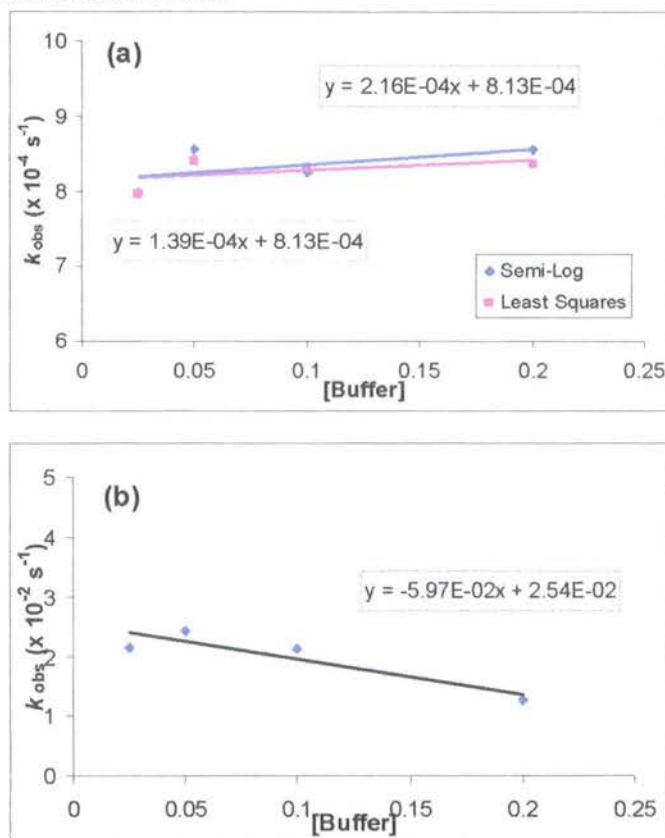
[Buffer] (M)	pH ^(b)	[H ⁺] ^(c) (x 10 ⁻⁶)	$k_{\text{obs}}^{\beta(d)}$ (x 10 ⁻²) s ⁻¹	$k_{\text{obs}}^{\alpha(d)}$ (x 10 ⁻⁴) s ⁻¹	R ²	$k_{\text{int}}^{i(e)}$ (s ⁻¹)	$k_{\text{int}}^{\alpha(e)}$ (s ⁻¹)
0.2	5.59	7.82	1.25	8.35	0.999		
0.1	5.60	7.60	2.12	8.32	0.999	2.54 x 10 ⁻²	8.13 x 10 ⁻⁴
0.05	5.61	7.50	2.42	8.40	0.999	(1.99 x 10 ^{-2(f)})	(8.26 x 10 ^{-4(f)})
0.025	5.62	7.24	2.15	7.76	0.999		

(a) Measurements were made at a substrate concentration of 0.05 mM and 1 % acetonitrile (b) pH was determined using a MeterLabTM PHM 290 pH-Stat Controller equipped with a radiometer (pH 4 - 7 - 10 @ 25 °C) combination electrode (type pHC4006) with a saturated LiTCA filling solution. (c) [H⁺] was calculated using $[H^+] = 10^{-(\text{pH}/\gamma_H)}$ where $\gamma_H = 1$ is the activity coefficient of the hydronium ion under the experimental conditions. (d) The value of the first-order rate constant (k_{obs}), was obtained from the least squares analysis of Figure 2.3-16 (a). (e) k_{int} is defined as the intercept of the plot of k_{obs} against buffer concentration Figure 2.3-17(a & b). (f) Mean of k_{obs}

The double exponential least squares analysis of Figure 2.3-16(a) shows a very good fit with the t-values for the estimate of the first rate constant in the order of 75 and 615 for the second rate constant. The error of the estimate of the single exponential regression is 1.1×10^{-3} whereas for the double exponential regression it is 2.8×10^{-4} . The semi-logarithmic plot (Fig 2.3-16(b)) shows a poor correlation due to its non-linearity.

The buffer catalysis plots (Fig 2.3-16(a) and (b)) show no evidence of buffer catalysis. There is an overall increase in rate with decreasing buffer concentration for the first rate constant with the slopes on the order of $2 \times 10^{-4} \text{ M}^{-1} \text{ s}^{-1}$.

Figure 2.3-17: Aromatisation of 2-methylcyclohexa-2,4-dienol and 1-methylcyclohexa-2,4-dienol in 10 % FB phosphate at pH 5.6 (a) plot of $k_{\text{obs}}(\textit{ipso})$ against buffer concentration; (b) plot of $k_{\text{obs}}(\textit{ortho})$ against buffer concentration.



The mean of the first order rate constants for aromatisation of 1-methylcyclohexa-2,4-dienol at pH 5.6 is $1.99 \pm 0.3 \times 10^{-2} \text{ s}^{-1}$. The mean first order rate constant of aromatisation of 2-methylcyclohexa-2,4-dienol is $8.26 \pm 0.1 \times 10^{-4} \text{ s}^{-1}$. These correspond to half-lives of 35 and 839 seconds respectively.

An example of the double exponential least squares analysis of the data from 25 % FB phosphate (pH = 6.09) is shown below in Figure 2.3-18. The green line shows the collected data and the black line shows the double exponential regression line. The single and double exponential residuals are also shown (Fig 2.3-18(inset)). The single

exponential equation clearly does not fit the initial data. The double exponential residuals show the error of the regression line is ± 0.002 whereas in the single exponential case the error is ± 0.02 .

Figure 2.3-18: Double exponential fit of the aromatisation reaction of 2-methylcyclohexa-2,4-dienol and 1-methylcyclohexa-2,4-dienol in 0.1 M 25 % FB phosphate at pH 6.09. (Inset: single and double exponential residuals).

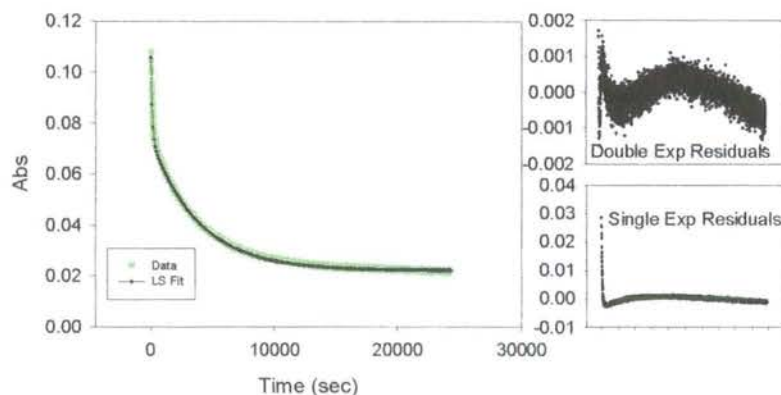
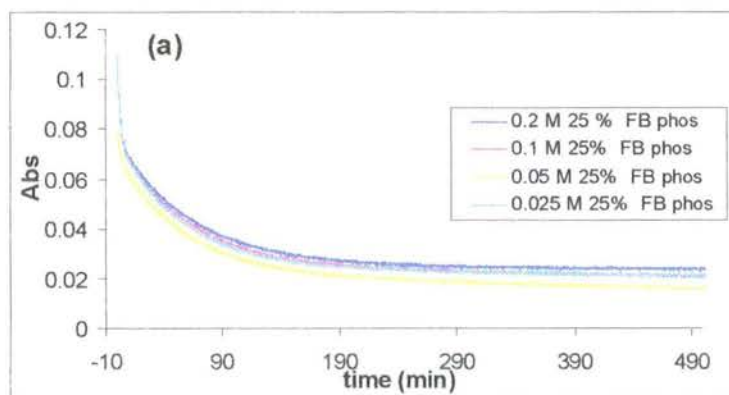
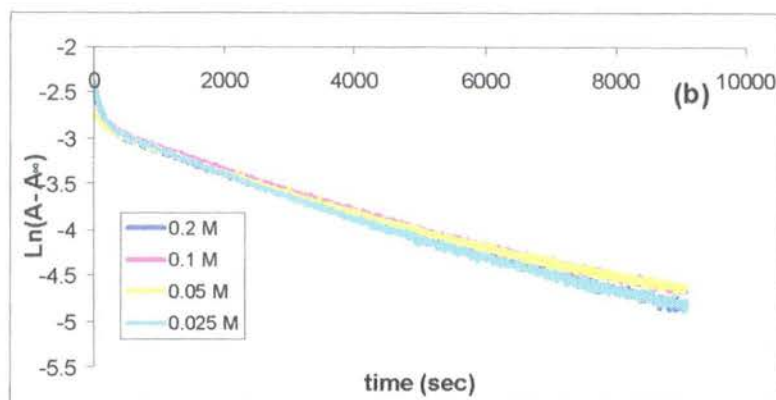


Figure 2.3-19(a) (below) shows the experimental data from the aromatisation of 2-methylcyclohexa-2,4-dienol and 1-methylcyclohexa-2,4-dienol in phosphate buffer (25 % FB, pH 6.1) at 25 °C. A corresponding semi-logarithmic plot of $\Delta A = A - A_{\infty}$ against time is shown in Figure 2.3-19(b) where A_{∞} refers to the absorbance at the end of the reaction.

Figure 2.3-19: Aromatisation of 2-methylcyclohexa-2,4-dienol and 1-methylcyclohexa-2,4-dienol in 25 % FB phosphate at pH 6.1 (a) Plot of absorbance versus time; (b) plot of $\ln(A - A_{\infty})$ against time





The table below shows the rate of aromatisation of 2-methylcyclohexa-2,4-dienol and 1-methylcyclohexa-2,4-dienol in phosphate buffer (25 % FB, pH 6.1).

Table 2.3-7: First-order rate constants for aromatisation of toluene hydrate obtained using least squares analysis in 25 % FB phosphate buffers (0.2 – 0.025 M) at 25 °C and I = 0.5 M (NaOCl₄)^(a).

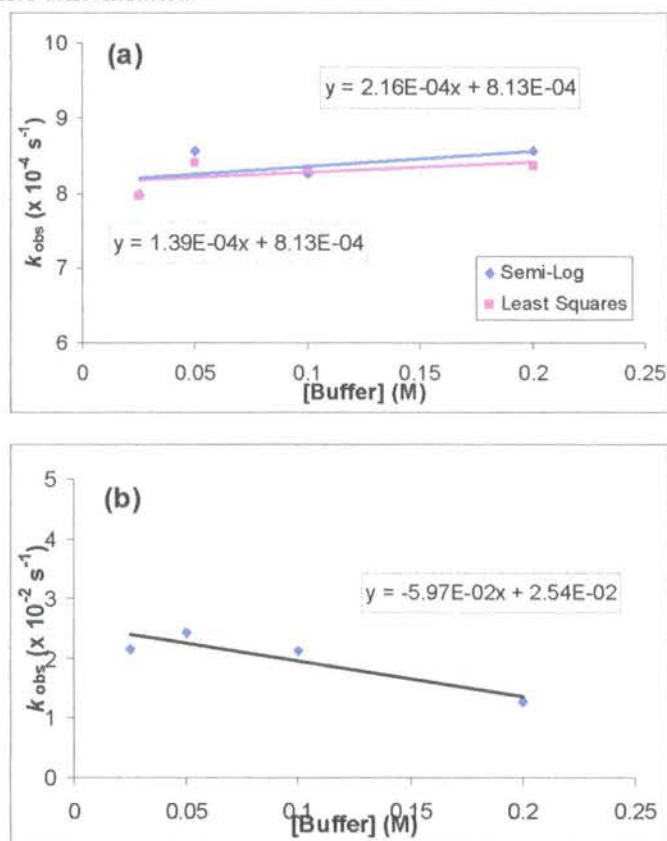
[Buffer] (M)	pH ^(b)	[H ⁺] ^(c) (x 10 ⁻⁶) (M)	$k_{\text{obs}}^{i(d)}$ (x 10 ⁻²) s ⁻¹	$k_{\text{obs}}^{o(d)}$ (x 10 ⁻⁴) s ⁻¹	R ²	$k_{\text{int}}^{i(e)}$ (s ⁻¹)	$k_{\text{int}}^{\alpha(e)}$ (s ⁻¹)
0.20	6.09	8.22	8.20	2.57	0.9998		
0.10	6.08	8.28	8.21	2.62	0.9995	4.96 x 10 ⁻³	2.43 x 10 ⁻⁴
0.05	6.08	8.34	-	1.95	0.9992	(6.31 x 10 ⁻³)	(2.49 x 10 ⁻⁴)
0.025	6.07	8.45	8.82	2.80	0.9996		

(a) Measurements were made at a substrate concentration of 0.05 mM and 1 % acetonitrile (b) pH was measured using an X electrode with a 5 M LiTCA filling solution pH was determined using a MeterLabTM PHM 290 pH-Stat Controller equipped with a radiometer (pH 4 - 7 - 10 @ 25 °C) combination electrode (type pHC4006) with a saturated LiTCA filling solution. (c) [H⁺] was calculated using $[H^+] = 10^{-(\text{pH} / \gamma_H)}$ where $\gamma_H = 1$ is the activity coefficient of the hydronium ion under the experimental conditions. (d) The value of the first-order rate constant (k_{obs}), was obtained from the least squares analysis of Figure 2.3-19(a). (e) k_{int} is defined as the intercept of the plot of k_{obs} against buffer concentration Figure 2.3-20(a&b). (f) Mean of k_{obs}

The data above shows the results from the semi-logarithmic and least squares analysis of the aromatisation reactions at pH 6.1. The double exponential least squares fit of the data in Fig 2.3-19(a) has t-values for the estimate of the first order rate constant of 120 and 760 for the second. The single exponential regression shows error of the estimate in the order of 1.5×10^{-3} whereas the double exponential regression line has an error of 4×10^{-4} . The semi-logarithmic plot (see Fig 2.3-19(b)) clearly shows non-linearity and so only estimates one rate constant.

The buffer catalysis plots (Fig 2.3-20(a & b) show no evidence of buffer catalysis. There is an 8 % increase in the value of the first order rate constant with decreasing buffer concentration.

Figure 2.3-20: Aromatisation of 2-methylcyclohexa-2,4-dienol and 1-methylcyclohexa-2,4-dienol in 25 % FB phosphate at pH 6.1: (a) plot of k_{obs} (*ipso*) against buffer concentration; (d) plot of k_{obs} (*ortho*) against buffer concentration.



The mean of the first order rate constants for the aromatisation of 1-methylcyclohexa-2,4-dienol at pH 6.1 is $8.41 \pm 0.2 \times 10^{-3} \text{ s}^{-1}$. The mean first order rate constant of aromatisation of 2-methylcyclohexa-2,4-dienol is $2.49 \pm 0.2 \times 10^{-4} \text{ s}^{-1}$. These correspond to half-lives of 82 and 2784 seconds respectively.

Figure 2.3-21 (below) shows the experimental data for the aromatisation of 2-methylcyclohexa-2,4-dienol and 1-methylcyclohexa-2,4-dienol in phosphate buffer (50 % FB, pH 6.6) at 25 °C. A corresponding semi-logarithmic plot of $\Delta A = A - A_{\infty}$

against time is shown in Figure 2.3-16(b) where A_{∞} refers to the absorbance at the end of the reaction.

Figure 2.3-21: Aromatisation of 2-methylcyclohexa-2,4-dienol and 1-methylcyclohexa-2,4-dienol in 50 % FB phosphate at pH 6.6 (a) Plot of absorbance versus time; (b) plot of $\ln(A - A_{\infty})$ against time

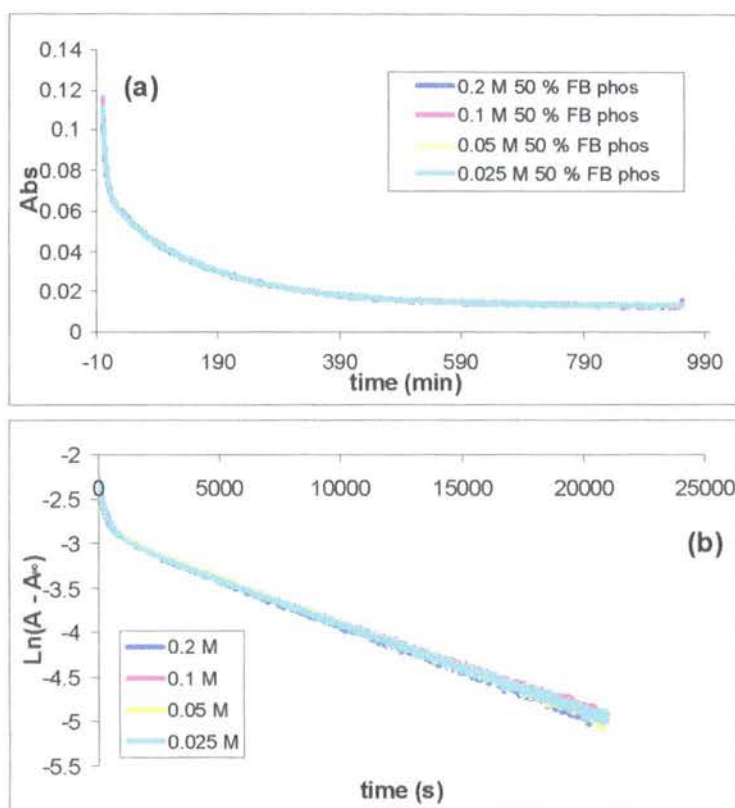


Table 2.3-8 (below) summarises the first order rate constants for the aromatisation of 2-methylcyclohexa-2,4-dienol and 1-methylcyclohexa-2,4-dienol in 50 % FB acetate at pH 6.6.

Table 2.3-8: : First-order rate constants for aromatisation of toluene hydrate obtained using both semi-log and least squares analysis in 50 % FB phosphate buffers (0.2 – 0.025 M) at 25 °C and I = 0.5 M (NaClO₄)^(a)

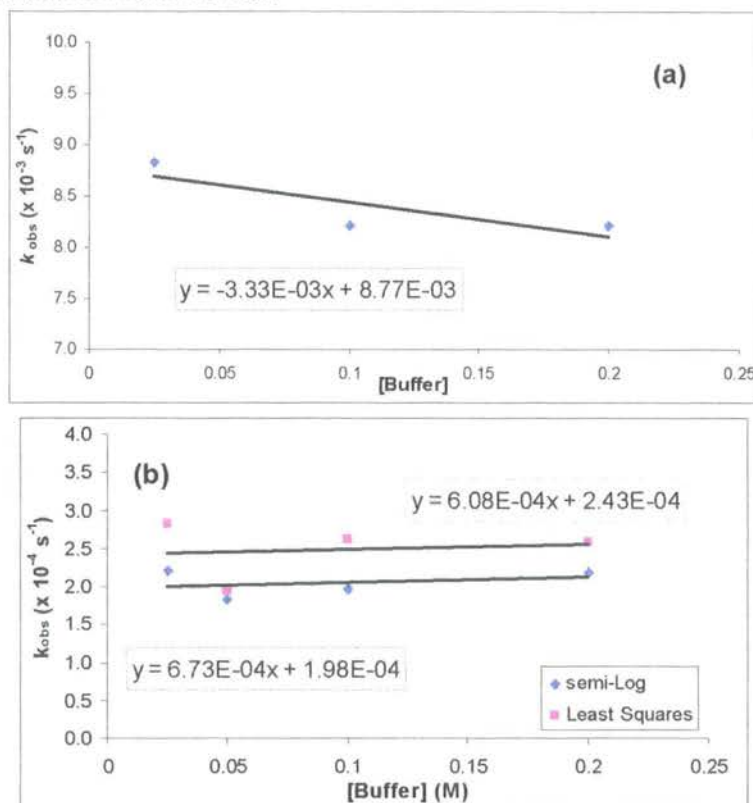
[Buffer] (M)	pH ^(b)	[H ⁺] ^(c) (x 10 ⁻⁷)	k_{obs}^i ^(d) (x 10 ⁻²) s ⁻¹	k_{obs}^o ^(d) (x 10 ⁻⁴) s ⁻¹	R ²	k_{int}^i ^(e) (s ⁻¹)	k_{int}^o ^(e) (s ⁻¹)
0.2	6.55	2.83	2.87	1.03	0.9997		
0.1	6.62	2.42	2.91	1.02	0.9998	2.83 x 10 ⁻³	1.02 x 10 ⁻⁴
0.05	6.59	2.55	2.80	1.03	0.9998	(2.85 x 10 ^{-3(g)})	(1.02 x 10 ^{-4(g)})
0.025	6.59	2.57	2.84	1.02	0.9998		

(a) Measurements were made at a substrate concentration of 0.05 mM and 1 % acetonitrile (b) pH was measured using an X electrode with a 5 M LiTCA filling solution pH was determined using a MeterLab™ PHM 290 pH-Stat Controller equipped with a radiometer (pH 4 - 7 - 10 @ 25 °C) combination electrode (type pHC4006) with a saturated LiTCA filling solution. (c) [H⁺] was calculated using $[H^+] = 10^{-(pH / \gamma_H)}$ where $\gamma_H = 1$ is the activity coefficient of the hydronium ion under the experimental conditions. (d) The value of the first-order rate constant (k_{obs}), was obtained from the least squares analysis of Figure 2.3-21(a). (e) k_{int} is defined as the intercept of the plot of k_{obs} against buffer concentration Figure 2.3-22(a&b). (f) Mean of k_{obs}

The results from the double exponential regression are shown above. The fit was very good with an error of the estimate of 3×10^{-4} and t-values for the estimate of the two rate constants of 374 and 1593; whereas for the single exponential fit the error of the estimate is 2×10^{-3} , with an average R² of 0.98. The semi-logarithmic plot (Fig 2.3-21(b)) shows non-linearity and the rate constants cannot be extracted.

The buffer catalysis plots (Fig 2.3-22(a & b) show no buffer catalysis, in fact, the rate constants show little change over the buffer range and so the values of the mean of k_{obs} and k_{int} are the same.

Figure 2.3-22: Aromatisation of 2-methylcyclohexa-2,4-dienol and 1-methylcyclohexa-2,4-dienol in 50 % FB phosphate at pH 6.6 (a) plot of $k_{\text{obs}}(\textit{ipso})$ against buffer concentration; (d) plot of $k_{\text{obs}}(\textit{ortho})$ against buffer concentration.



The mean of the first order rate constants for the aromatisation of 1-methylcyclohexa-2,4-dienol at pH 6.6 is $2.85 \pm 0.02 \times 10^{-3} \text{ s}^{-1}$. The mean of the first order rate constants for the aromatisation of 2-methylcyclohexa-2,4-dienol is $1.02 \pm 0.003 \times 10^{-4} \text{ s}^{-1}$. These correspond to half-lives of 243 and 6795 seconds respectively.

Table 2.3-9 (below) summarises the rate constants for aromatisation of 1-methylcyclohexa-2,4-dienol and 2-methylcyclohexa-2,4-dienol in acetate and phosphate buffers (pH 4.2 – 6.6).

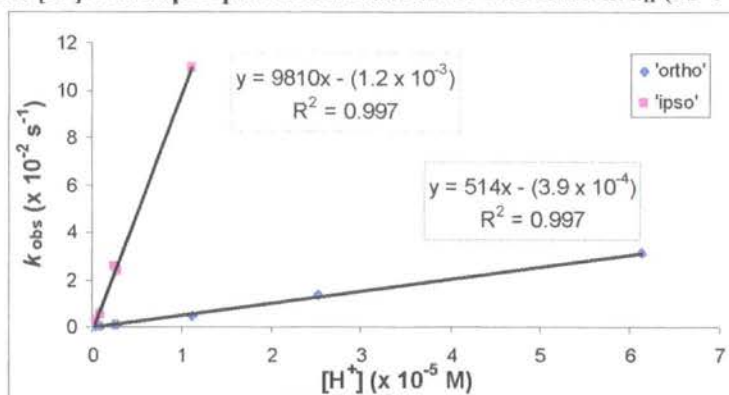
Table 2.3-9: Summary of the first-order rate constants for the aromatisation of 1-methylcyclohexa-2,4-dienol and 2-methylcyclohexa-2,4-dienol in acetate and phosphate buffers, I = 0.5 M (NaClO₄) at 25 °C

pH ^(a)	[H ⁺] ^(b) M	k_{int}^o s ⁻¹	$k_{\text{H}}^{o(c)}$ M ⁻¹ s ⁻¹	k_{int}^i s ⁻¹	$k_{\text{H}}^{i(c)}$ M ⁻¹ s ⁻¹
4.21	6.14 x 10 ⁻⁵	3.10 x 10 ⁻²		-	
4.60	2.51 x 10 ⁻⁵	1.34 x 10 ⁻²		-	
4.95	1.12 x 10 ⁻⁵	4.24 x 10 ⁻³	514	1.09 x 10 ⁻¹	9810
5.56	2.75 x 10 ⁻⁶	8.84 x 10 ⁻⁴		2.34 x 10 ⁻²	
5.62	2.40 x 10 ⁻⁶	8.13 x 10 ⁻⁴		2.54 x 10 ⁻²	
6.07	8.45 x 10 ⁻⁷	2.43 x 10 ⁻⁴		4.96 x 10 ⁻³	
6.59	2.57 x 10 ⁻⁷	1.02 x 10 ⁻⁴		2.83 x 10 ⁻³	

(a) Measurement of pH using a MeterLabTM PHM 290 pH-Stat Controller equipped with a radiometer (pH 4 - 7 - 10 @ 25 °C) combination electrode (type pHC4006) electrode with a 5 M LiTCA filling solution. (b) [H⁺] was calculated using $[H^+] = 10^{-(\text{pH}/\gamma_{\text{H}})}$ where $\gamma_{\text{H}} = 1$ is the activity coefficient of the hydronium ion under the experimental conditions. (c) The value of the second-order rate constant (k_{H}) is the slope of the plot of k_{int} against [H⁺].

As with the previous hydrate, the second-order rate constant for acid-catalysed aromatisation, k_{H} , could be obtained as the slope of a plot of k_{obs} (or k_{int}) values against acid concentration (see Fig. 2.3-23). Figure 2.3-23 (below) shows an excellent fit of the first-order data. For the 'ortho' hydrate the error of the estimate is 7×10^{-4} and the t-value for the estimate of the second-order rate constant is 42. The estimate of the y-intercept is not good with a t-value of -1.2. Similarly for the 'ipso' hydrate the t-value for the estimate of k_{H} is 32 and for the estimate of the y-intercept it is -0.73. The error of the estimate is higher in this case (2.7×10^{-3}); this is expected as there are fewer first-order rate constants for this compound to predict k_{H} .

Figure 2.3-23: Aromatisation of 1-methylcyclohexa-2,4-dienol and 2-methylcyclohexa-2,4-dienol, plot of k_{int} against $[\text{H}^+]$ with slope equal to the second-order rate constant k_{H} ($\text{M}^{-1}\text{s}^{-1}$)

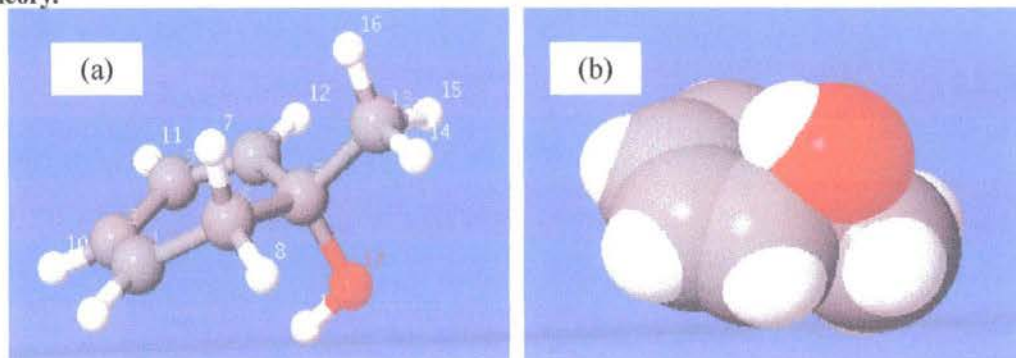


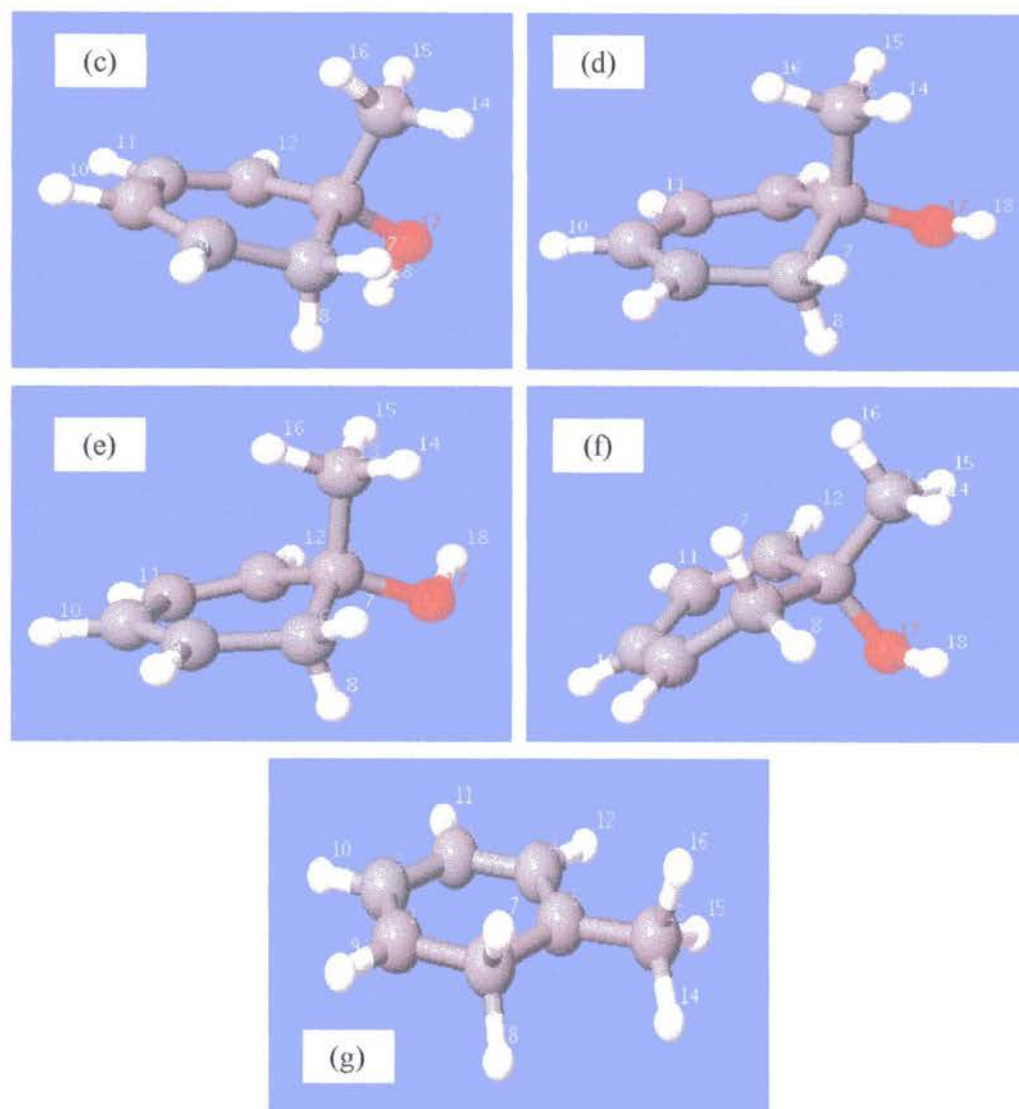
The second order rate constant for the aromatisation of 1-methylcyclohexa-2,4-dienol is $9810 \text{ M}^{-1} \text{ s}^{-1}$, corresponding to a half-life in 1 M acid of $7.1 \times 10^{-5} \text{ s}$. The second order rate constant for the aromatisation of 2-methylcyclohexa-2,4-dienol is $514 \text{ M}^{-1}\text{s}^{-1}$, corresponding to a half-life of $1.4 \times 10^{-3} \text{ s}$ in 1 M acid.

2.3.3 Computational studies of toluene hydrates

The starting structures were generated using the Maestro program employing semi-empirical Monte Carlo simulations to the MM3 level of theory. A number of conformers were found and the five lowest energy conformers were calculated to the B3LYP/6-31g** level of theory using the Gaussian '03 program.⁷⁶ The structure of the putative carbocation intermediate for aromatisation reaction of each hydrate was also calculated and only one minimum energy structure was found in each case.

Figure 2.3-24: Conformers of the 'ipso' toluene hydrate calculated to the B3LYP/6-31g** level of theory.





The lowest energy conformer (Fig 2.3-25(a)) shows the hydroxyl group in the axial position and the methyl substituent in a forced equatorial position. The space-filling model shows the hydroxyl group directed towards the conjugated diene and the methyl group co-planar with the ring. The second hydrate structure (b) has the hydroxyl group in the equatorial position as do conformers (c) and (d); the difference between these structures is in the orientation of the hydrogen of the hydroxyl group and the orientation of the hydrogens on the methyl substituent relative to the ring. Conformer (e) shows the hydroxyl group in the axial position, similar to conformer (a); however, the hydrogen on the hydroxyl group is directed away from the centre of the

cyclohexadiene. The carbocation shown in the Figure 2.3-25(g) is completely planar with the methyl group co-planar with the ring. The CH₃ group of the carbocation is orientated with one hydrogen parallel with the plane of the ring.

The energies of the conformers shown in Fig 2.3-25 are given in Table 2.3-11. The energy differences between the conformers in the gas phase are reasonably high. The energy differences between the conformers are smaller in the aqueous phase. The fifth column shows the stabilising effect of an aqueous sphere. The approximate stabilisation of the hydrate is 28 kJ/mol and for the carbocation it is 216 kJ/mol.

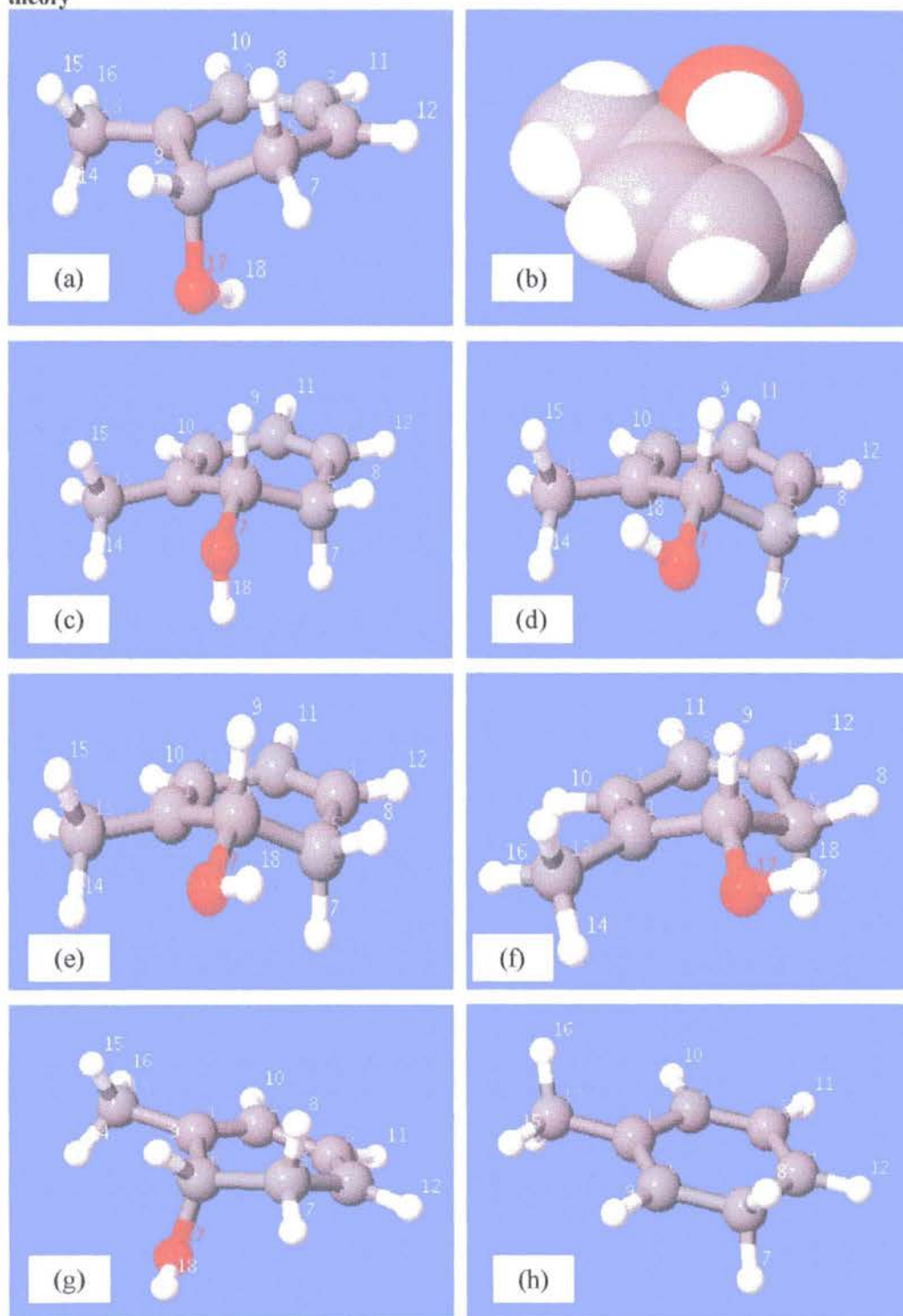
Table 2.3-10: Summary of the energies of *ipso* toluene hydrate (2.13) and corresponding carbocation (2.14) from the Gaussian calculations at the B3LYP/6-31 g level of theory**

	Gas Phase		With water sphere		Stabilisation
	kJ/mol	$\Delta^{(a)}$	kJ/mol	$\Delta^{(a)}$	$\Delta^{(b)}$
Hydrate					
Fig 2.3-25 (a)	-913586.63	0.00	-913612.43	0.00	-25.80
Fig 2.3-25 (b)	-913582.87	3.76	-913612.08	0.35	-29.20
Fig 2.3-25 (c)	-913578.90	7.73	-913608.88	3.55	-29.98
Fig 2.3-25 (d)	-913582.87	8.21	-913608.89	3.54	-30.47
Fig 2.3-25 (e)	-913574.24	12.30	-913607.18	5.25	-32.94
Fig 2.3-25 (f) (carbocation)	-713871.66	199714.97	-714087.56	199524.87	-215.90

(a) Difference in energy between the lowest energy structure (b) Difference in energy between the gas phase and water sphere calculation.

The conformers are of '*ortho*' toluene hydrate are shown in Fig 2.3-26.

Figure 2.3-25: Conformers of the *ortho* toluene hydrate calculated to the B3LYP/6-31g** level of theory



The lowest energy conformer of hydrate (2.13) is shown in Fig 2.3-26 (a). The hydroxyl group is in the axial position and the methyl substituent is co-planar with the dienyl system. The space-filling model shows the hydroxyl group's orientation relative to the conjugated diene. Structures (c), (d), (e) and (f) show the hydroxyl group in the equatorial position; the difference between these structures is in the orientation of the hydrogen of the hydroxyl group and the orientation of the hydrogens on the methyl substituent relative to the ring. Structure (g) shows the highest energy structure of hydrate (2.13) calculated using Gaussian '03, which has the hydroxyl group in the axial position with the hydrogen pointing away from the cyclohexadiene. Structure (h) shows the carbocation (2.15), which is completely planar, with the carbon of the methyl substituent co-planar with the ring. There are no hydrogens on the methyl substituent of carbocation (2.15) exactly parallel with the plane of the ring.

Table 2.3-11: Summary of the energies of *ortho* toluene hydrate (2.13) and corresponding carbocation (y) from the Gaussian calculations at the B3LYP/6-31g level of theory⁷⁶**

	Gas Phase		With water sphere		Stabilization
	kJ/mol	Δ	kJ/mol	Δ	Δ
Hydrate					
THo-1	-913592.97	0.00	-913619.81	0.00	-26.84
THo-2	-913586.40	6.57	-913615.93	3.88	-29.53
THo-5	-913584.02	8.95	-913613.57	6.24	-29.55
THo-4	-913584.02	8.95	-913613.57	6.24	-29.55
THo-3	-913582.77	10.20	-913612.49	7.32	-29.72
THo-6	-913581.34	11.63	-913614.53	5.28	-33.20
carbocation	-713856.04	199736.93	-714074.62	199545.19	-218.58

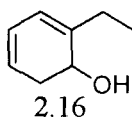
Table 2.3-12 (above) shows the calculated energies of the conformers of '*ortho*' toluene hydrate (2.14) corresponding to the structures shown in Figure 2.3-26. As with the '*ipso*' hydrate (2.13), the energy differences between conformers are larger in the gas phase than in the aqueous phase. Overall there is stabilisation of the hydrate on moving from the gas phase to the aqueous phase. The stabilisation of the hydrates is



approximately 30 kJ/mol. The stabilisation of the carbocation is much higher at 218 kJ/mol.

2.4 Ethylbenzene Hydrate

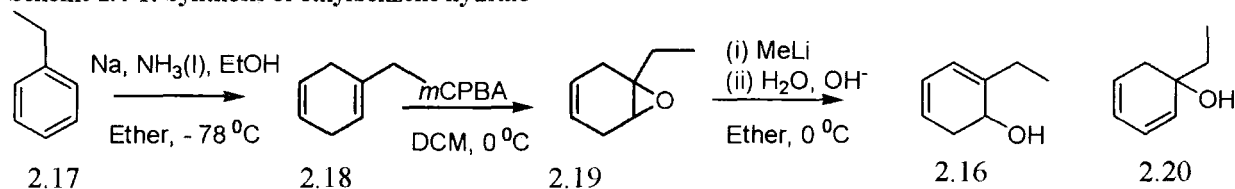
This section will discuss the synthesis and kinetics of aromatisation of ethylbenzene hydrate (2.16).



2.4.1 Synthesis of ethylbenzene hydrate

The hydrate of ethylbenzene was synthesised using the route outlined in Scheme 2.4-1. The Birch reduction of ethylbenzene (2.17) proceeded with a reasonable yield (48 %) giving the cyclohexadiene (2.18). The epoxidation step proceeded in excellent yields (70 % after column chromatography).

Scheme 2.4-1: Synthesis of ethylbenzene hydrate



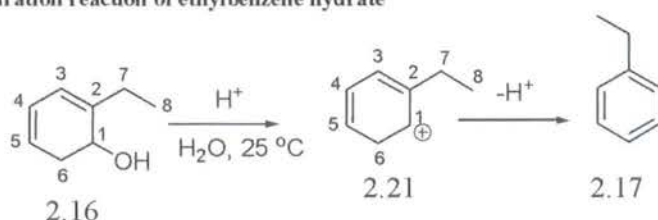
Synthesis of the hydrate from the epoxide (2.19) was more troublesome. The ring-opening proceeded as expected; however, the *ipso* hydrate was isolated in a particularly low yield (5 %) so it could not be characterised, and its presence was inferred from the total integration of the allylic hydrogens relative to the C1- hydrogen of the '*ortho*' hydrate. The low yield of *ipso* hydrate is attributed to its aromatisation to ethylbenzene in either the ether-methyl lithium environment and/or the work-up conditions (quenched with 10 % sodium hydroxide solution).

As discussed previously (section 2.3.1) the arene hydrates under investigation do not appear to be stable to purification techniques. It was decided to continue with the kinetic studies of the aromatisation of the '*ortho*' hydrate (2.16) as the major impurity is the arene which is the product of the irreversible aromatisation/dehydration reaction.

2.4.2 Kinetic analysis of the aromatisation via dehydration of ethylbenzene hydrate

The dehydration reactions of hydrate (2.16) to arene (2.17) were followed in a range of acetic acid buffers (pH 4.2 – 5.6) at ionic strength 0.5 M maintained with sodium perchlorate and 25 °C. The substrate solution was prepared in acetonitrile to a concentration of 5 mM. Typically a 1/100 dilution of this solution into the relevant buffer solution was made to initiate the reaction. The total substrate concentration that could be used was limited by product arene solubility. The solubility of ethylbenzene in water is reported to be between 1.6 and 0.3 mM.^{78, 82, 83}

Scheme 2.4-2: Dehydration reaction of ethylbenzene hydrate



A typical repetitive scan for the aromatisation reaction is shown in Fig 2.4-1. As reaction proceeds a decrease in absorbance due to hydrate at $\lambda = 254\text{ nm}$ is observed concomitant with an increase in absorbance at $\lambda = 220\text{ nm}$ due to product. The former wavelength $\lambda = 254\text{ nm}$ was chosen as the analytical wavelength.

Figure 2.4-1: Representative repetitive scan of the dehydration of hydrate (2.16) in 0.05 M 25 % FB phosphate at pH 5.6

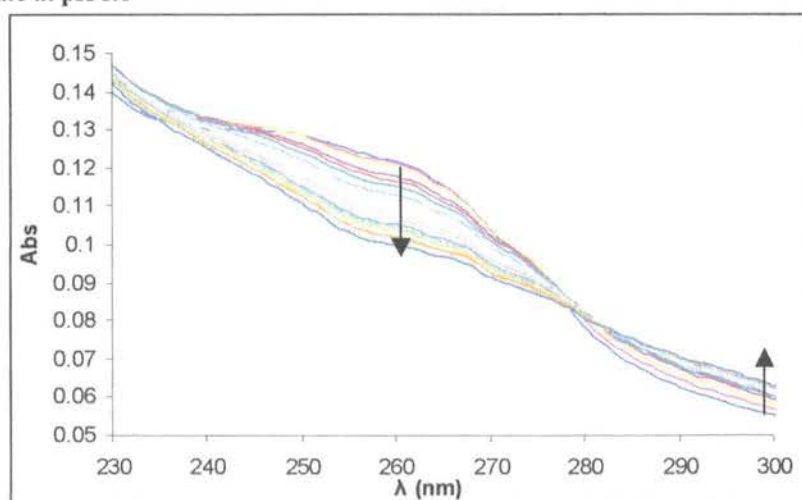


Figure 2.4-2(a) shows the change in absorbance against time at 254 nm as a result of the reaction of ethylbenzene hydrate in acetate buffer (25 % FB, pH 4.2). A corresponding semi-logarithmic plot of $\Delta A = A - A_{\infty}$ against time is shown in Figure 2.4-2(b) where A_{∞} refers to the absorbance at the end of the reaction.

Figure 2.4-2: Aromatisation of ethylbenzene hydrate in acetate buffer (25 % FB, pH 4.2) at 25 °C and $I = 0.5 \text{ M}$ (NaClO_4) (a) Plot of absorbance versus time; (b) plot of $\ln(A - A_{\infty})$ against time with slope equal to k_{obs}

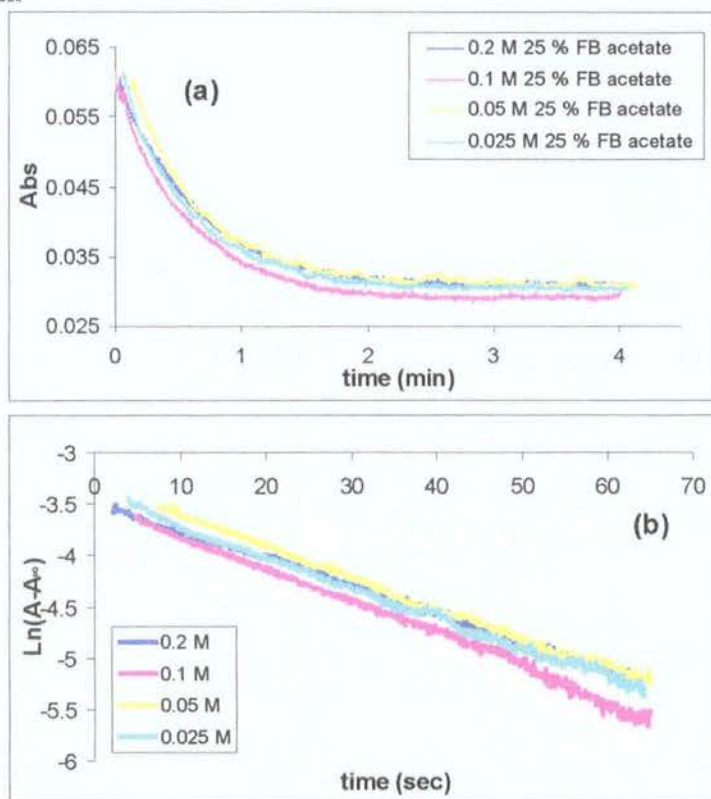


Table 2.4-1 shows there is a good agreement between the single exponential least squares and semi-logarithmic analyses of the experimental data shown in Fig 2.4-2(a & b). The least squares analysis of Figure 2.4-2(a) gave a mean value of $k_{\text{obs}} = 2.95 \pm 0.1 \times 10^{-2} \text{ s}^{-1}$. The mean t-value for the estimate of k_{obs} was 503 with an error of the estimate of 3×10^{-4} . The semi-logarithmic analysis (see Fig 2.4-2(b)) also gave a mean value of $k_{\text{obs}} = 2.95 \pm 0.1 \times 10^{-2}$.

Table 2.4-1: First-order rate constants for aromatisation of ethylbenzene hydrate (2.16) in 25% FB acetate buffers (0.2 – 0.025 M) at 25 °C and I = 0.5 M (NaClO₄)^(a).

[Buffer] (M)	pH ^(b)	[H ⁺] ^(c) x 10 ⁻⁵ M	Semi-log Plot		Least Squares Plot			
			k_{obs} ^(d) (x 10 ⁻²) s ⁻¹	R ²	k_{int} ^(f) (x 10 ⁻²) s ⁻¹	k_{obs} ^(e) (x 10 ⁻²) s ⁻¹	R ²	k_{int} ^(f) (x 10 ⁻²) s ⁻¹
0.20	4.21	6.14	2.74	0.998		2.68	0.999	
0.10	4.21	6.12	3.22	0.995	3.04	2.99	0.999	3.16
0.05	4.22	6.08	2.89	0.992	(2.95 ^(g))	3.06	0.998	(2.95 ^(g))
0.025	4.22	6.07	2.95	0.996		3.06	0.999	

(a) Measurements were made at a substrate concentration of 0.05 mM and 1 % acetonitrile (b) pH was determined using a MeterLabTM PHM 290 pH-Stat Controller equipped with a radiometer (pH 4 - 7 - 10 @ 25 °C) combination electrode (type pHC4006) with a saturated LiTCA filling solution. (c) [H⁺] was calculated using $[H^+] = 10^{-(\text{pH} / \gamma_H)}$ where $\gamma_H = 1$ is the activity coefficient of the hydronium ion under the experimental conditions. (d) The value of the first-order rate constant (k_{obs}), was obtained from the slope of the plot of $\ln(A - A_\infty)$ against time in Figure 2.4.2-2(b). (e) k_{int} is defined as the intercept of the plot of k_{obs} against buffer concentration Figure 2.4.2-3 (f) The value of the first-order rate constant (k_{obs}), was obtained from the least squares analysis of Figure 2.4.2-2(a). (g) mean of k_{obs}

The plot of k_{obs} against buffer concentration (Figure 2.4-3, below) shows no evidence of buffer catalysis, in fact there is an increase in the value of the rate constant of 14 % with decreasing buffer concentration. The mean rate of aromatisation of ethylbenzene hydrate at pH 4.2 is $2.95 \times 10^{-2} \text{ s}^{-1}$ with a corresponding half-life of 23 seconds.

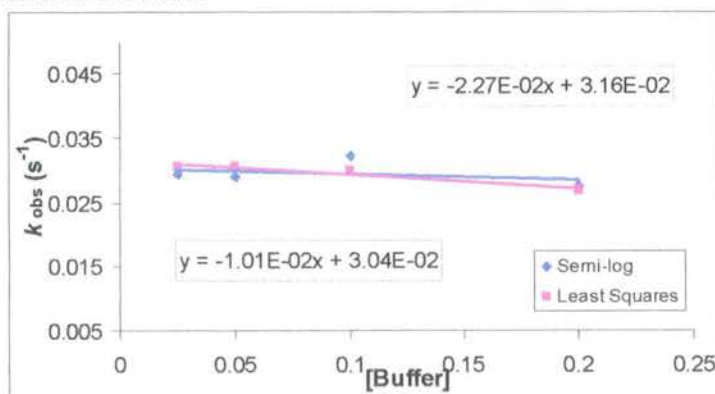
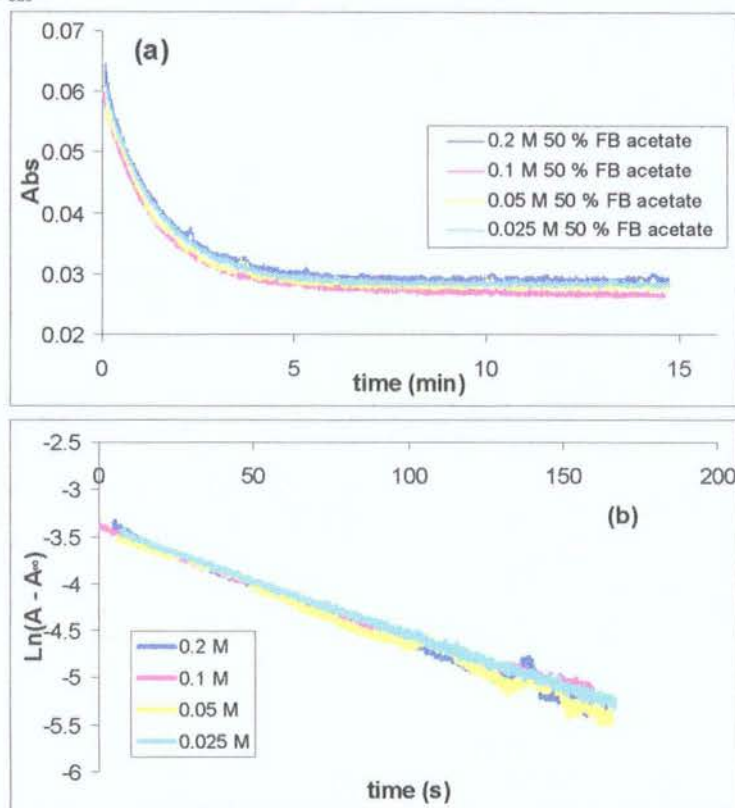
Figure 2.4-3: Aromatisation of ethylbenzene hydrate in 25 % FB acetate at pH 4.2 and 25 °C : Plot of k_{obs} against buffer concentration

Figure 2.4-4(a) shows the change in absorbance against time at 254 nm as a result of the reaction of ethylbenzene hydrate in acetate buffer (50 % FB, pH 4.6). A

corresponding semi-logarithmic plot of $\Delta A = A - A_\infty$ against time is shown in Figure 2.4-4(b) where A_∞ refers to the absorbance at the end of the reaction.

Figure 2.4-4: Aromatisation of ethylbenzene hydrate (2.16) in 50 % FB acetate at pH 4.6, $I=0.5$ M (NaClO_4) and 25 °C (a) Plot of absorbance versus time; (b) plot of $\ln(A - A_\infty)$ against time with slope equal to k_{obs}



The table below summarises the first order rate constants of aromatisation of ethylbenzene hydrate in 50 % FB acetate at pH 4.6. The data shows a good consistency between the semi-logarithmic and single exponential least squares analysis of the data. The least squares analysis of Figure 2.4-4(a) gives a mean value of k_{obs} of $1.19 \pm 0.01 \times 10^{-2} \text{ s}^{-1}$. The error of the estimate is 3×10^{-4} and the mean of the t-values for the estimate of k_{obs} is 918. The semi-logarithmic analysis gives a mean value of $k_{\text{obs}} = 1.15 \pm 0.03 \times 10^{-2} \text{ s}^{-1}$.

Table 2.4-2: First-order rate constants for aromatisation of ethylbenzene hydrate (2.16) in 50 % FB acetate buffers (0.2 – 0.025 M) at 25 °C and I = 0.5 M (NaOCl₄)^(a).

[Buffer] (M)	pH ^(b)	[H ⁺] ^(c) x 10 ⁻⁶ M	Semi-log Plot			Least Squares Plot		
			k_{obs} ^(d) (x 10 ⁻²) s ⁻¹	R ²	k_{int} ^(e) (x 10 ⁻²) s ⁻¹	k_{obs} ^(f) (x 10 ⁻²) s ⁻¹	R ²	k_{int} ^(e) (x 10 ⁻²) s ⁻¹
0.20	4.58	2.63	1.20	0.992		1.19	0.9987	
0.10	4.54	2.88	1.07	0.995	1.14	1.18	0.9987	1.19
0.05	4.56	2.75	1.21	0.994	(1.15 ^(g))	1.23	0.9979	(1.19 ^(g))
0.025	4.56	2.75	1.13	0.998		1.17	0.9994	

(a) Measurements were made at a substrate concentration of 0.05 mM and 1 % acetonitrile (b) pH was determined using a MeterLabTM PHM 290 pH-Stat Controller equipped with a radiometer (pH 4 - 7 - 10 @ 25 °C) combination electrode (type pHC4006) with a saturated LiTCA filling solution. (c) [H⁺] was calculated using $[H^+] = 10^{-(\text{pH} / \gamma_{\text{H}})}$ where $\gamma_{\text{H}} = 1$ is the activity coefficient of the hydronium ion under the experimental conditions. (d) The value of the first-order rate constant (k_{obs}), was obtained from the slope of the plot of $\ln(A - A_{\infty})$ against time in Figure 2.4-4(b). (e) k_{int} is defined as the intercept of the plot of k_{obs} against buffer concentration Figure 2.4-5 (f) The value of the first-order rate constant (k_{obs}), was obtained from the least squares analysis of Figure 2.4-4(a). (g) mean of k_{obs}

The plot of k_{obs} against buffer concentration (Fig 2.4-5, below) shows no evidence of buffer catalysis. The mean rate of aromatisation of ethylbenzene hydrate at pH 4.6 is $1.19 \times 10^{-2} \text{ s}^{-1}$ with a corresponding half-life of 58 seconds.

Figure 2.4-5: Aromatisation of ethylbenzene hydrate (2.16) in acetate buffer (50 % FB, pH 4.6) at 25 °C and I = 0.5 M (NaClO₄): Plot of k_{obs} against buffer concentration

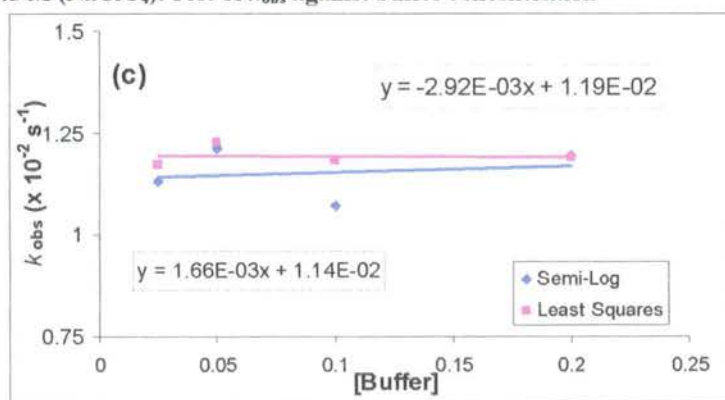
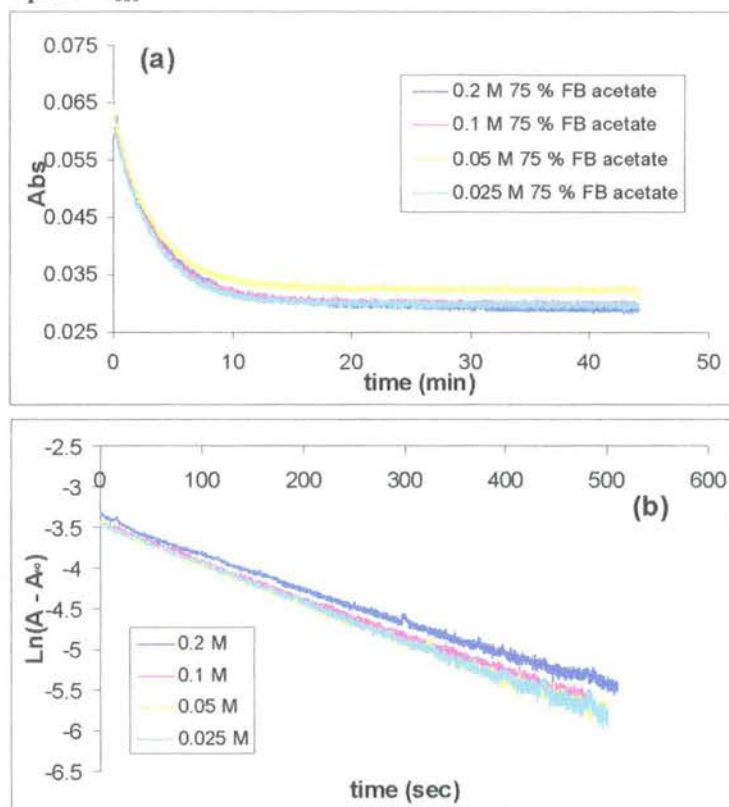


Figure 2.4.2-6(a) shows the change in absorbance against time at 254 nm as a result of the reaction of ethylbenzene hydrate in acetate buffer (50 % FB, pH 4.6). A corresponding semi-logarithmic plot of $\Delta A = A - A_{\infty}$ against time is shown in Figure 2.4.2-6(b) where A_{∞} refers to the absorbance at the end of the reaction.

Figure 2.4-6: Aromatisation of ethylbenzene hydrate (2.16) in acetate buffer (75 % FB, pH 4.9) at 25 °C and $I = 0.5 \text{ M}(\text{NaClO}_4)$: (a) Plot of absorbance versus time; (b) plot of $\ln(A - A_\infty)$ against time with slope equal to k_{obs}



The table below shows the rate of aromatisation of ethylbenzene hydrate in 75 % FB acetate at pH 4.9. The mean first order rate constant of aromatisation of ethylbenzene hydrate from the single exponential least squares analysis of Figure 2.4-6(a) is $4.76 \pm 0.1 \times 10^{-3} \text{ s}^{-1}$. The error of the estimate is 2.25×10^{-4} and the mean t-value for the estimate of k_{obs} is 1814. There is no evidence for a second exponential term in the fit of the data. The double exponential analysis gave low t-values for the estimate of the rate constants and the second pre-exponential term is very small (3×10^{-3}) suggesting it is not relevant.

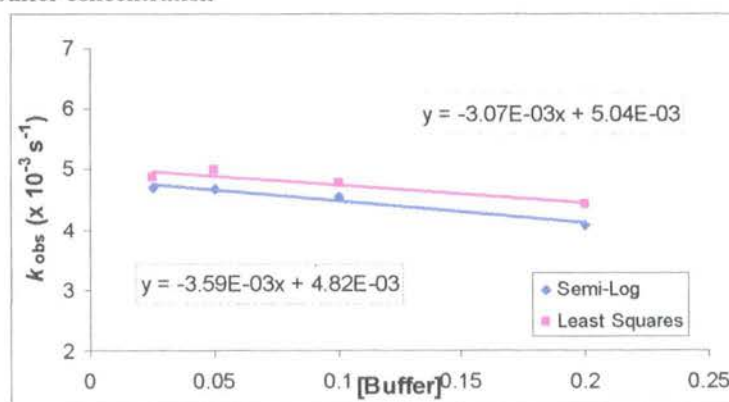
The mean first order rate constant of aromatisation from the semi-logarithmic analysis of the data (Fig 2.4-6(b)) is $4.48 \pm 0.14 \times 10^{-3} \text{ s}^{-1}$.

Table 2.4-3: First-order rate constants for aromatisation of ethylbenzene hydrate (2.16) in 75% FB acetate buffers (0.2 – 0.025 M) at 25 °C and I = 0.5 M (NaOCl)^(a).

[Buffer] (M)	pH ^(b)	[H ⁺] ^(c) x 10 ⁻⁵ M	Semi-log Plot			Least Squares Plot		
			k_{obs} ^(d) (x 10 ⁻³) s ⁻¹	R ²	k_{int} ^(f) (x 10 ⁻³) s ⁻¹	k_{obs} ^(e) (x 10 ⁻³) s ⁻¹	R ²	k_{int} ^(f) (x 10 ⁻³) s ⁻¹
0.20	4.93	1.17	4.07	0.996		4.41	0.9986	
0.10	4.93	1.16	4.54	0.998	4.82	4.77	0.9992	5.04
0.05	4.94	1.14	4.65	0.997	(4.48 ^(g))	4.99	0.9991	(4.76 ^(g))
0.025	4.95	1.13	4.68	0.997		4.87	0.9992	

(a) Measurements were made at a substrate concentration of 0.05 mM and 1 % acetonitrile (b) pH was determined using a MeterLabTM PHM 290 pH-Stat Controller equipped with a radiometer (pH 4 - 7 - 10 @ 25 °C) combination electrode (type pHC4006) with a saturated LiTCA filling solution. (c) [H⁺] was calculated using $[H^+] = 10^{-(\text{pH} / \gamma_{\text{H}})}$ where $\gamma_{\text{H}} = 1$ is the activity coefficient of the hydronium ion under the experimental conditions. (d) The value of the first-order rate constant (k_{obs}), was obtained from the slope of the plot of $\ln(A - A_{\infty})$ against time in Figure 2.4-6(b). (e) k_{int} is defined as the intercept of the plot of k_{obs} against buffer concentration Figure 2.4-7 (f) The value of the first-order rate constant (k_{obs}), was obtained from the least squares analysis of Figure 2.4-6(a). (g) mean of k_{obs}

Figure 2.4-7 shows no evidence of buffer catalysis, there is small increase in the rate with decreasing buffer concentration, however the change in rate over the buffer range is 10 % from the least squares analysis and 15 % from the semi-logarithmic analysis.

Figure 2.4-7: Aromatisation of ethylbenzene hydrate in 75 % FB acetate at pH 4.9 and 25 °C: Plot of k_{obs} against buffer concentration

The mean of the first order rate constants of aromatisation of ethylbenzene hydrate at pH 4.9 is $4.76 \times 10^{-3} \text{ s}^{-1}$ corresponding to a half-life of 146 seconds.

Figure 2.4-8(a) shows the change in absorbance against time at 254 nm as a result of the reaction of ethylbenzene hydrate in acetate buffer (50 % FB, pH 4.6). A corresponding semi-logarithmic plot of $\Delta A = A - A_{\infty}$ against time is shown in Figure 2.4-8(b) where A_{∞} refers to the absorbance at the end of the reaction.

Figure 2.4-8: Aromatisation of ethylbenzene hydrate at pH 5.6 (a) Plot of absorbance versus time; (b) plot of $\ln(A - A_{\infty})$ against time with slope equal to k_{obs}

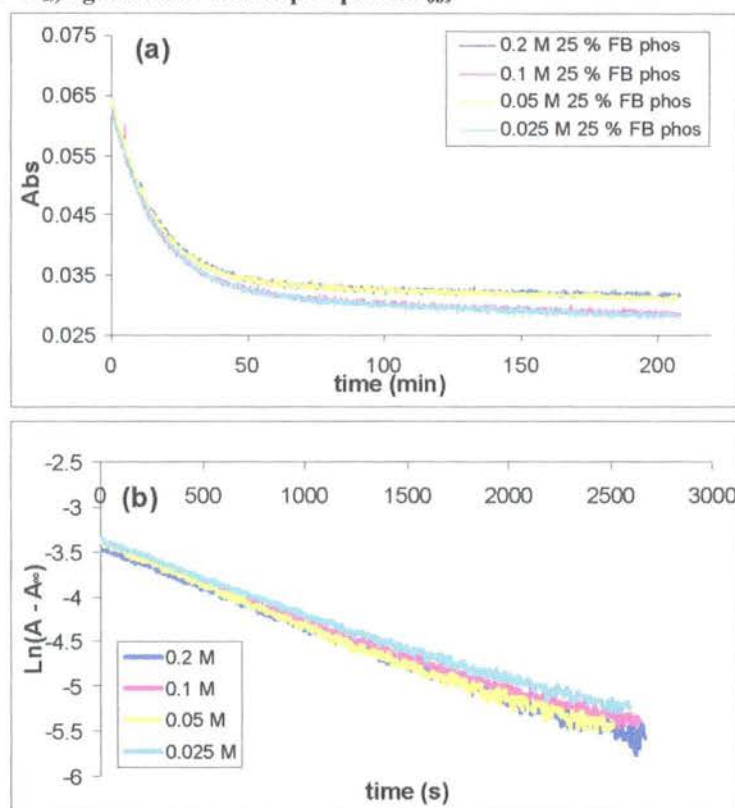


Table 2.4-4 (below) summarises the first order rate constants of aromatisation of ethylbenzene hydrate at pH 5.6. The data below do not show the same precision as obtained for the previous results; this is due to the extensive drift in the end point of the reaction. The single exponential least squares analysis of the data in Fig 2.4-8(a) shows a larger error than the data from the semi-logarithmic analysis (Fig 2.4-8(b)). Figure 2.4-8(a) shows the drift in the endpoint.

The mean from the data by the least squares analysis is $k_{obs} = (8.68 \pm 0.3) \times 10^{-4} \text{ s}^{-1}$. The error of the estimate is 5.3×10^{-4} and the mean t-value for the estimate of k_{obs} is

293. The mean k_{obs} value from the semi-logarithmic analysis is $(7.90 \pm 0.2) \times 10^{-4} \text{ s}^{-1}$. At this particular pH the semi-logarithmic analysis gives the more accurate results.

Table 2.4-4: First-order rate constants for aromatisation of ethylbenzene hydrate (2.16) in 90 % FB acetate buffers (0.2 – 0.025 M) at 25 °C and I = 0.5 M (NaClO₄)^(a)

[Buffer] (M)	pH ^(a)	$[\text{H}^+]^{(c)}$ $\times 10^{-6}$ M	Semi-log Plot			Least Squares Plot		
			$k_{\text{obs}}^{(d)}$ ($\times 10^{-4}$) s^{-1}	R^2	$k_{\text{int}}^{(f)}$ ($\times 10^{-4}$) s^{-1}	$k_{\text{obs}}^{(e)}$ ($\times 10^{-4}$) s^{-1}	R^2	$k_{\text{int}}^{(g)}$ ($\times 10^{-4}$) s^{-1}
0.20	5.55	2.82	7.35	0.993		8.93	0.998	
0.10	5.55	2.82	8.40	0.992	8.23	8.33	0.999	8.45
0.05	5.54	2.87	7.76	0.992	$(7.90^{(g)})$	9.39	0.995	$(8.68^{(g)})$
0.025	5.56	2.74	8.09	0.994		8.01	0.996	

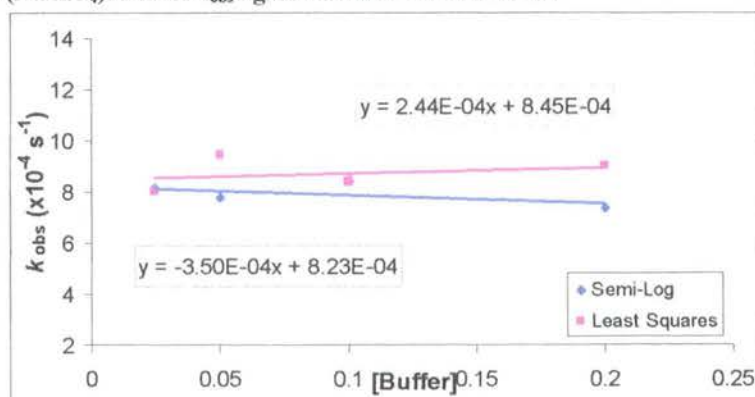
(a) Measurements were made at a substrate concentration of 0.05 mM and 1 % acetonitrile (b) pH was determined using a MeterLab™ PHM 290 pH-Stat Controller equipped with a radiometer (pH 4 - 7 - 10 @ 25 °C) combination electrode (type pHC4006) with a saturated LiTCA filling solution.

(c) $[\text{H}^+]$ was calculated using $[\text{H}^+] = 10^{-(\text{pH} / \gamma_{\text{H}})}$ where $\gamma_{\text{H}} = 1$ is the activity coefficient of the hydronium ion under the experimental conditions. (d) The value of the first-order rate constant (k_{obs}), was obtained from the slope of the plot of $\ln(A - A_{\infty})$ against time in Figure 2.4.2-8(b). (e) k_{int} is defined as the intercept of the plot of k_{obs} against buffer concentration Figure 2.4.2-9 (f) The value of the first-order rate constant (k_{obs}), was obtained from the least squares analysis of Figure 2.4.2-8(a).

(g) Mean of k_{obs}

Figure 2.4.2-9 (below) shows, again, there is no evidence of buffer catalysis. The mean first order rate constant of aromatisation of ethylbenzene hydrate is $7.90 \times 10^{-4} \text{ s}^{-1}$ corresponding to a half-life of 877 seconds.

Figure 2.4-9: Aromatisation of ethylbenzene hydrate in acetate buffer (75 % FB, pH 4.9) at 25 °C and I = 0.5 M (NaClO₄): Plot of k_{obs} against buffer concentration.



The results from similar analyses at higher pHs (5.6 to 7) showed no stable endpoint and so accurate k_{obs} values could not be determined. As in this case we were studying the reaction of one hydrate rather than a mixture, it was decided that a second-order rate constant (k_{H}) for aromatisation could be determined using data at four pH values. Table 2.3-5 (below) summarises the results from the study at pH 4.2 to 5.6

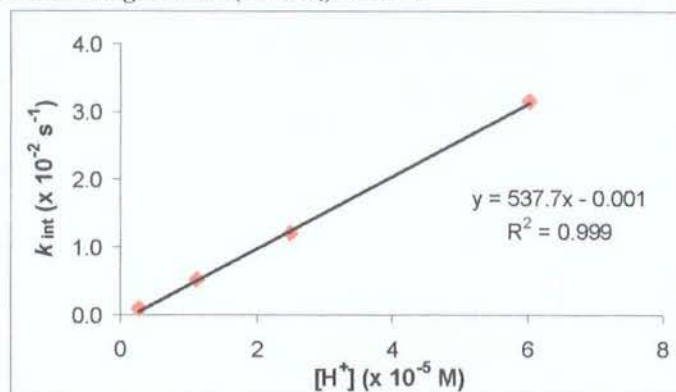
Table 2.4-5: Summary of the first-order rate constants for the aromatisation of ethylbenzene hydrate in acetate buffers, I = 0.5 M (NaClO₄)

pH ^(a)	[H ⁺] ^(b) M	k_{int} s ⁻¹	k_{H} ^(c) M ⁻¹ s ⁻¹	Log(k_{int}) s ⁻¹	Log (k_{H}) ^(c)
4.21	6.14 x 10 ⁻⁵	3.16 x 10 ⁻²		-1.50	
4.60	2.51 x 10 ⁻⁵	1.19 x 10 ⁻²		-1.92	
4.95	1.12 x 10 ⁻⁵	5.04 x 10 ⁻³	534	-2.30	3.56
5.56	2.75 x 10 ⁻⁶	7.90 x 10 ⁻⁴		-3.10	

(a) pH was determined using a MeterLabTM PHM 290 pH-Stat Controller equipped with a radiometer (pH 4 - 7 - 10 @ 25 °C) combination electrode (type pHC4006) with a saturated LiTCA filling solution. (b) [H⁺] was calculated using $[\text{H}^+] = 10^{-(\text{pH}/\gamma_{\text{H}})}$ where $\gamma_{\text{H}} = 1$ is the activity coefficient of the hydronium ion under the experimental conditions. (c) The value of the second-order rate constant (k_{H}) is the slope of the plot of k_{int} against [H⁺].

The data above shows the results for the aromatisation reaction of ethylbenzene hydrate. The plot of k_{int} against hydronium ion concentration is shown in Fig 2.4-10; the slope of this plot gives a value of $k_{\text{H}} = 534 \text{ M}^{-1}\text{s}^{-1}$. A pH-rate profile gave a y-intercept of 3.56 which corresponds to second-order rate constant of $3631 \text{ M}^{-1} \text{ s}^{-1}$. The value from the pH-rate profile is 10-fold larger than the value obtained from Figure 2.4-10. The slope of this line was -1.19 which is a large deviation from unity and so it was disregarded.

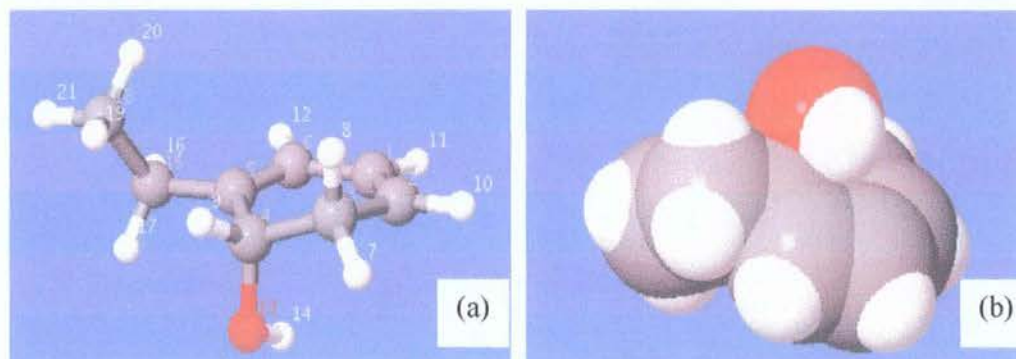
Figure 2.4-10: Plot of k_{obs} for aromatisation of ethylbenzene hydrate (2.16) against concentration of hydronium ion at ionic strength 0.5 M (NaClO_4) at 25 °C.

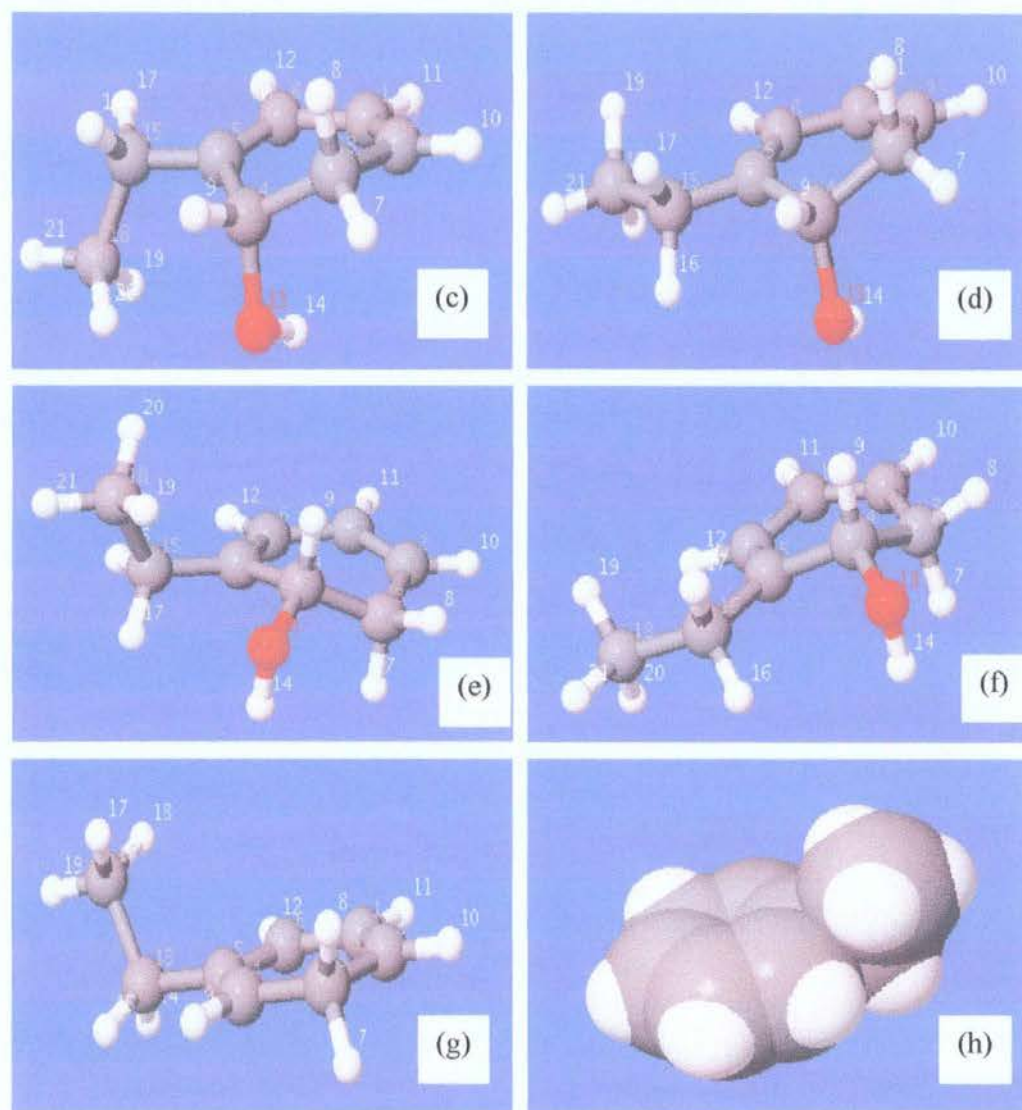


2.4.3 Computational studies of ethylbenzene hydrate

The structures of 2-ethylcyclohexa-2,4-dienol (2.16) and corresponding carbocation are shown below (see Fig 2.4-11), calculated to the B3LYP/6-31g** level of theory. The starting structures were generated using the Maestro program employing semi-empirical Monte Carlo simulations to the MM3 level of theory. A number of conformers were found and the five lowest energy conformers were calculated to the B3Lyp/6-31g** level of theory using the Gaussian '03 program.⁷⁶ The structure of the putative carbocation (2.21) intermediate for the aromatisation reaction of the hydrate was also calculated and only one minimum energy structure was found in each case.

Figure 2.4-11: Structures of 2-ethylcyclohexa-2,4-dienol (2.16) and corresponding carbocation(2.21) calculated to the B3LYP/6-31g** level of theory





The first structure above (Fig 2.4-12(a)) shows the lowest energy structure of the 'ortho' hydrate (2.16). The hydroxyl group is in the axial position with the ethyl group directed in the opposite direction to the hydroxyl group. The space-filling model (b) shows the orientation of the hydrogen of the hydroxyl group - hydrogen pointing towards the cyclohexadiene. Structures (c) and (d) also show the hydroxyl group in the axial position; the difference is only the rotation of the ethyl group. This is further shown in the small energy difference between structures (a), (c) and (d) (see Table 2.4-6). Structures (e) and (f) both have the hydroxyl groups in a pseudoequatorial position,

where (e) is a ring-flip of (a) and (f) is a ring-flip of (d). All the hydrate conformers have a planar *cis*-diene component with the hydrogens co-planar with the ring-structure.

The calculated structure of the carbocation intermediate (2.21) is shown in (g) and (h). It is completely planar, with the ethyl group lying in a similar arrangement to conformer (a). The space-filling model of the carbocation shows the ethyl-group sitting almost perpendicular to the ring (h). Table 2.4-6 (below) shows the energies of the structures illustrated in Figure 2.4-12.

Table 2.4-6: Summary of the energies of *ortho* ethylbenzene hydrate (2.16) and corresponding carbocation (2.21) from the Gaussian calculations at the B3LYP/6-31g level of theory**

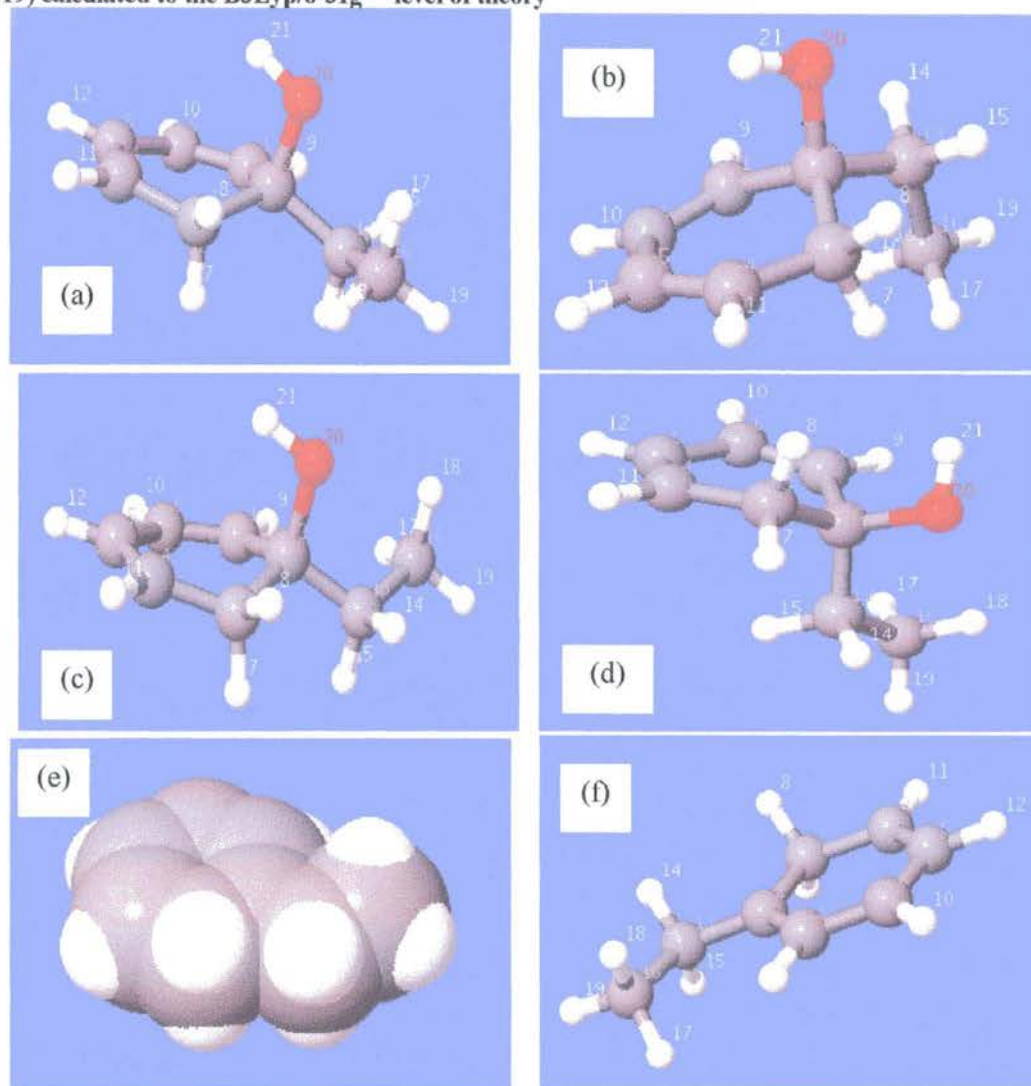
Hydrate	Gas phase		With water sphere		Stabilization
	kJ/mol	$\Delta^{(a)}$	kJ/mol	$\Delta^{(a)}$	$\Delta^{(b)}$
Fig 2.4-12 (a)	-1016816.25	0.00	-1016842.87	0.00	26.62
Fig 2.4-12 (c)	-1016815.99	0.26	-1016841.92	3.88	25.93
Fig 2.4-12 (d)	-1016815.89	0.36	-1016842.51	6.24	26.62
Fig 2.4-12 (e)	-1016810.24	6.01	-1016839.47	6.24	29.23
Fig 2.4-12 (f)	-1016808.95	7.30	-1016838.41	7.32	29.46
Fig 2.4-12 (g) carbocation	-817084.02	199731.98	-817300.41	199542.46	216.40

(a) Difference in energy between the lowest energy structure (b) Difference in energy between the gas phase and water sphere calculation.

The energies of the conformers (a)-(f) and carbocation (g) are shown in Table 2.4-6. Rotation of the methyl group does not appear to require much energy in the gas phase, as is shown by the very small difference between Figures 2.4-12 (a) – (c). The structures with the hydroxyl in the equatorial position are considerably higher in energy than the axial conformers. The energy differences between the conformers are higher with the aqueous sphere, but overall there is stabilisation. The carbocation is lowered in energy by 216 kJ/mol on transferring from the gas phase to the aqueous phase.

The structures of the '*ipso*' ethylbenzene hydrate (2.19) are shown below in Figure 2.4-13 calculated to the B3Lyp/6-31g** level of theory using Gaussian 03.⁷⁶

Figure 2.4-12: Structures of 1-ethylcyclohexa-2,4-dienol (2.16) and corresponding carbocation (2.19) calculated to the B3Lyp/6-31g** level of theory



The lowest energy structure (a) shows the hydroxyl group in the pseudoaxial position and the ethyl group in the pseudoequatorial position with the ethyl group parallel to the ring facing away from the conjugated diene. The second conformer (b) also shows the hydroxyl group in the axial position with the ethyl group perpendicular to the ring in a pseudoequatorial position. The fourth conformer shows the hydroxyl group in the axial position and the ethyl group parallel to the ring with the ethyl group facing the conjugated diene slightly above the plane of the ring. The highest energy conformer calculated (Fig 2.4-13(d)) shows the hydroxyl group in a pseudoequatorial position and

the ethyl group in a pseudoaxial position. In the case of the carbocation structure is shown in Fig 2.4-13(e), the structure is completely planar with the ethyl group parallel to the ring, as illustrated clearly by the space-filling model (f).

The energies of the conformers of the ‘*ipso*’ ethylbenzene hydrate (2.19) are shown in Table 2.4-7 (below) calculated to the B3LYP/6-31g** level of theory using Gaussian 03.⁷⁶

Table 2.4-7: Summary of the energies of *ortho* ethylbenzene hydrate (2.19) and corresponding carbocation (2.21) from the Gaussian calculations at the B3LYP/6-31g level of theory**

	Gas Phase		With water sphere		Stabilization
	kJ/mol	Δ	kJ/mol	Δ	Δ
Hydrate					
Fig 2.4-13 (a)	-1016808.88	0.00	-1016834.12	0.00	25.25
Fig 2.4-13 (b)	-1016808.43	0.45	-1016835.50	-1.38	27.07
Fig 2.4-13 (c)	-1016808.42	0.46	-1016833.07	1.05	24.65
Fig 2.4-13 (d)	-1016805.51	3.37	-1016834.16	-0.04	28.65
Carbocation					
Fig 2.4-13 (e)	-817099.10	199709.78	-817311.27	199522.85	212.16

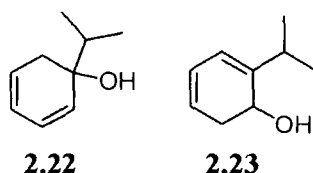
(a) Difference in energy between the lowest energy structure (b) Difference in energy between the gas phase and water sphere calculation.

Table 2.4-7 shows the energies of the conformers in Fig 2.4-7 calculated in the gas phase and with a water sphere using the polarisable continuum model. Overall, the hydrate conformers are stabilised on moving to the aqueous phase by approximately 26 kJ/mol. The carbocation is stabilised by 212 kJ/mol in the aqueous phase.

Interestingly, the relative energies of the conformers change on moving from the gas phase to the aqueous phase. The conformer shown in Fig 2.4-13(b) is lower in energy in the aqueous phase than conformer (a). More interestingly, the conformer with the hydroxyl group in the equatorial position is also lower in energy than conformer (a).

2.5 Cumene Hydrate

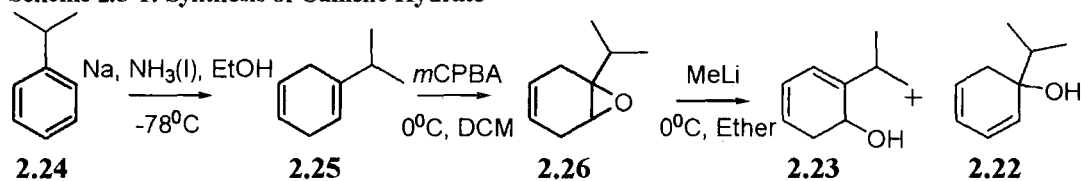
This section presents the results from the synthesis and kinetic studies of aromatisation of the '*ipso*' (2.22) and '*ortho*' (2.23) cumene hydrates.



2.5.1 Synthesis of Cumene Hydrate

The Birch reduction proceeded as outlined in the first step of Scheme 2.5-1 (below). The reaction proceeded with a yield of 42 %. The epoxidation proceeded as expected with selective epoxidation of the isopropyl-substituted double bond. The reaction proceeded with a yield of 50 % after purification.

Scheme 2.5-1: Synthesis of Cumene Hydrate

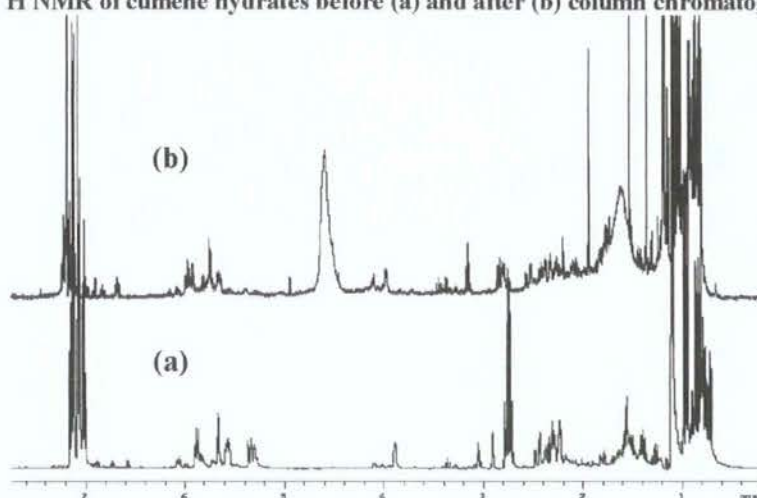


The final ring-opening step was troublesome due to the instability of the hydrate product. The reaction proceeded as outline in Scheme 2.5-1 (above) with a respectable crude yield of 77 %. In this case a mixture of *ortho* and *ipso* hydrates were obtained in a 1.1:1.0 ratio determined from the integration of the zerotime spectra below (see Fig 2.5-2).

Generally the arene hydrates could not be purified by standard purification techniques due to their acid, thermal and water sensitivities. Flash column chromatography was attempted for which the silica gel column was eluted with pure diethyl ether over 5 minutes. The ¹H NMR spectrum in Figure 2.5-1 (below) shows the effect of flash column chromatography on the cumene hydrates, for example, the appearance of unidentifiable multiplets below 3 ppm and the appearance of a broad singlet at 4.5 ppm. The hydrates quickly decomposed after chromatography. The GC-MS of the hydrates

after chromatography showed multiple peaks with m/z greater than the expected molecular ion for the hydrates

Figure 2.5-1: ^1H NMR of cumene hydrates before (a) and after (b) column chromatography



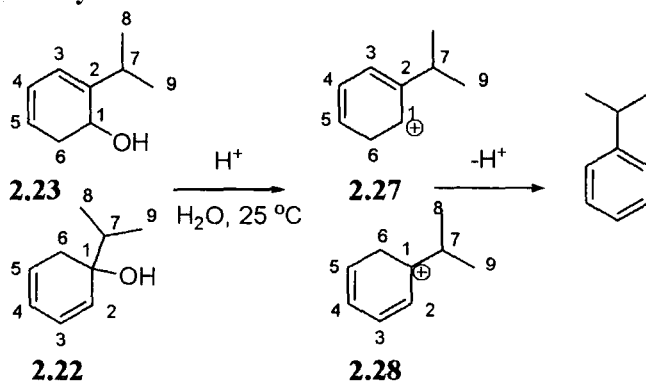
The synthesis of the hydrates (2.22 and 2.23) was repeated with an excess of methyllithium (2 equivalents) to force the reaction to completion. The problem with this approach was that a proportion of the hydrates were lost to aromatisation in either the methyllithium-ether reaction mixture and/or in work-up. As the major impurity from the hydrate synthesis appeared to be cumene (the parent arene), it was decided to continue with the kinetic studies as the product formed in the irreversible aromatisation reaction is cumene. Any other impurities were assumed to be UV inactive and as they only appeared to constitute $< 1\%$ of the product, thus their affect on final UV absorbance would be minimal.

2.5.2 Kinetic analysis of the aromatisation reaction of the cumene hydrates

The aromatisation reactions of the mixture of 2-isopropylcyclohexa-2,4-dienol (2.23) and 1-isopropylcyclohexa-2,4-dienol (2.22) were followed in acetate and phosphate buffers (pH 4.2 – 7) at ionic strength 0.5, maintained with sodium perchlorate (see Scheme 2.5-1, below). For the UV-Vis studies, the substrate solution was prepared in acetonitrile to a concentration of 8 mM. Typically a 1/100 dilution of this solution into

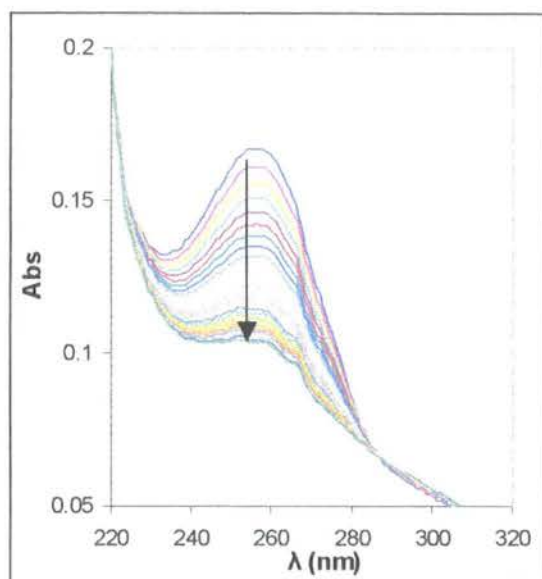
the relevant buffer was made to initiate the reaction. The total substrate concentration (0.08 mM) was limited due to the solubility of the reactant and product. The reported solubility of cumene in water is between 0.61 and 0.51 mM^{80, 82}. The final substrate concentration used in these kinetic experiments was lower than these values as the solubility of the arene was further decreased by the buffer and perchlorate salts.

Scheme 2.5-2: Aromatisation reaction via carbocation intermediates (2.27) and 2.28 of *ipso* (2.23) and *ortho* (2.22) cumene hydrates



A representative repetitive scan is shown below (Fig 2.5-1) for the aromatisation reaction. The scan shows a decrease in absorbance at 254 nm due to the disappearance of the hydrates. The increasing absorbance of the arene at 220 nm is not shown due to the high absorbance of the buffer at this wavelength (between 2 and 3 Abs). The analytical wavelength chosen was 254 nm.

Figure 2.5-2: Representative repetitive scan of the aromatisation reaction of 1-isopropylcyclohexa-2,4-dienol and 2-isopropylcyclohexa-2,4-dienol in phosphate buffer (0.025 M, 50 % FB) at pH 6.6, IS = 0.5 M (NaClO₄).



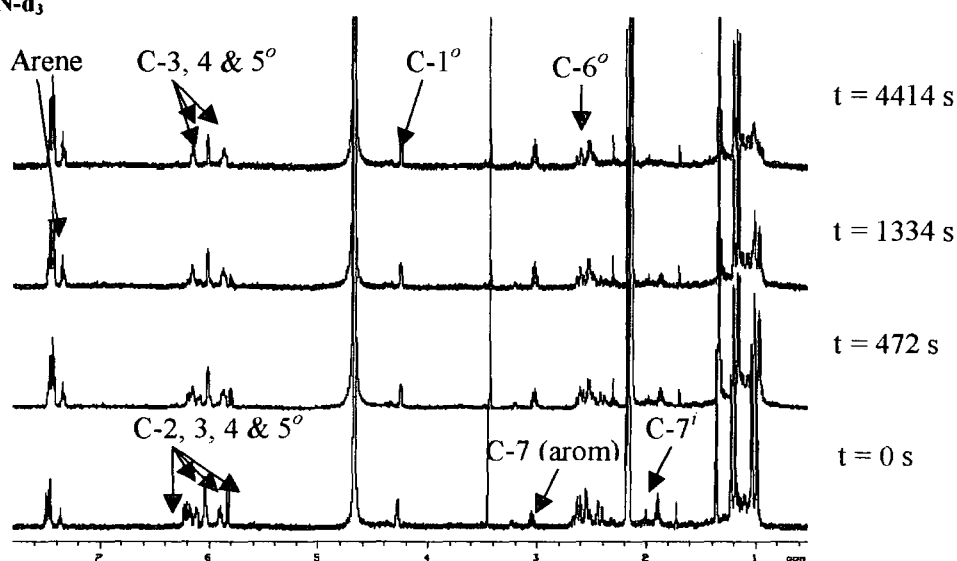
The reaction of the 2-isopropylcyclohexa-2,4-dienol (*ortho* hydrate 2.23) was slower than the corresponding 1-isopropylcyclohexa-2,4-dienol (*ipso* hydrate 2.22) and the absorbance versus time plot above shows the simultaneous reactions of both hydrates. At higher pH values the reaction of both hydrates could be followed, whereas, below pH 4.6 the reaction of the '*ipso*' hydrate was too fast to be monitored by standard UV-Vis spectrophotometry.

The reaction was initially followed by ¹H NMR spectroscopy as illustrated in Figure 2.5-3 (below). The reaction was run in deuterated phosphate buffer (0.1 M, 50 % FB) at pD 7.20 (pH 6.90) with the ionic strength maintained at 0.5 M with sodium perchlorate. The ¹H NMR-time profile shows the disappearance of two multiplets at 5.8 and 6.2 ppm for the allylic hydrogens (C-2 and C-5) of the '*ipso*' hydrate and the disappearance of the doublet of doublets at 1.0 ppm due to the CH₃ groups of the isopropyl substituent of this hydrate. Figure 2.5-3 also shows the slow disappearance of the multiplet at 4.2 ppm due to the C-1 hydrogen of the '*ortho*' hydrate and the disappearance of the doublet of doublets at 1.2 ppm due to the CH₃ groups of the isopropyl group. The decrease in the areas of the hydrate peaks is matched by an

increase in the area of the aromatic multiplet at 7.5 ppm, and the septet and doublet at 3 and 1.4 ppm, respectively, due to the isopropyl substituent of the product.

The NMR-time profile clearly shows the rapid reaction of the ‘*ipso*’ hydrate; the reaction is almost complete before the first spectrum is taken. The zero time spectrum was taken in 5 mM sodium deuterioxide at ionic strength 0.5 M (NaClO₄), due to the reactivity of the hydrates at pH 7.

Figure 2.5-3: Aromatisation reaction of 1-isopropylcyclohexa-2,4-dienol and 2-isopropylcyclohexa-2,4-dienol in deuterated phosphate buffer (0.1 M, 50 % FB) at pD = 7.30, I = 0.5 M (NaClO₄) and 20 % MeCN-d₃



The fraction of substrate ($f(s)$), for the ‘*ortho*’ hydrate, was calculated using equation 2.4. The term $A_{4.2}$ refers to the area of the multiplet at 4.2 ppm due to the C-1 hydrogen of the hydrate. The term A_3 refers to the area of the septet due to the C-7 hydrogen of the product arene. A correction was made to $f(s)$ to account for the presence of arene at time zero ($A_{3(t)} - A_{3(0)}$).

$$f(s) = \frac{A_{4.2(t)}}{A_{4.2(t)} + (A_{3(t)} - A_{3(0)})} \quad \text{Equation 2-4}$$

The fraction of substrate ($f(s)$), for the ‘*ipso*’ hydrate, was calculated using equation 2.5. The term $A_{1.8}$ refers to the area of the multiplet at 1.8 ppm due to the C-7 hydrogen

of the hydrate ($\text{CH}(\text{CH}_3)_2$). The term A_3 refers to the area of the septet due to the C-7 hydrogen of the product arene. A correction was made to $f(s)$ to account for the presence of arene at time zero ($A_{3(t)} - A_{3(0)}$).

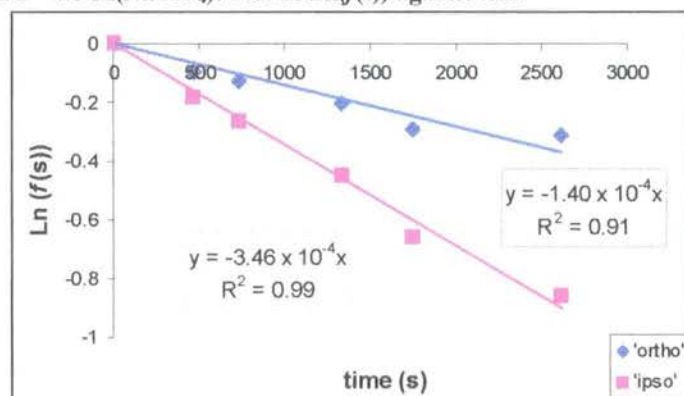
$$f(s) = \frac{A_{1.8(t)}}{A_{1.8(t)} + (A_{3(t)} - A_{3(0)})} \quad \text{Equation 2-5}$$

Experimental data for the change in $f(s)$ versus time are listed in Table 2.5-1. The first order rate constant, k_{obs} (s^{-1}), for aromatisation could be obtained as the slope of a semi-logarithmic plot of $f(s)$ against time (Fig 2.5-4), and is given in Table 2.5-1.

Table 2.5-1: Fraction of substrate over time for the *ortho* (2.23) and *ipso* (2.24) cumene hydrates

Time(s)	<i>ortho</i>			<i>ipso</i>		
	$f(s)$	$\text{Ln}(f(s))$	$k_{\text{obs}}(\text{s}^{-1})$	$f(s)$	$\text{Ln}(f(s))$	$k_{\text{obs}}(\text{s}^{-1})$
0	1.00	0.00		1.00	0.00	
472	0.91	-0.09		0.83	-0.19	
730	0.88	-0.13	1.40×10^{-4}	0.76	-0.29	3.46×10^{-4}
1334	0.82	-0.20		0.64	-0.45	
1750	0.74	-0.29		0.52	-0.66	
2613	0.73	-0.31		0.42	-0.86	

Figure 2.5-4: Aromatisation of *ipso* and *ortho* cumene hydrates in phosphate buffer (0.1 M, 50 % FB) at pD 7.3 and $I = 0.5 \text{ M}(\text{NaClO}_4)$: Plot of $\text{Ln}(f(s))$ against time

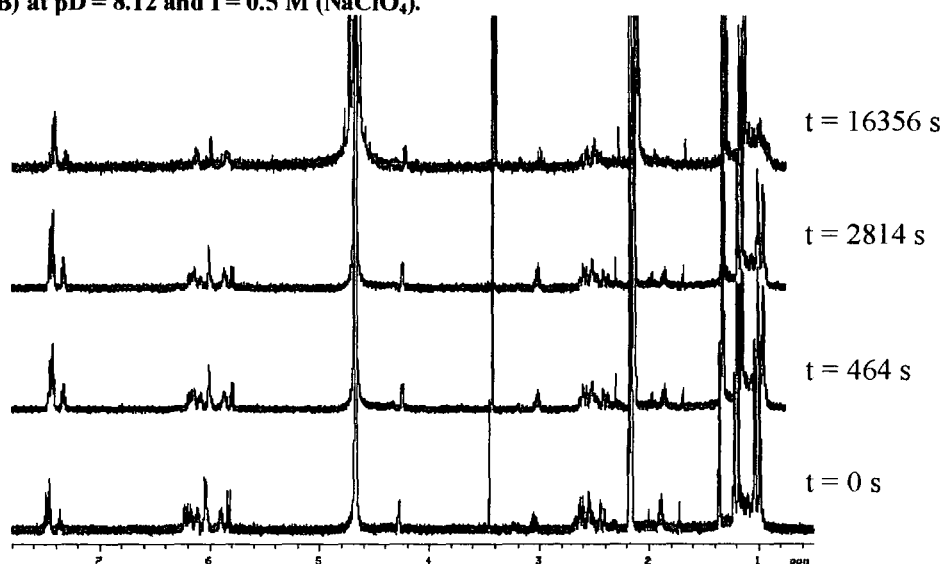


The ^1H NMR-time profile for the reaction of *ipso* (2.22) and *ortho* (2.23) cumene hydrates in deuterated phosphate buffer (0.1 M, 90 % FB) at pD 8.12 is shown below. Figure 2.5-5 shows the faster reaction of the *ipso* hydrate; the hydrate has completely

reacted before the reaction of the *ortho* hydrate has started. Over the time period illustrated, none of the *ortho* hydrate had reacted and so the area of the C1-H^o, at 4.2 ppm remains constant (A^o). A^{sept} is the area of the septet for the C7-Hⁱ at 1.9 ppm, for *ipso* cumene hydrate. The $f(s)$ was determined using equation 2.6 (below) and the crude rate constant for aromatisation of the '*ipso*' hydrate at pD 8.12 is $9.1 \times 10^{-5} \text{ s}^{-1}$.

$$f(s) = \frac{\left(\frac{A^{sept}}{A^o}\right)_t}{\left(\frac{A^{sept}}{A^o}\right)_0} \quad \text{Equation 2-6}$$

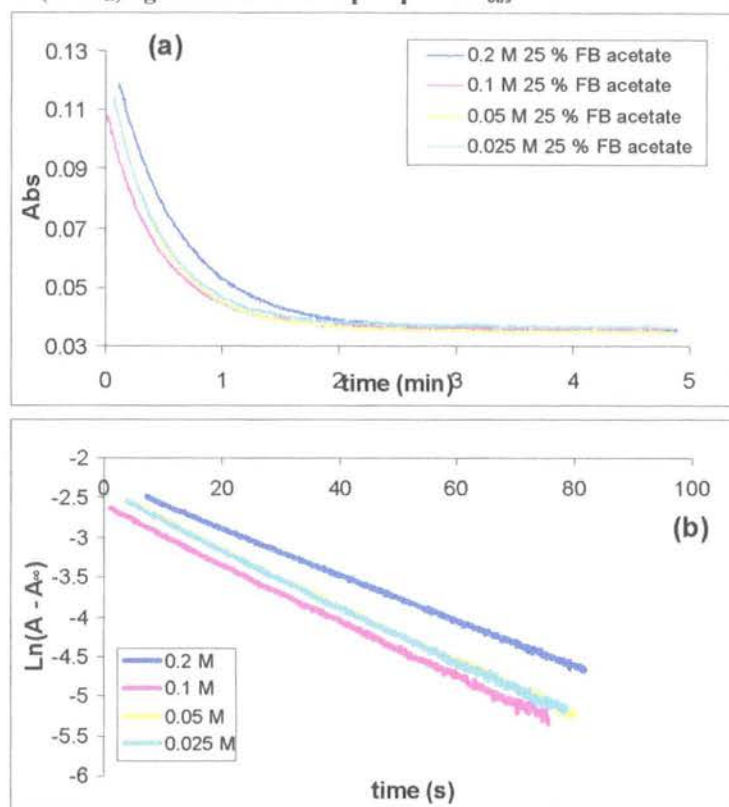
Figure 2.5-5: Aromatisation of *ortho* and *ipso* cumene hydrates in deuterated phosphate buffer (0.1 M, 90 % FB) at pD = 8.12 and I = 0.5 M (NaClO₄).



Due to the solubility issues associated with the hydrates studied and the resulting low signal/noise values of the NMR spectra in D₂O, NMR kinetics were judged to be relatively inaccurate in this case and so the second-order rate constant for aromatisation was determined by UV-Vis spectrophotometry.

Figure 2.4-6(a) shows the change in absorbance against time at 254 nm as a result of the reaction of the isopropylbenzene hydrates in acetate buffer (25 % FB, pH 4.2). A corresponding semi-logarithmic plot of $\Delta A = A - A_\infty$ against time is shown in Figure 2.4-6(b) where A_∞ refers to the absorbance at the end of the reaction.

Figure 2.5-6: Aromatisation reaction of *ortho* cumene hydrate (2.23) in acetate buffer (25 % FB, pH 4.2) at 25 °C and $I = 0.5 \text{ M}$ (NaClO_4) followed at $\lambda = 254 \text{ nm}$. (a) Plot of absorbance versus time; (b) plot of $\ln(A - A_\infty)$ against time with slope equal to k_{obs}



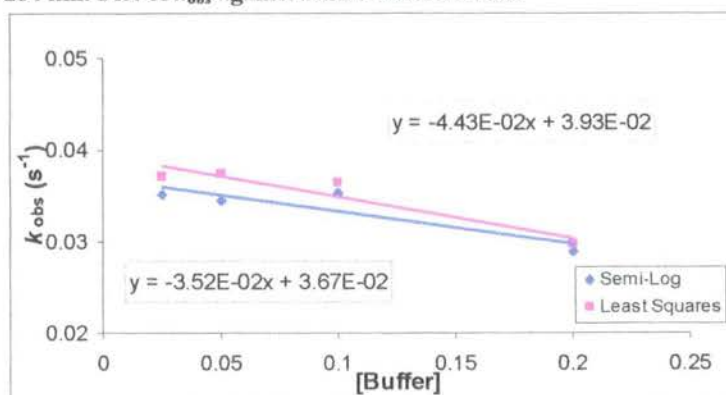
The table below summarises the first order rate constants of aromatisation for 2-isopropylcyclohexa-2,4-dienol (k_{obs}^o) in 25 % FB acetate buffer at pH 4.2 and ionic strength 0.5, maintained with sodium perchlorate. At this pH value the rate of aromatisation of 1-isopropylcyclohexa-2,4-dienol is too fast to be monitored by standard UV-vis methods.

Table 2.5-2: First-order rate constants for aromatisation of *ortho* cumene hydrate (2.23) in acetate buffer (25 % FB, pH 4.2) at I = 0.5 M (NaClO₄) and 25 °C

[Buffer] (M)	pH ^(b)	[H ⁺] ^(c) x 10 ⁻⁵ M	Semi-log Plot		Least Squares Plot			
			$k_{\text{obs}}^{\circ(d)}$ (x 10 ⁻²) s ⁻¹	R ²	$k_{\text{int}}^{\circ(e)}$ (x 10 ⁻²) s ⁻¹	$k_{\text{obs}}^{\circ(f)}$ (x 10 ⁻²) s ⁻¹	R ²	$k_{\text{int}}^{\circ(e)}$ (x 10 ⁻²) s ⁻¹
0.20	4.21	6.14	2.89	0.999		2.97	0.999	
0.10	4.21	6.12	3.52	0.998	3.67	3.64	0.999	3.93
0.05	4.22	6.08	3.45	0.997	(3.34 ^(g))	3.74	0.999	(3.51 ^(g))
0.025	4.22	6.07	3.51	0.998		3.70	0.999	

(a) Measurements were made at a substrate concentration of 0.05 mM and 1 % acetonitrile (b) pH was determined using a MeterLab™ PHM 290 pH-Stat Controller equipped with a radiometer (pH 4 - 7 - 10 @ 25 °C) combination electrode (type pHC4006) with a saturated LiTCA filling solution. (c) [H⁺] was calculated using $[H^+] = 10^{-(\text{pH} / \gamma_{\text{H}^+})}$ where $\gamma_{\text{H}^+} = 1$ is the activity coefficient of the hydronium ion under the experimental conditions. (d) The value of the first-order rate constant (k_{obs}°), was obtained from the slope of the plot of $\ln(A - A_{\infty})$ against time in Figure 2.5.2-5(b). (e) k_{int}° is defined as the intercept of the plot of k_{obs}° against buffer concentration Figure 2.5.-7. (f) The value of the first-order rate constant (k_{obs}°), was obtained from the least squares analysis of Figure 2.5-6(a). (g) mean of k_{obs}°

Both methods of analysis show very good correlations. The least squares fit gave an error of the estimate of k_{obs}° as $3.5 \times 10^{-4} \text{ s}^{-1}$; the t-values for the fit of the rate-constant were greater than 1000 with p-values less than 1×10^{-4} . The least squares analysis gave a mean value of k_{obs}° of $3.51 \pm 0.18 \times 10^{-2} \text{ s}^{-1}$. The semi-logarithmic analysis gave a mean value of k_{obs}° of $3.34 \pm 0.15 \times 10^{-2} \text{ s}^{-1}$. An unpaired t-test gave a p-value of 0.50 whereas a paired t-test gave a p-value of 0.03.

Figure 2.5-7: Aromatisation reaction of *ortho* cumene hydrate in 25 % FB acetate buffer at pH 4.2 followed at $\lambda = 254 \text{ nm}$: Plot of k_{obs}° against buffer concentration

The buffer catalysis plot (see Fig 2.5-7, above) shows no evidence of buffer catalysis, in fact there is a negative slope on the order of $4 \times 10^{-2} \text{ M}^{-1}\text{s}^{-1}$. The difference in rate between the highest and lowest buffer concentration is 25 %. The mean first order rate constant of aromatisation of *ortho* cumene hydrate at pH 4.2 is $3.4 \times 10^{-2} \text{ s}^{-1}$ which corresponds to a half-life of 20 seconds.

Figure 2.4-8(a) shows the change in absorbance against time at 254 nm as a result of the reaction of the isopropylbenzene hydrates in acetate buffer (50 % FB, pH 4.6). A corresponding semi-logarithmic plot of $\Delta A = A - A_{\infty}$ against time is shown in Figure 2.4-8(b) where A_{∞} refers to the absorbance at the end of the reaction.

Figure 2.5-8: Aromatisation of *ortho* cumene hydrate (2.23) in acetate buffer (50 % FB, pH 4.6) at 25 °C and $I = 0.5 \text{ M}(\text{NaClO}_4)$ (a) Plot of absorbance versus time; (b) plot of $\ln(A - A_{\infty})$ against time with slope equal to k_{obs}

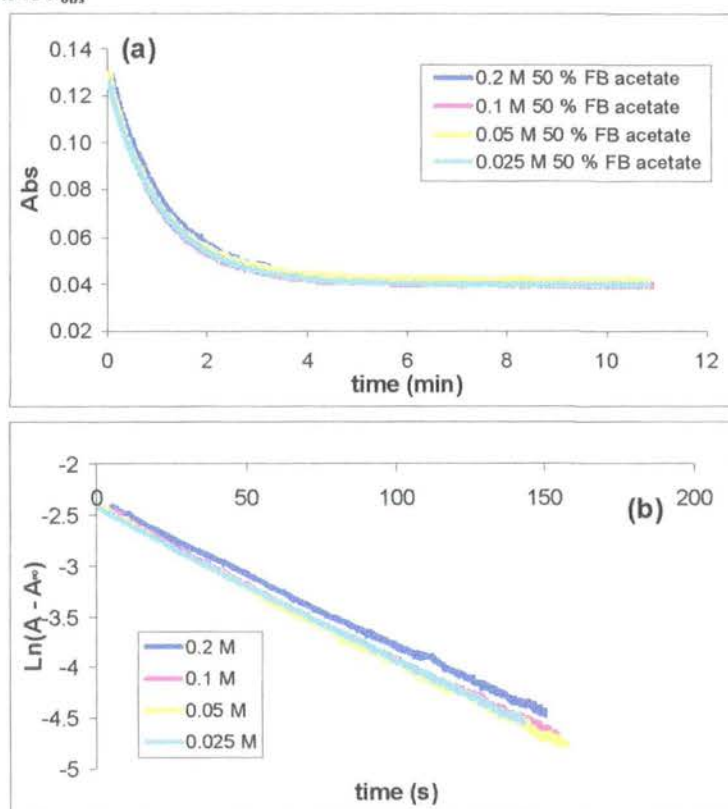


Table 2.5-3 (below) summarises the first order rate constants of aromatisation of *ortho* cumene hydrate in acetate buffer (50 % FB, pH 4.6) at ionic strength 0.5 maintained

with sodium perchlorate and 25 °C. The results below show a very good correlation between the two methods of analysis. The least squares analysis of Figure 2.5-8(a) gave an error of the estimate of 4×10^{-4} . The mean of the t-values for the fit of the rate constant was 1755, with the p-values below 1×10^{-4} . The data did not give a reasonable estimate of the rate constant when fitting a double exponential equation (t-value < 50). The mean of the first order rate constants from the least squares analysis was $1.52 \pm 0.03 \times 10^{-2} \text{ s}^{-1}$. The semi-logarithmic analysis (see Fig 2.5-8(b)) gave a mean of k_{obs} of $1.45 \pm 0.02 \times 10^{-2}$. An unpaired t-test gave a p-value of 0.16 and a paired t-test gave a p-value of 0.03.

Table 2.5-3: First-order rate constants for aromatisation of cumene hydrate in 50% FB acetate buffers (0.2 – 0.025 M) at 25 °C and I = 0.5 M(NaClO₄)^(a)

[Buffer] (M)	pH ^(b)	$[\text{H}^+]^{(c)}$ $\times 10^{-5}$ M	Semi-log Plot			Least Squares Plot		
			$k_{\text{obs}}^{(d)}$ ($\times 10^{-2}$) s^{-1}	R^2	$k_{\text{int}}^{(e)}$ ($\times 10^{-2}$) s^{-1}	$k_{\text{obs}}^{(f)}$ ($\times 10^{-2}$) s^{-1}	R^2	$k_{\text{int}}^{(e)}$ ($\times 10^{-2}$) s^{-1}
0.20	4.58	2.63	1.39	0.999		1.43	0.999	
0.10	4.54	2.88	1.47	0.998	1.50	1.57	0.999	1.57
0.05	4.56	2.75	1.49	0.998	(1.45 ^(g))	1.56	0.999	(1.52 ^(g))
0.025	4.56	2.75	1.47	0.999		1.50	0.999	

(a) Measurements were made at a substrate concentration of 0.05 mM and 1 % acetonitrile (b) pH was determined using a MeterLab™ PHM 290 pH-Stat Controller equipped with a radiometer (pH 4 - 7 - 10 @ 25 °C) combination electrode (type pHC4006) with a saturated LiTCA filling solution. (c) $[\text{H}^+]$ was calculated using $[\text{H}^+] = 10^{-(\text{pH} / \gamma_{\text{H}})}$ where $\gamma_{\text{H}} = 1$ is the activity coefficient of the hydronium ion under the experimental conditions. (d) The value of the first-order rate constant (k_{obs}), was obtained from the slope of the plot of $\ln(A - A_{\infty})$ against time in Figure 2.5.2-8(b). (e) k_{int} is defined as the intercept of the plot of k_{obs} against buffer concentration Figure 2.5.2-9. (f) The value of the first-order rate constant (k_{obs}), was obtained from the least squares analysis of Figure 2.5.2-8(a). (g) mean of k_{obs}

The buffer catalysis plot (fig 2.5-9) has a slightly negative slope (-5×10^{-3}), the difference in rate between the highest and lowest buffer concentration is 5 %. The average first order rate constant for the aromatisation of *ortho* cumene hydrate at pH 4.6 is $1.52 \times 10^{-2} \text{ s}^{-1}$ which corresponds to a half-life of 46 seconds.

Figure 2.5-9: Aromatisation of cumene hydrate in 50 % FB acetate buffer at pH 4.6: Plot of k_{obs} against buffer concentration

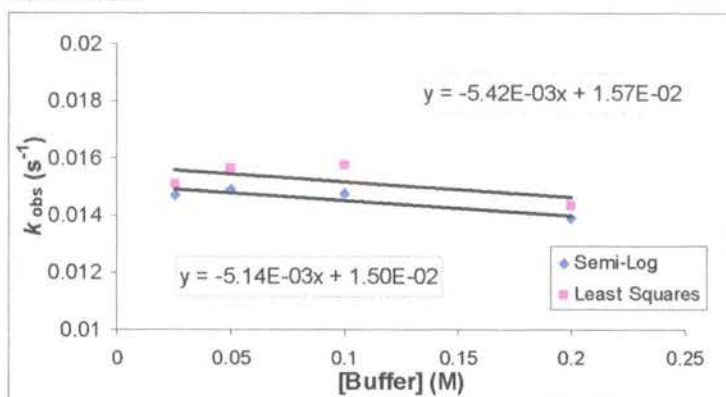


Figure 2.4-10(a) shows the change in absorbance against time at 254 nm as a result of the reaction of the isopropylbenzene hydrates in acetate buffer (75 % FB, pH 4.9). A corresponding semi-logarithmic plot of $\Delta A = A - A_{\infty}$ against time is shown in Figure 2.4-10(b) where A_{∞} refers to the absorbance at the end of the reaction.

Figure 2.5-10: : Aromatisation of cumene hydrate in 75 % FB acetate buffer at pH 4.9 (a) Plot of absorbance versus time; (b) plot of $\ln(A - A_{\infty})$ against time with slope equal to k_{obs}

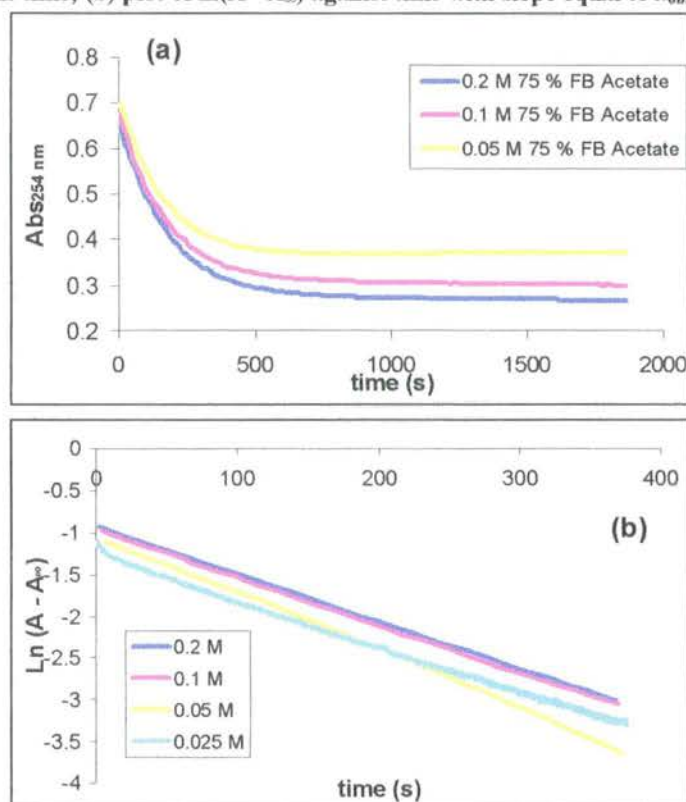


Table 2.5-4 (below) summarises the first order rate constants for the aromatisation of *ortho* cumene hydrate at pH 4.9. Both the least squares and semi-logarithmic analyses gave similar results. The mean of the first order rate constants for the aromatisation reaction from the semi-logarithmic analysis (see Fig 2.5-10(b)) is $5.93 \pm 0.35 \times 10^{-3} \text{ s}^{-1}$. The least squares analysis of the experimental data (see Fig 2.5-10(b)) shows the error of the estimate on the order of 1.5×10^{-3} and a mean t-value for the estimate of k_{obs} of 539. The mean of the first order rate constants is $5.96 \pm 0.28 \times 10^{-3} \text{ s}^{-1}$. An unpaired t-test of the results from the different analyses gave a p-value of 0.94 and a paired t-test of the same data gave a p-value of 0.77.

Table 2.5-4: First-order rate constants for aromatisation of *ortho* cumene hydrate (2.23) in 75% FB acetate buffers (0.2 – 0.025 M) at 25 °C and I = 0.5 M (NaClO₄)^(a).

[Buffer] (M)	pH ^(b)	$[\text{H}^+]^{(c)}$ $\times 10^{-5}$ M	Semi-log Plot			Least Squares Plot		
			$k_{\text{obs}}^{(d)}$ ($\times 10^{-3}$) s^{-1}	R ²	$k_{\text{int}}^{(e)}$ ($\times 10^{-3}$) s^{-1}	$k_{\text{obs}}^{(f)}$ ($\times 10^{-3}$) s^{-1}	R ²	$k_{\text{int}}^{(e)}$ ($\times 10^{-3}$) s^{-1}
0.20	4.93	3.11	5.65	0.999		5.57	0.999	
0.10	4.93	3.10	5.66	0.999	6.15	5.77	0.999	6.28
0.05	4.94	3.03	6.96	0.999	5.93 ^(g)	6.80	0.999	5.96 ^(g)
0.025	4.95	3.00	5.44	0.998		5.70	0.999	

(a) Measurements were made at a substrate concentration of 0.05 mM and 1 % acetonitrile (b) pH was determined using a MeterLab™ PHM 290 pH-Stat Controller equipped with a radiometer (pH 4 - 7 - 10 @ 25 °C) combination electrode (type pHC4006) with a saturated LiTCA filling solution. (c) $[\text{H}^+]$ was calculated using $[\text{H}^+] = 10^{-(\text{pH}/\gamma_{\text{H}})}$ where $\gamma_{\text{H}} = 1$ is the activity coefficient of the hydronium ion under our experimental conditions. (d) The value of the first-order rate constant (k_{obs}), was obtained from the slope of the plot of $\ln(A_{\infty} - A)$ against time in Figure 2.5.2-10(b). (e) k_{int} is defined as the intercept of the plot of k_{obs} against buffer concentration Figure 2.5.2-11. (f) The value of the first-order rate constant (k_{obs}), was obtained from the least squares analysis of Figure 2.5.2-10(a) (g) Mean of k_{obs} for 0.2- 0.05 M solutions at constant pH.

The plot of k_{obs} against buffer concentration (Fig 2.5-11) showed no evidence of buffer catalysis, there is, however a negative slope on the order of $3 \times 10^{-3} \text{ M}^{-1} \text{ s}^{-1}$. The rate of aromatisation of *ortho* cumene hydrate at pH 4.9 is $5.96 \times 10^{-3} \text{ s}^{-1}$.

Figure 2.5-11: Aromatisation of cumene hydrate in acetate buffer (75 % FB, pH 4.9) at 25 °C and I = 0.5 M (NaClO₄): Plot of k_{obs} against buffer concentration

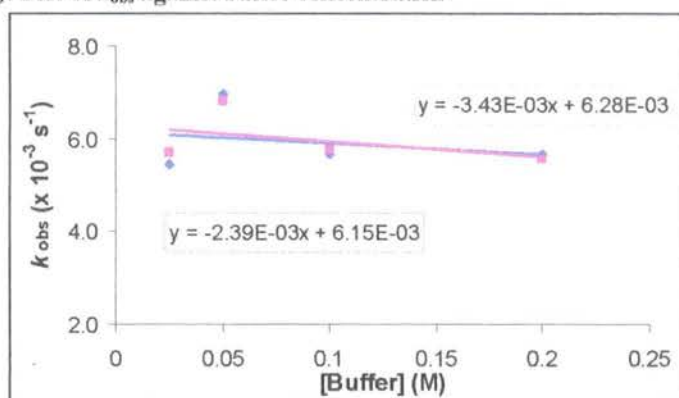


Figure 2.4-12(a) shows the change in absorbance against time at 254 nm as a result of the reaction of the isopropylbenzene hydrates in acetate buffer (90 % FB, pH 5.6). A corresponding semi-logarithmic plot of $\Delta A = A - A_{\infty}$ against time is shown in Figure 2.4-12(b) where A_{∞} refers to the absorbance at the end of the reaction.

Figure 2.5-12: Aromatisation reaction of *ortho* cumene hydrate in acetate buffer (90 % FB, pH 5.6) at 25 °C and I = 0.5 M (NaClO₄). (a) Plot of absorbance versus time; (b) plot of $\ln(A - A_{\infty})$ against time with slope equal to k_{obs}

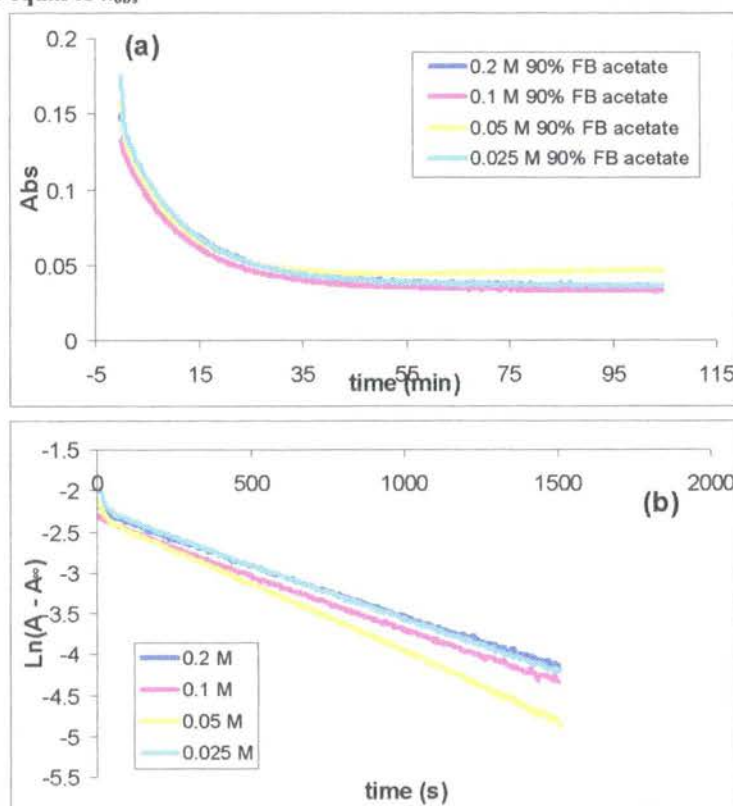
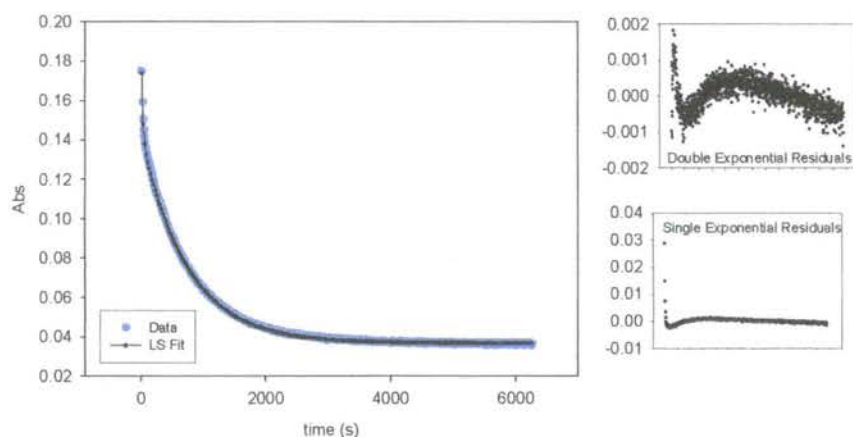


Table 2.5-5 (below) summarises the results from the aromatisation reaction of the cumene hydrates in 90 % FB acetate buffer. The data below show the correlation between the semi-logarithmic and the least squares analyses. At this pH, it is possible to see the fast reaction of the '*ipso*' hydrate (see Fig 2.5-12(a)), however, the reaction is too fast to be accurately separated from the slower reaction of the '*ortho*' hydrate. Only in the case of the 0.025 M buffer (see Fig 2.5-13) was the faster reaction estimated; this estimated a first order rate constant for the aromatisation of *ipso* cumene hydrate of $4.82 \times 10^{-2} \text{ s}^{-1}$ corresponding to a half-life of 14 seconds.

Figure 2.5-13: UV-vis spectrophotometric data from the aromatisation of the cumene hydrates: Acetate buffer (90 % FB, 0.025 M), least squares analysis. Inset: Single and double exponential residuals



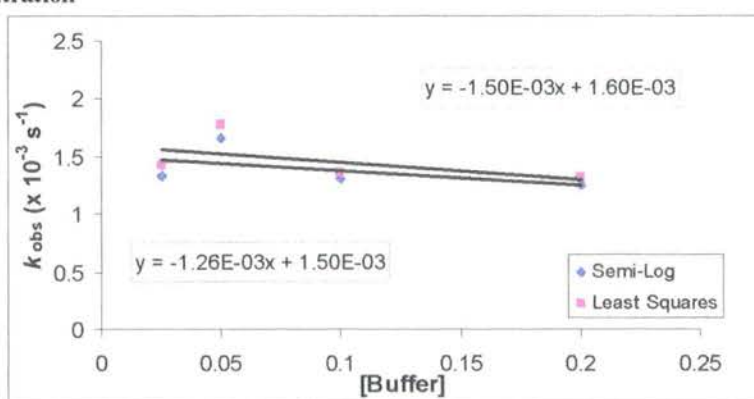
The least squares analysis using a single exponential equation gives a reasonable fit with the error of the estimate on the order of 1.0×10^{-3} . The t-values for the estimate of the first order rate constants had a mean of 400 with all p-values less than 1×10^{-4} . The estimates of the rate constants from fitting the double exponential equation were unreasonable except in the case of 0.025 M (Fig 2.5-13). The t-values for the faster reaction were in one case below 1 and had a mean of 30. Using the single exponential equation, the mean of the rate constants for aromatisation was $1.46 \pm 0.10 \times 10^{-3} \text{ s}^{-1}$. This corresponds well with the results from the semi-logarithmic analysis (see Fig 2.5.2-12(b)) which has a mean of $1.39 \pm 0.21 \times 10^{-3} \text{ s}^{-1}$.

Table 2.5-5: First-order rate constants for aromatisation of cumene hydrate in 90 % FB acetate buffers (0.20 – 0.025 M) at 25 °C and I = 0.5 M (NaClO₄)^(a).

[Buffer] (M)	pH ^(b)	Semi-log Plot				Least Squares Plot			
		[H ⁺] ^(c) x 10 ⁻⁶ M	k_{obs} ^(d) (x 10 ⁻³) s ⁻¹	R ²	k_{int} ^(f) (x 10 ⁻³) s ⁻¹	k_{obs} ^(e) (x 10 ⁻³) s ⁻¹	R ²	k_{int} ^(f) (x 10 ⁻³) s ⁻¹	
0.20	5.55	2.84	1.25	0.998		1.31	0.999		
0.10	5.55	2.85	1.31	0.998	1.50	1.36	0.999	1.60	
0.05	5.54	2.88	1.66	0.999	(1.34 ^(g))	1.77	0.998	(1.46 ^(g))	
0.025	5.56	2.74	1.32	0.997		1.41	0.997		

(a) Measurements were made at a substrate concentration of 0.05 mM and 1 % acetonitrile (b) pH was determined using a MeterLab™ PHM 290 pH-Stat Controller equipped with a radiometer (pH 4 - 7 - 10 @ 25 °C) combination electrode (type pHC4006) with a saturated LiTCA filling solution. (c) [H⁺] was calculated using $[H^+] = 10^{-(\text{pH}/\gamma_{\text{H}})}$ where $\gamma_{\text{H}} = 1$ is the activity coefficient of the hydronium ion under our experimental conditions. (d) The value of the first-order rate constant (k_{obs}), was obtained from the slope of the plot of $\ln(A_{\infty} - A)$ against time in Figure 2.5-12(b). (e) k_{int} is defined as the intercept of the plot of k_{obs} against buffer concentration Figure 2.5-13. (f) The value of the first-order rate constant (k_{obs}), was obtained from the least squares analysis of Figure 2.5-12(a) (g) Mean of k_{obs} for 0.2- 0.05 M solutions at constant pH.

Figure 2.5-14 shows no evidence of buffer catalysis; the slope is on the order of $-1 \times 10^{-3} \text{ M}^{-1} \text{ s}^{-1}$. The mean first order rate constant for the aromatisation of *ortho* cumene hydrate at pH 5.6 is $1.46 \times 10^{-3} \text{ s}^{-1}$.

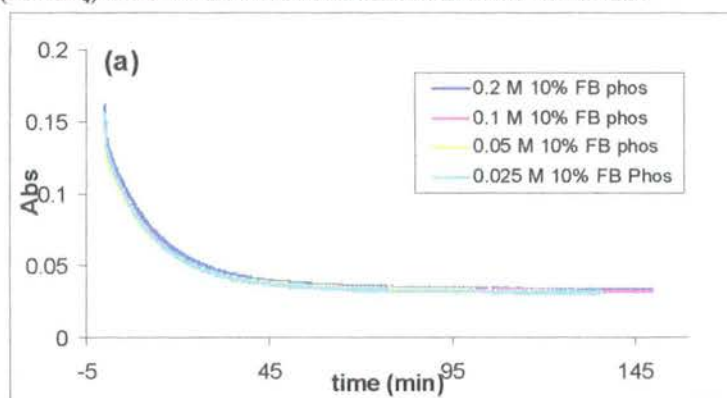
Figure 2.5-14: Aromatisation reaction of cumene hydrate in 90 % FB acetate: Plot of k_{obs} against buffer concentration

At pH values above ~5.5, the contribution of the faster reaction of the *ipso*-hydrate became significant. This could be deduced on the basis of whether the data were fitted better by a double exponential least squares analysis rather than a single exponential analysis. To extract the two first order rate constants a double exponential least squares fit of the experimental absorbance versus time, data is used (eqn 2.7).

$$y = y_0 + Ae^{-bx} + Ce^{-dx} \quad \text{Equation 2-7}$$

In Equation 2-7 A and b are the pre-exponential factor and first order rate constant of the first reaction and C and d are the pre-exponential factor and first order rate constant for the second reaction.

Figure 2.5-15: Aromatisation reaction of the cumene hydrates in phosphate buffer (10 % FB, pH 5.6) , I = 0.5 M(NaClO₄) at 25 °C: Plot of absorbance at 254 nm versus time



The data in the Table 2.5-6 (below) show the single and double exponential fits of the experimental data shown in Fig 2.5-15. The double exponential equation gives a better fit for the first order rate constants as it has an error of the estimate of the regression of 4×10^{-4} whereas the single exponential has a regression error of 1.1×10^{-3} . The t-values for the estimate of the rate constant from the single-exponential equation are on the order of 600. However, the t-values for the estimate of the first rate constant have a mean of 54 and for the second rate constant it is 1019.

Table 2.5-6: First-order rate constants for aromatisation of cumene hydrate using least squares analysis in 10% FB phosphate buffers (0.2 – 0.025 M) at 25 °C^(a)

[Buffer] (M)	pH ^(b)	[H ⁺] ^(c) x 10 ⁻⁶ M	Single Exponential ^(d)		Double Exponential ^(e)		
			k_{obs} (x 10 ⁻³ s ⁻¹)	R ²	k_{obs}^i (x 10 ⁻² s ⁻¹)	k_{obs}^o (x 10 ⁻³ s ⁻¹)	R ²
0.2	5.59	7.82	1.17	0.9986	3.63	1.16	0.9996
0.10	5.60	7.60	1.22	0.9990	3.73	1.21	0.9996
0.05	5.61	7.50	1.16	0.9990	3.65	1.17	0.9998
0.025	5.62	7.24	1.20	0.9982	3.42	1.18	0.9994

(a) Measurements were made at a substrate concentration of 0.05 mM and 1 % acetonitrile (b) pH was determined using a MeterLabTM PHM 290 pH-Stat Controller equipped with a radiometer (pH 4 - 7 - 10 @ 25 °C) combination electrode (type pHC4006) with a saturated LiTCA filling solution. (c) [H⁺] was calculated using $[H^+] = 10^{-(\text{pH}/\gamma_H)}$ where $\gamma_H = 1$ is the activity coefficient of the hydronium ion under our experimental conditions. (d) The value of the first-order rate constant (k_{obs}), was obtained from the least squares fit of the experimental data below Figure 2.5-15 (a) using a single exponential equation (e) The value of the first-order rate constants k_{obs}^i and k_{obs}^o was obtained from the least squares analysis of Figure 2.5-15(a) using the double exponential equation (2.7).

An example of the double exponential fit is shown below. The residuals (Fig 2.5-16(inset)) compare the errors of the single and double exponential equations. In the double exponential fit the error is ± 0.0025 whereas in the single exponential regression the fit is ± 0.025 .

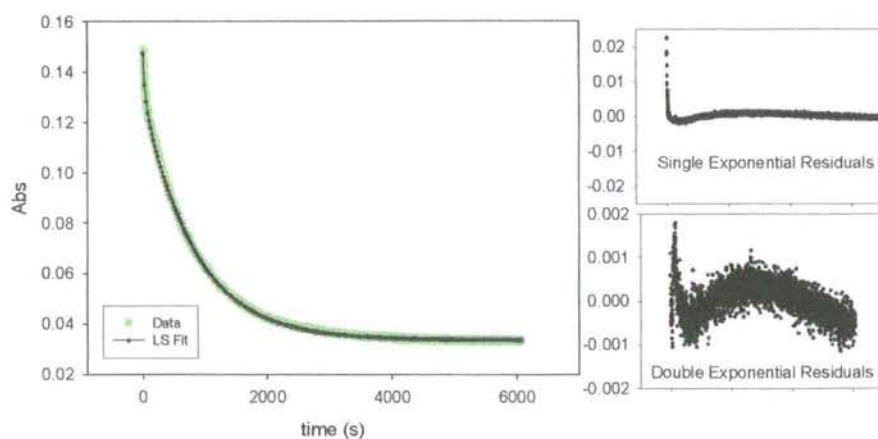
Figure 2.5-16: UV-vis spectrophotometric data from the aromatisation reaction of 1-isopropylcyclohexa-2,4-dienol and 2-isopropylcyclohexa-2,4-dienol in phosphate buffer (0.1 M, 10 % FB) at pH 5.60 and I = 0.5 M (NaClO₄) (inset: single and double exponential residuals)

Figure 2.5-17: Aromatisation reaction of the cumene hydrates in phosphate buffer (10 % FB, pH 5.6) at I = 0.5 M (NaClO₄) and 25 °C: Semi-logarithmic plot of (A-A_∞) against time

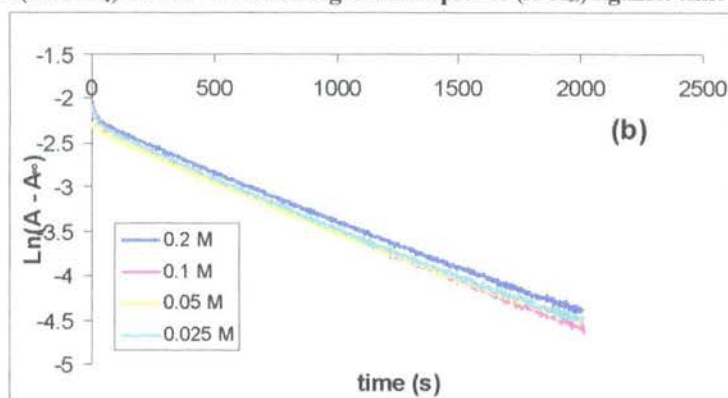


Figure 2.5-17 shows the semi-logarithmic plot of $A - A_{\infty}$ against time. The plot shows non-linearity at the beginning, which is further evidence of a second parallel reaction. The results from the semi-logarithmic analysis are summarised in Table 2.5-7 and compared with the double exponential least squares analysis presented above.

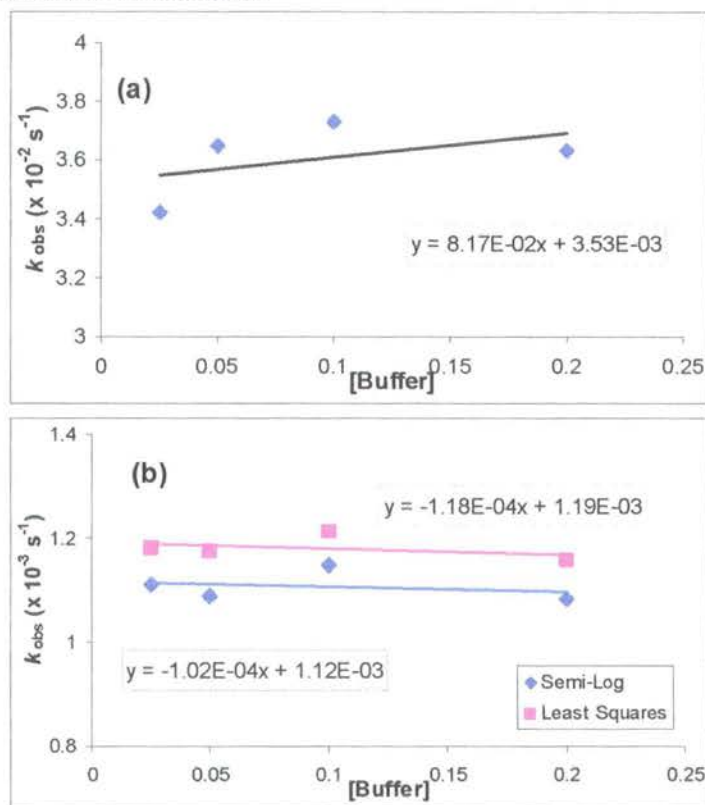
Table 2.5-7: First-order rate constants for aromatisation of cumene hydrate in 10% FB phosphate buffers (0.2 – 0.025 M) at 25 °C and I = 0.5 M (NaClO₄)^(a)

[Buffer] (M)	pH ^(b)	Semi-log Plot			Least Squares Plot			$k_{\text{int}}^{(d)}$ (s ⁻¹)
		$k_{\text{obs}}^{o(c)}$ (x 10 ⁻⁴) s ⁻¹	R ²	$k_{\text{int}}^{(d)}$ (x 10 ⁻³) s ⁻¹	$k_{\text{obs}}^{i(e)}$ (x 10 ⁻²) s ⁻¹	$k_{\text{obs}}^{o(e)}$ (x 10 ⁻³) s ⁻¹	R ²	
0.20	5.59	1.08	0.997		3.63	1.16	0.999	<i>ipso</i> : 3.53 x 10 ⁻²
0.10	5.60	1.15	0.998	1.12	3.73	1.21	0.999	(3.61 x 10 ^{-2(f)})
0.05	5.61	1.09	0.998	(1.11 ^(f))	3.65	1.17	0.999	<i>ortho</i> : 1.19 x 10 ⁻⁴
0.025	5.62	1.11	0.997		3.42	1.18	0.999	(1.18 x 10 ^{-4(f)})

(a) Measurements were made at a substrate concentration of 0.05 mM and 1 % acetonitrile (b) pH was determined using a MeterLab™ PHM 290 pH-Stat Controller equipped with a radiometer (pH 4 - 7 - 10 @ 25 °C) combination electrode (type pHC4006) with a saturated LiTCA filling solution. (c) The value of the first-order rate constant (k_{obs}), was obtained from the slope of the plot of $\ln(A - A_{\infty})$ against time in Figure 2.5-17. (d) k_{int} is defined as the intercept of the plot of k_{obs} against buffer concentration. (e) The value of the first-order rate constant (k_{obs}), was obtained from the least squares analysis of Figure 2.5-14. (f) mean of k_{obs}

Figure 2.5.2-18(a & b) shows the plots of the first order rate constants for aromatisation of the *ipso* (k_{obs}^i) and *ortho* (k_{obs}^o) cumene hydrates against buffer concentration. The plots (Fig 2.5-18 (a) and (b)) show no evidence for buffer catalysis.

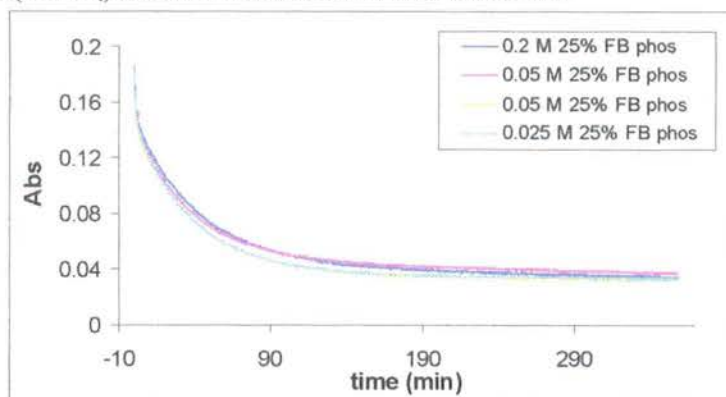
Figure 2.5-18: The aromatisation reactions of *ipso* and *ortho* cumene hydrates phosphate buffers (10 % FB, pH 5.6) at I = 0.5 M(NaClO₄) and 25 °C. (a) plot of k_{obs}^i against buffer concentration; (b) plot of k_{obs}^o against buffer concentration.



The mean first order rate constant for the aromatisation of 1-isopropylcyclohexa-2,4-dienol (*ipso* cumene hydrate) is $3.61 \pm 0.07 \times 10^{-2}$ s $^{-1}$ at pH 5.6. The mean first order rate constant for the aromatisation of 2-isopropylcyclohexa-2,4-dienol (*ortho* cumene hydrate) is $1.18 \pm 0.01 \times 10^{-3}$ s $^{-1}$ at pH 5.6. These correspond to half-lives of 19 and 587 seconds, respectively.

Figure 2.4-19(a) shows the change in absorbance against time at 254 nm as a result of the reaction of *ipso* and *ortho* cumene hydrates in phosphate buffer (25 % FB, pH 6.1).

Figure 2.5-19: The aromatisation reaction of cumene hydrate in phosphate buffer (25 % FB, pH 6.1) at I = 0.5 M(NaClO₄) and 25 °C: Plot of absorbance versus time



The table below summarises the results from the double exponential least squares fit (using equation 2.7) of the experimental data in Figure 2.5-19.

Table 2.5-8: First-order rate constants for aromatisation of 1-isopropylcyclohexa-2,4-dienol (2.22) and 2-isopropylcyclohexa-2,4-dienol (2.23) using least squares analysis in 25 % FB phosphate buffers (0.2 – 0.025 M) at 25 °C and I = 0.5 M(NaClO₄)^(a)

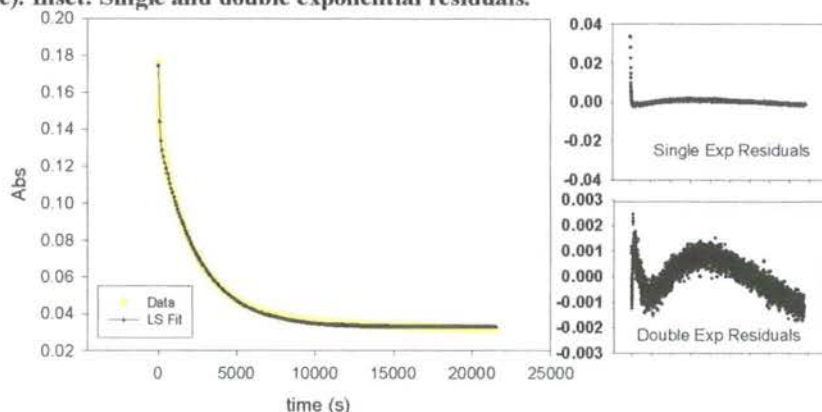
[Buffer] (M)	pH ^(b)	[H ⁺] ^(c) (x 10 ⁻⁷) M	$k_{\text{obs}}^{\text{(d)}}$ (x 10 ⁻²) s ⁻¹	$k_{\text{obs}}^{\text{(e)}}$ (x 10 ⁻⁴) s ⁻¹	R ²	$k_{\text{int}}^{\text{(f)}}$ (x 10 ⁻²) s ⁻¹	$k_{\text{obs}}^{\text{(g)}}$ (x 10 ⁻⁴) s ⁻¹
0.20	6.09	8.22	1.10	3.46	0.9992		
0.10	6.08	8.28	1.14	3.78	0.9987	1.64	4.17
0.05	6.08	8.34	1.60	3.96	0.9996	(1.35 ^(g))	(3.83 ^(g))
0.025	6.07	8.45	1.58	4.12	0.9997		

(a) Measurements were made at a substrate concentration of 0.05 mM and 1 % acetonitrile (b) pH was determined using a MeterLabTM PHM 290 pH-Stat Controller equipped with a radiometer (pH 4 - 7 - 10 @ 25 °C) combination electrode (type pH4006) with a saturated LiTCA filling solution. (c) [H⁺] was calculated using $[\text{H}^+] = 10^{-(\text{pH}/\gamma_{\text{H}})}$ where $\gamma_{\text{H}} = 1$ is the activity coefficient of the hydronium ion under the experimental conditions. (d) The value of the first-order rate constant ($k_{\text{obs}}^{\text{(d)}}$), was obtained from the least squares fit of the data below Figure 2.5-19 using equation 2.7. (e) The value of the first-order rate constant ($k_{\text{obs}}^{\text{(e)}}$), was obtained from the least squares fit of the data below Figure 2.5-19 using equation 2.7. (f) k_{int} is defined as the intercept of the plot of k_{obs} against buffer concentration. (g) mean of k_{obs} .

An example of the double exponential fit of the data with double and single exponential residuals (Figure 2.5-20(inset)) is shown in Fig 2.5-20. The residuals, inset below,

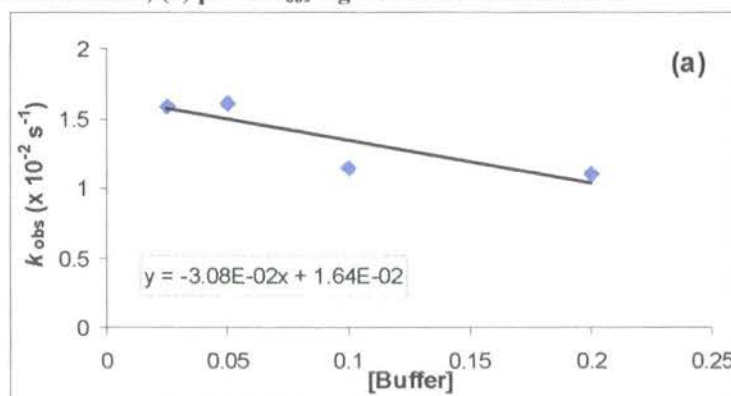
show that the total error around the regression line in the single exponential fit is ± 0.02 ; whereas for the double exponential fit the error is ± 0.003 .

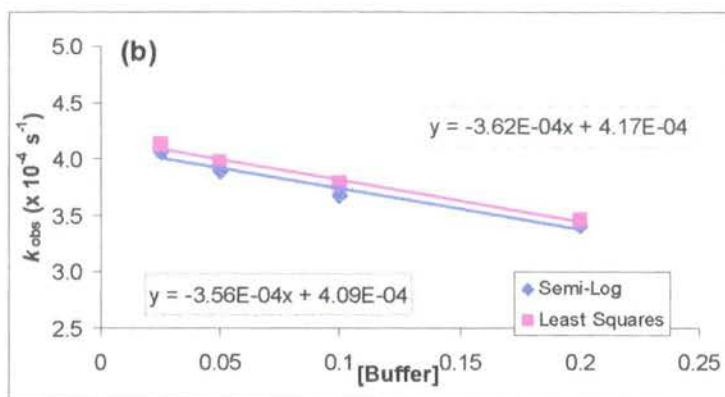
Figure 2.5-20: UV-vis spectrophotometric data from the aromatisation reaction of 1-isopropylcyclohexa-2,4-dienol and 2-isopropylcyclohexa-2,4-dienol in phosphate buffer (0.05 M, 25 % FB) at pH 5.60 and $I = 0.5 \text{ M}(\text{NaClO}_4)$ (yellow line) and the double exponential least squares fit (black line). Inset: Single and double exponential residuals.



The error of the estimate for the single exponential fit of Fig 2.5-20 is 1.8×10^{-3} and for the double exponential equation 3.8×10^{-4} . The mean t-value for the estimate of the rate constant for the single exponential equation is 421 whereas for the two rate constants of the double exponential equation the mean t-values were 66 and 823. A semi-logarithmic plot shows non-linearity which, as discussed previously, is further proof of two parallel reactions. The buffer catalysis plots show no evidence for buffer catalysis.

Figure 2.5-21: The aromatisation reaction of *ipso* and *ortho* cumene hydrates in phosphate buffer (25 % FB, pH 6.1) at $I = 0.5 \text{ M}(\text{NaClO}_4)$ and $25 \text{ }^\circ\text{C}$: Plot of absorbance versus time (a) plot of k_{obs}^i against buffer concentration; (b) plot of k_{obs}^o against buffer concentration





The mean rate of aromatisation of 1-isopropylcyclohexa-2,4-dienol is $1.35 \pm 0.14 \times 10^{-2} \text{ s}^{-1}$ at pH 6.1. The mean rate of aromatisation of 2-isopropylcyclohexa-2,4-dienol is $3.83 \pm 0.14 \times 10^{-4} \text{ s}^{-1}$ at pH 5.6. These correspond to half-lives of 51 and 1810 seconds respectively.

Figure 2.5-22 (below) shows the experimental UV-vis spectrophotometric data from the aromatisation reaction of the *ipso* and *ortho* cumene hydrates in phosphate buffer (50 % FB, pH 6.6).

Figure 2.5-22: Aromatisation of *ipso* and *ortho* cumene hydrates in phosphate buffer (50 % FB, pH 6.6) at I = 0.5 M (NaClO₄) and 25 °C: Plot of absorbance at 254 nm against time

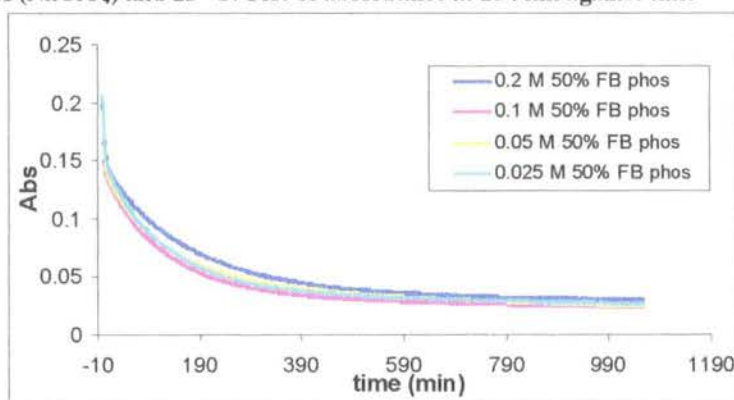


Table 2.5-9 (below) summarises the results from the double exponential least squares fit of the absorbance against time data using equation 2.7

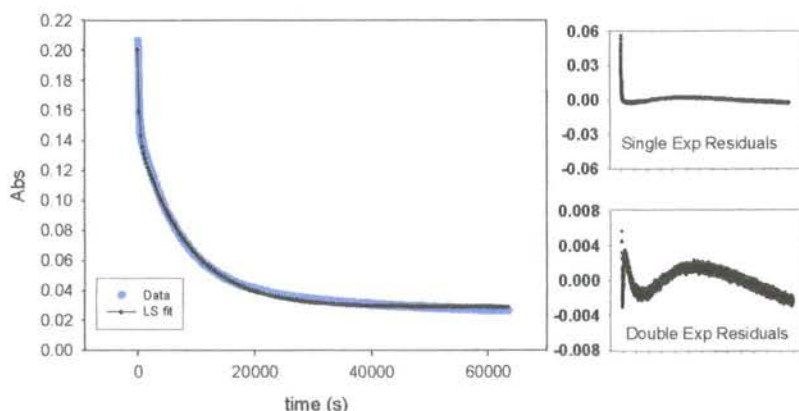
Table 2.5-9: First-order rate constants for aromatisation of 1-isopropylcyclohexa-2,4-dienol (2.22) and 2-isopropylcyclohexa-2,4-dienol (2.23) using double exponential least squares analysis in 50 % FB phosphate buffers (0.2 – 0.025 M) at 25 °C and I = 0.5 M(NaClO₄)^(a)

[Buffer] (M)	pH ^(b)	[H ⁺] ^(c) (x 10 ⁻⁷) M	$k_{\text{obs}}^{\kappa(d)}$ (x 10 ⁻³) s ⁻¹	$k_{\text{obs}}^{\sigma(e)}$ (x 10 ⁻⁴) s ⁻¹	R ²	$k_{\text{int}}^{\kappa(f)}$ (x 10 ⁻³) s ⁻¹	$k_{\text{obs}}^{\alpha(f)}$ (x 10 ⁻⁴) s ⁻¹
0.20	6.65	2.25	3.65	0.97	0.9999		
0.10	6.62	2.42	3.85	1.27	0.9997	1.64	4.17
0.05	6.59	2.55	3.75	1.13	0.9994	(1.35 ^(g))	(3.83 ^(g))
0.025	6.59	2.57	5.42	1.28	0.9997		

(a) Measurements were made at a substrate concentration of 0.05 mM and 1 % acetonitrile (b) pH was determined using a MeterLab™ PHM 290 pH-Stat Controller equipped with a radiometer (pH 4 - 7 - 10 @ 25 °C) combination electrode (type pHC4006) with a saturated LiTCA filling solution. (c) [H⁺] was calculated using $[H^+] = 10^{-(\text{pH}/\gamma_{\text{H}^+})}$ where $\gamma_{\text{H}^+} = 1$ is the activity coefficient of the hydronium ion under our experimental conditions. (d) The value of the first-order rate constant (k_{obs}), was obtained from the least squares fit of the data in Figure 2.22 using equation 2.7. (e) The value of the first-order rate constant (k_{obs}), was obtained from the least squares fit of the data below Figure 2.22 using equation 2.7. (f) k_{int} is defined as the intercept of the plot of k_{obs} against buffer concentration. (g) mean of k_{obs} .

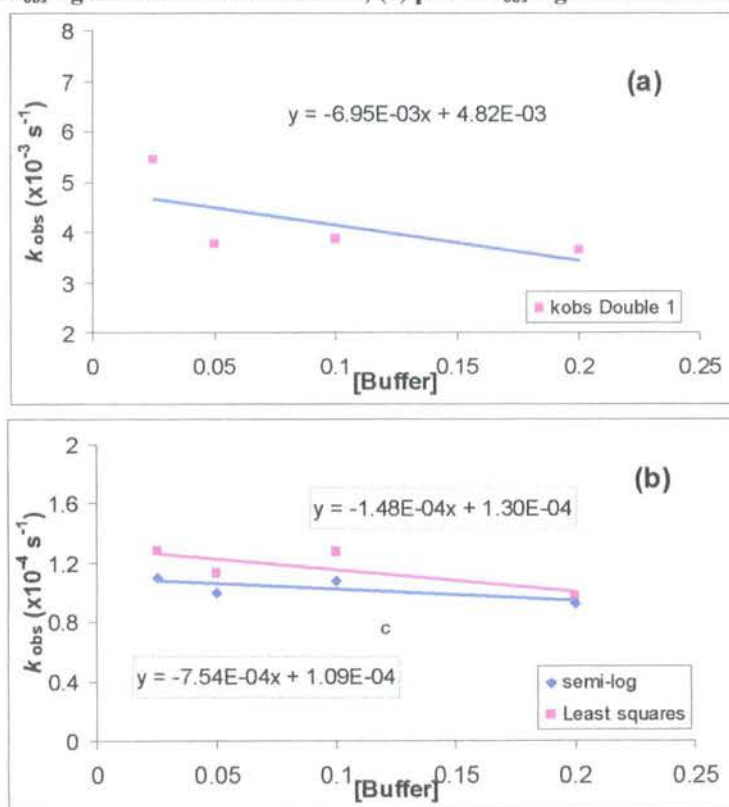
The data in the table above shows the results for a double exponential analysis of the results from the aromatisation reaction in 50 % FB phosphate. An example of the double exponential fit is shown in Fig 2.5-23. The residuals (Fig 2.5-23(inset)) show that the total error around the regression line in the single exponential fit is ± 0.06 ; whereas for the double exponential fit the error is ± 0.008 .

Figure 2.5-23: UV-vis spectrophotometric data from the aromatisation reaction of 1-isopropylcyclohexa-2,4-dienol and 2-isopropylcyclohexa-2,4-dienol in phosphate buffer (0.025 M, 50 % FB) at pH 6.59 and I = 0.5 M (NaClO₄) (blue line). The double exponential least squares fit is shown in black. Inset: single and double exponential residuals.



The mean error of the estimate for the single exponential fit of Fig 2.5-22 is 2.3×10^{-3} and for the double exponential equation 7.0×10^{-4} . The mean t-value for the estimate of the rate constant for the single exponential equation is 620; whereas for the two rate constants of the double exponential equation the mean t-values were 157 and 1413. A semi-logarithmic plot shows non-linearity. The buffer catalysis plots show no evidence for buffer catalysis (see Fig 2.5-24(a & b)). The buffer catalysis plot for k_{obs}^i (Fig 2.5-24(a)) has a negative slope of -7×10^{-3} . The change in first order rate constant over the buffer range is 48 %. For k_{obs}^o (Fig 2.5-24(b)) the slope is also negative, however the change in rate constant over the buffer range is smaller (32 %)

Figure 2.5-24: The aromatisation reaction of cumene hydrate in phosphate buffer (50 % FB, pH 6.6). (a) plot of k_{obs}^i against buffer concentration; (b) plot of k_{obs}^o against buffer concentration.



The mean rate of aromatisation of 1-isopropylcyclohexa-2,4-dienol is $4.17 \pm 0.42 \times 10^{-3} \text{ s}^{-1}$. The mean rate of aromatisation of 2-isopropylcyclohexa-2,4-dienol is $1.16 \pm 0.07 \times 10^{-4} \text{ s}^{-1}$ at pH 6.6. These correspond to half-lives of 166 and 5975 seconds respectively.

Table 2.5-10 (below) summarises the first order rate constants for the aromatisation reactions of 1-isopropylcyclohexa-2,4-dienol (*ipso*) and 2-isopropylcyclohexa-2,4-dienol (*ortho*) in acetate and phosphate buffers (pH 4.2 – 6.6).

Table 2.5-10: Summary of the first-order rate constants for the aromatisation of 1-isopropylcyclohexa-2,4-dienol (k_{int}^i) and 2-isopropylcyclohexa-2,4-dienol (k_{int}^o) in acetate and phosphate buffers, I = 0.5 M (NaClO₄)

pH ^(a)	[H ⁺] ^(b) M	$k_{int}^{o(c)}$ s ⁻¹	$k_H^{o(d)}$ M ⁻¹ s ⁻¹	$k_{int}^{i(c)}$ s ⁻¹	$k_H^{i(d)}$ M ⁻¹ s ⁻¹
4.21	6.14 x 10 ⁻⁵	3.93 x 10 ⁻²		-	
4.60	2.51 x 10 ⁻⁵	1.57 x 10 ⁻²		-	
4.95	1.12 x 10 ⁻⁵	5.46 x 10 ⁻³		-	
5.56	2.75 x 10 ⁻⁶	1.60 x 10 ⁻³	644	4.82 x 10 ^{-2(e)}	16140
5.62	2.40 x 10 ⁻⁶	1.17 x 10 ⁻³		3.53 x 10 ⁻²	
6.07	8.45 x 10 ⁻⁷	4.17 x 10 ⁻⁴		1.64 x 10 ⁻²	
6.59	2.57 x 10 ⁻⁷	1.11 x 10 ⁻⁴		4.38 x 10 ⁻³	

(a) pH was determined using a MeterLabTM PHM 290 pH-Stat Controller equipped with a radiometer (pH 4 - 7 - 10 @ 25 °C) combination electrode (type pHC4006) with a saturated LiTCA filling solution. (b) [H⁺] was calculated using $[H^+] = 10^{-(pH/\gamma_H)}$ where $\gamma_H = 1$ is the activity coefficient of the hydronium ion under our experimental conditions. (c) The value of the first-order rate constant (k_{int}) was obtained from the plot of k_{obs} against [buffer], where k_{obs} is calculated from the least squares fit using equation 2.7. (d) The value of the second-order rate constant (k_H) is the slope of the plot of k_{int} against [H⁺]. (e) First order rate constant from the double exponential fit of data from the aromatisation reaction in 0.025 M 90 % FB acetate buffer.

Plots of buffer independent first order rate constants for aromatisation (k_{int}) against acid concentration yield as slope the second order rate constant for aromatisation catalysed by hydronium ion. Figure 2.5-25 (below) shows an excellent linear correlation of the first-order data with hydronium ion concentration. For the '*ortho*' hydrate the error of the estimate of k_H is 7×10^{-4} and the t-value for the estimate of the second-order rate constant is 53. The estimate of the y-intercept is not good with a t-value of -1.5. Similarly for the '*ipso*' hydrate the t-value for the estimate of k_H is 8.7 and for the estimate of the y-intercept it is -0.29. The error of the estimate is higher in this case (3.8×10^{-3}); this is expected as fewer first-order rate constants for this compound are used in the prediction of k_H .

Figure 2.5-25: Acid-catalysed aromatisation of 1-methylcyclohexa-2,4-dienol and 2-methylcyclohexa-2,4-dienol: plot of k_{int} against $[\text{H}^+]$ with slope equal to the second-order rate constant

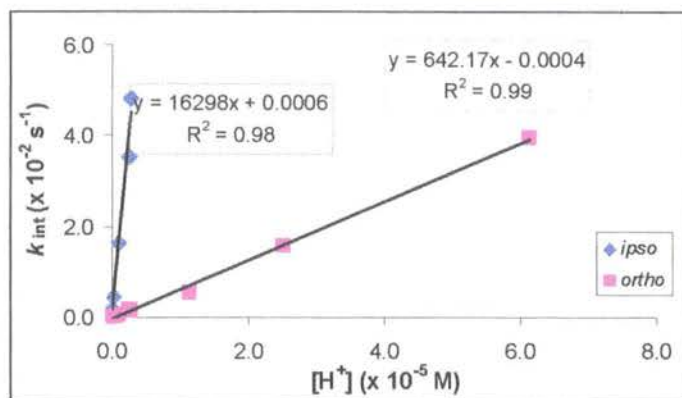


Table 2.5-11 (below) shows the logarithm of the first order rate constants for the aromatisation reaction of 1-isopropylcyclohexa-2,4-dienol and 2-isopropylcyclohexa-2,4-dienol.

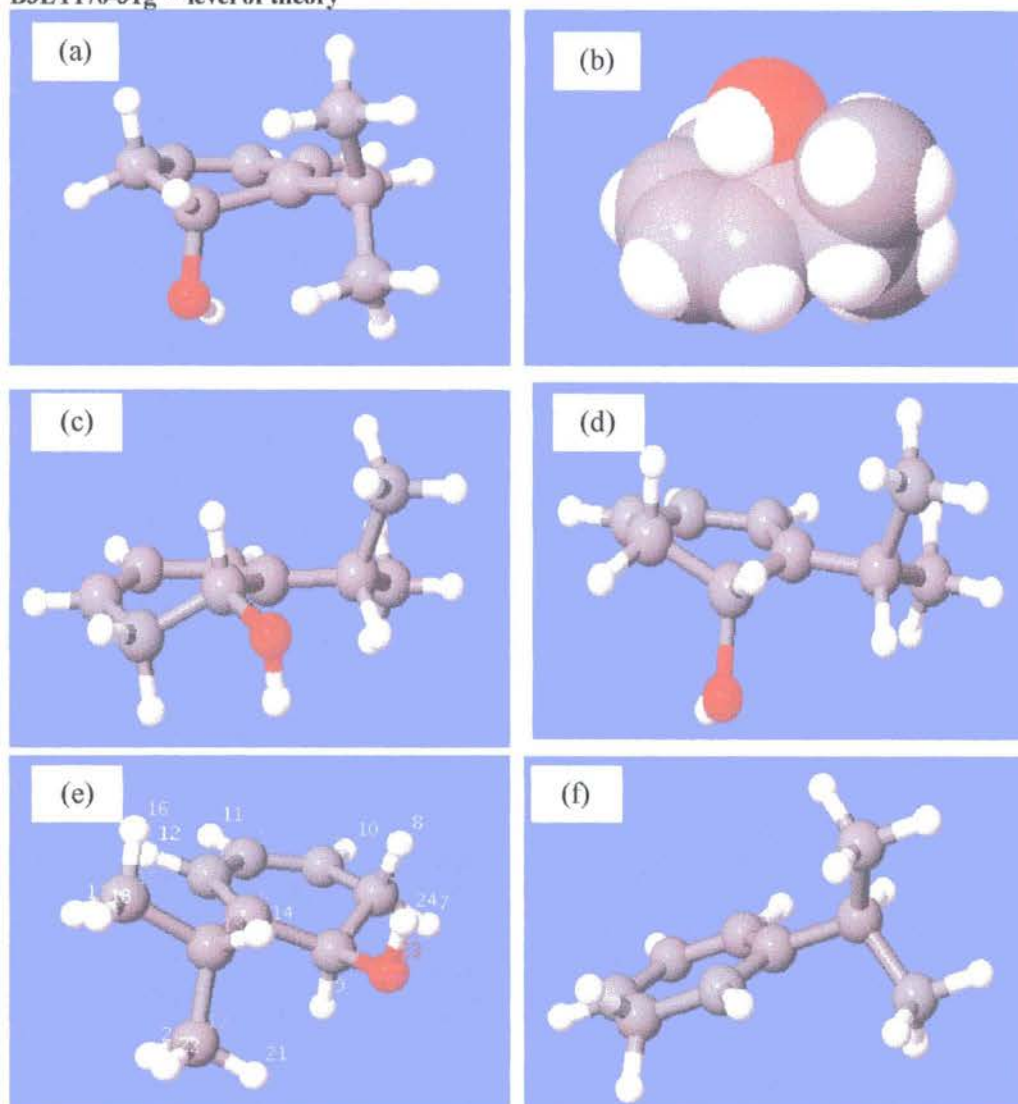
Using the logarithm of the k_{obs} data in Table 2.5-10, a pH-rate profile was constructed (Fig 2.5-26). The y-axis intercept of this plot gives values of $\log k_{\text{H}} = 4.05$ and 3.06 respectively for the *ipso* and *ortho* cumene hydrates. The corresponding k_{H} value for the *ortho* hydrate is $1148 \text{ M}^{-1} \text{ s}^{-1}$ and for the *ipso* hydrate it is $11220 \text{ M}^{-1} \text{ s}^{-1}$. The '*ortho*' hydrate second-order rate constant from the pH-rate profile is almost double the value obtained from the plot of k_{obs} against concentration of hydronium ion (1148 versus $644 \text{ M}^{-1} \text{ s}^{-1}$). This value was disregarded. In the case of the '*ipso*' hydrate the rate constant from the pH-rate profile is closer to the rate constant from the plot of k_{int} against concentration of hydronium ion (11220 and $16140 \text{ M}^{-1} \text{ s}^{-1}$). However, this value was also disregarded due to the error associated with pH-rate profiles.

2.5.3 Computational Studies of the isopropylbenzene hydrates

The structures and energies of 2-isopropylcyclohexa-2,4-dienol (2.22) and carbocation (2.28) were calculated using Gaussian '03 at the B3LYP/6-31g** level of theory.⁷⁶ The starting point for the calculations were generated from Monte-Carlo calculations

(MM3* level of theory) using the Maestro program. The structures below are the lowest energy structures calculated.

Figure 2.5-26: Lowest energy structure of 2-isopropylcyclohexa-2,4-dienol (2.22) calculated to B3LYP/6-31g level of theory**



Structure (a) above in Fig 2.5-27 is the lowest energy conformer. The structure shows the hydroxyl group in the axial position with the hydrogen pointing towards the cyclohexadiene portion of the ring structure. The isopropyl substituent is in an equatorial position with the two CH₃ groups pointing towards the hydroxyl group. The conjugated diene moiety is planar with all the hydrogens co-planar. The CH₂ group adjacent to the hydroxyl-carbon is situated below the plane of the dienyl moiety

and so the ring is puckered. The space-filling model (Fig 2.5-27 (b)) shows the packing with the hydroxyl group lying on top of the ring structure.

The next lowest energy conformer is shown in Figure 2.5-27 (c). This is a ring-flip of structure (a). The hydroxyl group is in an equatorial position. The central carbon at the isopropyl group is still co-planar with the conjugated moiety of the ring-structure and the two CH₃ groups have twisted and the C-H of the isopropyl group is pointing towards the hydroxyl group. Figure 2.5-27 (d) shows the next lowest energy structure calculated. In this case the hydroxyl group is in the axial position and the orientation of the isopropyl group is similar to structure (c). Figure 2.5-27 (e) shows the highest energy structure calculated. The hydroxyl group is in the equatorial position with the hydrogen pointing orientated parallel to the centre of the ring.

The carbocation is shown in Figure 2.5-27(f). The ring is completely planar with the isopropyl group in a pseudo-equatorial position. The isopropyl group is side on to the ring with the C-H parallel to the ring centre.

Scheme 2.5-3: 'ortho' cumene hydrate and hydrate energies calculated to B3LYP/6-31g level of theory**

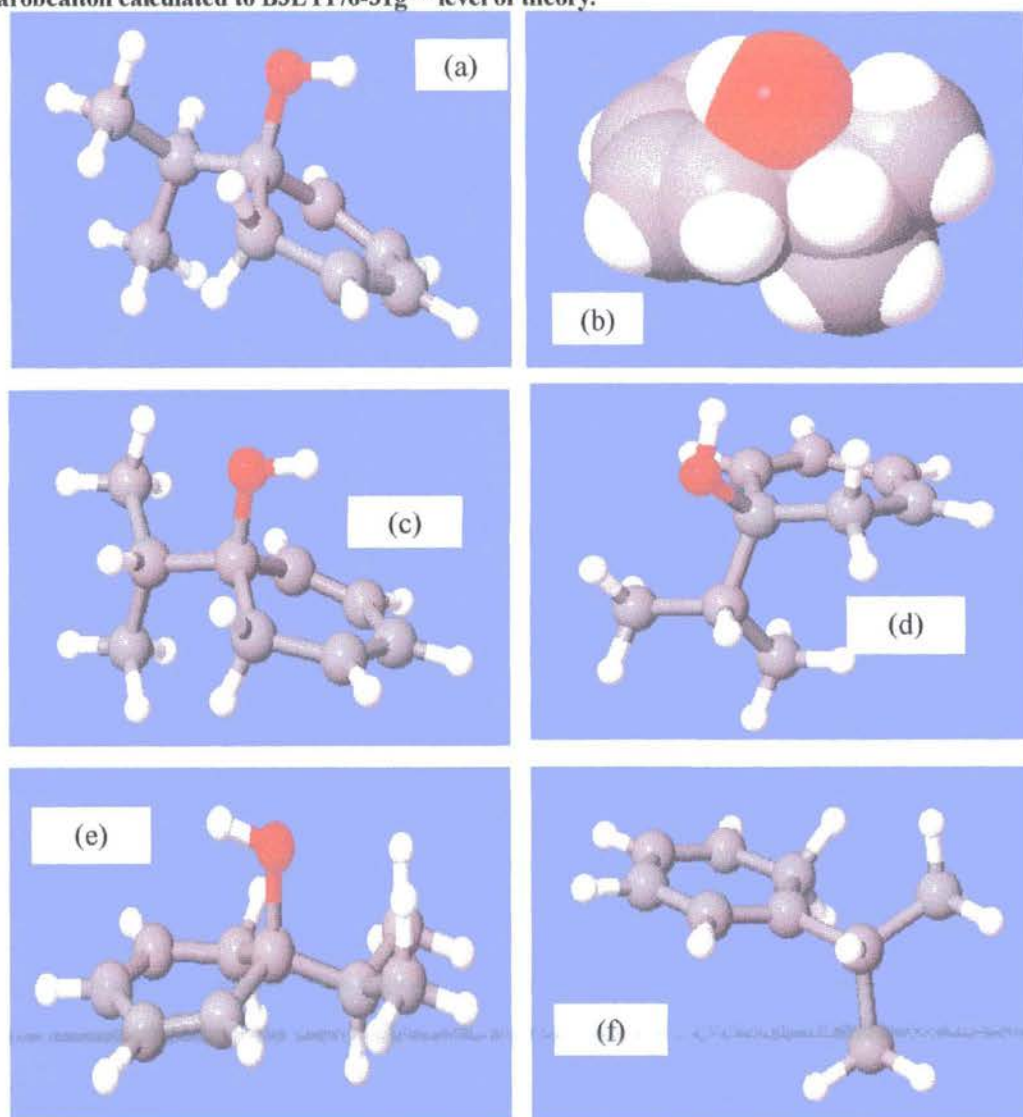
Hydrate	Gas phase		With water sphere		
	kJ/mol	Δ	kJ/mol	Δ	Δ
Fig 2.5-27(a)	-1120039.41	0.00	-1120064.91	0.00	-25.49
Fig 2.5-27(c)	-1120039.17	0.24	-1120065.60	-0.69	-26.43
Fig 2.5-27(d)	-1120038.50	0.91	-	-	-
Fig 2.5-27(e)	-1120032.94	6.47	1120061.91	3.00	-28.96
Fig 2.5-27(f) carbocation	-920309.77	199729	-920523.47	199541.44	-213.70

The table above shows the absolute and relative energies of the conformers and carbocation of 2-isopropylcyclohexa-2,4-dienol in the gas phase and with a aqueous sphere (polarized continuum model). The first structure (a) is the most stable in the gas phase, however in the 'aqueous' phase the second conformer (c) is more stable. However, the energy differences are very small between the first three conformers. The

highest energy conformer is the fourth conformer (e). The carbocation is considerably higher in energy than the neutral hydrate. The effect of the water sphere is to stabilize the positively charged species by 214 kJ/mol.

The structure and energy of 1-isopropylcyclohexa-2,4-dienol (2.23) and carbocation (2.27) were calculated using Gaussian '03 to the B3LYP/6-31g** level of theory.⁷⁶ The starting point for the calculation were generated from Monte-Carlo calculations (MM3* level of theory) using the Maestro program. The structures below are the lowest energy structures calculated.

Figure 2.5-27: Lowest energy structure of 1-isopropylcyclohexa-2,4-dienol and its putative carbocation calculated to B3LYP/6-31g level of theory.**



The lowest energy conformer (Fig 2.5-28(a)) has the hydroxyl group in the axial position with the hydrogen pointing towards the conjugated diene of the ring. The space filling model shows this better (Fig 2.5-28(b)). The isopropyl group is held in a pseudo-equatorial position with the C-H bond facing the dienyl hydrogens. The ring is not entirely planar; the unsaturated portion is orientated below the plane of the conjugated diene. Structure (c) is the second lowest energy structure and it differs from structure (a) in the rotation of the isopropyl group. The isopropyl group is facing towards the CH₂ of the ring with the C-H bond at a 90° angle to the hydroxyl group. Structure (d) shows another rotation of the isopropyl group; the C-H bond is *anti* to the hydroxyl group. Structure (e) is a ring-flip of structure (a). The hydroxyl group is in the equatorial position and the isopropyl group is forced almost into an axial position. The carbocation shown in Figure 2.5-28(f) is planar, as expected. The isopropyl group is orientated with the C₇-H bond almost parallel with the C-C bonds of the ring.

Table 2.5-11: 'Ipsa' cumene hydrate and carbocation energies calculated to B3LYP/6-31g level of theory**

Hydrate	Gas phase		With water sphere		
	kJ/mol	Δ	kJ/mol	Δ	Δ
Fig 2.5-28(a)	-1120031.52	0.00	-1120224.34	0.00	-26.15
Fig 2.5-28(c)	-1120028.49	3.03	-1120052.71	4.96	-24.23
Fig 2.5-28(d)	-1120027.01	4.51	1120052.06	5.61	-25.05
Fig 2.5-28(e)	-1120024.65	6.87	-1120052.64	5.03	-27.98
Fig 2.5-28(f) carbocation	-920328.53	199703	-920535.96	199521.71	-207.43

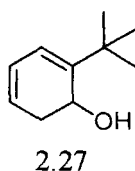
Table 2.5-12 (above) shows the absolute and relative energies of the conformers and carbocation of 1-isopropylcyclohexa-2,4-dienol in the gas phase and with a aqueous sphere (polarized continuum model). The first structure has the lowest energy in the gas phase and the aqueous phase. The second and third conformers show rotation of the isopropyl group which is of a higher energy than structure (a). Conformer (e) is the ring-flip of (a) and it shows the largest increase in energy probably due to the axial

orientation of the isopropyl group. The carbocation is significantly higher in energy, as expected.

Overall the effect of the water sphere is stabilizing. This is most notable in the carbocation which is lowered in energy by over 200 kJ/mol.

2.6 *tert*-butylbenzene Hydrate

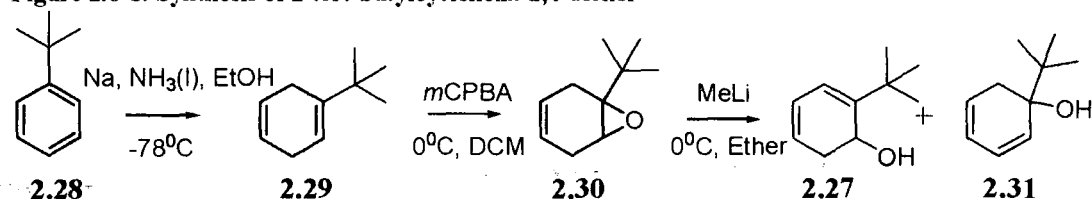
This section presents the results from the synthesis and kinetic studies of the aromatisation reaction of 2-*tert*-butylcyclohexa-2,4-dienol in aqueous buffers.



2.6.1 Synthesis of 2-*tert*-butylcyclohexa-2,4-dienol.

The Birch reduction of *tert*-butylbenzene (2.28) proceeded with a respectable yield of 75 %. The epoxidation step showed the major epoxide (shown below in Scheme 2.6-1), minor regioisomers and some epoxidation on the less sterically hindered alkene. Fortunately these different products could be separated by column chromatography (silica gel, 99:1 petroleum ether: diethyl ether). The final step using methyl lithium as the ring-opening reagent was troublesome. Using similar equivalents of methyl lithium and substrate epoxide, the products isolated were unreacted epoxide, the parent arene and 2-*tert*-butylcyclohexa-2,4-dienol. It is assumed the more reactive 1-*tert*-butylcyclohexa-2,4-dienol (2.31) either aromatized in work-up or in the methyl lithium solution and so could not be isolated. As with the other hydrates, purification of the *tert*-butyl substituted hydrate was difficult due to the reactivity of the hydrate towards acid and water. The products were not stable over long periods of time.

Figure 2.6-1: Synthesis of 2-*tert*-butylcyclohexa-2,4-dienol

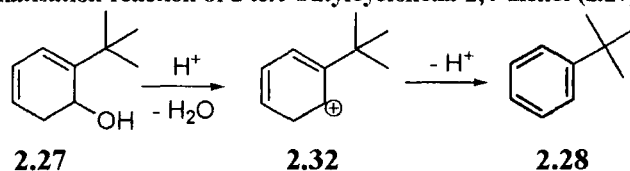


The reaction was pushed to completion with a large excess of methyl lithium so the only impurity could be assumed to be the parent arene. Although the hydrate was not totally pure; it was decided to continue with the kinetic studies as the presence of the parent arene should not affect the rate as it is stable to further reaction under the conditions of these experiments.

2.6.2 Kinetic analysis of the aromatisation reaction of 2-*tert*-butylcyclohexa-2,4-dienol.

The aromatisation reaction (see Scheme 2.6-1) of 2-*tert*-butylcyclohexa-2,4-dienol (2.27) was followed in acetate and phosphate buffers (pH 4.2 – 6.6) at ionic strength 0.5 M, maintained with sodium perchlorate. Typically a 1/100 dilution into the relevant buffer was made to initiate the reaction with the stock solution of hydrate in acetonitrile. The total substrate concentration (0.05 mM) was limited due to the solubility of the reactant and product. The reported solubility of *tert*-butylbenzene in water is 1.41×10^{-5} M.⁸⁰

Scheme 2.6-1: Aromatisation reaction of 2-*tert*-butylcyclohexa-2,4-dienol (2.27)



A typical repetitive scan of the aromatisation reaction is shown below. The scan shows the disappearance of the hydrate at $\lambda = 260$ nm. The increasing absorbance of the arene at 220 nm is not shown due to the high absorbance of the buffer at this wavelength. The analytical wavelength chosen is 260 nm.

Figure 2.6-2: Repetitive scan of the aromatisation reaction of 2-*tert*-butylcyclohexa-2,4-dienol (2.27) in acetate buffer (90 % FB, pH 5.6) at I=0.5 M (NaClO₄) and 25 °C

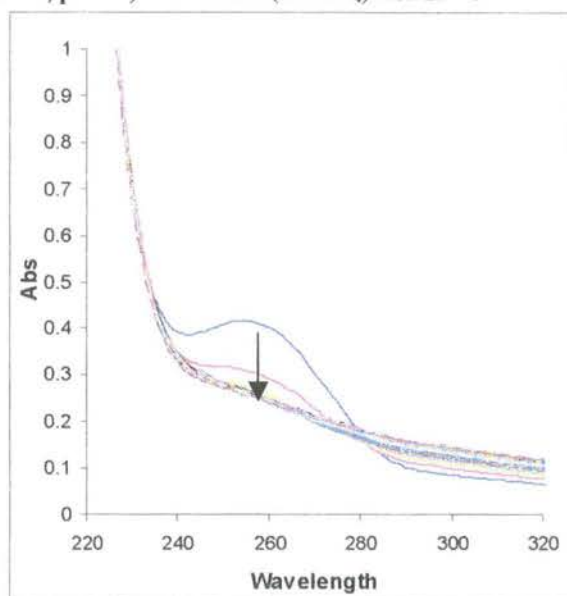
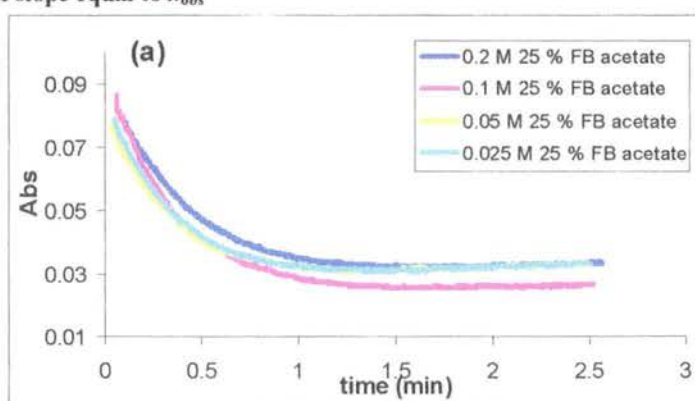
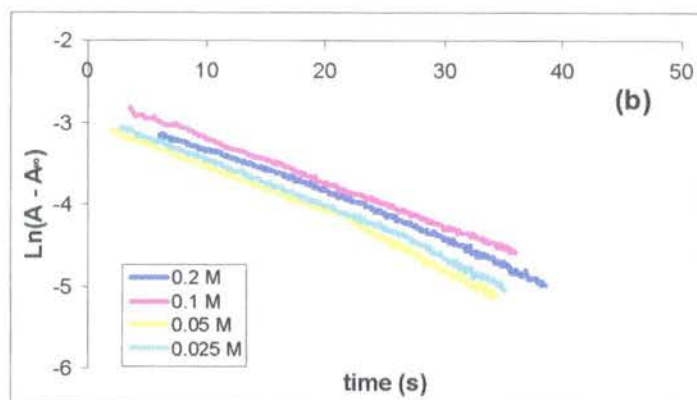


Figure 2.6-3(a) shows the change in absorbance against time at 260 nm as a result of the reaction of *tert*-butylbenzene hydrate in acetate buffer (25 % FB, pH 4.2). A corresponding semilogarithmic plot of $\Delta A = A - A_{\infty}$ against time is shown in Figure 2.6-3(b) where A_{∞} refers to the absorbance at the end of the reaction.

Figure 2.6-3: Aromatisation of 2-*tert*-butylbenzene hydrate (2.27) in acetate buffer (25 % FB, pH 4.2) at I = 0.5 M (NaClO₄) and 25 °C: (a) Plot of absorbance versus time; (b) plot of $\ln(A - A_{\infty})$ against time with slope equal to k_{obs}





The table below summarises the first order rate constants for the aromatisation reaction of 2-*tert*-butylcyclohexa-2,4-dienol in 25 % FB acetate buffer at pH 4.2.

Table 2.6-1: First-order rate constants for aromatisation of 2-*tert*-butylbenzene hydrate (2.27) in 25 % FB acetate buffers (0.2 – 0.025 M) at 25 °C and I = 0.5 M (NaClO₄)^(a)

[Buffer] (M)	pH ^(b)	[H ⁺] ^(c) x 10 ⁻⁵ M	Semi-log Plot			Least Squares Plot		
			k_{obs} ^(d) (x 10 ⁻²) s ⁻¹	R ²	k_{int} ^(e) (x 10 ⁻²) s ⁻¹	k_{obs} ^(f) (x 10 ⁻²) s ⁻¹	R ²	k_{int} ^(e) (x 10 ⁻²) s ⁻¹
0.20	4.21	6.14	5.37	0.997		4.85	0.998	
0.10	4.21	6.12	5.49	0.998	5.92	5.09	0.999	5.97
0.05	4.22	6.08	5.87	0.996	(5.64 ^(g))	5.82	0.997	(5.40 ^(g))
0.025	4.22	6.07	5.84	0.997		5.84	0.997	

(a) Measurements were made at a substrate concentration of 0.05 mM and 1 % acetonitrile (b) pH was determined using a MeterLab™ PHM 290 pH-Stat Controller equipped with a radiometer (pH 4 - 7 - 10 @ 25 °C) combination electrode (type pH4006) with a saturated LiTCA filling solution. (c) [H⁺] was calculated using $[H^+] = 10^{-(\text{pH}/\gamma_{\text{H}})}$ where $\gamma_{\text{H}} = 1$ is the activity coefficient of the hydronium ion under our experimental conditions. (d) The value of the first-order rate constant (k_{obs}), was obtained from the slope of the plot of $\ln(A_{\infty} - A)$ against time in Figure 2.6-3(b). (e) k_{int} is defined as the intercept of the plot of k_{obs} against buffer concentration Figure 2.6-4. (f) The value of the first-order rate constant (k_{obs}), was obtained from the least squares analysis of Figure 2.6 -3(a). (g) mean of k_{obs}

The least squares fit of the data in Fig 2.6-3(a) showed an estimate of error of 6×10^{-4} and the t-values for the estimate of k_{obs} were greater than 300. For the semi-logarithmic plot (Fig 2.6-3(b)) all A_{∞} values could be measured except for reactions in 0.025 M buffer where an A_{∞} value estimated by the least-squares analysis was used. Overall the R² values were good with the error in the third decimal.

The results from the semi-logarithmic analysis have a mean of $5.64 \times 10^{-2} \text{ s}^{-1}$; the least squares analysis gives a mean of $5.40 \times 10^{-2} \text{ s}^{-1}$.

Figure 2.6-4: Aromatisation of 2-*tert*-butylbenzene hydrate (2.27) in acetate buffer (25 % FB, pH 4.2) at $I = 0.5 \text{ M}$ (NaClO_4) and $25 \text{ }^\circ\text{C}$: Plot of k_{obs} against buffer concentration

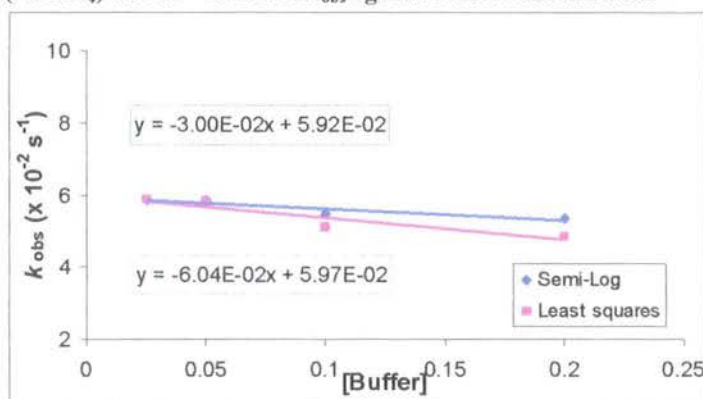
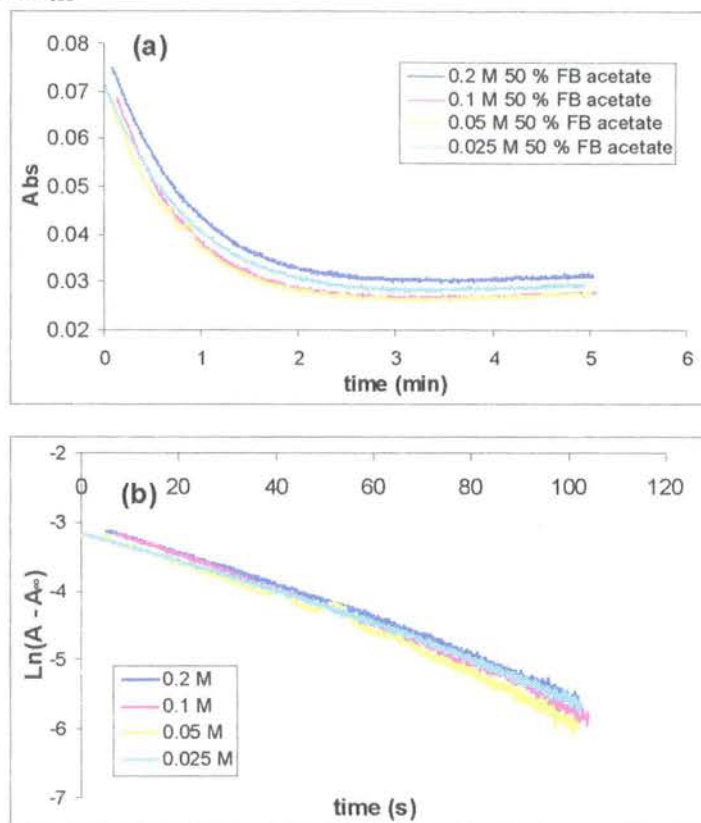


Figure 2.6-4 shows no evidence of buffer catalysis, in fact the rate increases as the buffer concentration decreases. The slopes are small and as shown above, and the error over the four buffer concentrations is low. The intercept value (k_{int}) differs from the mean of the data only by a factor of 0.003 and 0.006 in the semi-logarithmic and least squares analyses, respectively. This is a change of 5 and 10 % respectively.

The first order rate constant for aromatisation of *tert*-butylbenzene hydrate at pH 4.2 is $5.73 \times 10^{-2} \text{ s}^{-1}$.

Figure 2.6-5(a) shows the change in absorbance against time at 260 nm as a result of the reaction of *tert*-butylbenzene hydrate in acetate buffer (50 % FB, pH 4.6). A corresponding semi-logarithmic plot of $\Delta A = A - A_{\infty}$ against time is shown in Figure 2.6-5(b) where A_{∞} refers to the absorbance at the end of the reaction.

Figure 2.6-5: Aromatisation of *tert*-butylbenzene hydrate in acetate buffer (50 % FB, pH 4.6) at $I = 0.5 \text{ M}$ (NaClO_4) and $25 \text{ }^\circ\text{C}$: (a) Plot of absorbance versus time; (b) plot of $\ln(A - A_\infty)$ against time with slope equal to k_{obs}



The experimental data in Figure 2.6-5(a) (above) shows a good correlation with a stable A_∞ value. Over time the data drifted upwards, however, as this occurred after 10 half-lives the calculated rate constant is not affected. The table below summarises the results for the aromatisation reaction of *ortho-tert*-butylbenzene hydrate in 50 % FB acetate at pH 4.6. The results from the semi-logarithmic analysis gave a mean value of $k_{\text{obs}} = 2.60 \pm 0.08 \times 10^{-2} \text{ s}^{-1}$. The results from the least square analysis of the experimental data in Figure 2.6-5(a) have a mean value of $k_{\text{obs}} = 2.38 \pm 0.08 \times 10^{-2} \text{ s}^{-1}$.

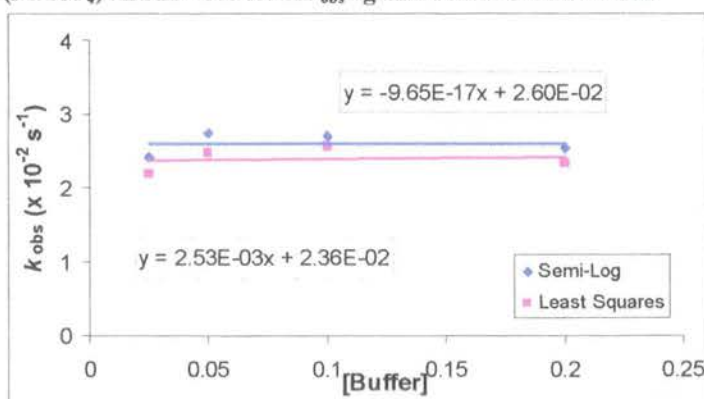
Table 2.6-2: First-order rate constants for aromatisation of *t*Butylbenzene hydrate (2.27) in 50 % FB acetate buffers (0.2 – 0.025 M) at 25 °C and I = 0.5 M (NaClO₄)^(a)

[Buffer] (M)	pH ^(b)	[H ⁺] ^(c) x 10 ⁻⁵ M	Semi-logarithmic			Least Squares		
			<i>k</i> _{obs} ^(d) (x 10 ⁻³) s ⁻¹	R ²	<i>k</i> _{int} ^(e) (x 10 ⁻³) s ⁻¹	<i>k</i> _{obs} ^(f) (x 10 ⁻³) s ⁻¹	R ²	<i>k</i> _{int} ^(g) (x 10 ⁻³) s ⁻¹
0.20	4.58	2.63	2.53	0.995		2.32	0.998	
0.10	4.54	2.88	2.70	0.995	2.60	2.56	0.998	2.38
0.05	4.56	2.75	2.74	0.989	(2.60 ^(g))	2.47	0.997	(2.36 ^(g))
0.025	4.56	2.75	2.41	0.995		2.18	0.998	

(a) Measurements were made at a substrate concentration of 0.05 mM and 1 % acetonitrile (b) pH was determined using a MeterLab™ PHM 290 pH-Stat Controller equipped with a radiometer (pH 4 - 7 - 10 @ 25 °C) combination electrode (type pHC4006) with a saturated LiTCA filling solution. (c) [H⁺] was calculated using $[H^+] = 10^{-(pH/\gamma_H)}$ where $\gamma_H = 1$ is the activity coefficient of the hydronium ion under our experimental conditions. (d) The value of the first-order rate constant (*k*_{obs}), was obtained from the slope of the plot of ln (*A*_∞ - *A*) against time in Figure 2.6-5(b). (e) *k*_{int} is defined as the intercept of the plot of *k*_{obs} against buffer concentration Figure 2.6-6. (f) The value of the first-order rate constant (*k*_{obs}), was obtained from the least squares analysis of Figure 2.6-5(a). (g) mean of *k*_{obs}.

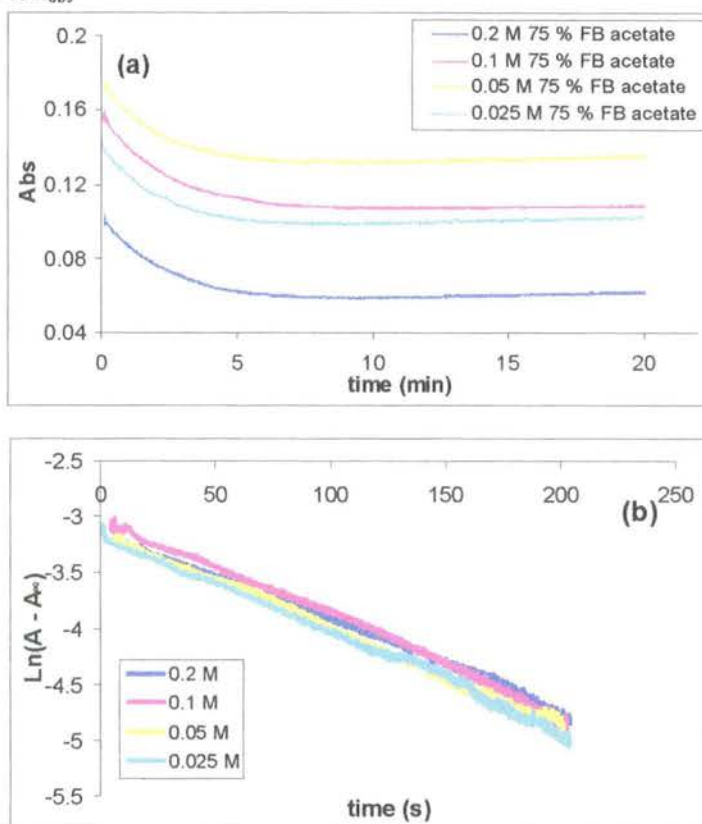
The error of the estimate for the least squares analysis was 6×10^{-4} and the *t* values for the estimate of *k*_{obs} were over 400. The error in the semi-logarithmic and least squares analysis of 0.05 M data is higher; however this does not appear to affect the rate, when compared to the other data at the same pH. Figure 2.6-6 (below) shows no evidence of buffer catalysis. The y-axis intercept of this plot gave the same value for the first order rate constant for aromatisation as the mean of the values obtained at each buffer concentration @ constant pH.

Figure 2.6-6: Aromatisation of 2-*tert*-butylbenzene hydrate (2.27) in acetate buffer (50 % FB, pH 4.6) at I = 0.5 M (NaClO₄) and 25 °C: Plot of *k*_{obs} against buffer concentration



The mean rate of aromatisation of *ortho-tert*-butylbenzene hydrate (2.27) at pH 4.6 is $2.48 \times 10^{-2} \text{ s}^{-1}$.

Figure 2.6-7: Aromatisation of *tert*-butylbenzene hydrate in acetate buffer (75 % FB, pH 4.9) at $I = 0.5 \text{ M}$ (NaClO_4) and $25 \text{ }^\circ\text{C}$: (a) Plot of absorbance versus time; (b) plot of $\ln(A - A_\infty)$ against time with slope equal to k_{obs}



The table below summarises the first order rate constants for the aromatisation reaction of *tert*-butylbenzene hydrate in acetate buffer (75 % FB, pH 4.9). The least squares analysis of the data in Figure 2.6-7(a) to ten half-lives gave an error of the estimate of the fit on the order of 6×10^{-4} . The semi-logarithmic analysis (Fig 2.6-7(b)) gives a reasonable fit to 2.5 half-lives (200 s) with the error in third decimal place. The results from the semi-logarithmic analysis have a mean value of $k_{\text{obs}} = 8.20 \pm 0.34 \times 10^{-3} \text{ s}^{-1}$; the least squares analysis gives a mean value of $k_{\text{obs}} = 8.50 \pm 0.22 \times 10^{-3} \text{ s}^{-1}$.

Table 2.6-3: First-order rate constants for aromatisation of *tert*-butylbenzene hydrate (2.27) in 75 % FB acetate buffers (0.2 – 0.025 M) at 25 °C and I = 0.5 M (NaClO₄)^(a)

[Buffer] (M)	pH ^(b)	[H ⁺] ^(c) x 10 ⁻⁵ M	Semi-log Plot		Least Squares Plot			
			k_{obs} ^(d) (x 10 ⁻³) s ⁻¹	R ²	k_{int} ^(e) (x 10 ⁻⁴) s ⁻¹	k_{obs} ^(f) (x 10 ⁻⁴) s ⁻¹	R ²	k_{int} ^(e) (x 10 ⁻⁴) s ⁻¹
0.20	4.93	3.11	7.84	0.997		7.88	0.998	
0.10	4.93	3.10	8.82	0.993	8.96	7.38	0.999	8.73
0.05	4.94	3.03	8.68	0.997	(8.20 ^(g))	8.68	0.998	(8.50 ^(g))
0.025	4.95	3.00	8.67	0.996		8.83	0.997	

(a) Measurements were made at a substrate concentration of 0.05 mM and 1 % acetonitrile (b) pH was determined using a MeterLab™ PHM 290 pH-Stat Controller equipped with a radiometer (pH 4 - 7 - 10 @ 25 °C) combination electrode (type pHC4006) with a saturated LiTCA filling solution. (c) [H⁺] was calculated using $[H^+] = 10^{-(\text{pH}/\gamma_H)}$ where $\gamma_H = 1$ is the activity coefficient of the hydronium ion under our experimental conditions. (d) The value of the first-order rate constant (k_{obs}), was obtained from the slope of the plot of $\ln(A_\infty - A)$ against time in Figure 2.6-7(b). (e) k_{int} is defined as the intercept of the plot of k_{obs} against buffer concentration Figure 2.6-8. (f) The value of the first-order rate constant (k_{obs}), was obtained from the least squares analysis of Figure 2.6-7(a). (g) mean of k_{obs}

Figure 2.6-8 (below) shows no evidence of buffer catalysis; there is an overall increase in the first order rate constant for aromatisation on the order of 10 % with decreasing buffer concentration. The first order rate constant for the aromatisation of *tert*-butylbenzene hydrate at pH 4.9 is $8.60 \times 10^{-3} \text{ s}^{-1}$ corresponding to a half-life of 81 seconds.

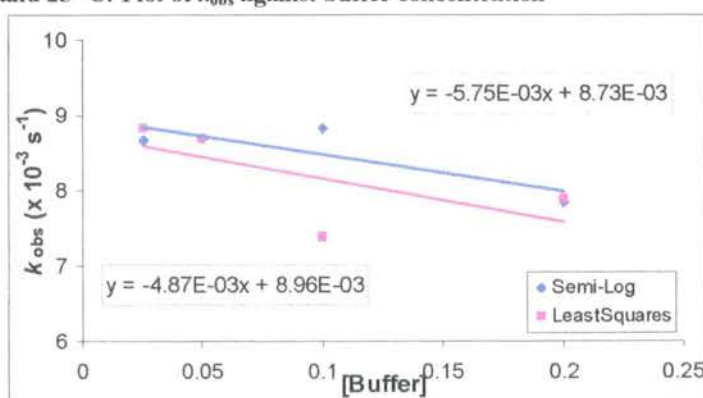
Figure 2.6-8: Aromatisation of *tert*-butylbenzene hydrate in acetate buffer (75 % FB, pH 4.9) at I = 0.5 M (NaClO₄) and 25 °C: Plot of k_{obs} against buffer concentration

Figure 2.6-9(a) shows the change in absorbance against time at 260 nm as a result of the reaction of *tert*-butylbenzene hydrate in acetate buffer (90 % FB, pH 5.6). A

corresponding semi-logarithmic plot of $\Delta A = A - A_\infty$ against time is shown in Figure 2.6-9(b) where A_∞ refers to the absorbance at the end of the reaction.

Figure 2.6-9: Aromatisation of *tert*-butylbenzene hydrate in acetate buffer (90 % FB, pH 5.6) at I = 0.5 M (NaClO₄) and 25 °C: (a) Plot of absorbance versus time; (b) plot of $\ln(A - A_\infty)$ against time with slope equal to k_{obs}

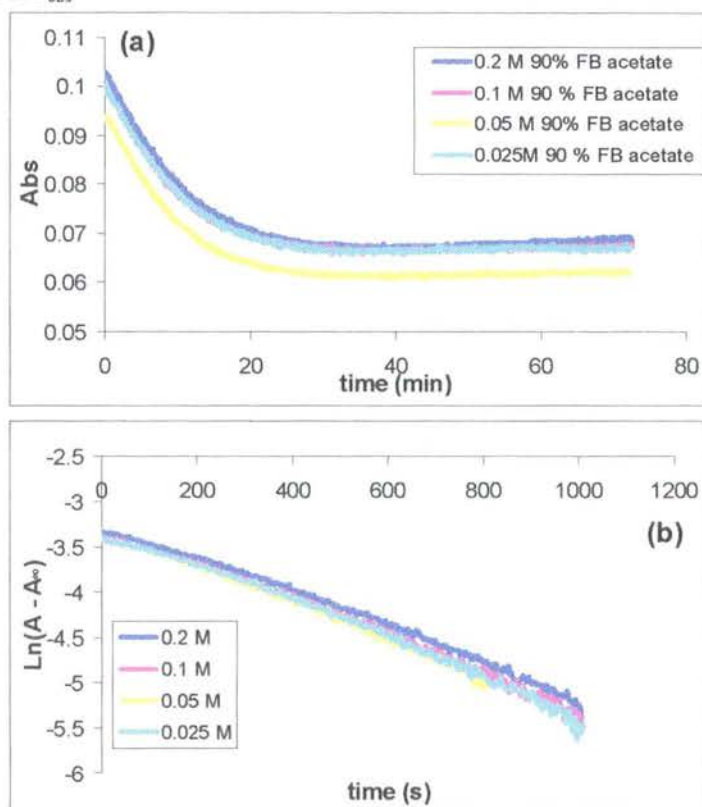
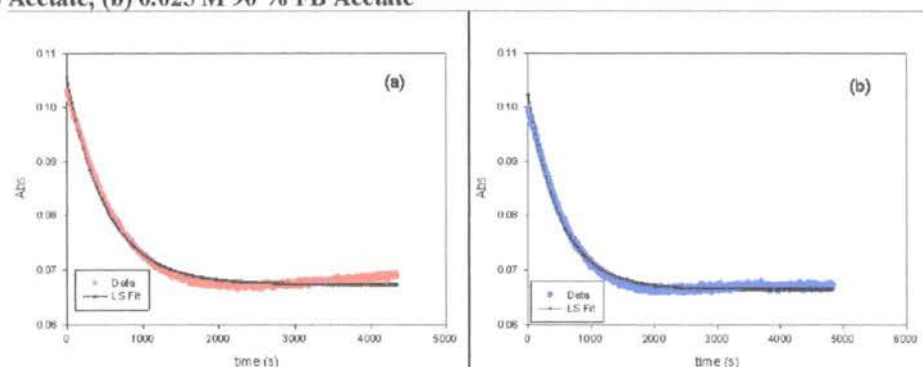


Figure 2.6-9(a) shows the instability of the endpoint (A_∞) at this particular pH value. In this case, the semi-logarithmic plot (fig 2.6-9(b)) estimated A_∞ from the y_0 -value in the least squares fit shown below (Fig 2.6-9 (a & b)). Examples of the least square analysis of the UV-vis spectrophotometric data are shown in Figure 2.6-10(a). The red and blue lines are the collected data and the black line is the least-squares predicted fit.

Figure 2.6-10: Examples of least-squares analysis of UV-vis spectrophotometric data; (a) 0.2 M 90 % FB Acetate, (b) 0.025 M 90 % FB Acetate



The table below summarizes the first order rate constants for the aromatisation of *tert*-butylbenzene hydrate in 90 % FB acetate buffers at pH 5.6. The least squares analysis of the data in Figure 2.6-9(a) was good, with an error of estimate of 7×10^{-4} and *t*-values for the estimate of k_{obs} greater than 250. The results from the semi-logarithmic analysis have mean k_{obs} of $2.00 \pm 0.03 \times 10^{-3} \text{ s}^{-1}$; the least squares analysis gives a mean of $1.99 \pm 0.03 \times 10^{-3} \text{ s}^{-1}$.

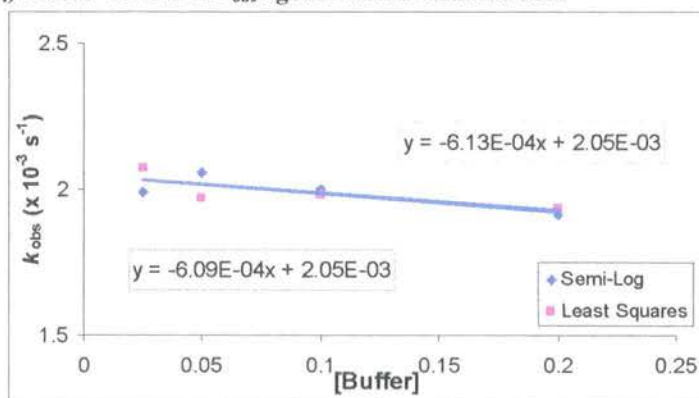
Table 2.6-4: First-order rate constants for aromatisation of *tert*-butylbenzene hydrate (2.17) in 90 % FB acetate buffers (0.2 – 0.025 M) at 25 °C and $I = 0.5 \text{ M}$ (NaClO_4)^(a)

[Buffer] (M)	pH ^(b)	$[\text{H}^+]^{(c)}$ $\times 10^{-6}$ M	Semi-log Plot		Least Squares Plot			
			$k_{\text{obs}}^{(d)}$ ($\times 10^{-3}$) s^{-1}	R^2	$k_{\text{int}}^{(e)}$ ($\times 10^{-3}$) s^{-1}	$k_{\text{obs}}^{(f)}$ ($\times 10^{-3}$) s^{-1}	R^2	$k_{\text{int}}^{(e)}$ ($\times 10^{-3}$) s^{-1}
0.20	5.55	2.84	1.91	0.994		1.93	0.994	
0.10	5.55	2.85	2.00	0.994	1.99	1.98	0.996	1.99
0.05	5.54	2.88	1.99	0.995	(2.05 ^(g))	2.07	0.996	(2.05 ^(g))
0.025	5.56	2.74	2.06	0.992		1.97	0.996	

(a) Measurements were made at a substrate concentration of 0.05 mM and 1 % acetonitrile (b) pH was determined using a MeterLabTM PHM 290 pH-Stat Controller equipped with a radiometer (pH 4 - 7 - 10 @ 25 °C) combination electrode (type pH4006) with a saturated LiTCA filling solution. (c) $[\text{H}^+]$ was calculated using $[\text{H}^+] = 10^{-(\text{pH}/\gamma_{\text{H}})}$ where $\gamma_{\text{H}} = 1$ is the activity coefficient of the hydronium ion under our experimental conditions. (d) The value of the first-order rate constant (k_{obs}), was obtained from the slope of the plot of $\ln(A - A_{\infty})$ against time in Figure 2.6-9(b). (e) k_{int} is defined as the intercept of the plot of k_{obs} against buffer concentration Figure 2.6-11. (f) The value of the first-order rate constant (k_{obs}), was obtained from the least squares analysis of Figure 2.6-9(a). (g) mean of k_{obs} .

The first order rate constant values obtained as the y-intercept values (k_{int}) of Fig 2.6-11 only differ by 5×10^{-5} from the mean of the values obtained at each buffer concentration at constant pH, showing both results are reasonable. Figure 2.6-11 shows no evidence of buffer catalysis and the slope is on the order of $-6 \times 10^{-4} \text{ M}^{-1} \text{ s}^{-1}$.

Figure 2.6-11: Aromatisation of *tert*-butylbenzene hydrate in acetate buffer (90 % FB, pH 5.6) at I = 0.5 M (NaClO_4) and 25 °C: Plot of k_{obs} against buffer concentration



The first order rate constant for the aromatisation of *tert*-butylbenzene hydrate at pH 5.6 is $2.02 \times 10^{-3} \text{ s}^{-1}$.

Figure 2.6-12(a) shows the change in absorbance against time at 260 nm as a result of the reaction of *tert*-butylbenzene hydrate in phosphate buffer (10 % FB, pH 5.6). A corresponding semi-logarithmic plot of $\Delta A = A - A_{\infty}$ against time is shown in Figure 2.6-12(b) where A_{∞} refers to the absorbance at the end of the reaction.

Figure 2.6-12: Aromatisation of 2-*tert*-butylbenzene hydrate (2.27) in phosphate buffer (10 % FB, pH 5.6) at $I = 0.5 \text{ M}$ (NaClO_4) and $25 \text{ }^\circ\text{C}$: (a) Plot of absorbance versus time; (b) plot of $\ln(A - A_\infty)$ against time with slope equal to k_{obs}

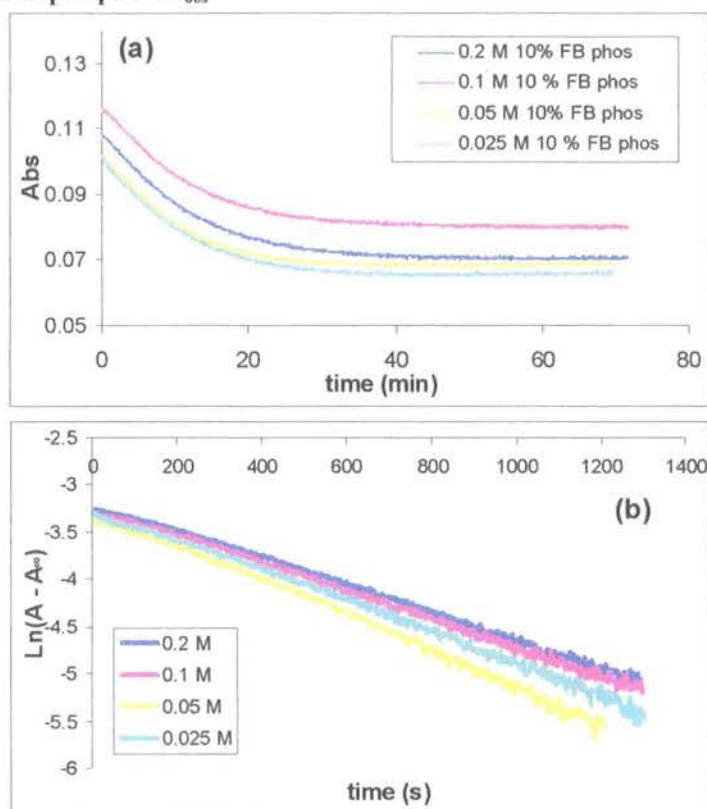


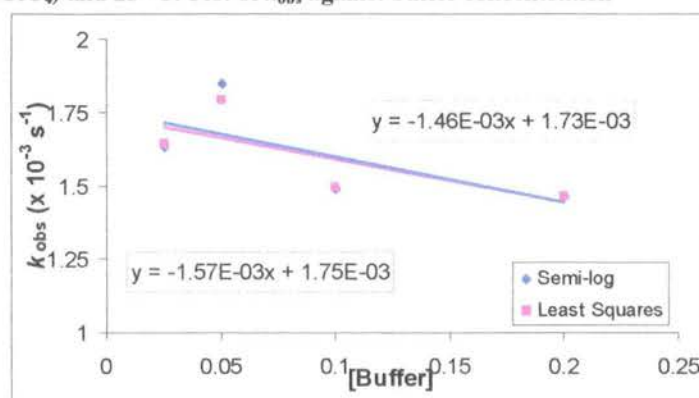
Table 2.6-5 (below) summarises the results for the aromatisation of *tert*-butylbenzene in 10% FB phosphate buffers at pH 5.6. The least squares analysis of the data in Figure 2.6-12(a) gave a mean t -value for the estimate of k_{obs} of 300 and the error of the estimate of the fit was on the order of 5×10^{-3} . All the data in Figure 2.6-12(a) show a stable A_∞ , and so the least squares and semi-logarithmic results are very similar. The mean of the results from the semi-logarithmic analysis is $k_{\text{obs}} = 1.61 \pm 0.09 \times 10^{-3} \text{ s}^{-1}$. The mean of the results from the least squares analysis is $k_{\text{obs}} = 1.60 \pm 0.08 \times 10^{-3} \text{ s}^{-1}$.

Table 2.6-5: First-order rate constants for aromatisation of 2-*tert*-butylbenzene hydrate (2.27) in 10 % FB phosphate buffers (0.2 – 0.025 M) at 25 °C and I = 0.5 M (NaClO₄)^(a)

[Buffer] (M)	pH ^(b)	[H ⁺] ^(c) x 10 ⁻⁶ M	Semi-log Plot		Least Squares Plot			
			k_{obs} ^(d) (x 10 ⁻³) s ⁻¹	R ²	k_{int} ^(e) (x 10 ⁻³) s ⁻¹	k_{obs} ^(f) (x 10 ⁻³) s ⁻¹	R ²	k_{int} ^(e) (x 10 ⁻³) s ⁻¹
0.20	5.59	7.82	1.46	0.998		1.46	0.998	
0.10	5.60	7.60	1.49	0.997	1.65	1.49	0.999	1.67
0.05	5.61	7.50	1.85	0.992	(1.60 ^(g))	1.79	0.998	(1.60 ^(g))
0.025	5.62	7.24	1.63	0.996		1.64	0.997	

(a) Measurements were made at a substrate concentration of 0.05 mM and 1 % acetonitrile (b) pH was determined using a MeterLabTM PHM 290 pH-Stat Controller equipped with a radiometer (pH 4 - 7 - 10 @ 25 °C) combination electrode (type pHC4006) with a saturated LiTCA filling solution. (c) [H⁺] was calculated using $[H^+] = 10^{-(\text{pH}/\gamma_{\text{H}})}$ where $\gamma_{\text{H}} = 1$ is the activity coefficient of the hydronium ion under our experimental conditions. (d) The value of the first-order rate constant (k_{obs}), was obtained from the slope of the plot of $\ln(A - A_{\infty})$ against time in Figure 2.6-12(b). (e) k_{int} is defined as the intercept of the plot of k_{obs} against buffer concentration Figure 2.6-13. (f) The value of the first-order rate constant (k_{obs}), was obtained from the least squares analysis of Figure 2.6-12(a). (g) mean of k_{obs} .

Figure 2.6-13 shows no evidence for buffer catalysis however, there is an increase in the first order rate constant of 10 % with decreasing buffer concentration. The slopes are on the order of 1.5×10^{-3} .

Figure 2.6-13: Aromatisation of *tert*-butylbenzene hydrate in phosphate buffer (10 % FB, pH 5.6) at I = 0.5 M (NaClO₄) and 25 °C: Plot of k_{obs} against buffer concentration

The mean first order rate constant for the aromatisation of *tert*-butylbenzene hydrate at pH 5.6 is $1.67 \times 10^{-3} \text{ s}^{-1}$.

Figure 2.6-14(a) shows the change in absorbance against time at 260 nm as a result of the reaction of *tert*-butylbenzene hydrate in phosphate buffer (25 % FB, pH 6.1). A corresponding semi-logarithmic plot of $\Delta A = A - A_{\infty}$ against time is shown in Figure 2.6-14(b) where A_{∞} refers to the absorbance at the end of the reaction.

Figure 2.6-14: Aromatisation of *tert*-butylbenzene hydrate (2.27) in phosphate buffer (25 % FB, pH 6.1) at $I = 0.5 \text{ M}$ (NaClO_4) and $25 \text{ }^{\circ}\text{C}$: (a) Plot of absorbance versus time; (b) plot of $\ln(A - A_{\infty})$ against time with slope equal to k_{obs}

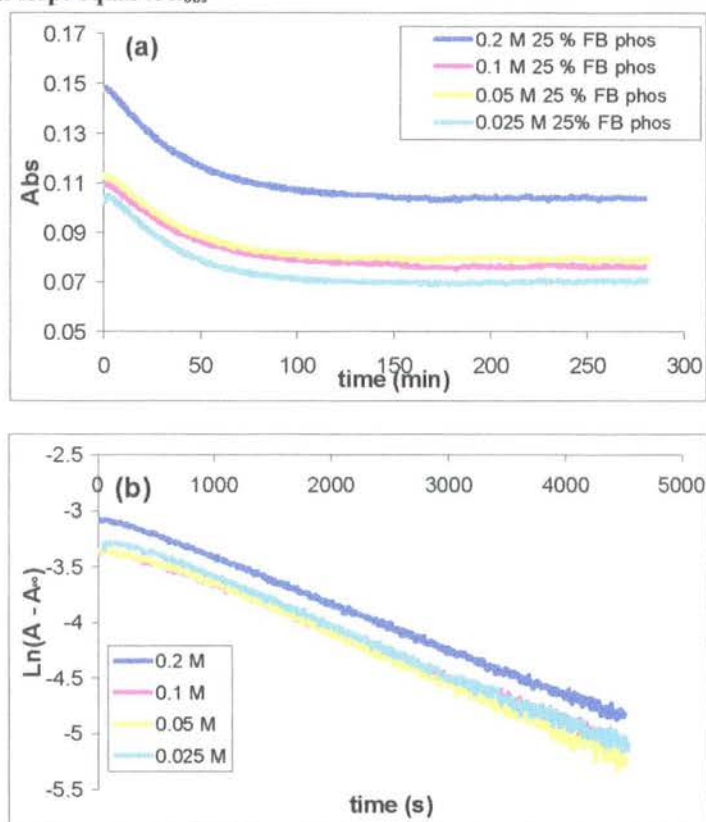


Table 2.6-6 summarises the results from the analysis of the aromatisation reaction of *tert*-butylbenzene hydrate in phosphate buffer (25 % FB, pH 6.1) at ionic strength 0.5 M maintained with sodium perchlorate. The least squares analysis of Fig 2.6-14(a) was good with the error of the estimate of the fit on the order of 6×10^{-4} with a mean t -values for the estimate of $k_{\text{obs}} = 430 \text{ s}^{-1}$. The mean first order rate constant for the aromatisation reaction from the least squares analysis is $4.42 \pm 0.14 \times 10^{-4}$. The semi-logarithmic plots also showed good consistency (see Fig 2.6-14(b)). The mean first order rate constant is $4.18 \pm 0.09 \times 10^{-4} \text{ s}^{-1}$.

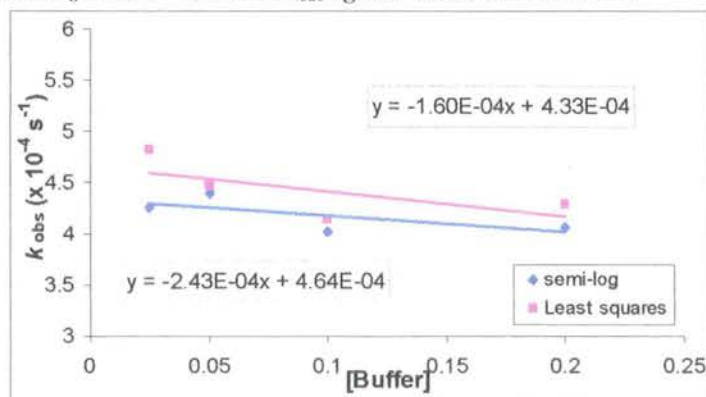
Table 2.6-6: First-order rate constants for aromatisation of *t*-butylbenzene hydrate (2.27) in 25 % FB phosphate buffers (0.2 – 0.025 M) at 25 °C and I = 0.5 M (NaClO₄)^(a)

[Buffer] (M)	pH ^(b)	[H ⁺] ^(c) (x 10 ⁻⁷) M	Semi-log Plot			Least Squares Plot		
			k_{obs} ^(d) (x 10 ⁻⁴) s ⁻¹	R ²	k_{int} ^(e) (x 10 ⁻⁴) s ⁻¹	k_{obs} ^(f) (x 10 ⁻⁴) s ⁻¹	R ²	k_{int} ^(e) (x 10 ⁻⁴) s ⁻¹
0.20	6.09	8.22	4.05	0.999		4.29	0.999	
0.10	6.08	8.28	4.02	0.997	4.33	4.13	0.998	4.64
0.05	6.08	8.34	4.39	0.997	(4.18 ^(g))	4.45	0.998	(4.42 ^(g))
0.025	6.07	8.45	4.26	0.997		4.80	0.997	

(a) Measurements were made at a substrate concentration of 0.05 mM and 1 % acetonitrile (b) pH was determined using a MeterLabTM PHM 290 pH-Stat Controller equipped with a radiometer (pH 4 - 7 - 10 @ 25 °C) combination electrode (type pHC4006) with a saturated LiTCA filling solution. (c) [H⁺] was calculated using $[H^+] = 10^{-(\text{pH}/\gamma_{\text{H}})}$ where $\gamma_{\text{H}} = 1$ is the activity coefficient of the hydronium ion under our experimental conditions. (d) The value of the first-order rate constant (k_{obs}), was obtained from the slope of the plot of $\ln(A - A_{\infty})$ against time in Figure 2.6-14(b). (e) k_{int} is defined as the intercept of the plot of k_{obs} against buffer concentration Figure 2.6-15. (f) The value of the first-order rate constant (k_{obs}), was obtained from the least squares analysis of Figure 2.6-14(a). (g) mean of k_{obs} .

The buffer catalysis plot (Fig 2.6-15) shows no evidence of buffer catalysis. The slope of the plot is on the order of $2 \times 10^{-4} \text{ M}^{-1} \text{ s}^{-1}$.

Figure 2.6-15: Aromatisation of *tert*-butylbenzene hydrate in phosphate buffer (25 % FB, pH 6.1) at I = 0.5 M (NaClO₄) and 25 °C: Plot of k_{obs} against buffer concentration



The mean first order rate constant for the aromatisation of *tert*-butylbenzene hydrate in 25 % FB phosphate buffer at pH 6.1 is $4.49 \times 10^{-4} \text{ s}^{-1}$ which corresponds to a half-life of 1544 seconds.

Figure 2.6-16(a) shows the change in absorbance against time at 260 nm as a result of the reaction of *tert*-butylbenzene hydrate in phosphate buffer (50 % FB, pH 6.6). A corresponding semi-logarithmic plot of $\Delta A = A - A_{\infty}$ against time is shown in Figure 2.6-16(b) where A_{∞} refers to the absorbance at the end of the reaction.

Figure 2.6-16: Aromatisation of *tert*-butylbenzene hydrate in phosphate buffer (50 % FB, pH 6.6) at $I = 0.5 \text{ M}$ (NaClO_4) and $25 \text{ }^{\circ}\text{C}$: (a) Plot of absorbance versus time; (b) plot of $\ln(A - A_{\infty})$ against time with slope equal to k_{obs}

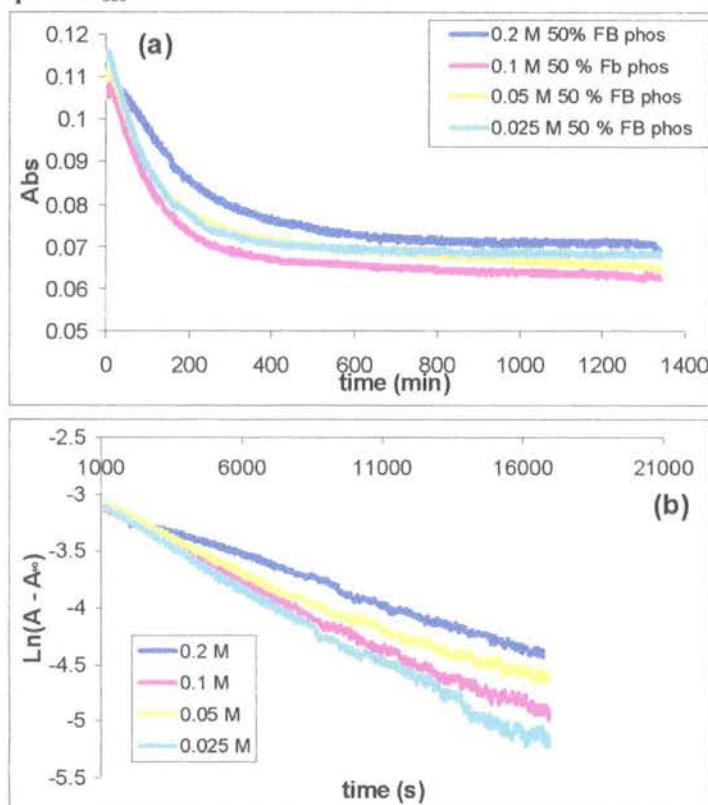


Table 2.6-7 summarises the results from the analysis of the experimental data in Figure 2.6-16 (a & b). The least squares analysis of the data in Figure 2.6-16(a) gave a good fit with the error of the estimate for the fit on the order of 2×10^{-4} . The mean t-value for the estimate of $k_{\text{obs}} = 550 \text{ s}^{-1}$. The raw data below (Fig 2.6-16(a)) show an unstable endpoint, thus the need to estimate A_{∞} . The semi-logarithmic analysis used the value for A_{∞} predicted from the fit of the least squares data. Also the first 30 minutes of the reaction appears to still show mixing or some other physical process; excluding these data points has little effect on the rate constant. The results for the data in 0.1 to 0.025 M buffers were fit to 3 half-lives, but the data obtained in 0.2 M buffer could only be fit

to 2 half-lives. The results from the 0.2 M buffer are almost two-fold slower than the other buffer concentrations. This could be put down to experimental error, or a medium effect. The data at the early stages of the reaction appear to be more affected than for the reaction in 0.2 M buffer than at the other buffer concentrations, perhaps accounting for the difference in rate constant.

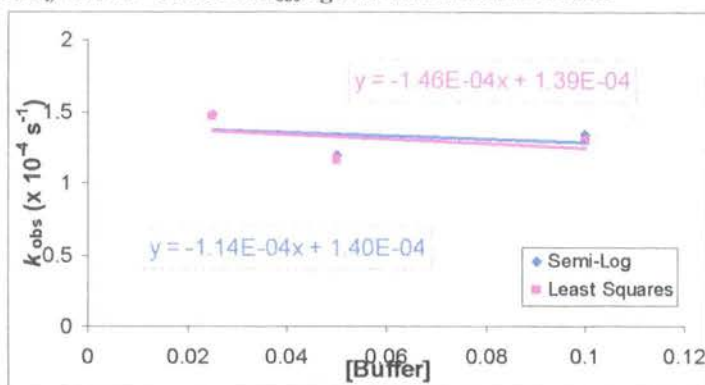
Table 2.6-7: First-order rate constants for aromatisation of *tert*-butylbenzene hydrate (2.27) in 50 % FB phosphate buffers (0.2 – 0.025 M) at 25 °C and I = 0.5 M (NaClO₄)^(a)

[Buffer] (M)	pH ^(b)	[H ⁺] ^(c) (x 10 ⁻⁷) M	<i>k</i> _{obs} ^(d) (x 10 ⁻⁴) s ⁻¹	Semi-log Plot		Least Squares Plot		
				R ²	<i>k</i> _{int} ^(e) (x 10 ⁻⁴) s ⁻¹	<i>k</i> _{obs} ^(f) (x 10 ⁻⁴) s ⁻¹	R ²	<i>k</i> _{int} ^(e) (x 10 ⁻⁴) s ⁻¹
0.20	6.65	2.25	0.91	0.994		(0.79) ^(h)	0.997	
0.10	6.62	2.42	1.34	0.996	1.14	1.30	0.998	1.46
0.05	6.59	2.55	1.19	0.994	(1.34) ^(g)	1.16	0.996	(1.33) ^(g)
0.025	6.59	2.57	1.47	0.998		1.46	0.999	

(a) Measurements were made at a substrate concentration of 0.05 mM and 1 % acetonitrile (b) pH was determined using a MeterLabTM PHM 290 pH-Stat Controller equipped with a radiometer (pH 4 - 7 - 10 @ 25 °C) combination electrode (type pHC4006) with a saturated LiTCA filling solution. (c) [H⁺] was calculated using $[H^+] = 10^{-(pH/\gamma_H)}$ where $\gamma_H = 1$ is the activity coefficient of the hydronium ion under our experimental conditions. (d) The value of the first-order rate constant (*k*_{obs}), was obtained from the slope of the plot of ln (A - A_∞) against time in Figure 2.6.2-15(b). (e) *k*_{int} is defined as the intercept of the plot of *k*_{obs} against buffer concentration Figure 2.6.2-16. (f) The value of the first-order rate constant (*k*_{obs}), was obtained from the least squares analysis of Figure 2.6.2-15(a). (g) mean of *k*_{obs} (h) rejected

Figure 2.6-17 shows the plot of k_{obs} against buffer concentration; again, there is no evidence of buffer catalysis.

Figure 2.6-17: Aromatisation of *tert*-butylbenzene hydrate in phosphate buffer (50 % FB, pH 6.6) at $I = 0.5 \text{ M}$ (NaClO_4) and $25 \text{ }^\circ\text{C}$: Plot of k_{obs} against buffer concentration



The first order rate constant for the aromatisation of *tert*-butylbenzene hydrate at pH 6.5 is $1.34 \times 10^{-4} \text{ s}^{-1}$.

Table 2.6-8 is a summary of the first order rate constants for the aromatisation reaction of *tert*-butylbenzene hydrate in acetate and phosphate buffers. The results from the semi-logarithmic and least squares analysis are shown and the analysis of the corresponding second-order plot is discussed.

Table 2.6-8: Summary of the results for the aromatisation reaction of *tert*-butylbenzene hydrate (2.27) in phosphate and acetate buffers at I = 0.5 M (NaClO₄) and 25 °C

pH ^(a)	[H ⁺] ^(b) M	<i>k</i> _{obs}	
		<i>k</i> _{int} ^(c) (<i>k</i> _{int} ^(d)) s ⁻¹	<i>k</i> _H ^(e) (<i>k</i> _H ^(f)) M ⁻¹ s ⁻¹
4.22	6.03 × 10 ⁻⁵	5.40 × 10 ⁻² (5.92 × 10 ⁻²)	
4.56	2.75 × 10 ⁻⁵	2.36 × 10 ⁻² (2.60 × 10 ⁻²)	
4.95	1.12 × 10 ⁻⁵	8.73 × 10 ⁻³ (8.96 × 10 ⁻³)	902
5.52	2.75 × 10 ⁻⁶	1.73 × 10 ⁻³ (1.75 × 10 ⁻²)	(949)
5.56	3.02 × 10 ⁻⁶	2.05 × 10 ⁻⁴ (2.05 × 10 ⁻²)	
6.07	8.51 × 10 ⁻⁷	4.64 × 10 ⁻⁴ (4.33 × 10 ⁻⁴)	
6.59	2.57 × 10 ⁻⁷	1.48 × 10 ⁻⁴ (1.48 × 10 ⁻²)	

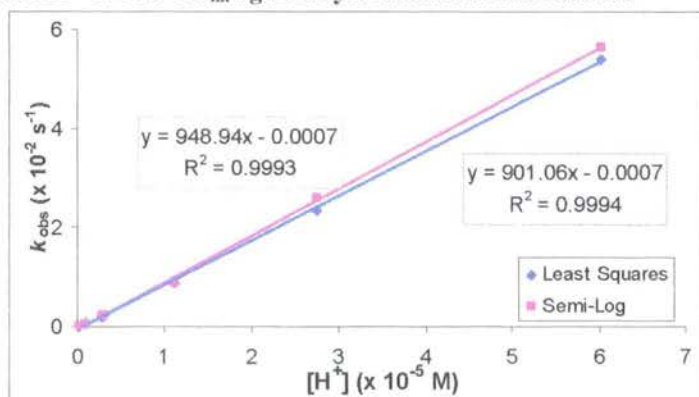
(a) pH was determined using a MeterLabTM PHM 290 pH-Stat Controller equipped with a radiometer (pH 4-7-10 @ 25 °C) combination electrode (type pHC4006) with a saturated LiTCA filling solution. (b) [H⁺] was calculated using [H⁺] = 10^{-(pH/γ_H)} where γ_H = 1 is the activity coefficient of the hydronium ion under our experimental conditions. (c) The value of the first-order rate constant (*k*_{int}) was obtained from the plot of *k*_{obs} against [buffer], where *k*_{obs} is calculated from the least squares fit using equation 2.3. (e) The value of the first-order rate constant (*k*_{int}) was obtained from the plot of *k*_{obs} against [buffer], where *k*_{obs} is calculated from the semi-logarithmic fit. (f) The value of the second-order rate constant (*k*_H) is the slope of the plot of *k*_{int} against [H⁺].

The data shows strong dependence on acid concentration. The difference in results between the least squares and semi-logarithmic analysis is negligible when compared to the change in rate with decreasing acid concentration. The methods gave slightly different *k*_H values.

The plots of *k*_{int} against increasing acid concentration (Fig 2.6-18) both gave very good linear correlations with R² values of 0.9994 and 0.9993 for the least squares and semi-logarithmic results, respectively. Analysis of both linear regressions shows the least squares analysis gives a slope (*k*_H) of 901 ± 10 M⁻¹ s⁻¹ and an intercept of -7 ± 3 × 10⁻⁴ and the semi-logarithmic analysis gives a *k*_H of 948 ± 11 M⁻¹ s⁻¹ and an intercept of -7 ± 3 × 10⁻⁴. In both cases the intercept is negative, however the value is so small when compared to the slope it can be treated as zero and also there are negative t-values and

high p-values for the intercept variable showing a poor estimate. The slopes both gave positive t-values for the estimate, with the least squares data giving a t-value of 92 and the semi-log data giving a t-value of 85. Both had p-values of less than 1×10^{-4} . All this shows the least squares regression gives a better value for k_H .

Figure 2.6-18: Aromatisation of *tert*-butylbenzene hydrate in acetate and phosphate buffers at I = 0.5 M (NaClO₄) and 25 °C: Plot of k_{int} against hydronium ion concentration



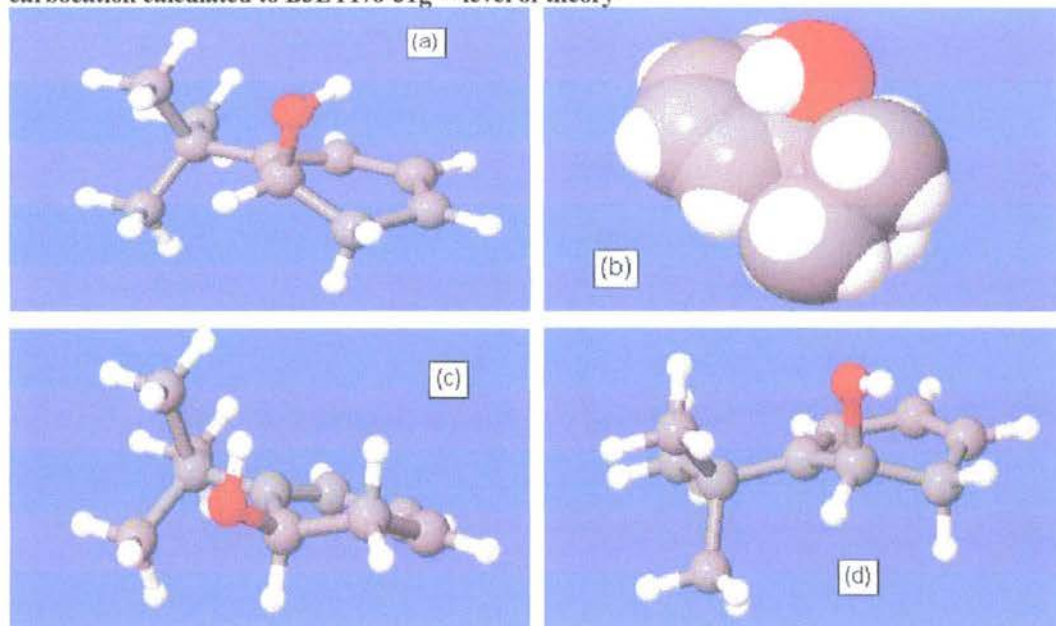
The values of $\text{Log } k_H$ calculated from the pH-rate profile for the semi-logarithmic and least squares analysis are 3.47 and 3.36, respectively. The values of k_H obtained are very different to those obtained from the slope of the plot of k_{obs} against hydronium ion concentration (Fig 2.6-19) corresponding to a mean k_H of $2600 \text{ M}^{-1} \text{ s}^{-1}$. A number of factors could lead to a difference in the values of the second order rate constant. The highest acid concentration used was $6.03 \times 10^{-5} \text{ M}$, and this is a long way from 1 M acid, so the error in the reverse extrapolation is quite high. The slopes of the pH-rate profiles also deviate from 1 (1.12 and 1.10) and both show negative t-values. The statistical analysis of the least squares data shows an intercept of 3.36 ± 0.07 and an intercept of 3.47 ± 0.1 from the semi-logarithmic data; in both cases the t-values were positive. The results from the pH-rate profile were rejected.

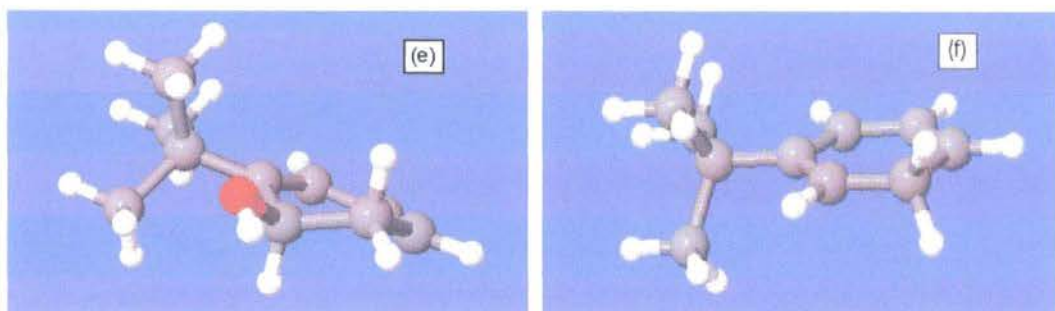
The second-order rate constant for the aromatisation of 1,2-*tert*-butylbenzene hydrate is $901 \pm 10 \text{ M}^{-1} \text{ s}^{-1}$, this corresponds to a lifetime of 1.1 *ms* in 1 M acid.

2.6.3 Computational studies of *tert*-butylbenzene hydrates

The structures and energies of 2-*tert*-butylcyclohexa-2,4-dienol (2.27) and corresponding carbocation (2.32) were calculated using Gaussian '03 at the B3LYP/6-31g** level of theory.⁷⁶ The starting points for the calculations were generated from Monte Carlo calculations (MM3* level of theory) using the Maestro program. The structures below are the lowest energy structures calculated.

Figure 2.6-19: Lowest energy structures of 2-*tert*-butylcyclohexa-2,4-dienol and the corresponding carbocation calculated to B3LYP/6-31g** level of theory





The lowest energy structure (Fig 2.6-19(a)) shows the hydroxyl group in the axial position and the *tert*-butyl group is in a pseudoequatorial position. The space-filling model of structure (a) (Fig 2.6-19(b)) shows the position of the hydroxyl group, pointing towards the conjugated diene. Figure 2.6-19(c) shows the second lowest energy structure with the hydroxyl group in an equatorial position. The third structure shows the hydroxyl group in an axial position again (Fig 2.6-19(d)); however the hydrogen is pointing away from the centre of the cyclohexadienyl ring. Structure (e) is similar to (d), however the hydrogen of the hydroxyl group is pointing down and not up. Fig 2.6-19(f) shows the structure of the carbocation. It is planar with the carbon atoms of the *tert*-butyl group co-planar with the ring. The CH₂ group adjacent to the carbocation centre has both hydrogens in a pseudo-equatorial position.

The table below shows the calculated energies of the structures in Fig 2.6-19(a – f) above.

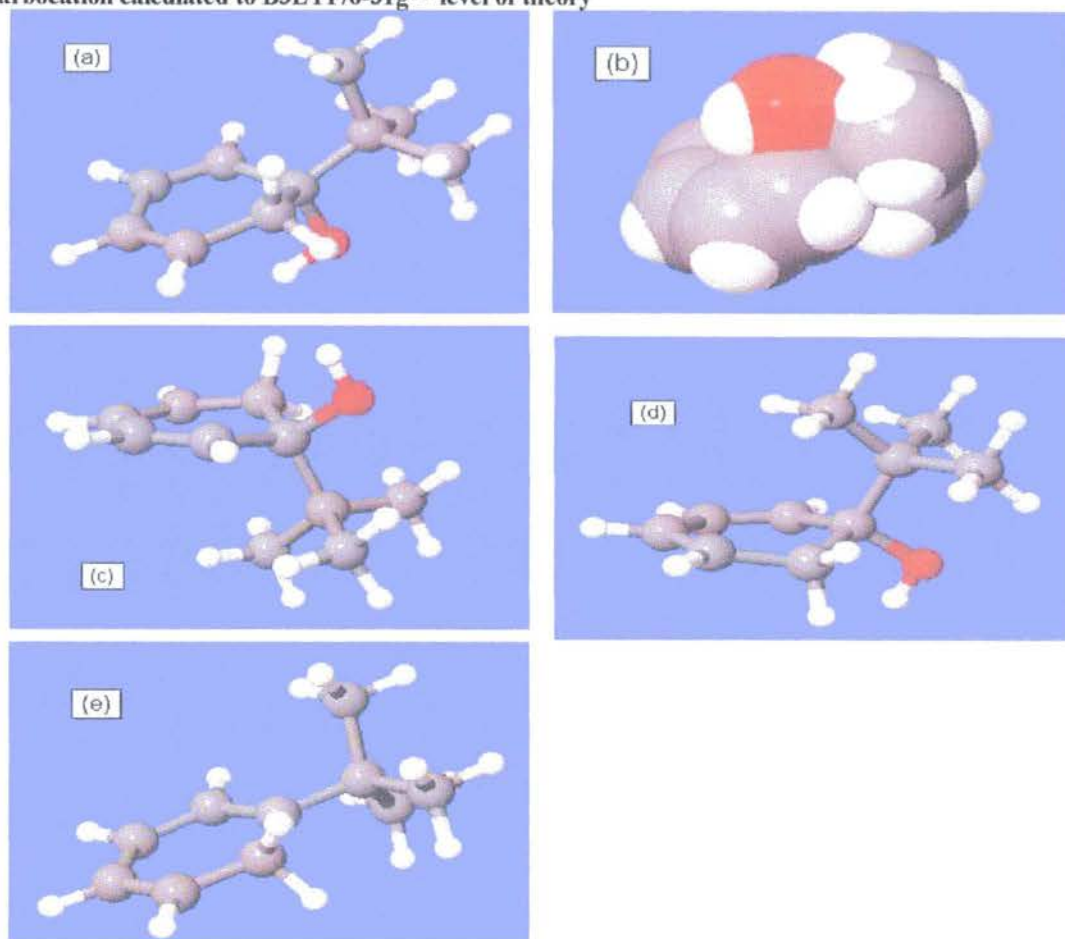
Table 2.6-9: 'ortho' tert-butylbenzene hydrate energies and corresponding carbocation calculated to B3LYP/6-31g level of theory.**

Hydrate	Gas phase		With water sphere		
	kJ/mol	Δ	kJ/mol	Δ	Δ
Fig 2.6-19 (a)	- 1223257.38	0.00	-1223281.65	0.00	-24.27
Fig 2.6-19 (c)	- 1223245.12	12.26	-1223276.82	4.83	-31.70
Fig 2.6-19 (d)	- 1223245.57	11.54	-1223271.63	10.02	-26.06
Fig 2.6-19 (e)	- 1223243.57	13.81	-1223271.08	10.57	-27.51
Carbocation Fig 2.6-19 (f)	- 1023531.06	199726.32	-1023737.33	199519	-206.27

The energies above show the stabilising affect of a water sphere. The water sphere lowers the energy of the hydrate, most notably for structure (c). It also reduces the conformational energy differences ie the ring-flip between structures (a) and (c) drops from 12.26 to 4.83 kJ/mol. Interestingly, in this case, the energy of a ring-flip is lower than the energy for the rotation of the hydroxyl group. This was not predicted by the MM3* calculations. The carbocation is 206.27 kJ/mol more stable in the aqueous sphere than in the gas phase.

Although the 1-tert-butylcyclohexa-2,4-dienol was not isolated, the computational studies were carried out to understand the reason why it could not be isolated and to compare it with the other tert-butyl substituted hydrates. The putative carbocation was also studied. The structures and energies of were calculated using Gaussian '03 at the B3Lyp/6-31g** level of theory.⁷⁶ The starting points for the calculations were generated from Monte Carlo calculations (MM3* level of theory) using the Maestro program. The structures below are the lowest energy structures calculated.

Figure 2.6-20: Lowest energy structures of 1-*tert*-butylcyclohexa-2,4-dienol and the corresponding carbocation calculated to B3LYP/6-31g** level of theory



The lowest energy *ipso* structure (Fig 2.6-20 (a)) shows the same preference for the hydroxyl group in the axial position as the rest of the series. The space-filling model shows the hydroxyl group sitting on top of the cyclohexadienyl ring with the hydrogen pointing towards the diene. The next lowest energy structure (c) is a ring-flip of (a) with both the hydroxyl and *tert*-butyl groups in a pseudo equatorial position. Structure (d) is similar to (c). The carbocation (Fig 2.6-20(e)) is planar with the *tert*-butyl group co-planar with the ring. The CH₂ group beside the carbocation centre has both hydrogens in a pseudo-equatorial position.

Table 2.6-20 (below) shows the energies of the above hydrate and corresponding carbocation structures calculated to the B3LYP/6-31g** level of theory using Gaussian 03.⁷⁶

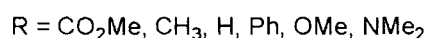
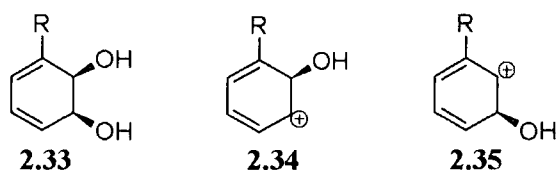
Table 2.6-10: 'ipso' tert-butylbenzene hydrate and corresponding carbocation energies calculated to B3LYP/6-31g level of theory.**

Hydrate	Gas phase		With water sphere		
	kJ/mol	Δ	kJ/mol	Δ	Δ
Fig 2.6-20(a)	-1223246.40	0.00	-1223270.71	0.00	-24.31
Fig 2.6-20(c)	-1223240.41	5.99	-1223266.99	3.72	-26.58
Fig 2.6-20(d)	-1223234.86	11.54	-1223260.11	10.60	-25.25
carbocation Fig 2.6-20(e)	-1023549.49	199697	-1023751.63	199519	-202.14

The table shows the stabilizing affect of the water sphere. As mentioned above, this lowers the energy of the structure and decreases the inter-conformational energy. The carbocation is the most stabilized (202.14 kJ/mol) by a water sphere.

2.7 Computational Studies of the *cis*-dihydrodiols

The synthesis and kinetics of the *cis*-dihydrodiols were studied by Boyd *et al*¹. The Hammett plot for the aromatisation reaction of the *cis*-dihydrodiols will be discussed and compared with the Hammett plot for the arene hydrates in section 2.8 and 3.2. This section will present the results from the computational study of the structures and energies of the *cis*-dihydrodiols (2.33) and corresponding carbocations (2.34). The structures were calculated using Gaussian '03 at the B3LYP/6-31g** level of theory.⁷⁶ In the case of biphenyl *cis*-dihydrodiol (2.33, R = Ph), the major product formed from the aromatisation reaction is the *meta*-phenol and so the structure calculated is based on structure (2.35).



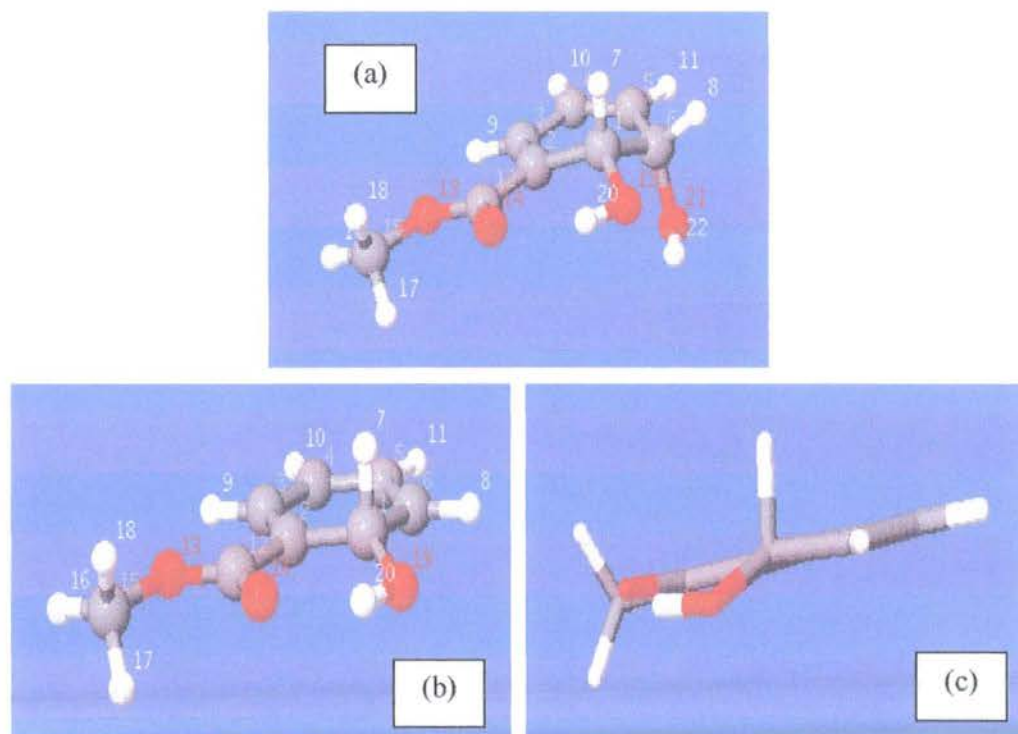
The starting points for the calculations were generated from Monte Carlo calculations (MM3* level of theory) using the Maestro program. The structures shown are the lowest energy structures calculated.

2.7.1 Lowest energy structures of the *cis*-dihydrodiols and corresponding carbocations

Figure 2.7-1 shows the structures of the ester-substituted diols and the corresponding carbocation. The calculated energies are shown in Figure 2.7-1.

The structures below show the lowest energy structure methyl 5,6-dihydroxycyclohexa-1,3-dienecarboxylate and the corresponding carbocation. Figure 2.7-1(a) shows the structure of the parent *diol*. The structure shows a hydrogen-bonding interaction between the two hydroxyl groups and the C=O of the ester substituent. The ring is a half-envelope type structure. The conjugated diene is planar and the two saturated carbons lie above and below the plane of the diene.

Figure 2.7-1: Structures of the CO₂Me-substituted *cis*-dihydrodiols calculated at the B3LYP/6-31g level of theory: (a) Diol (b) carbocation and (c) side-on view of the carbocation.**

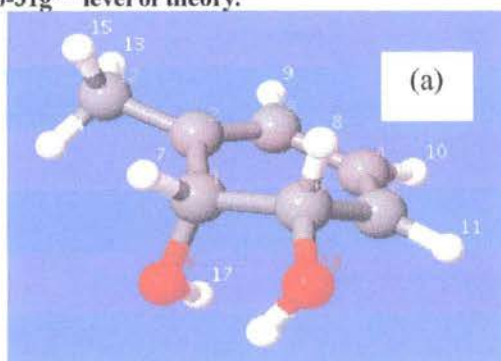


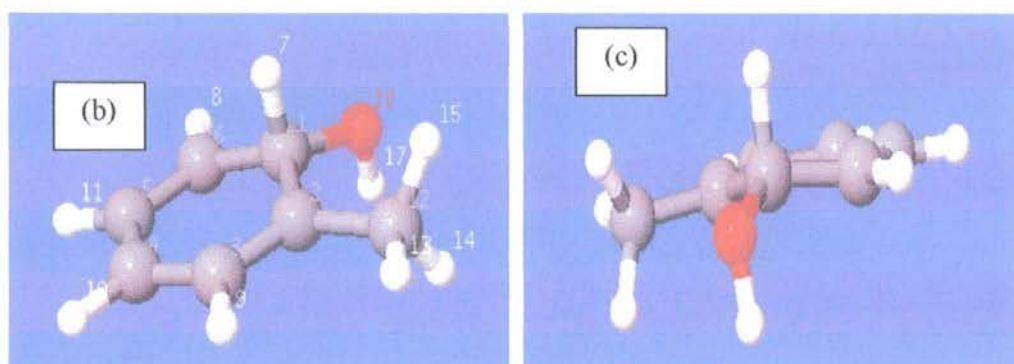
The carbocation (see Fig 2.7-1(b)) also shows a hydrogen bonding interaction between the remaining hydroxyl group and the C=O bond of the ester substituent. The ring is almost planar, the carbon with the hydroxyl group sits slightly above the plane of the ring giving a slightly puckered structure; the wire-structure in Figure 2.7-1(c) shows this more clearly.

Figure 2.7-2 shows the structures of the methyl-substituted diol and the corresponding carbocation. The calculated energies are shown in Figure 2.7-1.

The structures show the CH₃-substituted diol and corresponding carbocation, Figure 2.7-2(a) shows the diol. There is a hydrogen bonding interaction between the two adjacent hydroxyl groups, as with the ester in Figure 2.7-1(a) (above). The hydroxyl group on C-1 is in an axial position, with the hydrogen pointing towards the centre of the ring. The hydroxyl group on C-6 is in the equatorial position. The conjugated diene of the ring is planar, while the two saturated carbons lie above and below the plane of the ring. The carbon of the CH₃-substituent is co-planar with the alkenyl C-Hs.

Figure 2.7-2: Structures of the CH₃-substituted diol ((1S,2R)-3-methylcyclohexa-3,5-diene-1,2-diol) calculated to the B3LYP/6-31g level of theory.**





The carbocation structure shown in Figure 2.7-2 (b) and (c) shows the hydroxyl group in an equatorial position. Figure 2.7-2(c) shows the puckering of the ring at the hydroxyl substituted carbon. The structure is not fully planar.

Figure 2.7-3 shows the structures of the phenyl-substituted diol and the corresponding carbocation. The calculated energies are shown in Figure 2.7-1.

Figure 2.7-3: Structures of the phenyl-substituted diol - (1S,2R)-3-phenylcyclohexa-3,5-diene-1,2-diol - calculated to the B3LYP/6-31g level of theory**

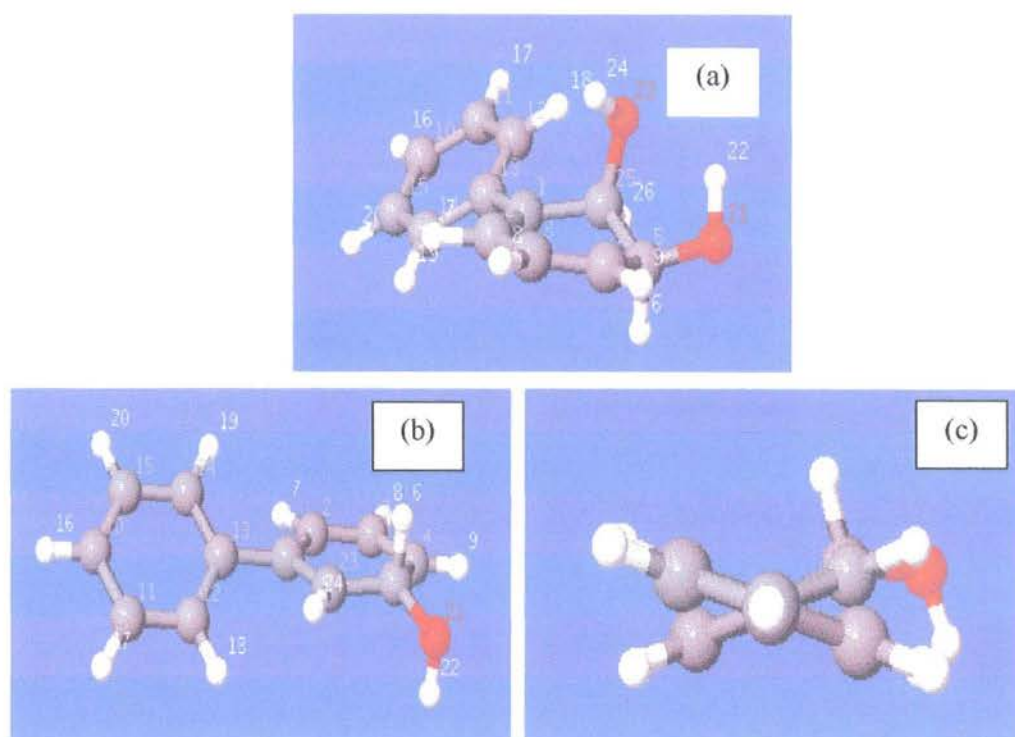
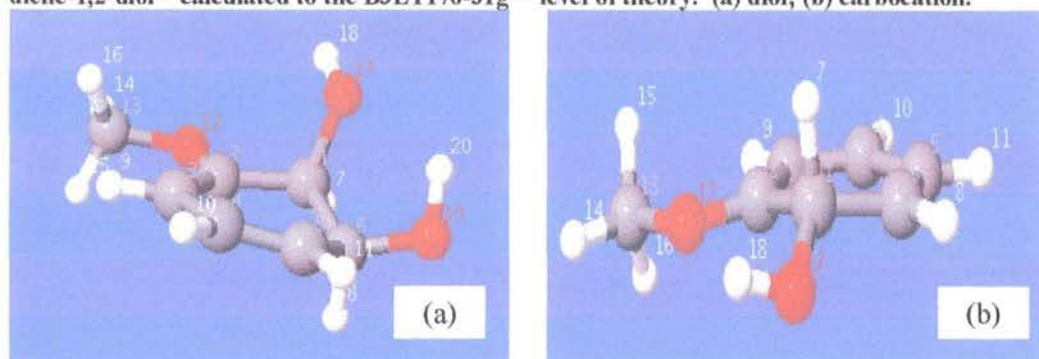


Figure 2.7-3(a) shows the calculated structure of (1S,2R)-3-phenylcyclohexa-3,5-diene-1,2-diol. The structure shows hydrogen bonding between the two hydroxyl groups. The hydroxyl group on C-6 is not fully in the axial position; the hydroxyl group on C-5 is in an equatorial position. The phenyl ring is twisted 30° relative to the core ring structure. The carbocation shown in Figure 2.7-3 ((b) and (c)) shows once again the puckering of the ring at the carbon with the hydroxyl group attached. The phenyl ring is turned approximately 10° relative to the core ring. The hydroxyl group is in the equatorial position with the hydrogen pointing down.

Figure 2.7-4 shows the structures of the methoxy-substituted diol and the corresponding carbocation. The calculated energies are shown in Figure 2.7-1.

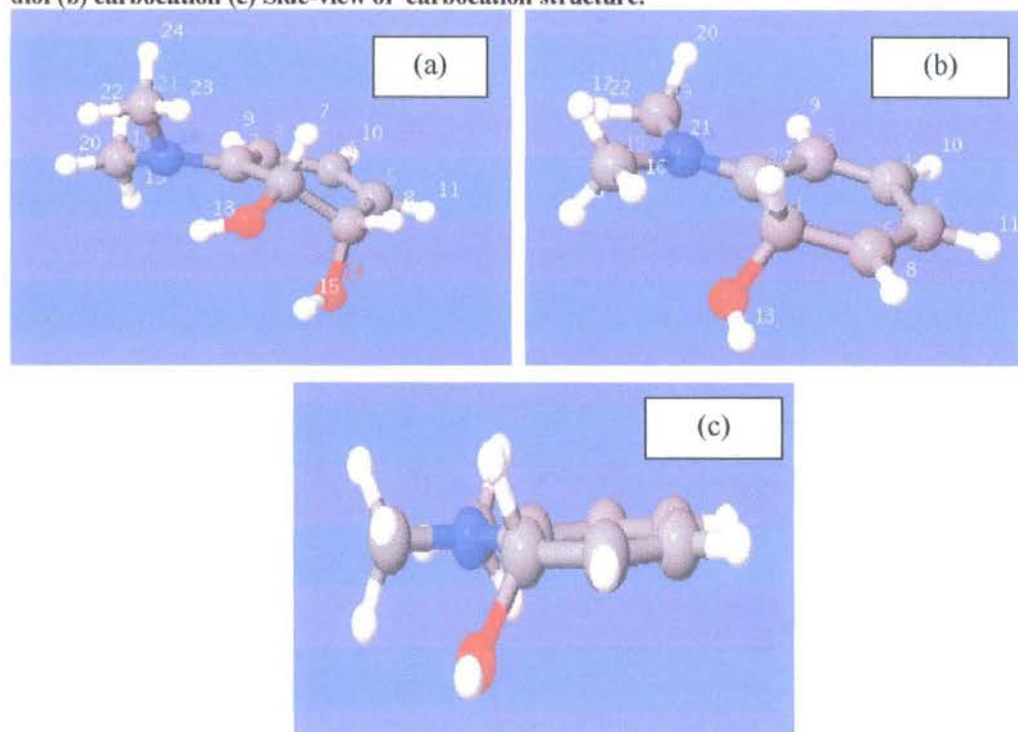
Figure 2.7-4: The structures of the methoxy-substituted diol - (1S,2S)-3-methoxycyclohexa-3,5-diene-1,2-diol – calculated to the B3LYP/6-31g level of theory. (a) diol; (b) carbocation.**



The structures show the methoxy-substituted diol and corresponding carbocation. Figure 2.7-4(a) shows the diol; as with the other diols above (Fig 2.7-4(a)) there is hydrogen bonding between the two hydroxyl groups ($H\cdots OH$ distance equals 2.1 \AA). The hydroxyl-group on C-1 is axial and the hydroxyl group on C-6 is equatorial. The structure next lowest in energy is a ring-flip of structure (a). Interestingly, the methoxy substituent does not appear to be available for hydrogen bonding in the diol. However, there is hydrogen bonding between the hydroxyl group and the methoxy substituent in the carbocation (Fig 2.7-4(b)). The distance between the oxygen of the OMe group and the hydrogen of the OH group is 2.5 \AA . Once again the ring is puckered at the hydroxyl substituted carbon (C-1) of the carbocation, with the hydroxyl group in an equatorial position.

Figure 2.7-5 shows the structures of the dimethylamino-substituted diol and the corresponding carbocation. The calculated energies are shown in Figure 2.7-1.

Figure 2.7-5: Lowest energy structures for the dimethylamino-substituted diol - (1S,2R)-3-(dimethylamino)cyclohexa-3,5-diene-1,2-diol – calculated to the B3LYP/6-31g** level of theory. (a) diol (b) carbocation (c) Side-view of carbocation structure.



The structures above show the dimethylamino-substituted diol and corresponding carbocation. Figure 2.7-5(a) shows the diol and there appears to be hydrogen-bonding between the *cis*-hydroxyl groups ($H\cdots OH$ distance equals 2.2 Å). There also appears to be hydrogen bonding between the hydroxyl group on C-1 and the nitrogen lone-pair ($H\cdots NMe_2$ distance equals 2.6 Å). Unlike in the methoxy-substituted diol, the hydroxyl group on C-1 is equatorial. The dimethylamino group is twisted relative to the cyclohexadiene in the diol with one CH_3 group 6° above the ring and the other 30° below. The carbocation intermediate shown in Figure 2.7-5 (b) and (c) appears to have a planar structure, unlike the other carbocations mentioned in this section (Fig 2.7 1-4(b)) due to complete delocalization of the N-lone pair. There is also no hydrogen bonding between the remaining hydroxyl group on C-1 and the nitrogen lone-pair, in fact the hydrogen of the hydroxyl group is pointing away from the ring structure with the hydroxyl group in a pseudo-equatorial position. The dimethylamino group is almost co-planar with the ring; one CH_3 group is 3° above the plane of the cyclohexadiene and the other 3° below.

2.7.2 Calculated Energies of the *cis*-dihydrodiols

Table 2.7-1 (below) shows the calculated energies of the substituted *cis*-dihydrodiols (2.33). As with the hydrates, incorporating a water sphere in the calculation lowers the energy of the diols and the carbocation intermediates. The greatest stabilisation is seen in the phenyl-substituted dihydrodiol and the weakest stabilisation effect was seen with the ester substituent.

Table 2.7-1: Energies of the R-substituted *cis*-dihydrodiols (2.33) calculated to the B3LYP/6-31g level of theory.**

Substituent (R)	Diol (kJ/mol)			Carbocation (kJ/mol)		
	Gas phase	With water sphere	Δ	Gas phase	With water sphere	Δ
CO ₂ Me	-1606141.40	-1606179.56	-38.16	-1406349.90	-1406582.51	-232.61
CH ₃	-1111069.36	-1111109.51	-40.15	-911306.04	-911553.56	-247.52
H	-1007826.91	-1007868.15	-42.24	-808033.70	-808299.45	-265.25
Ph	-1614493.29	-1614542.43	-49.14	-1414710.38	-1414960.40	-250.02
OMe	-1308519.57	-1308561.70	-42.13	-1108802.34	-1109036.95	-234.61
NMe ₂	-1359581.93	-1359625.83	-43.90	-1159936.46	-1160153.81	-217.354

2.7.3 Relative energies of the *cis*-dihydrodiols

Table 2.7-2: Relative energies of the *cis*-diol structures shown in section 2.7.2*

Substituent	<i>cis</i> -dihydrodiol		Carbocation		Energy C ⁺ - Energy diol
	kJ/mol	Δ kJ/mol ($\times 10^3$)	kJ/mol	Δ kJ/mol ($\times 10^3$)	
Ph	-1614542.43	0.00	-1414960.40	0.00	199582
CO ₂ Me	-1606179.56	8.36	-1406582.51	8.37	199597
NMe ₂	-1359625.83	254.92	-1160153.81	254.81	199472
OMe	-1308561.70	305.98	-1109036.95	305.92	199524
CH ₃	-1111109.51	503.43	-911553.56	503.41	199556
H	-1007868.15	606.67	-808298.70	606.66	199570

* Energies calculated to the B3LYP/6-31g** level of theory incorporating PCM with water as the solvent.⁷⁶

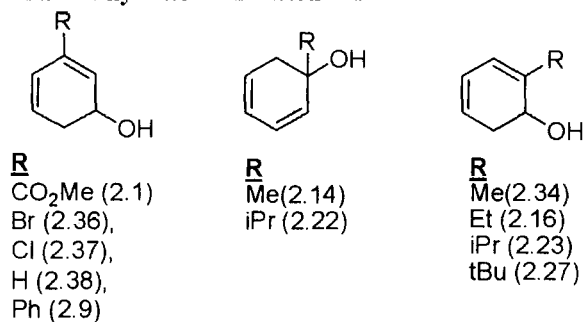
The table above shows the relative energies of the hydrated dihydrodiols; the third column shows the increasing energy of the diol with changing substituent, relative to the diol with a phenyl substituent. The fifth column shows the increasing energy of the carbocation intermediate, relative to that with a phenyl substituent. The final column shows the energy difference between the carbocation and the diol for each substituent. The smallest calculated energy difference between the carbocation and the dihydrodiol is seen with the dimethylamino substituent, whereas the largest energy difference between carbocation and dihydrodiol is seen with the ester-substituent. This is consistent with the published results¹, showing the rate of aromatisation of the dihydrodiol bearing an electron-donating substituent is faster than a *cis*-diol with an electron-withdrawing substituent.

2.8 Linear Free Energy Correlations

This section displays the possible linear free energy correlations between the kinetic data for dehydration of the various hydrates and the available σ -values. The following hydrates shall be discussed: methylbenzoate hydrate (2.1), bromobenzene hydrate (2.36), chlorobenzene hydrate (2.37), benzene hydrate (2.38), biphenyl hydrate (2.9), *ipso*-

toluene hydrate (2.14), *ipso*-cumene hydrate (2.22) and *ortho*-toluene hydrate (2.13), ethylbenzene hydrate (2.16), cumene hydrate (2.23) and *tert*-butylbenzene hydrate(2.27).

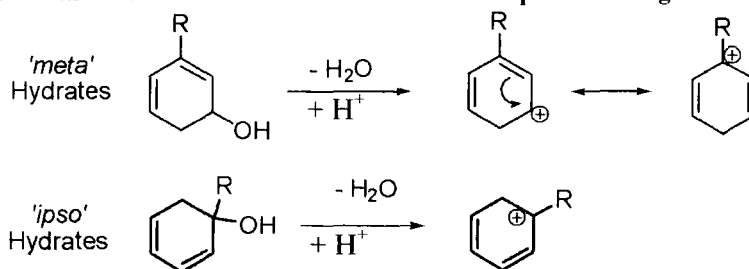
Chart 2.8-1: Structures of arene hydrates to be discussed



2.8.1 Hydrates with substituents at the '*ipso*' and '*meta*' position

Scheme 2.8-1 (below) shows the hydrates that form carbocation intermediates which possess contributing resonance structures with positive charge at the substituted carbon. The kinetic data for these hydrates will be considered together.

Scheme 2.8-1: Formation of carbocation intermediates with positive charge on the '*ipso*' carbon



2.8.1.1 Correlation of kinetic data for aromatisation with σ^+ , σ_p and σ_m .

The σ_m and σ_p constants are based on the pK_a values for ionization of *meta* and *para* substituted benzoic acids. The σ^+ parameter is based on the rate of solvolysis of a *para*-substituted cumyl chloride and better accounts for direct resonance interactions between an electron-donating substituent and a carbocation centre than the original Hammett σ_m and σ_p values. Table 2.8-1 (below) summarises the second-order rate constants for aromatisation of the '*ipso*' and '*meta*' hydrates and the relevant substituent constants.

Table 2.8-1: Summary of second-order rate constants for aromatisation for arene hydrates (see Chart 2.8-1 for structures)

Hydrate	$k_H^{(a)}$ ($M^{-1} s^{-1}$)	Log k_H	σ_p^+ (b)	σ_p (b)	σ_m (b)
Methylbenzoate Hydrate (2.1)	0.0962	-1.02	0.48	0.45	0.37
Bromobenzene Hydrate (2.36)	20	1.30	0.15	0.23	0.39
Chlorobenzene Hydrate (2.37)	27	1.43	0.11	0.23	0.39
Benzene Hydrate (2.38)	190	2.28	0	0	0
Biphenyl Hydrate (2.9)	2203	3.34	-0.18	-0.01	0.06
' <i>ipso</i> ' Toluene Hydrate (2.14)	9810	3.99	-0.31	-0.17	-0.07
' <i>ipso</i> ' Cumene Hydrate (2.22)	14700	4.17	-0.28	-0.15	-0.04

(a) Obtained from slope of the plot of k_{obs} against hydronium ion concentration (b) From ref⁽⁸⁴⁾

Figure 2.7.1.1-1((a) – (c)) shows plots of the log of the second-order rate constants for dehydration, k_H , against σ_p^+ , σ_p and σ_m according to equations 2.8 – 2.10 respectively.

$$\text{Log}(k_H) = \rho^+ \sigma_p^+ + C \quad \text{Equation 2-8}$$

$$\text{Log}(k_H) = \rho_m \sigma_m + C \quad \text{Equation 2-9}$$

$$\text{Log}(k_H) = \rho_p \sigma_p + C \quad \text{Equation 2-10}$$

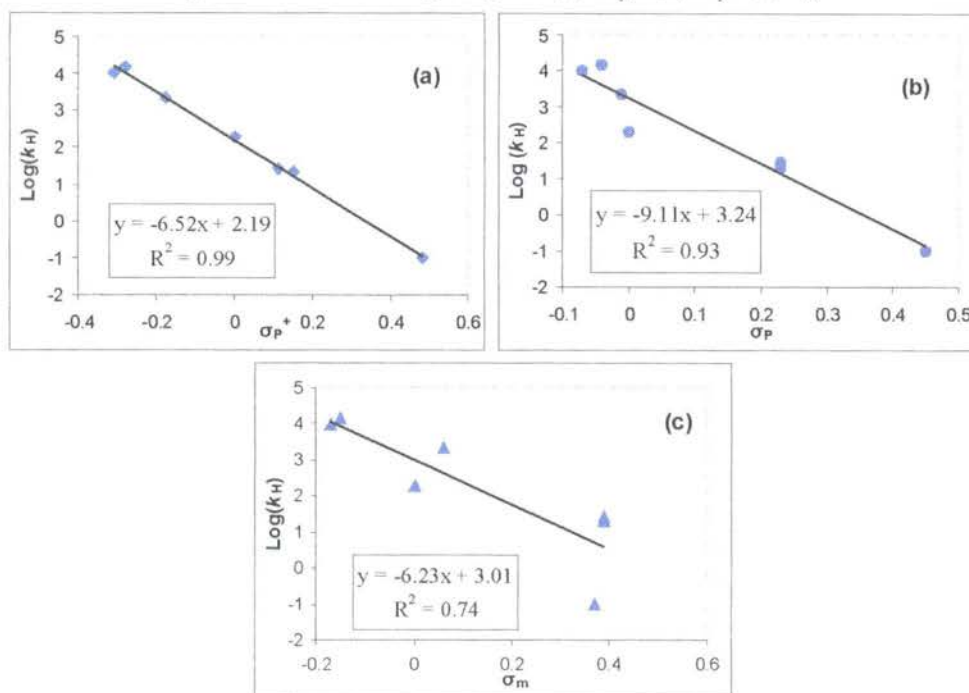
Figure 2.8-1: Plots of $\text{Log } k_H$ against (a) σ_p^+ (b) σ_p (c) σ_m 

Figure 2.8-1(a) shows an excellent correlation with R^2 equal to 0.997. The slope (ρ^+) is equal to $-(6.52 \pm 0.20)$. The correlation with σ_p (Fig 2.7.1-1(b)) predicts a ρ^p of $-(9.11 \pm 1.11)$ with an $R^2 = 0.93$. The error is higher here with the point for benzene hydrate (2.38) being the major outlier. The correlation with σ_m (Fig 2.9-1(c)) predicts a ρ^m of $-(6.23 \pm 1.66)$ with an $R^2 = 0.74$. The correlation is poor in this case, with the standard error of the estimate equal to 1.03, which is almost ten times the error for the fit in Figure 2.8-1(a).

2.8.1.2 Correlation of kinetic data for aromatisation with σ_I , σ_R and Taft E_s values

Substituent parameters that reflect purely inductive effects were measured by a number of different groups using different model systems. The Taft and Charton model systems listed below are based on acid and base-catalysed aliphatic ester hydrolyses and pK_a values of aliphatic acetic acids respectively. The Taft σ_I values were measured based on the change in ^{19}F chemical shift in a series of substituted fluorobenzenes is also given below. Also a correlation with Taft E_s values, based on the acid-catalysed hydrolysis of aliphatic esters, is shown.

Table 2.8-2: Summary of second-order rate constants for aromatization of arene hydrates and σ_I , σ_R and Taft E_s values. (For structures see Chart 2.8-1)

Hydrate	k_H ($M^{-1}s^{-1}$)	Log k_H	$\sigma_I^{(b)}$	$\sigma_I^{(b)}$	$\sigma_I^{(b)}$	Taft $E_s^{(b)}$	F ^(b)	R ^(b)
Methylbenzoate Hydrate (2.1)	0.0962	-1.02	0.31	0.30	0.19	-	0.34	0.11
Bromobenzene Hydrate (2.36)	20	1.30	0.45	0.47	0.49	-1.16	0.45	-0.22
Chlorobenzene Hydrate (2.37)	27	1.43	0.47	0.47	0.43	-0.97	0.42	-0.19
Benzene Hydrate (2.38)	190	2.28	0	0	0	0	0.03	0
Biphenyl Hydrate (2.9)	2203	3.34	0.10	0.12	0.14	d:-1.01 w:-3.82	0.12	-0.13
' <i>ipso</i> ' Toluene Hydrate (2.14)	9810	3.99	-0.04	-0.01	-0.01	-1.24	0.01	-0.18
' <i>ipso</i> ' Cumene Hydrate (2.22)	14700	4.17	-0.06	0.01	-	-1.71	0.04	-0.19

(a) Obtained from slope of the plot of k_{obs} against hydronium ion concentration (b) From ref⁽⁸⁴⁾

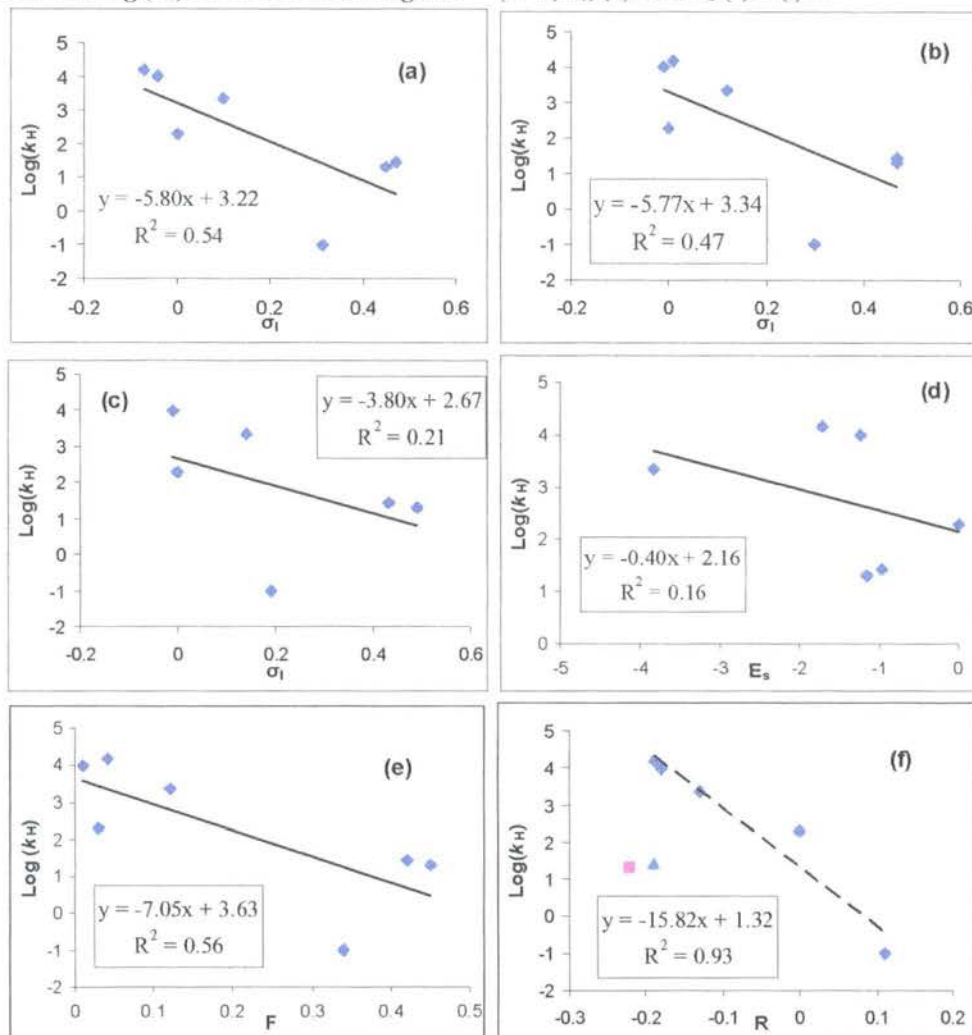
Figure 2.8-2((a) – (c)) shows plots the log of the second-order rate constants for dehydration, k_H , against σ_I , Taft E_s , F and R values according to equations 2.11 – 2.14 respectively.

$$\text{Log}(k_H) = \rho^I \sigma_I + C \quad \text{Equation 2-11}$$

$$\text{Log}(k_H) = \rho_{E_s} E_s + C \quad \text{Equation 2-12}$$

$$\text{Log}(k_H) = \rho_F F + C \quad \text{Equation 2-13}$$

$$\text{Log}(k_H) = \rho_R R + C \quad \text{Equation 2-14}$$

Figure 2.8-2: $\text{Log}(k_H)$ for aromatization against (a–c) σ_I , (d) Taft E_s (e) F (f) R.

The above correlations generally gave poor fits. Figure 2.7-2(a) gave a ρ^I of -5.80 ± 2.39 with a standard error of the estimate of 1.36; R^2 is equal to 0.54. Correlation with Charton's σ_I -values gave a ρ^I of -5.77 ± 2.76 with the error of the estimate in the order of 1.5 and $R^2 = 0.47$. The correlation with Taft's σ^I from the chemical shift of fluorobenzenes gives a ρ^I of -3.80 ± 3.72 , the standard error of the estimate is 1.76 and $R^2 = 0.21$. Correlation with the steric factor, Taft's E_s values, gives a slope of -0.40 ± 0.45 with an $R^2 = 0.16$.

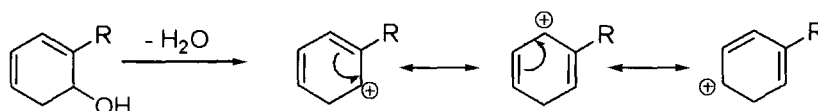
Figure 2.7-2(e) and (f) show the correlation between $\text{Log}(k_H)$ for the aromatisation reaction and the Field (F) and resonance (R) effects. The outlier in Figure 2.7-2(e) is the

methyl benzoate ester and the overall the fit is poor. The slope is equal to -7.05 ± 2.79 with $R^2 = 0.74$. Figure 2.7-2(f), the correlation with R, shows a good correlation when two outliers, the chloro and bromo substituted hydrates are excluded. The slope is equal to -15.82 ± 2.57 , with $R^2 = 0.93$.

2.8.2 Hydrates with 'ortho' substituents

The 'ortho' hydrates show no resonance structure with the carbocation stabilized at a tertiary position, as shown below (Scheme 2.8-2).

Scheme 2.8-2: Resonance structures for the carbocation intermediate generated from the 'ortho' hydrates



2.8.2.1 Correlation of hydrates with σ^+ , σ_p and σ_m .

The table below shows the 'ortho' hydrates and the corresponding σ_p^+ , σ_p and σ_m values. Although the rate data span only a 2-fold range of activity, the Hammett correlations were attempted in any case and the results interpreted qualitatively.

Table 2.8-3: Summary of second-order rate constants for aromatization of the 'ortho' arene hydrates and the corresponding σ_p^+ , σ_p , σ_m values.

'ortho' Hydrate	k_H ($M^{-1} s^{-1}$)	Log k_H	σ_p^+	σ_p	σ_m
Toluene Hydrate (2.13)	514	2.71	-0.31	-0.17	-0.07
Ethylbenzene Hydrate (2.16)	538	2.73	-0.30	-0.15	-0.07
Cumene Hydrate (2.23)	642	2.81	-0.28	-0.15	-0.04
<i>tert</i> -butylbenzene Hydrate (2.27)	949	2.98	-0.26	-0.20	-0.10

(a) Obtained from slope of the plot of k_{obs} against hydronium ion concentration (b) From ref.⁽⁸⁴⁾

Figure 2.8-3 ((a) – (c)) (below) shows plots of the log of the second-order rate constants for dehydration of the *ortho* hydrates against σ_p^+ , σ_p and σ_m according to equations 2.8 – 2.10 respectively.

Figure 2.8-3: Plots of $\text{Log}(k_H)$ against (a) σ_p^+ (b) σ_p (c) σ_m

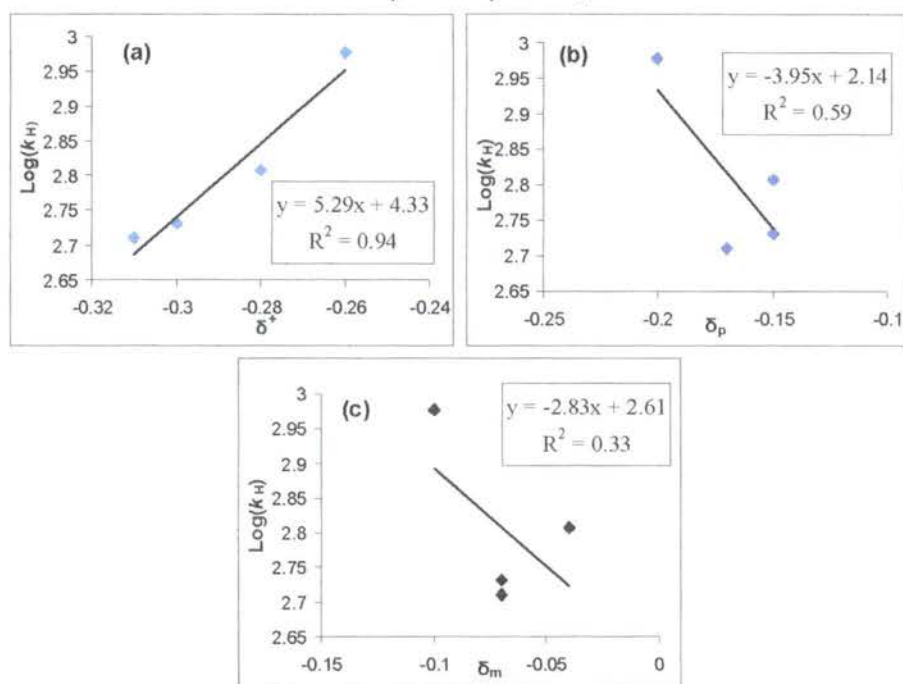


Figure 2.8-3(a) shows a reasonable correlation with $R^2 = 0.94$. The slope (ρ^+) is equal to 5.28 ± 0.97 . The correlation with σ_p (Fig 2.8-3(b)) predicts a ρ^p of $-(3.95 \pm 2.31)$ with an $R^2 = 0.59$. The correlation with σ_m (Fig 2.8-3(c)) predicts a ρ^m of $-(2.83 \pm 2.86)$ with $R^2 = 0.33$.

2.8.2.2 Correlations with σ_I , σ_R and Taft Es

The kinetic data for aromatization of the *ortho* hydrates was also correlated against σ_I , σ_R and Taft Es values.

Table 2.8-4: Summary of second-order rate constants for the '*ortho*' arene hydrates and σ_I , Taft Es, R and F values.

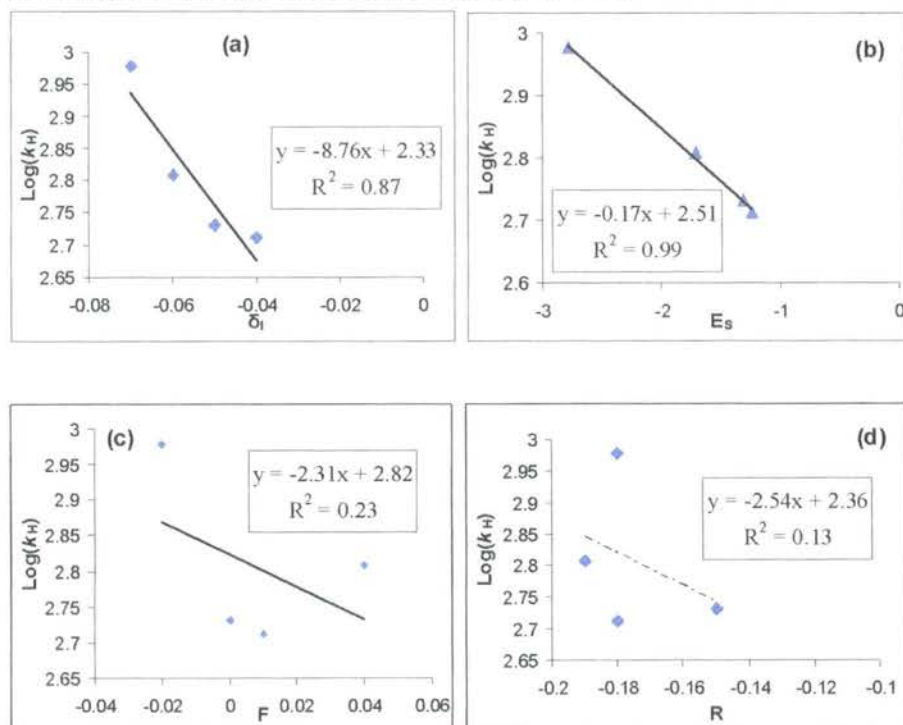
' <i>ortho</i> ' Hydrate	$k_H^{(a)}$ ($M^{-1} s^{-1}$)	$\text{Log } k_H$	$\sigma_I^{(b)}$	$Es^{(b)}$	$F^{(b)}$	$R^{(b)}$	$\sigma_R^{(b)}$
Toluene Hydrate	514	2.71	-0.04	1.24	0.01	-0.19	0.7

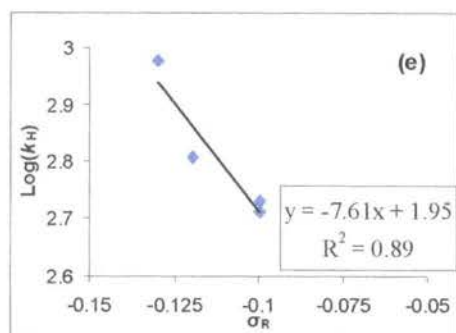
Ethylbenzene Hydrate	538	2.73	-0.05	1.31	0.00	-0.15	-0.5
Cumene Hydrate	642	2.81	-0.06	1.71	0.04	-0.19	-0.4
<i>tert</i> -butylbenzene Hydrate	949	2.98	-0.07	2.78	-0.02	-0.18	-0.07

(a) Obtained from slope of the plot of k_{obs} against hydronium ion concentration (b) From ref.⁽⁸⁴⁾

Figure 2.7-4((a) – (e)) shows for the logs of the second-order rate constants for dehydration, k_H , against σ_I , Taft E_s , F, R and σ_R^o values according to equations 2.11 – 2.14 respectively.

Figure 2.8-4: : Semi-logarithmic plots of the second-order rate constant for the aromatisation of the 'ortho' hydrates against (a) σ_I , (b) E_s , (c) R, (d) F and (e) σ_R^o values



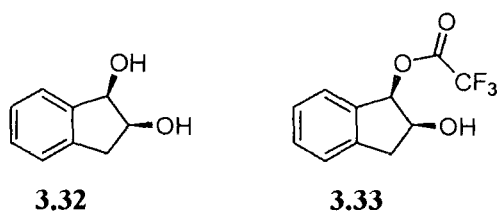


The above correlations generally gave a poor fit. Figure 2.7-3(a) gave a ρ^1 of -8.76 ± 2.38 with a standard error of the estimate of 0.053; $R^2 = 0.87$. Correlation with the steric factor, Taft's E_S values, gives a slope of -0.17 ± 0.007 with $R^2 = 0.99$.

Figure 2.7-4 (c), (d) and (e) show the correlation between $\log(k_H)$ for the aromatisation reaction and the calculated field (F) and resonance (R) effects and also σ_R^o . The correlations with R and F were particularly poor. For the correlation with F (see Fig 2.7.2-2(c), the slope is equal to -2.31 ± 3.01 with R^2 equal to 0.23. In figure 2.7-4(d), the correlation with R is also poor with the slope is equal to -2.54 ± 4.61 , with R^2 equal to 0.13. The correlation with σ_R^o was reasonable; the slope was calculated to be -7.61 ± 1.91 with an R^2 of 0.89.

2.9 Indene Diol

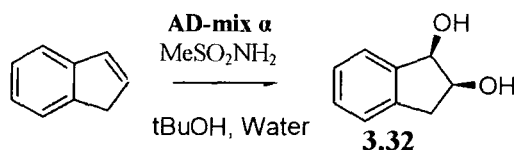
This section presents the synthesis and kinetic studies of indene diol (3.32). Enantiomerically pure *cis*-indene diol was prepared using the Sharpless dihydroxylating reagent. Acid-catalyzed rates of formation of the putative benzylic carbocation intermediate were determined by ^1H NMR spectroscopy in perchloric acid solution in D_2O . Azide-trapping experiments using ester derivative (3.33) were attempted with the aim of obtaining a first-order rate constant for the reaction of the putative carbocation intermediate with water. The combined data could be used to provide an estimate for the pK_R of the 2-hydroxyindanyl cation.



2.9.1 Synthesis of (1R,2S)-2,3-dihydro-1H-indene-1,2-diol (3.32) and ester derivative

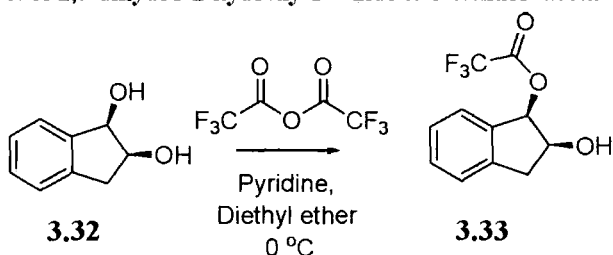
The synthesis of (1R,2S)-2,3-dihydro-1H-indene-1,2-diol (3.32) was carried out as shown in Scheme 2.9-1. The Sharpless dihydroxylation agent (AD-mix- α) was employed so that the product would be diastereomerically pure. The product was isolated and purified by recrystallisation.

Scheme 2.9-1: Synthesis of (1R,2S)-2,3-dihydro-1H-indene-1,2-diol (3.32)



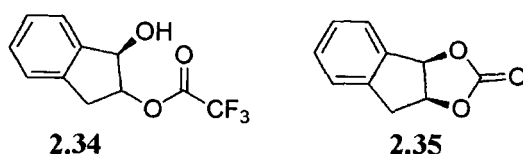
Scheme 2.9-2 (below) outlines the synthesis of the ester derivative 2,3-dihydro-2-hydroxy-1H-inden-3-yl 2,2,2-trifluoroacetate (3.33).

Scheme 2.9-2: Synthesis of 2,3-dihydro-2-hydroxy-1H-inden-3-yl 2,2,2-trifluoroacetate.



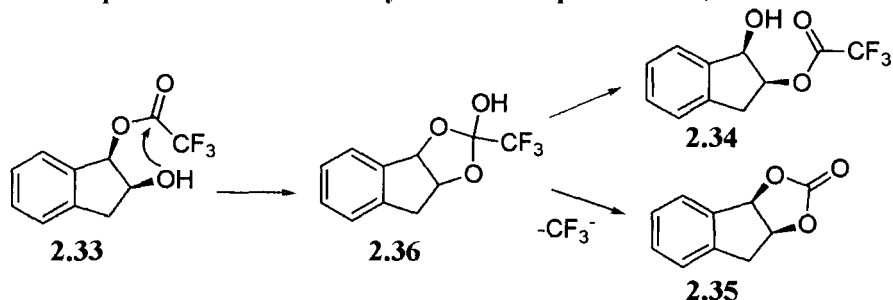
The synthesis of 2,3-dihydro-2-hydroxy-1H-inden-3-yl 2,2,2-trifluoroacetate proved to be problematic. The desired compound was only isolated in a 20 % yield; however fortunately it could be purified by flash column chromatography. A number of side-products were formed and these eluted from the column together. As all the side-products were eluted together, 1D and 2D NMR was required to identify the peaks of the individual compounds. The first expected side-product identified was 2,3-dihydro-1-hydroxy-1H-inden-2-yl 2,2,2-trifluoroacetate (2.34), a regioisomer of (2.35). The second

side-product identified was the tri-cyclic *cis*-1,2-dihydroxyindane carbonate (2.35) formed by the elimination of CF_3^- . This compound was previously prepared by White *et al*⁸⁵.



A third major side-product was formed and this proved difficult to identify. The ^1H NMR spectrum showed peaks in the aromatic region, a pseudo-quartet at 5.6 ppm, a doublet at 5.3 ppm both with J-values of 5 Hertz, and a multiplet at 3.3 ppm. The ^{13}C NMR spectrum showed peaks at 141, 138, 86, 80, 75 and 38 with some indistinguishable arene peaks. The latter spectrum also showed a doublet at 113.5 ppm, with a J-value of 9 Hertz, likely due to the trifluoromethyl carbon which should show coupling to fluorine. The mass spectrum showed a molecular ion at 229 and a signal at 131 which is consistent with loss of a trifluoroacetate group (m/z 131 ($M^+ - \text{OCOCF}_3$)). These results are consistent with 2-trifluoromethyl-8,8a-dihydro-3a*H*-indeno[1,2-*d*][1,3]dioxol-2-ol (2.36 below) which is formed as an intermediate between (2.34) and (2.35) as outlined in Scheme 2.9-3 (below). There were no carbon signals suggesting an elimination product (*e.g.* 1-trifluoroacetylindene) but the molecular ion shows the loss of 18 (H_2O) when compared to 2,3-dihydro-2-hydroxy-1*H*-inden-3-yl 2,2,2-trifluoroacetate (m/z 246). The mass spectrum confirms the presence of a trifluoro acetate group as does the doublet at 113.5 ppm in the ^{13}C NMR spectra. It is surprising that carbonyl addition adduct 2.36 is stable enough to isolate.

Scheme 2.9-3: Proposed mechanism for the synthesis of side-products 2.34, 2.35 and 2.36



2.9.2 Determination of the second-order rate constant for carbocation formation (k_{H}) from (1*R*,2*S*)-2,3-dihydro-1*H*-indene-1,2-diol

Scheme 2.9-4 (below) shows the possible reactions of (1R,2S)-2,3-dihydro-1H-indene-1,2-diol (2.32) reacting via carbocation (2.37). The carbocation intermediate can react with water either in the forward or in the reverse direction to form a mixture of *cis* and *trans* indene diols (3.32). There could also be deprotonation of the carbocation intermediate to form 2-indanone (2.39) via enol (2.40).

The reaction was followed by NMR in deuterated perchloric acid solutions (0.10 to 3.13 M). Typically a 1/20 dilution into the relevant acid solution was made to initiate the reaction with the stock solution of (2.33) in deuterated acetonitrile. The final substrate concentration was 10 mM. The reaction mixture contained sodium 3-(trimethylsilyl)propanoate as an internal standard at a final concentration of 1 mM.

Scheme 2.9-4: Isomerisation of indene diol (2.32)

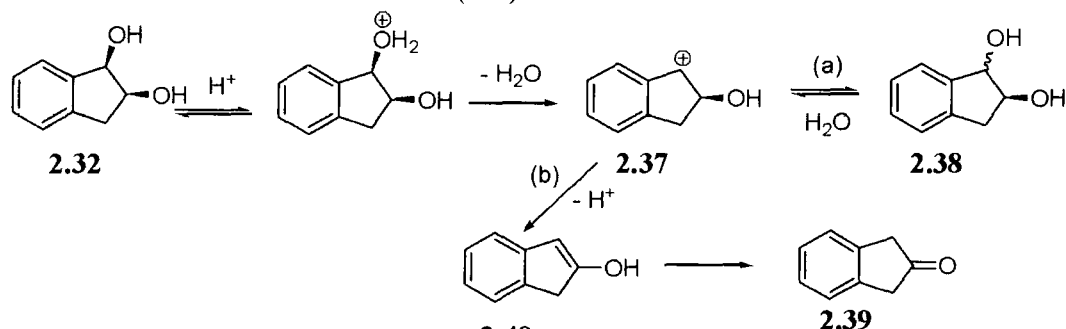
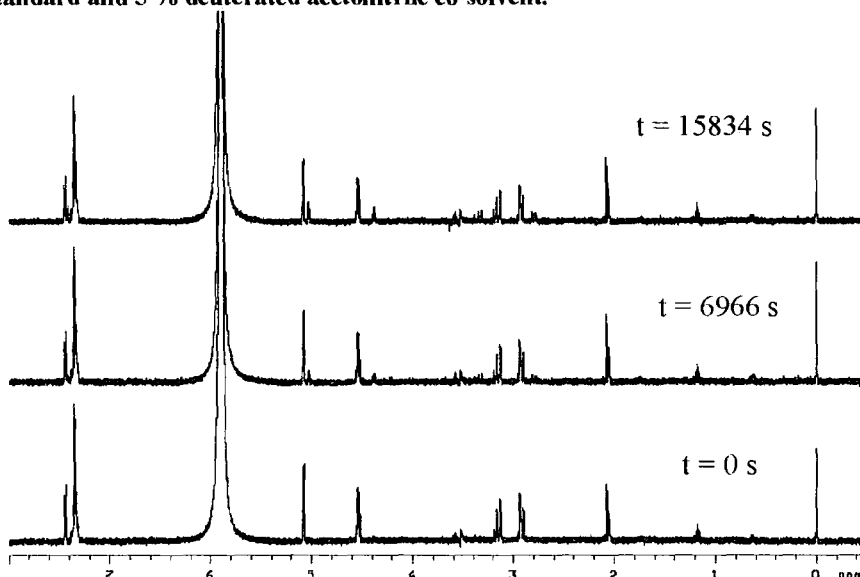


Figure 2.9-1: NMR-time profile for the racemisation of indene diol in 3.13 M $DClO_4$ with TMS internal standard and 5 % deuterated acetonitrile co-solvent.



The NMR-time profile (Fig 2.9-1) above shows the racemisation reaction of indene diol in 3.13 M DClO₄. The total area of the aromatic region at 7.2 ppm remains constant. The peaks at 5.1, 4.5, 3.1 and 2.9 ppm reduce in size concomitant with the appearance of the peaks at 5, 4.4, 3.2, 2.8 ppm. The peak at 2.05 ppm is the acetonitrile co-solvent. The internal standard appears at 0.0 and 1.1 ppm. At the end of the reaction the peaks due to reactant (1R, 2S)-2,3-dihydro-1H-indene-1,2-diol had decreased to half of their original areas and integrated 1:1 with analogous new product peaks due to (1S, 2S)-2,3-dihydro-1H-indene-1,2-diol. No peaks were observed due to 2-indanone (2.39), which would form as a result of deprotonation of the carbocation intermediate. Furthermore parallel UV-Vis spectrophotometric studies of the reaction of *cis*-indene diol in concentrated perchloric acid showed very little change in the UV-Vis spectra over the same timescale as the NMR experiment. The two diastomeric alcohol products would be expected to have almost identical UV-Vis spectra whereas that of 2-indanone is very different.

The progress of the reaction was monitored by determining the integrated area (A) of the quartet at 4.5 ppm due to the C2-H over time relative to the integrated area of the peaks due to aromatic protons (A_{arom}) which remain constant throughout the experiment. The fraction of substrate remaining, $f(s)$, was determined from Equation 2-15.

$$f(s) = \frac{(A/A_{arom})_t}{(A/A_{arom})_{t=0}} \quad \text{Equation 2-15}$$

Table 2.9-1 (below) shows a summary of the results for the isomerisation reaction.

The observed pseudo-first order rate constants for disappearance of substrate, k_{obs} , were determined as the slopes of semi-logarithmic plots of $f(s)$ against time: these plots were linear over the time course of the experiment, usually to 25 % reaction (see Fig 2.9-2). The pseudo-first order rate constants for disappearance of substrate were also determined by analysis of the decrease in peaks due to the C1 and C3 hydrogens in accordance with Equation 2-15. The pseudo-first order rate constants for isomerisation obtained from

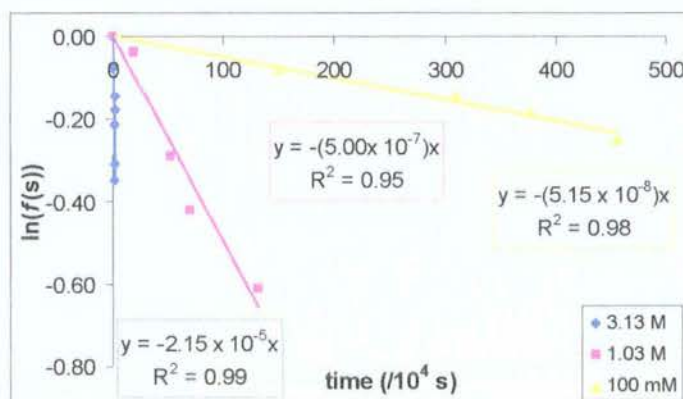
analysis of three different substrate peaks all agreed within 5-10%. The mean of the k_{obs} values from the data collected at 0.10 M DClO_4 is $5.47 \pm 0.23 \times 10^{-8} \text{ s}^{-1}$; at 1.03 M DClO_4 , $5.02 \pm 0.25 \times 10^{-7} \text{ s}^{-1}$; at 3.13 M DClO_4 , $2.07 \pm 0.21 \times 10^{-5} \text{ s}^{-1}$.

Table 2.9-1: Reaction data for the isomerisation of indene diol in DClO_4 solution^(a)

$[\text{H}^+]^{(b)}$ (M)	$X_0^{(c)}$	time (s)	$f(s)^{(d)}$	$\ln(f(s))$	$k_{\text{obs}}^{(e)}$ s^{-1}
3.13 (C1-H)	1.18	0	1.00	0.00	2.21×10^{-5}
		3708	0.93	-0.08	
		5233	0.87	-0.14	
		8728	0.84	-0.18	
		10449	0.81	-0.21	
		13985	0.73	-0.31	
		15834	0.71	-0.35	
1.03 (C2-H)	0.28	0	1.00	0.00	4.90×10^{-7}
		194797	0.96	-0.04	
		517393	0.75	-0.29	
		690732	0.66	-0.42	
		1307856	0.54	-0.61	
0.10 (C2-H)	-0.66	0	1.00	0.00	5.10×10^{-8}
		1507058	0.92	-0.08	
		3088490	0.87	-0.14	
		3770376	0.83	-0.19	
		4547556	0.78	-0.25	

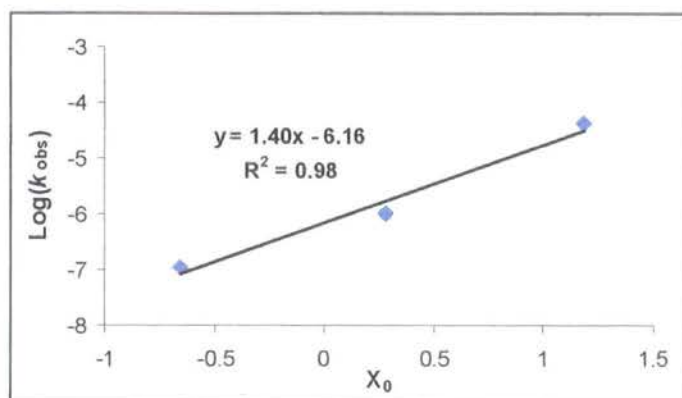
(a) A typical reaction involved a 1/20 dilution of a 100 mM indene diol stock solution in MeCN-d_3 into DClO_4 solution maintained at 25 °C. (b) Concentration determined by titration against a NaOH standard solution. (c) Hammett excess acidity function determined by a method outlined by Kresge *et al*²³ (d) $f(s)$ determined by application of equation 2.15 in this case for the decrease in the area of the quartet due to the C2 hydrogen over time. (e) k_{obs} is the slope of the plot $\ln(f(s))$ against time (see fig 2.9-2 and section 4.3.9).

Figure 2.9-2: First-order rate constants for the disappearance of indene diol.



The second-order rate constant for isomerisation, k_D ($M^{-1}s^{-1}$), could be obtained from a semilogarithmic plot of k_{obs} values against the Hammett excess acidity function (X_0): the slope of this plot is equivalent to $\log k_D$ (see Fig 2.9-3).

Figure 2.9-3: Isomerisation of indene diol in $DClO_4$: Plot of $\log(k_{obs})$ against the excess acidity function (X_0)



The second-order rate constant for carbocation formation is obtained as $k_D = 6.92 \times 10^{-7} M^{-1}s^{-1}$.

2.9.3 Determination of the rate constant for the reaction of the 2-hydroxyindanyl carbocation with water, k_{H_2O}

The rate constant for the reaction of the 2-hydroxyindanyl carbocation with water was estimated using the azide-clock method (see Scheme 2.9-4).¹¹ In this experiment the 2,3-dihydro-2-hydroxy-1H-indene-3-trifluoroacetate ester (2.33) is reacted in aqueous solution in the presence of increasing concentrations of azide ion. Quantification of the relative concentrations of the different products formed from further reaction of the carbocation (2.35) permits the determination of the relative rate constants for their formation.

Typically a 1/20 dilution into the relevant azide solution at ionic strength 0.5 M, maintained with sodium perchlorate, was made to initiate the reaction with the stock solution of (3.33) in deuterated acetonitrile. The total substrate concentration was 5 mM. The reaction was left at room temperature for 7 days to ensure complete product formation and the mixture was analysed by HPLC.

Scheme 2.9-5: Reaction of 2,3-dihydro-2-hydroxy-indene-3-trifluoroacetate in aqueous solution in the presence of azide ion

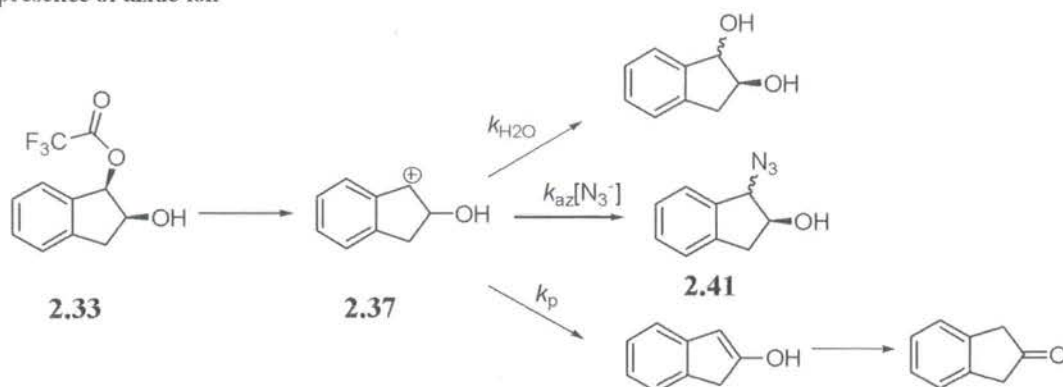
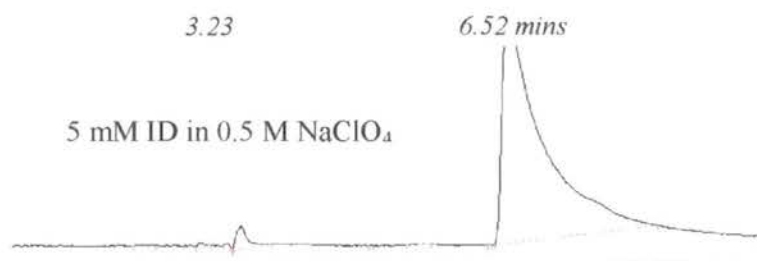


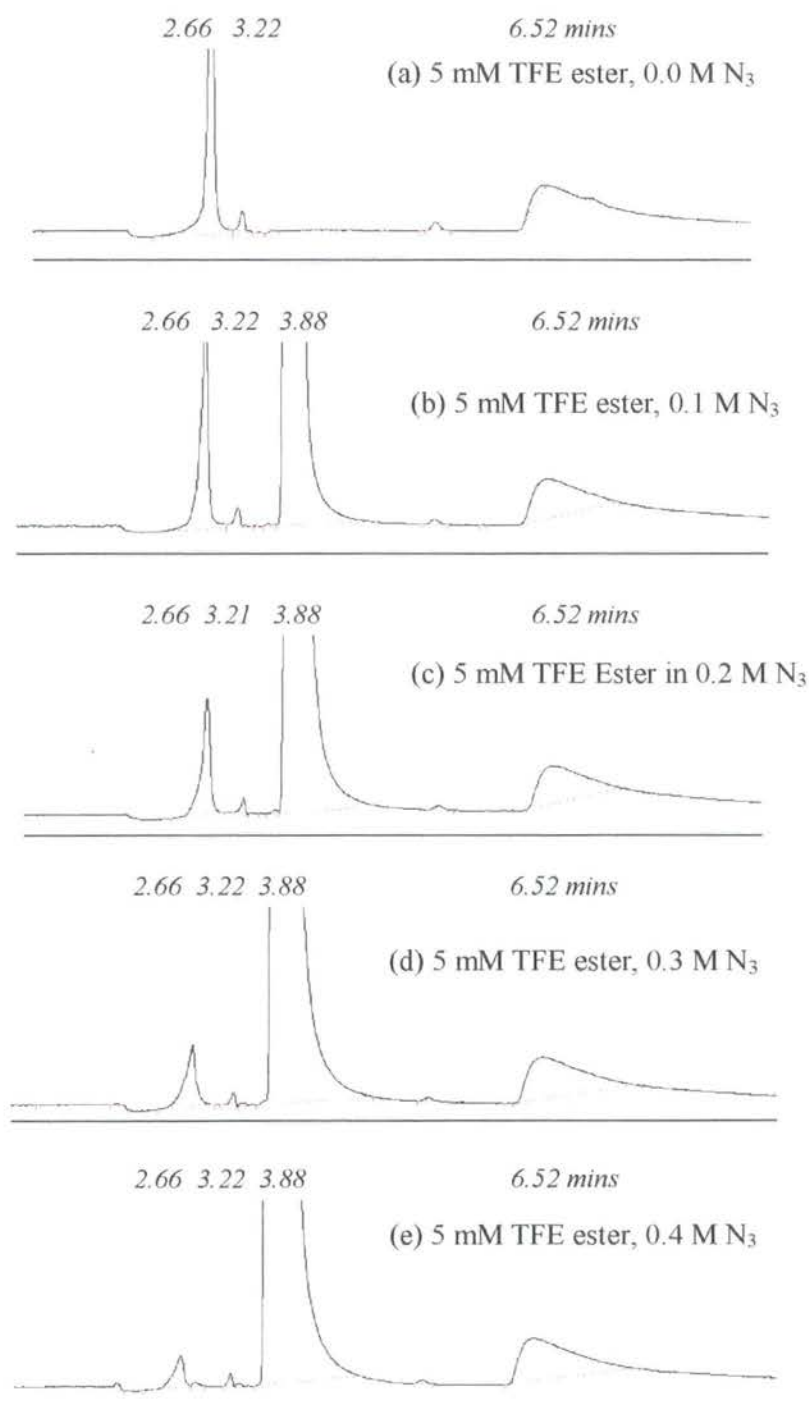
Figure 2.9-4 shows the HPLC trace of an authentic sample of pure *cis*-indene diol in 0.5 M NaClO₄. The peak at 3.2 minutes is assigned as the *cis*-diol and the peak at 7 minutes is assumed to be an artefact from the column.

Figure 2.9-4: Indene diol in aqueous solution containing at I = 0.5 M (NaClO₄) and 5 % MeCN: Product analysis by HPLC*



*Products were analysed using a Perkin-Elmer C-18 reverse phase column using 80:20 MeCN: water(v/v) at a flow rate of 1 mL/min and were analysed at 260 nm using a Perkin-Elmer diode array detector.

Figure 2.9-5: Solvolysis of 2,3-dihydro-2-hydroxy-indene-3-trifluoroacetate (2.33) in aqueous solution containing NaN_3 (0.0 – 0.5 M) at $I = 0.5 \text{ M}$ (NaClO_4) and 5 % MeCN: Product analysis by HPLC.



*Products were analysed using a Perkin-Elmer C-18 reverse phase column using 80:20 MeCN: water(v/v) at a flow rate of 1 mL/min and were analysed at 260 nm using a Perkin-Elmer diode array detector.

The HPLC traces of the products of the azide trapping experiments from the solvolysis of 2,3-dihydro-2-hydroxy-1H-indene-3-trifluoroacetate ester (2.33) in aqueous solution at different azide ion concentrations are shown in Figure 2.9-5. Figure 2.9-5(a) shows the product analysis of the solvolysis reactions of the ester derivative (3.33) in the absence of azide. Comparing this trace with the trace shown in Figure 2.9-5, the *cis* diol appears to be a minor product eluting at 3.2 minutes. The major peak eluting at 2.7 minutes has been assigned as the *trans* diol. The broad peak at 7 minutes which appears in all the traces has not been assigned to date but is assumed to be an artifact from the column.

Figure 2.9-5 (b) – (e) (above) shows the product analysis of the solvolysis reactions of the ester derivative (3.33) in the presence of increasing concentrations of azide. The area of the peaks assigned to the *trans* diol (2.8 minutes) and the *cis* diol (3.2 minutes) are decreasing as the concentration of azide increases. It is assumed that the decrease in concentration of the diols is concomitant with an increase in the concentration of the azido adduct (2.41) as it is known from the isomerisation studies (see section 2.9.2) that no elimination product is formed. However, no isolated peak for the azido adduct is present in these traces. The only peak changing with increasing azide concentration is at 3.8 minutes, this is assigned to be both the azide ion and the azido adduct.

It is assumed in the absence of azide, the only products formed are the *cis* and *trans* diols and so this is the total amount of diol formed. Assuming the decrease in diol with increasing azide results in an increase in azido adduct, Equation 2.16 can be used to determine the proportion of the azide adducts.

$$[RN_3] = (A_{ROH}^{trans} + A_{ROH}^{cis})_0 - (A_{ROH}^{trans} + A_{ROH}^{cis})_{N_3^-} \quad \text{Equation 2-16}$$

Table 2.9-2 (below) shows the percentages of the alcohol and azido products from the solvolysis reaction shown in Scheme 2.9-2.

Table 2.9-2: Product analysis for the solvolysis of 2,3-dihydro-2-hydroxy-inden-3-yl-2,2,2-trifluoroacetate in aqueous solution containing NaN_3 (0.0 – 0.5 M) at $I = 0.5 \text{ M}$ (NaClO_4) and 5 % MeCN^(a)

$[\text{N}_3^-]$ (M)	% ROH ^(b)	% RN_3 ^{(b), (c)}	$\frac{[\text{RN}_3]}{[\text{ROH}]}$ ^(d)	$k_{\text{az}}/k_{\text{H}_2\text{O}}$ ^(e)	$k_{\text{H}_2\text{O}}$ ^(f) (s^{-1})
0.0	100	0	0.0		
0.1	60	40	0.7		
0.2	34	66	2.0	557.67	$4.99 \times 10^8 \text{ s}^{-1}$
0.3	24	76	3.1		
0.4	3	97	37.1		

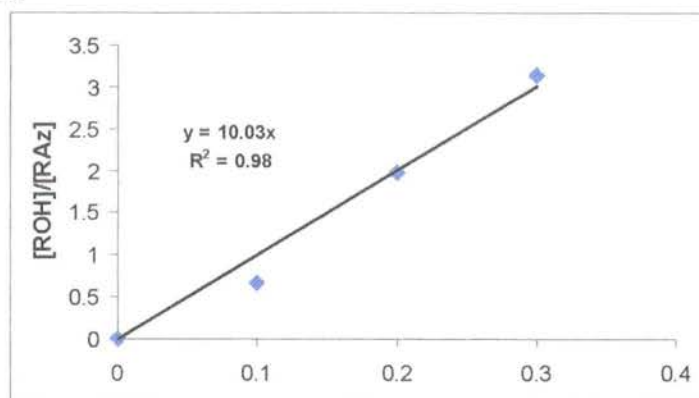
(a) Products were analysed using a Perkin-Elmer C-18 reverse phase column using 80:20 MeCN: water (v/v) at a flow rate of 1 mL/min and were analysed at 260 nm using a Perkin-Elmer diode array detector. (b) Peak areas were obtained by automated integration using the Perkin-Elmer software (c) The proportion of azido adduct was determined using equation 2.16. (d) Ratio given by (% RN_3 / % ROH) (e) Slope of plot of ($[\text{RN}_3]/[\text{ROH}]$) against $[\text{N}_3^-]$ multiplied by $[\text{H}_2\text{O}]$ ($= 55.6 \text{ M}$) (f) $k_{\text{H}_2\text{O}} = ([\text{H}_2\text{O}](5.0 \times 10^9 \text{ M}^{-1} \text{ s}^{-1}) / (k_{\text{az}}/k_{\text{H}_2\text{O}}))$: $k_{\text{az}} = (5.0 \times 10^9 \text{ M}^{-1} \text{ s}^{-1})$ is the estimated value for the diffusional reaction of azide ion with the 2-hydroxyindanyl carbocation (2.35).

The azide / alcohol product ratio ($[\text{RN}_3]/[\text{ROH}]$) from the solvolysis reaction can be equated with the corresponding ratio of rate constants for attack by the azide ion and water at the intermediate carbocation (k_{az} and $k_{\text{H}_2\text{O}}$, Scheme 2.9-2) as represented by Equation 2.17.

$$\frac{[\text{RN}_3]}{[\text{ROH}]} = \frac{(k_{\text{Az}}[\text{N}_3^-])}{(k_{\text{H}_2\text{O}}[\text{H}_2\text{O}])} \quad \text{Equation 2-17}$$

Thus a plot of $[\text{RN}_3]/[\text{ROH}]$ against azide ion concentration should give a straight line with a slope equal to $k_{\text{Az}}/(k_{\text{H}_2\text{O}}[\text{H}_2\text{O}])$ and a zero y-intercept. Figure 2.9-6 shows the plot of $[\text{RN}_3]/[\text{ROH}]$ against azide concentration for 2,3-dihydro-2-hydroxy-inden-3-yl-2,2,2-trifluoroacetate (2.33) in aqueous solution at ionic strength 0.5 M maintained with sodium perchlorate and 5 % acetonitrile co-solvent. The final entry at 0.5 M NaN_3 shows a large increase in the proportion of azido adduct and the plot of $[\text{RN}_3]/[\text{ROH}]$ showed upward curvature potentially due to a higher order dependence on azide ion and so it is excluded (see Fig 2.9-6).

Figure 2.9-6: Solvolysis of 2,3-dihydro-2-hydroxy-indene-3-trifluoroacetate in aqueous solution containing NaN₃ (0.0 – 0.5 M) at I = 0.5 M (NaClO₄) and 5 % MeCN: Plot of [RN₃]/[ROH] against azide concentration



The slope of the plot of [RN₃]/[ROH] against azide ion concentration is 10, thus $k_{az}/k_{H_2O} = 558$. Equation 2.18 was used to calculate a value for $k_{H_2O} = 5 \times 10^8 \text{ s}^{-1}$.

$$k_{H_2O} = ([H_2O]) \left(\frac{k_{Az}}{k_{Az}/k_{H_2O}} \right) \quad \text{Equation 2-18}$$

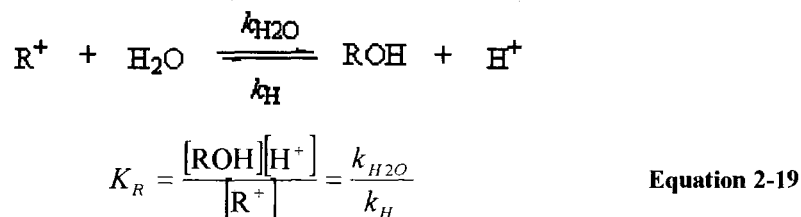
2.9.4 Determination of the pK_R of the 2-hydroxyindanyl carbocation

Measurements of the rate constant, k_{H_2O} , for reaction of water with the carbocation intermediate allows an equilibrium constant for this reaction to be evaluated. This is achieved by combining k_{H_2O} with the rate constant, k_H , for the acid-catalysed formation of the carbocation from the alcohol. The equilibrium between the 2-hydroxyindanyl carbocation and *cis*-indenediol is represented by Scheme 2.9-5. The corresponding equilibrium constant with units (M) can be expressed as the ratio of the concentrations of alcohol and carbocation present at equilibrium at known $[H^+]$ and $[H_2O]$, or alternatively as the ratio of the second order rate constants for the forward (k_{H_2O}) and reverse (k_H) reactions of the equilibrium (Scheme 2.9-5).

The rate constant for acid-catalyzed carbocation formation from the alcohol was determined as the rate constant for isomerisation by ¹H NMR spectroscopy as described in section 2.9.1 (above). However this value (k_D) was determined by NMR spectroscopy

in DClO_4 solution in D_2O and should be corrected to a value for reaction in HClO_4 solution in H_2O . In the absence of a specific literature value for such a solvent isotope effect on the reaction of dihydrodiols, we will employ the equivalent isotope effect determined for the dehydration reaction of methyl 3-hydroxycyclohexa-1,5-dienecarboxylate (2.1) in dilute perchloric acid (Section 2.1). In the case of ester (2.1) an isotope effect of $k_{\text{H}}^{\text{H}_2\text{O}}/k_{\text{D}}^{\text{D}_2\text{O}} = 1.6$ was obtained, this permits the determination of a value of $k_{\text{H}} = 1.11 \times 10^{-6} \text{ M}^{-1}\text{s}^{-1}$ for the rate of acid-catalysed carbocation formation from indenediol in H_2O . The rate constant for reaction of the carbocation with water ($k_{\text{H}_2\text{O}}$) was determined by an azide-trapping experiment described in section 2.9.2 (above).

Scheme 2.9-6: Equilibrium between a Carbocation intermediate and alcohol.



A K_{R} value for cation (2.37) was determined, using Equation 2.19, as $4.3 \times 10^{14} \text{ M}$, which corresponds to a $\text{p}K_{\text{R}}$ of -14.6.

Discussion

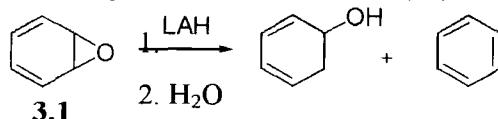
A suitable synthetic route to the hydrates has been developed during this project, which will be discussed in section 3.1. The results from the kinetic studies of dehydration will be discussed in section 3.2. The Hammett-type correlations of the dehydration kinetic data will be discussed in section 3.3. The computational studies will be discussed in section 3.4. Finally, the second-order rate constant for carbocation formation and the $\text{p}K_{\text{R}}$ of indene dihydrodiol cation will be discussed in section 3.5.

3.1 Synthesis of the Arene Hydrates

The successful synthesis of the arene hydrates depends on the nature of the substituent attached. The only hydrates for which chemical syntheses have been reported in the literature possess an electron-withdrawing substituent⁸⁶ or, in the case of benzene hydrate, no substituent.

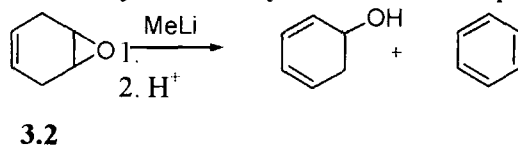
The earliest synthesis of benzene hydrate was reported by Vogel and Günther, and was via the reaction of lithium aluminium hydride with benzene oxide (see Scheme 3.1-1)⁸⁷. This synthetic methodology is, in general, not practical as the synthesis of benzene oxide is a three-step process. The formation of benzene as a side product was attributed to a wall-catalysed decomposition on standing.

Scheme 3.1-1: Synthesis of benzene hydrate from benzene oxide (3.4)⁸⁷



The synthesis of benzene hydrate was also reported in a brief communication on the effects of methylorganometallic reagents on cyclohexadiene monoepoxides (3.2)⁴⁴. The synthetic route is shown in Scheme 3.1-2 (below). The monoepoxide was prepared by epoxidation of the commercially available 1,4-cyclohexadiene. This synthetic route has been utilised by a number of research groups to synthesise benzene hydrate^{50, 88, 89}; however, the route has never been adapted to a range of hydrates.

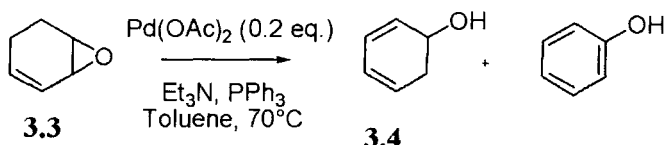
Scheme 3.1-2: Synthesis of benzene hydrate from cyclohexadiene monoepoxide (3.5)⁴⁴



There are a number of more recently reported syntheses of arene hydrates as a result of investigations into natural product synthetic methodology. For example, Scheme 3.1-3 shows the palladium mediated isomerisation of an allylic epoxide, followed by low temperature alkoxide-accelerated 1,5-hydrogen migration⁹⁰. This *transformation* was applied to more elaborate tricyclic structures in the total synthesis of a natural product (Ingenol). The production of phenol in a 1:3 ratio is attributed to a small amount of air

oxidation of the corresponding arene hydrate, which is known to be facilitated by the presence of $\text{Pd}(\text{OAc})_2$ ⁹⁰.

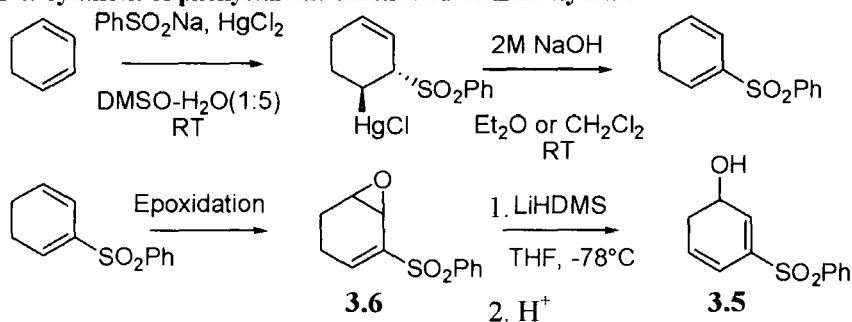
Scheme 3.1-3: Synthesis of benzene hydrate using palladium acetate⁹⁰



This methodology appears to be a useful general route to the hydrates. However, the route requires two steps to the epoxide precursor and so no advantage is achieved over the route in Scheme 3.1-2. Synthesis of the diene precursor to epoxide (3.6) was expected to be troublesome as only the 1,3-cyclohexadiene is commercially available. Also, the final step requires expensive palladium catalysts and Shlenck techniques, which are not essential for the route in Scheme 3.1-2.

A synthetic route to the phenylsulfone-substituted benzene hydrate (3.4, Scheme 3.1-4 below) is available in the literature. The steps through to the epoxide (3.5) in Scheme 3.1-4 have been scaled-up to 15 g, however, the number of synthetic steps (five, including the synthesis of 1,3-cyclohexadiene not shown) and the lack of diversity makes it an unappealing route to the arene hydrates and so was not pursued.

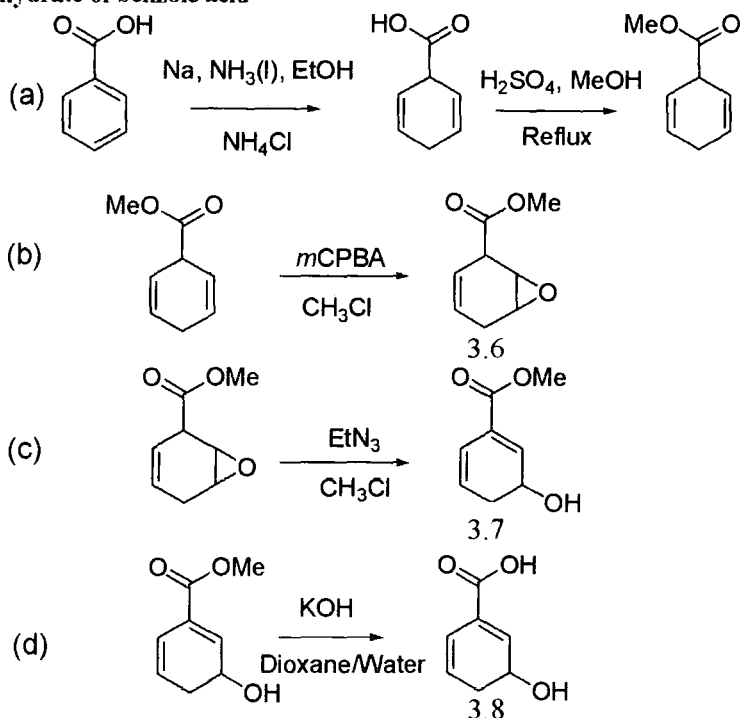
Scheme 3.1-4: Synthesis of phenylsulfone substituted benzene hydrate



The only other arene hydrate found in the literature was methylbenzoate hydrate (3.9, see section 2.1). The synthetic route is outlined in Scheme 3.1-5 (a) – (c). Drew et al⁹¹ reported the Birch reduction of benzoic acid followed by esterification in methanolic

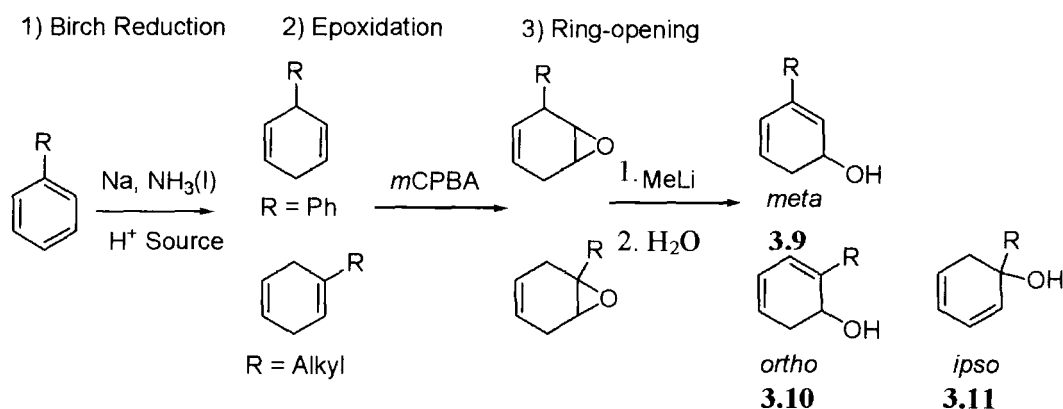
sulfuric acid and we found this was reproducible. We observed that the epoxidation of 3-methoxycarbonylcyclohexa-1,4-diene using mCPBA in chloroform gives two diastereomers which are separable by column chromatography using an ether/hexane gradient as reported by Mah et al.⁸⁶. Mah also reports isomerisation of the epoxide (3.6) to the hydrate *in situ*. A further publication by Sirate *et al*⁷⁵ reported the final conversion of the epoxide (3.6) to the hydrate (3.7), where only a weak base was required for deprotonation. We applied this synthetic route and the hydrate was isolated in good yields (see section 2.1.1). Sirate *et al*⁷⁵ also report the synthesis of the hydrate of benzoic acid (3.8) from the corresponding ester hydrate (3.7) using potassium hydroxide in dioxane/water, followed by acidification to pH 6 (see Scheme 3.1-5(d)). We attempted this procedure on a number of occasions; however the desired hydrate was never isolated and the major product was unreacted methyl benzoate.

Scheme 3.1-5: Synthetic route to methyl benzoate hydrate (a) synthesis of 3-methoxycarbonylcyclohexa-1,4-diene⁹¹ (b) epoxidation⁸⁶ and (c) ring-opening using Et₃N⁷⁵ (d) synthesis of the hydrate of benzoic acid



The method utilised in this work for the synthesis of the previously unreported hydrates is outlined below. The methodology is developed from the synthetic route outlined by Staroscik and Rickborn (see Scheme 3.1-2)⁴⁴. The synthetic route involves the Birch reduction of a series of mono substituted arenes, followed by mono epoxidation of the resulting diene, and then ring-opening of the epoxide using methyl lithium. The difficulties and yields for the individual steps are reported in the relevant sections in Chapters 2 and 4.

Scheme 3.1-6: General synthetic route used for the synthesis of the hydrates of alkyl benzenes and biphenyl



Overall the methodology was useful and the hydrates were isolated with reasonable purity. In the case of the phenyl substituent it was possible to purify the hydrate by flash chromatography with the compound staying on the column no longer than 5 minutes. The product was not particularly stable and the major decomposition product was the parent arene, biphenyl.

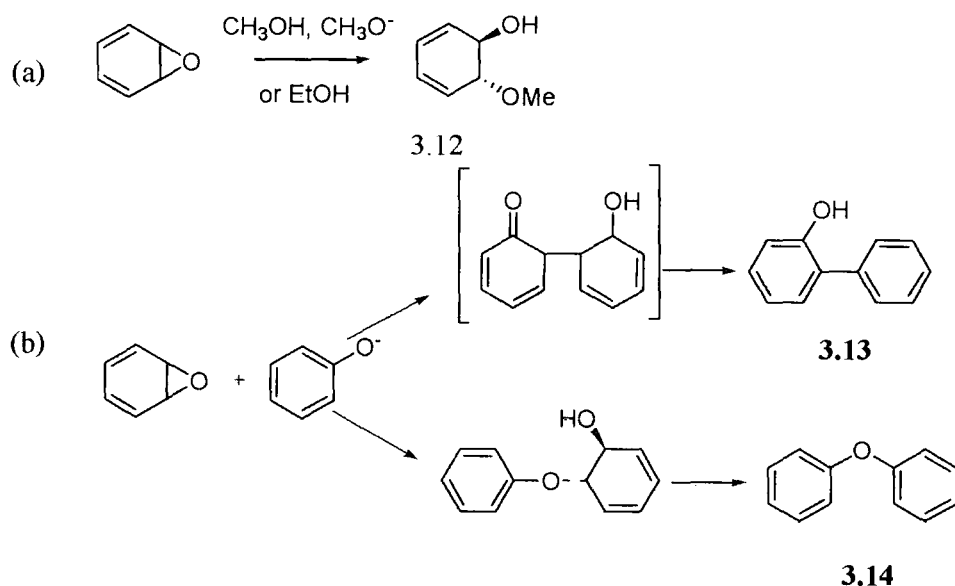
The alkyl-substituted hydrates were more difficult to purify (see Scheme 3.1-6). In most cases, the Birch reductions did not result in full conversion to the diene (see relevant section in chapter 4). As the only compounds isolated were the diene and the parent arene, it was decided to continue with the epoxidation step and purify the product at that stage. The epoxides could be purified easily by column chromatography using silica gel, leaving no remaining arene.

The final deprotonation step was troublesome. The identifiable products isolated from the reaction in the presence of equimolar quantities of methyllithium were the expected mixture of the *ortho* and *ipso* hydrates resulting from deprotonation at C-3 and C-6 respectively, the parent arene and unreacted epoxide. The epoxide starting material in all cases consisted only of pure epoxide; the arene had been removed completely by column chromatography prior to the reaction. The arene present after the deprotonation step was either formed as a result of reaction in the methyl lithium / diethyl ether reaction medium and/or during work-up. TLC analysis of the reaction mixture showed the presence of the

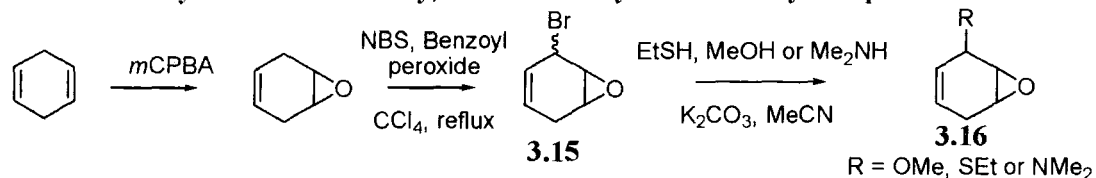
arene; however, this may have resulted from reaction of the hydrate on the silica gel TLC plate.

Further complications in the final step of the alkyl hydrate synthesis arose during purification. Standard purification techniques were attempted such as distillation and chromatography. The products were oils or liquids, and recrystallisation could not be used. In all cases decomposition to the parent arene and other unidentifiable compounds was observed. The arene hydrate could be isolated in very low yield from column chromatography; however, it would quickly decompose as is shown in the NMR spectra in Figure 2.5-1. It was decided to push the final deprotonation step to completion using excess methyl lithium and to use the hydrates without further purification. This is justified as the major side-product was the parent arene, which is the product of the irreversible aromatisation reaction studied. Any other impurities were assumed to be UV inactive and; as they only appeared to constitute at maximum 1 % of the product, their effect on the final UV absorbance would be minimal.

The only reported synthesis of an alkoxy-substituted hydrate was reported by Jeffrey et al. and is outlined in Scheme 3.1-7 (below). This particular paper discusses the synthesis of a number of derivatives of arene oxides resulting from nucleophilic substitution primarily at benzene epoxide (3.1). The reaction with methoxide in methanol was slow with a yield of 78 % of anisole hydrate (3.12) after 69 days (Scheme 3.1-7 (a)). The reaction of benzene oxide with *tert*butoxide attempted in this work, however, resulted in no arene hydrate. The only products identified were diphenylether and *o*-hydroxydiphenyl ether. The synthesis of (3.13) and (3.14) is explained as resulting from the enolization and dehydration of the dihydroaromatic produced when phenol, produced *in situ*, acts as a nucleophile⁴³.

Scheme 3.1-7: Attempted synthesis of heteroatom-substituted arene hydrates⁴³

In this work, the syntheses of the hydrates bearing electron-donating alkoxy and amino substituents were attempted (see Scheme 3.1-8). The methodology used was developed from Scheme 3.1-6. First, commercially available 1,4-cyclohexadiene was epoxidised using *m*CPBA. The resulting mono epoxide (3.2) was reacted with *N*-bromosuccinimide (NBS) in the presence of an initiator, benzoyl peroxide, forming the allylic bromination product (3.15)⁹². This bromo-epoxide was isolated as two diastereomers which could be separated by column chromatography. However, the two diastereomers could interconvert and on standing a mixture of the two epoxides were formed. This was previously noted by Kuhlmeier et al⁹³.

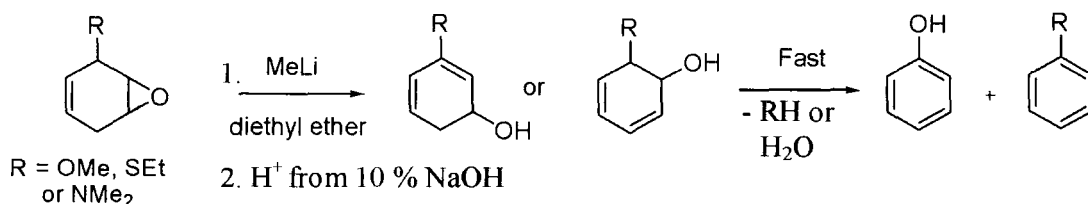
Scheme 3.1-8: Synthesis of the methoxy, thio and dimethylamino arene hydrate precursor

The substitution of the bromo-substituent of epoxide (3.15) by a variety of nucleophiles proceeded with reasonable yields with the exception of the methoxy substituted epoxide which reacted very slowly (5 days) and was low yielding. The details are presented in the relevant section in Chapter 4. The resulting epoxides could be purified by column chromatography. In the case of reaction of bromoepoxide (3.15) with dimethylamine, the

initial product was a conjugated diene epoxide, however, this appeared to isomerise to the desired non-conjugated regioisomer (3.16, R = NMe₂) on the alumina column used for purification. The substituted epoxides (3.16, R = NMe₂, OMe, SEt) were all unstable over time.

The reaction of the substituted epoxide (R = OMe, SEt and NMe₂) with methyl lithium did not lead to the successful isolation of hydrates. The only products isolated were the parent arene and phenol (see Scheme 3.1-9). This suggests that an arene hydrate species was formed, but this reacted quickly in either the methyl lithium / ether medium and/or under the work-up conditions eliminating either RH or water forming the phenol and the parent arene, respectively.

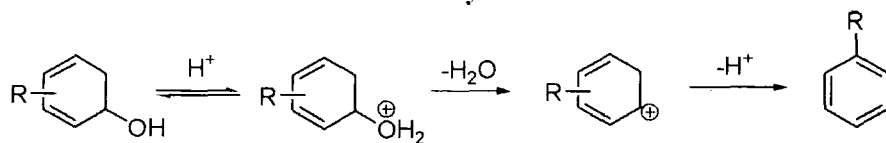
Scheme 3.1-9: Ring-opening of the NMe₂, SEt, and OMe substituted epoxides



3.2 Aromatisation reactions of the arene hydrates

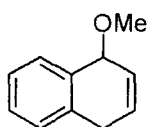
The aromatisation reaction of the arene hydrates is formally a dehydration reaction. The suggested mechanism, inferred from the study of naphthalene hydrate, involves the formation of a carbocation intermediate^{50, 51}. A generalised mechanism is shown below (Scheme 3.2-1). The rate of aromatisation of the individual hydrates will be discussed in this section.

Scheme 3.2-1: Aromatisation reaction of the arene hydrates

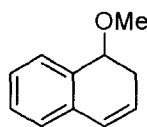


The second-order rate constants for aromatisation that were determined in this work will be compared with reference to a mechanism involving rate-determining carbocation formation as in Scheme 3.2-1. In our studies, no buffer catalysis was seen indicating the absence of general acid catalysis. This is consistent with the mechanism in Scheme 3.2-

1, which involves pre-equilibrium, non rate-limiting proton transfer to oxygen. This was also observed previously for benzene hydrate⁵⁴. The buffer catalysis plots did, however, show a negative slope i.e. an increase in rate with decreasing buffer concentration. Generally, the change in the rate constants was small with decreasing concentrations of total buffer and increasing total perchlorate and can be attributed to a medium effect rather than any catalysis. An increase in rate with increasing perchlorate concentration was noted by Pirinccioglu and Thibblin for the acid-catalyzed solvolysis of 1-methoxy-1,4-dihydronaphthalene (3.17) or 1-methoxy-1,2-dihydronaphthalene (3.18) in 25 vol. % acetonitrile in water at 25 °C forming naphthalene as the major product (98 %).⁵³



3.17



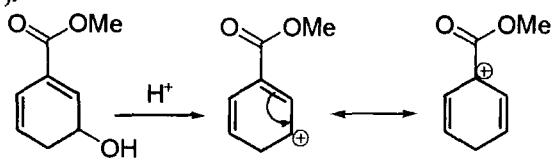
3.18

3.2.1 Methyl benzoate Hydrate

The kinetic studies of the aromatisation reaction of methyl benzoate hydrate (3.9) by ¹H NMR showed only the aromatisation reaction (see Figure 2.1-1). No competing ester hydrolysis reaction was noted at the acid-concentration used for preliminary NMR studies (2.5 mM DCIO₄). The second-order rate constant for aromatisation was determined as $9.62 \times 10^{-2} \text{ M}^{-1}\text{s}^{-1}$ by UV-vis spectrophotometry (see Section 2.1.2).

The electron-withdrawing ester substituent in the *meta* position relative to the hydroxyl group had the expected effect of slowing the aromatisation reaction when compared to benzene hydrate (R=H); $k_{\text{COOMe}}/k_{\text{H}} = 5.06 \times 10^{-4}$. An electron-withdrawing substituent would be expected to destabilise the carbocation intermediate and thus decrease the rate of carbocation formation which is rate-limiting.

Scheme 3.2-2: Resonance structures for the carbocation intermediate formed upon loss of the OH group of the hydrate (3.9).

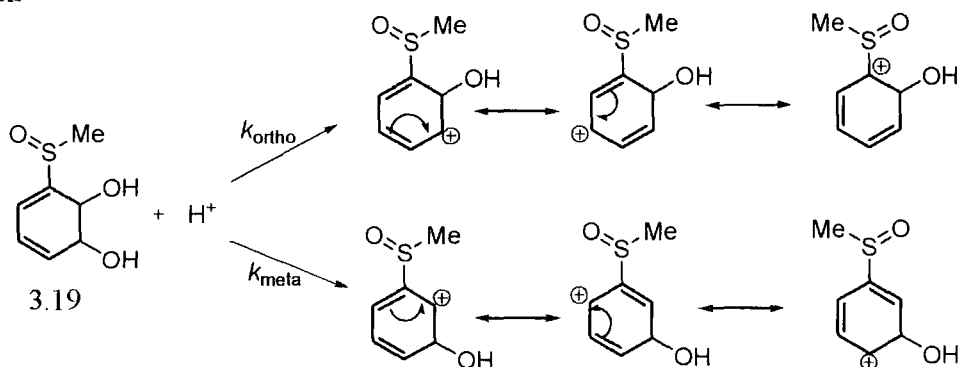


3.9

There are no published studies of the aromatisation of the analogous dihydrodiol with a methyl ester substituent. However, our results can be broadly compared with that for the PhSO_2 -substituted *cis*-dihydrodiol, which aromatised with a second-order rate constant of $4.3 \times 10^{-6} \text{ M}^{-1}\text{s}^{-1}$. This value is 10^4 -fold smaller than for the hydrate of methyl benzoate. However, the PhSO_2 group (σ^+ and $\sigma_p = 0.70$) is considerably more electron withdrawing than the CO_2Me group ($\sigma^+ = 0.48$ and $\sigma_p = 0.45$). The data for the ester (3.9) could be more directly compared with that for the PhSO -substituted dihydrodiol ($\sigma_p = 0.46$ and $\sigma^+ = 0.50$, respectively); the rate of aromatisation of PhSO -substituted diol is $1.9 \times 10^{-5} \text{ M}^{-1}\text{s}^{-1}$. This corresponds to a 5000-fold decrease in the rate constant when compared to the ester-substituted hydrate (see section 2.1).

The rate constant for the aromatisation of the sulphone-substituted diol is the combined rate constant for the formation of the *ortho* and *meta* phenol products (see Scheme 3.2-3, below). The resonance structures of *ortho*-substituted carbocation shown in Scheme 3.2-2(a) show the positive charge directly at the carbon bearing the electron withdrawing group; however, the *meta* substituted carbocation has no contributing resonance structures with the positive charge at this position. From the product analysis, the ratio of the rate constants (k_{meta}/k_{ortho}) is 0.28, which corresponds to a k_{ortho} of $1.5 \times 10^{-5} \text{ M}^{-1}\text{s}^{-1}$ and a k_{meta} of $5.4 \times 10^{-6} \text{ M}^{-1}\text{s}^{-1}$.

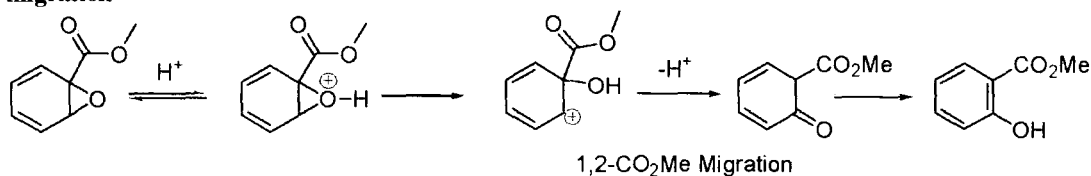
Scheme 3.2-3: Resonance structures for the carbocation intermediates leading to *ortho* and *meta* phenols



The ester hydrate (3.9) has the substituents in a 1,3-arrangement and the contributing resonance structures (Scheme 3.2-1)) show the positive charge at the *ipso* position, thus, comparison with only the reaction of dihydrodiol (3.19) to yield *ortho* product is more relevant. The ratio of the rate constants $k_{hyd}^{meta}/k_{diol}^{ortho}$ is 6500, which can be mostly attributed to the electron withdrawing effect of the extra hydroxyl of the dihydrodiol in destabilising the carbocation.

There is no rate constant for the aromatisation reaction of an ester substituted arene oxide. The only reported studies are in relation to a group migration during aromatisation. However, from inspection of the data, the oxides aromatised completely in neat 2,2,2-trifluoroacetic acid in 5 minutes⁹⁴. The proposed mechanism is shown below (see Scheme 3.2-4).

Scheme 3.2-4: Mechanism of aromatisation of CO₂Me-substituted arene oxide via 1,2-CO₂Me migration⁹⁴



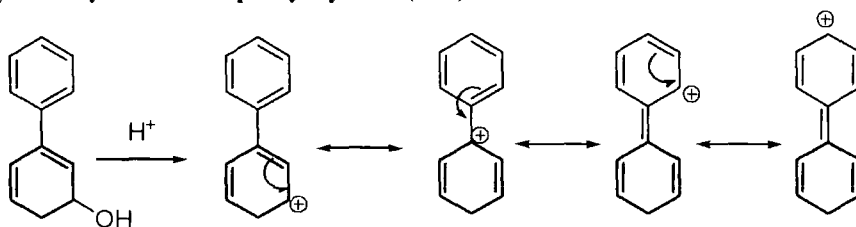
3.2.2 Biphenyl hydrate

The aromatisation of biphenyl hydrate could not be followed by ¹H NMR spectroscopy due to the insolubility of the hydrate in D₂O at the concentration necessary (5- 10 mM). The total substrate concentration that could be used was limited by product arene solubility. The solubility of biphenyl in water is 35 - 45 μM^{78, 79}. The second-order rate constant for the aromatisation of biphenyl hydrate was determined by UV-vis spectrophotometry as 2.20 x 10⁻³ M⁻¹ s⁻¹.

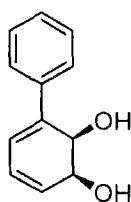
The phenyl substituent in the *meta* position relative to the hydroxyl group has the effect of increasing the rate of aromatisation when compared to benzene hydrate (R = H); k_{Ph}/k_H

= 11.6. The σ_P and σ_P^+ substituent constants for a phenyl-group are -0.01 and -0.18, respectively, and are consistent with an electron-donating substituent effect which would stabilize the carbocation intermediate. The resonance structures of the carbocation intermediate are shown below (Scheme 3.2-5). It shows there is a contributing resonance structure with the positive charge at the *ipso* position which permits further delocalization of charge around the phenyl ring.

Scheme 3.2-5: Contributing resonance structures for the carbocation intermediate generated in the acid-catalysed dehydration of biphenyl hydrate (3.12)



The rate of aromatisation of the phenyl-substituted *cis*-dihydrodiol (3.21) is $4.5 \times 10^{-2} \text{ M}^{-1}\text{s}^{-1}$, $k_{\text{hyd}}/k_{\text{diol}} = 4.9 \times 10^5$. As discussed in section 3.1.1, there are two possible products formed in the aromatisation of the *cis*-dihydrodiols. In the case of the dihydrodiol (3.21), 70 % *ortho*-phenol was formed and so $k_{\text{meta}}/k_{\text{ortho}}$ is 0.43. Thus, the second-order rate constant (k_{ortho}) for the *ortho* phenol forming reaction is $2.6 \times 10^{-2} \text{ M}^{-1}\text{s}^{-1}$. Biphenyl hydrate (3.12) has the substituents in a 1,3-arrangement and the contributing resonance structures (Scheme 3.2-5)) show the positive charge at the *ipso* position; thus, comparison with only the *ortho* phenol forming reaction of the diol is more relevant. The ratio of the rate constants $k_{\text{hyd}}/k_{\text{diol}}^{\text{ortho}} = 8.5 \times 10^5$.

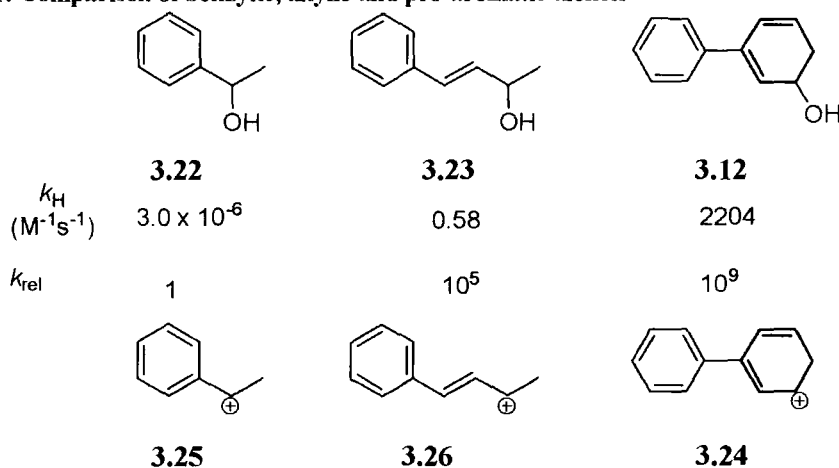


3.21

By contrast with hydrate (3.12), the phenyl substituent slows the rate of dehydration of the dihydrodiol when compared to the unsubstituted dihydrodiol ($k_{\text{Ph}}/k_{\text{H}} = 0.41$). The through-bond conjugation to the phenyl substituent in the hydrate must be more effective than in the dihydrodiol.

Chart 3.2-1 (below) compares the second order rate constants for dehydration of biphenyl hydrate (3.12) with analogous values for alcohols (3.22) and (3.23). The rate of carbocation formation in α -phenylethanol (3.22) is $3.0 \times 10^{-6} \text{ M}^{-1}\text{s}^{-1}$ and for the allylic alcohol (3.23) is $0.58 \text{ M}^{-1}\text{s}^{-1}$. The stabilising effect of one *ortho* alkenyl substituent on the benzylic carbocation increases the rate of carbocation formation 10^5 -fold. The effect of a second alkenyl substituent and cyclisation increases the rate of carbocation formation a further 10^4 -fold. The stability of the carbocation intermediate generated from the biphenyl hydrate (3.24) must be considerably greater than the stability of the benzylic carbocation (3.25) and the allylic carbocation (3.26). Dehydration of (3.12) yields a carbocation that is readily deprotonated unlike the phenyl ethyl cation (3.25) and the allylic cation (3.26). The elimination reaction of (3.23) requires hydroiodic acid (HI) at $180 - 200 \text{ }^\circ\text{C}$.

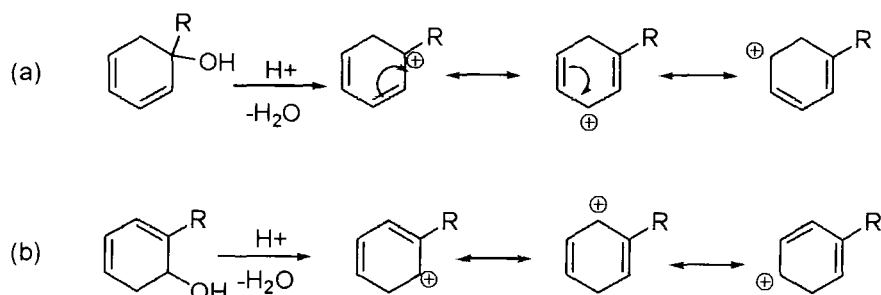
Chart 3.2-1: Comparison of benzylic, allylic and pro-aromatic alcohols



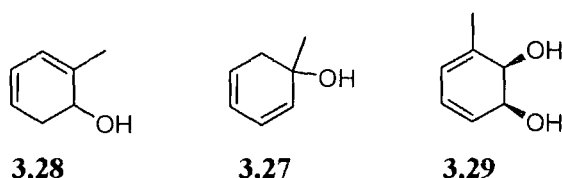
3.2.3 Alkyl substituted hydrates

The aromatisation reactions of the alkyl substituted hydrates will be discussed in this section. The substitution pattern is the same in each case and a general schematic for the contributing resonance structures for the cations formed from the *ipso* and *ortho* hydrates shown. Only the reaction of the *ipso* hydrate yields a carbocation with the charge on the *ipso* carbon.

Scheme 3.2-6: Contributing resonance structures for the aromatisation of (a) *ipso* and (b) *ortho* alkyl hydrates



The second-order rate constant for the aromatisation of the *ipso* hydrate of toluene (3.27) is $9810 \text{ M}^{-1}\text{s}^{-1}$ and the *ortho* hydrate (3.28) has a second-order rate constant for aromatisation of $514 \text{ M}^{-1}\text{s}^{-1}$ which gives $k_{ipso}/k_{ortho} = 19$. The contributing resonance structures for the carbocation intermediates are shown in Scheme 3.2-6 (a) and (b), $R = \text{CH}_3$.



The second-order rate constant for the aromatisation of the analogous methyl substituted *cis*-dihydrodiol (3.29) is $1.52 \text{ M}^{-1}\text{s}^{-1}$. The reaction forms $> 98\%$ *ortho* phenol and so the rate of reaction via the *meta*-pathway is negligible¹. The ratio $k_{hyd}^{ipso} / k_{diol}^{ortho} = 6454$ and

$$k_{hyd}^{ortho} / k_{diol}^{ortho} = 338.$$

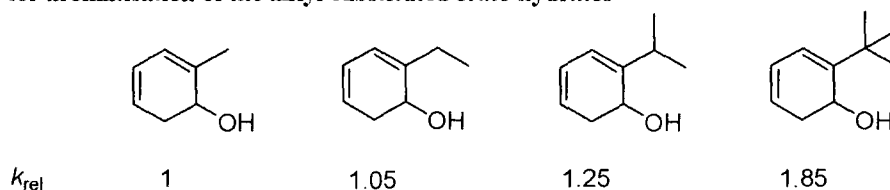
The *ipso* hydrate of ethylbenzene could not be isolated but the second order rate constant for aromatisation of this molecule is expected to be $> 10000 \text{ M}^{-1}\text{s}^{-1}$ based on the greater electron-donating inductive effect of an ethyl substituent compared with a methyl substituent (σ_I (Taft) -0.04 versus -0.05)⁹⁵. The second-order rate constant for the aromatisation reaction of the *ortho* hydrate is $538 \text{ M}^{-1}\text{s}^{-1}$. Comparing this with the ethyl substituted diol ($k_H = 1.46 \text{ M}^{-1}\text{s}^{-1}$), where $> 98\%$ reacts via the *ortho* phenol pathway, $k_{hyd}/k_{diol} = 361$.

Both hydrates of cumene were isolated and the second-order rate constant for the aromatisation of the *ipso* hydrate was found to be $14700 \text{ M}^{-1}\text{s}^{-1}$ and the *ortho* hydrate has a value of $642 \text{ M}^{-1}\text{s}^{-1}$. The ratio $k_{\text{hyd}}^{\text{ipso}} / k_{\text{hyd}}^{\text{ortho}} = 23$. The isopropyl group has a larger effect in the *ipso* position than in the *ortho*.

The *ipso* hydrate of *tert*-butylbenzene was not isolated. The second order rate constant for aromatisation of the *ortho* hydrate is $949 \text{ M}^{-1}\text{s}^{-1}$. As in the case of *ortho* cumene hydrate, there are no analogous studies of *tert*-butyl substituted dihydrodiols for comparison.

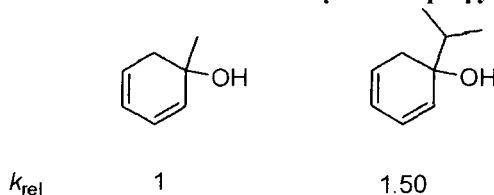
The *ortho* hydrates show increased rate with increasing steric bulk (see Fig 3.2-1) and this is reflected in the correlation with the Taft ES values (see section 2.10).

Figure 3.2-1: The effect of increasing the steric bulk of the substituent on the second-order rate constant for aromatisation of the alkyl-substituted *ortho* hydrates



Only two of the *ipso* hydrates were isolated. However, the overall effect is expected to increase the second-order rate constant as the steric bulk and inductive effect of the substituent increases. Figure 3.2-2 shows the relative rates of the methyl and isopropyl substituted hydrates.

Figure 3.2-2: Relative rates of aromatisation for the methyl and isopropyl substituted *ipso* hydrates.

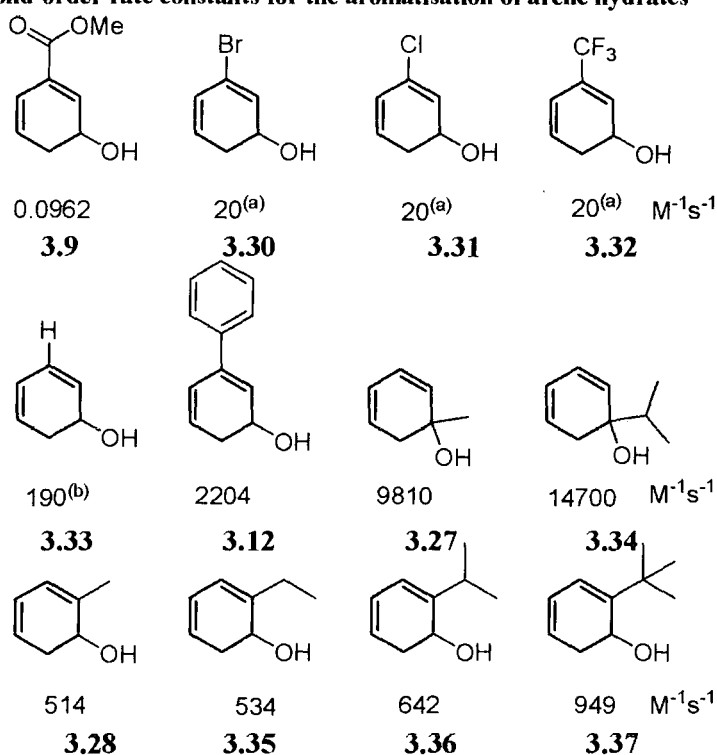


3.2.4 Summary of the second-order rate constants for aromatisation

Chart 3.1 (below) summarises the second-order rate constants for the aromatisation of the substituted hydrates. Overall, the electron-withdrawing groups retard the reaction and

electron-donating groups increase the overall rate. The position of the substituent in the ring has a large effect on the rate-constant.

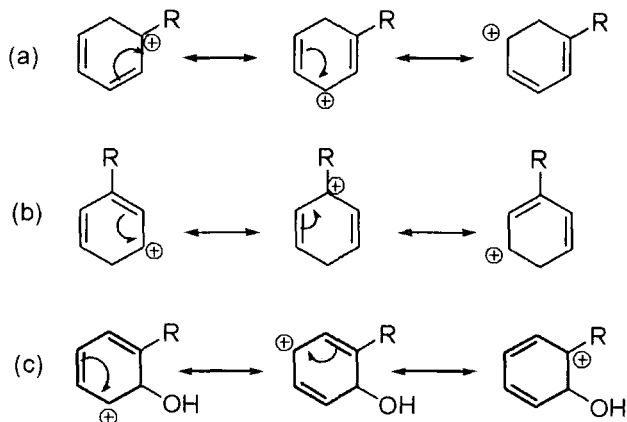
Chart 3.2-2: Second-order rate constants for the aromatisation of arene hydrates



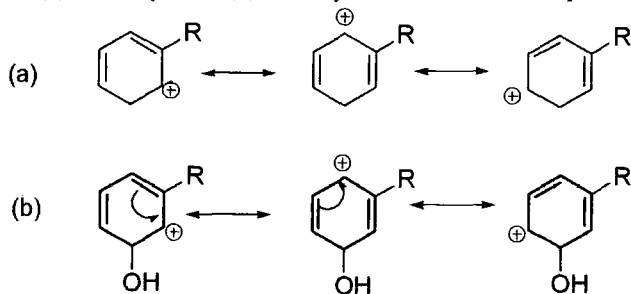
(a) Reported by O'Donoghue². (b) Reported by Rao *et al*⁵⁰

In terms of contributing resonance structures to the carbocation intermediate, kinetic data for the *ipso* hydrate can be best compared with the rate constants for the *ortho* phenol forming route whereas data for the *ortho* hydrate should be compared with that for formation of the *meta* phenol.

Scheme 3.2-7: Comparison of the contributing resonance structures to the carbocation formed during aromatisation of (a) *ipso* hydrate (b) *meta* hydrate (c) *cis* dihydrodiol via the *ortho* phenol pathway



Scheme 3.2-8: Comparison of the contributing resonance structures to the carbocation formed during aromatisation of (a) *ortho* hydrate (b) *cis* dihydrodiol via the *meta* phenol pathway



Where possible the comparison between the rate constant for aromatisation of the *ipso* hydrate is compared with the calculated second-order constant for the aromatisation of the *cis* diol via the *ortho* phenol forming route and the *ortho* hydrates have been compared with the second-order rate constant for the *meta* phenol forming route.

Table 3.2-1: Comparison of the contributing rate constants for the *cis* diols from the *ortho* and *meta* phenol pathways and the *ipso* and *ortho* hydrates

R	Diols (M ⁻¹ s ⁻¹)		Hydrates (M ⁻¹ s ⁻¹)		Compare	
	k_{diol}^{ortho}	k_{diol}^{meta}	k_{hyd}^{ipso}	k_{hyd}^{ortho}	$k_{hyd}^{ipso} / k_{diol}^{ortho}$	$k_{hyd}^{ortho} / k_{diol}^{meta}$
Me	1.49	< 0.03	9810	514	6854	> 17133
Et	1.46	< 0.03	-	538	6849	-
iPr	-	-	14700	614	-	-
tBu	-	-	-	962	-	-
Ph	3.2×10^{-2}	1.4×10^{-2}	2204 ^(a)	-	68875 ^(b)	-
CO ₂ Me	-	-	$9.62 \times 10^{-2(a)}$	-	-	-

(a) k_{hyd}^{meta} (b) $k_{hyd}^{meta} / k_{diol}^{ortho}$

Although the second order rate constant for the aromatisation of the *cis*-diols via the *meta* phenol forming route is only an estimate, it does show that the *ortho* hydrate is considerably more reactive than the equivalent *cis* diol.

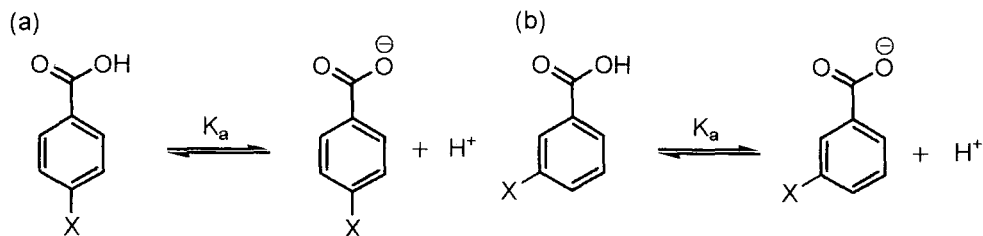
3.3 Hammett correlations

This section will discuss the various Hammett and other linear free energy correlations presented in section 2.9. Correlations with σ_p , σ_m , σ^+ , σ_I and σ_R parameters, Taft E_s and the field (F) and resonance (R) parameters were investigated.

3.3.1 Linear Free Energy Correlations

The σ -value for the substituent is the effect the substituent has on k or K_a for a standard reaction and is independent of the nature of the reaction being investigated. Electron-withdrawing groups have positive σ -values and electron-donating groups have negative σ -values. The magnitude of σ is a measure of the extent of the electron-donating and withdrawing effect. In defining σ -values Hammett only considered *para* and *meta*-substituents due to the steric factors associated with *ortho*-substituents. When there are multiple substitutions, the effects are largely additive.

Scheme 3.3-1: (a) Definition of σ_p : The effect the *para*-substituent (X) has on the dissociation constant of benzoic acid. (b) Definition of σ_m : The effect the *meta*-substituent(x) has on the dissociation constant of benzoic acid.



The sign and magnitude of ρ are important. If ρ is positive, then electron-withdrawing substituents increase the rate or equilibrium constant for a reaction. If ρ is negative, the opposite effect is seen. The magnitude of ρ reflects the sensitivity of the reaction to the substituents. Changing solvent greatly affects ρ ; for example, the dissociation of benzoic acids in ethanol gives a ρ value of 1.96, which is ascribed to a difference in solvation effects. Ethanol is not able to stabilise the charges generated as effectively as water upon dissociation of benzoic acid and so dissociation is more sensitive to substituent effects. Hammett σ -values are still widely used. Some non-classical examples include the correlation of ligand electronic effects with catalysts for polymerisation reactions⁹⁶ and the study of the effect of substituent on anaesthetic efficacy (via QSAR)⁹⁷.

The σ -value comprises both an inductive and a resonance effect,

$$\sigma = \sigma_I + \sigma_R \quad \text{Equation 3-1}$$

However, σ_m has no significant resonance interactions, and so σ_R is zero. Therefore, σ_I is approximately equal to σ_m .

Acidity constants, K_a , for ionisation of substituted anilinium ions and phenols give poor correlations with standard σ_m and σ_p values. Poor correlations are often obtained with σ -values when a reaction centre is formed which can interact directly with substituents through resonance. In these cases where there is through-conjugation between the substituent and the reaction site, a series of special parameters (σ^+ and σ^-) were developed. In general, they only differ from σ for *para* substituents that can mesomerically withdraw or donate electrons.

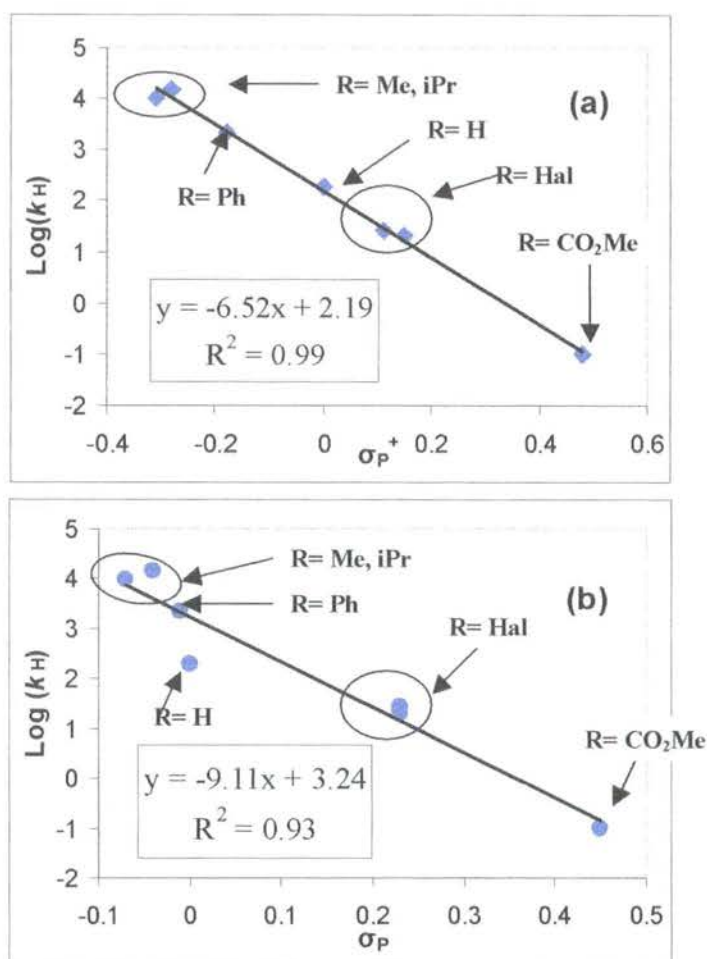
Nucleophilic aromatic substitution correlates better with σ^- than σ and electrophilic aromatic substitution correlates with σ^+ . These substituent constants are useful from a mechanistic point of view. If a reaction series correlates better with σ^+ or σ^- than with σ , it can be inferred that the transition state involves extensive through-bond conjugation between the reaction site and the substituent.

3.3.2 Hammett correlations for the arene hydrates

As described in section 2.8 for the aromatisation reactions of arene hydrates, the best correlation was found with σ^+ . The plot below (Fig 3.3-1) shows an excellent correlation with $R^2 = 0.997$. The slope (ρ^+) is obtained as $-(6.52 \pm 0.20)$. The correlation here includes the *ipso* toluene and cumene hydrates (3.14, R = Me, iPr) and the *meta*-substituted hydrates (3.13, R = Ph, CO₂Me, Cl, Br, H) shown in Chart 3.2-1. The only other acceptable correlation was with σ_p : this shows $R^2 = 0.93$ and a ρ^p obtained as $-(9.11 \pm 1.11)$. The greatest outlier in this later case is benzene hydrate (R = H), showing a negative deviation from the line.

As explained above (section 3.3.1), a negative ρ -value implies positive charge build-up in the transition state. The correlation with σ^+ suggests there is through bond conjugation with the positive charge. The correlation with σ_p shows the reaction is more sensitive to electron withdrawing groups than the hydrolysis of methyl benzoate. The large negative ρ in this case is in line with those expected for the electrophilic aromatic substitution.

Figure 3.3-1: Hammett correlations for second order rate constants for aromatisation for (a) σ^+ and (b) σ_p



As mentioned in section 2.8.2, the *ortho* hydrates were treated separately as the rate data spans only a 2-fold range of activity and so the results are interpreted qualitatively. In particular a positive ρ -value in a correlation with σ^+ implies that these correlations of the *ortho* hydrate cover too small a reactivity range. A negative ρ -value should be obtained for a carbocation forming mechanism. In general other attempted correlations with σ_I , σ_p and σ_m parameters yielded poor linear fits and thus should not be further interpreted.

Figure 3.3-2 shows the correlation of the logarithm of k_H for the alkyl substituted *ortho* hydrates against Tafts E_s values. From this correlation it can be deduced that the increasing the steric bulk of the substituent has less affect on the aromatisation reaction than on the hydrolysis of aliphatic esters.

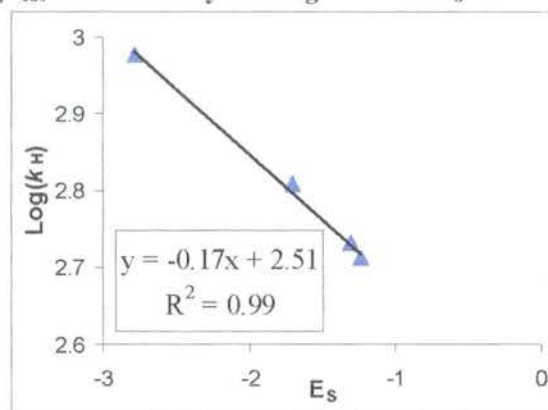
Figure 3.3-2: Plot of $\text{Log } k_{\text{obs}}$ for the *ortho* hydrates against Tafts E_s .

Table 3.3-1: Rate constants for acid-catalysed aromatisation of 3-substituted *cis*-dihydrodiols in HClO₄ (aq) at 25 °C¹.

Substituent	k_H ($\times 10^{-2} \text{ M}^{-1} \text{ s}^{-1}$)	<i>o</i> -Phenol (%)	σ_p	σ_p^+
EtO	1250	91	-0.24	-0.82
MeO	1110	99	-0.268	-0.78
MeS	200	>98	0.0	-0.60
Et	149	>98	-0.15	-0.30
Me	152	98	-0.12	-0.31
PhS	45	>98	0.13	-0.45
H	11	-	0	0
Ph	4.5	70	0.05	-0.18
CH ₂ CH	2.6	79	-0.08	-
F	0.64	91	0.062	-0.07
HCC	0.32	91	0.23	-0.18
I	0.31	-	0.18	0.14
Cl	0.26	99	0.227	0.11
Br	0.16	94	0.232	0.15
CF ₃	0.0033	9	0.54	0.53
PhSO	0.0019	78	0.46	0.50
PhSO ₂	0.00043	77	0.70	0.70

Table 3.3-1 summarises the results from the aromatisation reactions of the 3-substituted *cis*-dihydrodiols carried out by Boyd *et al*¹. The results show the rate-retarding affect of the second hydroxyl group on the rate of aromatisation when compared with the hydrates.

The linear free energy correlations are shown below. Figure 3.3-3 (a) and (b) show Log k_H values for the overall formation of *ortho* and *meta* phenols. The correlation with σ_p is slightly poorer than the correlation with σ^+ (R^2 of 0.88 versus 0.92). The correlation with σ_p shows the positive deviation of the MeS and PhS substituted *cis*-diols. The alkene substituted diol shows a negative deviation from the line, as does the fluoro substituent. The ρ -values we obtained have slopes of -6.70 and -4.36 differ from those obtained by Boyd *et al*. Furthermore, better correlation with σ_p rather than σ^+ was reported, whereas we see the opposite, although it is to a smaller extent.

Figure 3.3-3: Correlation of $\text{Log } k_{\text{H}}$ for the aromatisation of the 3-substituted *cis*-dihydrodiols with (a) σ_{p} and (b) σ^{+}

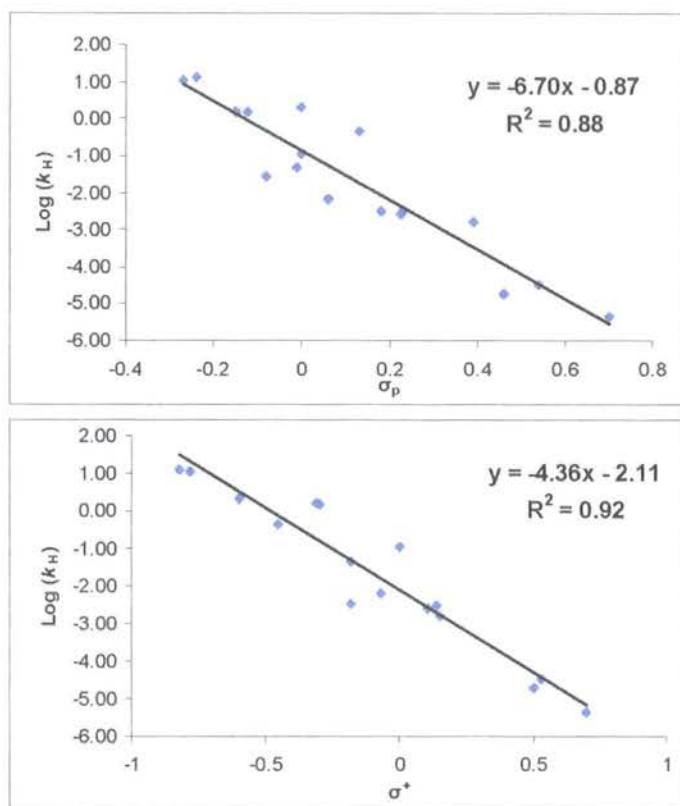
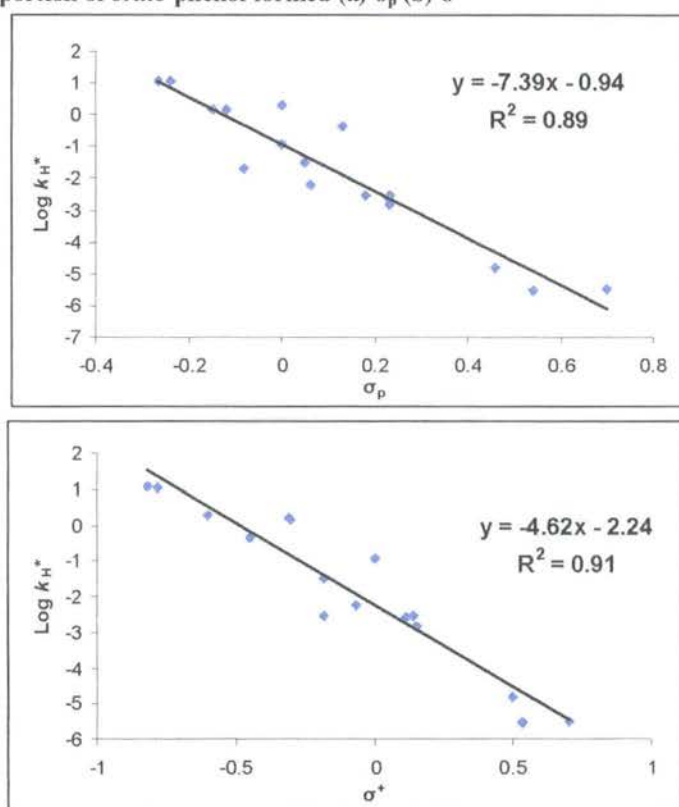


Figure 3.3-4 (a) and (b) show the correlation of $\text{Log}(k_{\text{H}})^*$ taking the formation of the *ortho* phenol into account and correcting for this. As with the correlations above, the correlation with σ^{+} gives a slightly better fit than the correlation with σ_{p} . The correlation with σ_{p} again shows positive deviation for the thiol substituents and a negative deviation for the fluoro and alkene substituted diols. The correlation with σ_{p} shows positive deviation for the alkyl substituted diols and the unsubstituted diol. The alkene substituted diol shows a negative deviation from the slope.

The correlation with σ^{+} here shows the positive deviation of the rate constants for the ethyl and methyl substituted diols and the unsubstituted diols. As there cannot be direct resonance between the carbocation centre and the alkyl substituent, one possible reason for the deviation is a hyperconjugation effect which the σ^{+} values do not take into account. The rate constant for the alkyne-substituted diols deviates negatively. There is the possibility of through bond conjugation between the alkynyl substituent and the

carbocation centre, the negative deviation of the alkynyl substituted *cis*-dihydrodiol suggests the σ^+ value has not fully taken this into account. The deviation of the unsubstituted *cis*-dihydrodiol may be due to the planarity of the carbocation centre. The calculations show the substituted *cis*-dihydrodiols generally give a non-planar carbocation intermediate.

Figure 3.3-4: Correlation of $\text{Log } k_{\text{H}}$ for the aromatisation of the 3-substituted *cis*-dihydrodiols taking account of the proportion of *ortho* phenol formed (a) σ_{p} (b) σ^+



When only the *cis*-dihydrodiols with σ -values spanning the same range as the hydrates are used, the correlations are poorer. For the ρ^{p} - correlation using σ -values from 0.43 to -0.15, the correlation was 0.78 and the ρ -value was -7.2. The ρ^+ correlation used σ -values from 0.5 to -0.31 and the ρ -value was -5.3 and the correlation value was also 0.78. The ρ -values are not very different than those presented above. It does show, however, that the ρ -value is more negative than for the corresponding hydrates ($\rho^{\text{p}} = -6.5$). This suggests the transition state to carbocation formation is earlier in the hydrates than in the *cis*-dihydrodiols and there is less positive charge build-up.

Figure 3.3-5: Hammett correlation for the aromatisation of the arene hydrates against σ_p^+ showing the predicted values for the electron-donating hydrates.

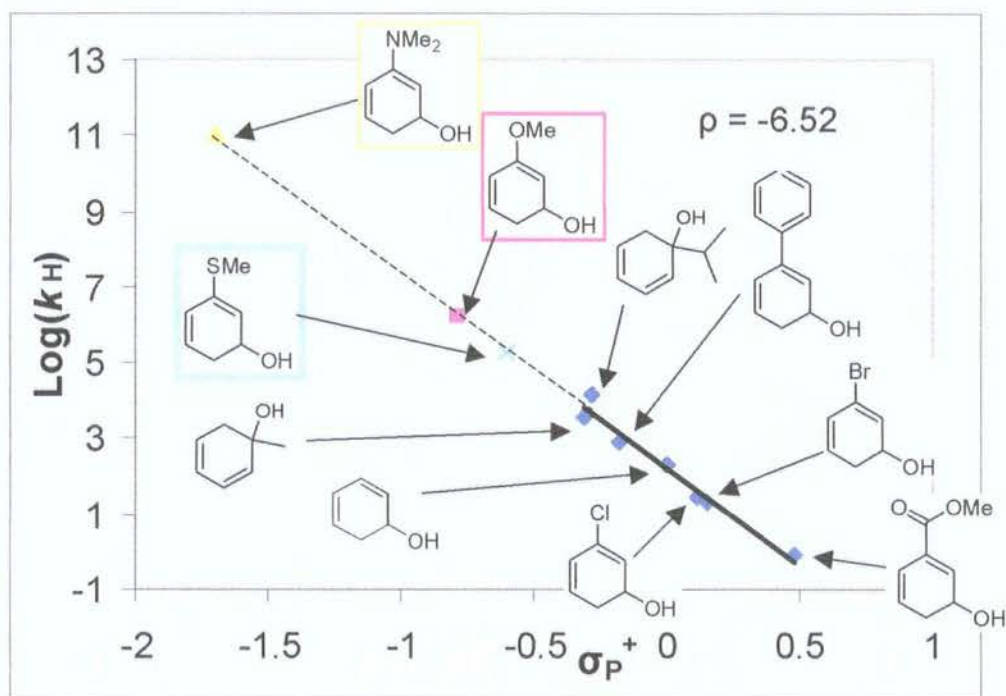


Figure 3.3-5 (above) shows the correlation with σ^+ for the hydrates and with the extrapolation to the electron donating substituents. Using the equation of the line, it is possible to predict the second-order rate constant for the reaction of the hydrates with electron-donating substituents, assuming they fall on the line. A summary of these predicted rate constants are shown in Table 3.3-2. The half-lives range from approximately 5 seconds to 10^{-7} seconds at pH 7, showing the reason for the difficulty in their isolation.

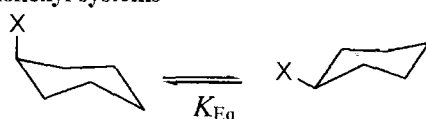
Table 3.3-2: Summary of the predicted rate constants from the aromatisation reaction of the hydrates with electron donating groups predicted from Fig3.3-5

Substituent	σ^+	$\text{Log } k_H$	k_H	$t_{1/2}$ at pH 7
OMe	-0.78	7.28	1.91×10^7	0.05 s
SMe	-0.6	6.10	1.26×10^6	5.5 s
NMe ₂	-1.7	13.27	1.86×10^{13}	3.7×10^{-7} s

3.4 Computational Studies

In parallel with the solution kinetic study of the reactivity of the arene hydrates, a computational study was carried out. The structures of the hydrates and putative carbocation were calculated using Gaussian '03 to B3Lyp6-31g** level of theory. The energies of the structures were also calculated. The structures of the lowest energy conformers are shown in the relevant section in Chapter 2. Here, the generalised structures and energies will be discussed and compared with the structures and energies of the *cis*-diols studied (see section 2.9).

Figure 3.4-1: A-values for cyclohexyl systems⁹⁸



X	A ^(a) (kJ/mol)
Me	1.70
Et	1.75
iPr	2.15
tBu	> 4.5
OH	0.87

(a) $A = -RT\text{Log}(K_{\text{eq}})$

In the case of the *meta* and *ortho*-substituted hydrates, the substituent is in a pseudoequatorial position as it is attached to a dienyl system. However, for the *ipso* alkyl hydrates the substituents can be either equatorial or axial. Generally, the lowest energy conformer of all the substituted hydrates showed the hydroxyl group in the axial position and the substituent either equatorial (*ipso* hydrate) or coplanar with the dienyl system. This is consistent with the substituent A-values for the cyclohexyl equivalent where the A-value for bulky substituents is greater than for a hydroxyl group (see Fig 3.3-1). In fact the A value of 0.8 kJ/mol for a hydroxyl substituent in chloroform is close to zero and indicates only a very slight preference for the axial position, which could easily be biased towards equatorial by a change in solvent⁹⁸.

Figure 3.4-2 shows four examples of the calculated minimum energy structures in chapter 2. Figure 3.4-2 (a) shows the calculated minimum energy structure of benzene hydrate (3.33, R = H), for which the hydroxyl group is in the equatorial position. Figure 3.4-2 (b) is *meta*-substituted phenyl hydrate (3.12) where the phenyl substituent is positioned on an unsaturated carbon and so is forced to be co-planar with the diene system. Figure 3.4-2 (c) and (d) show the *ortho* and *ipso* toluene hydrates, respectively. For hydrates (b) – (d), the hydroxyl group is in the axial position with the hydrogen orientated towards the centre of the cyclohexadiene.

Figure 3.4-2: Examples of the hydrate minimum energy structures calculated to the B3LYP/6-31g level of theory (a) methyl benzoate hydrate (b) biphenyl hydrate (c) *ipso* toluene hydrate and (d) *ortho* toluene hydrate**

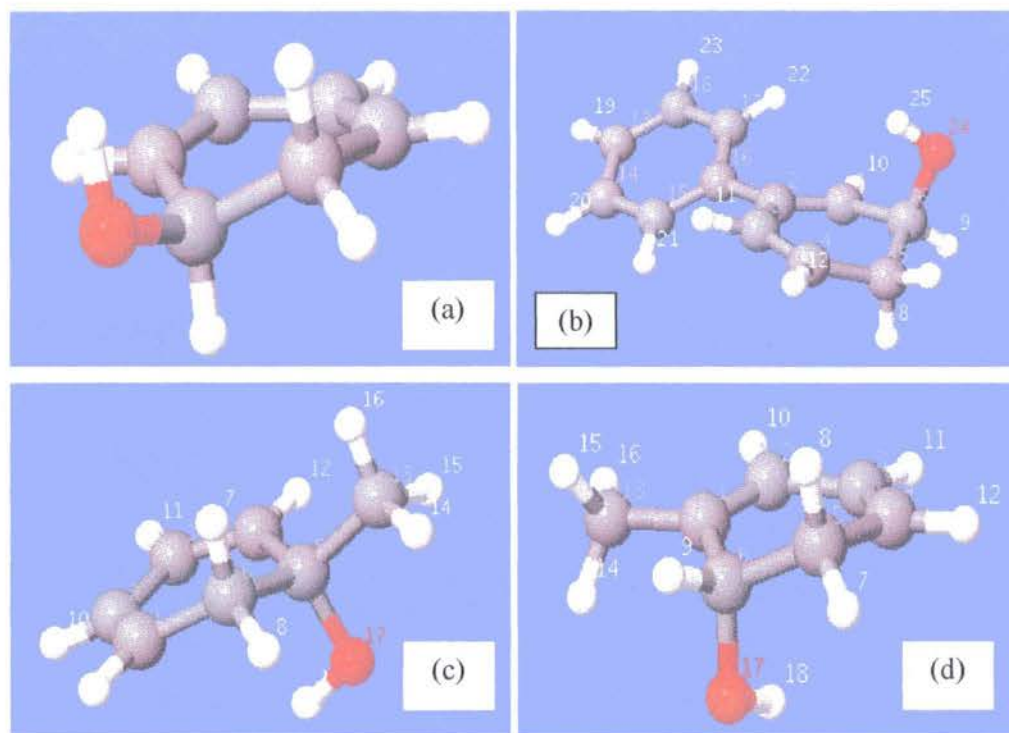


Figure 3.4-3 shows some examples of the calculated structures of the carbocation intermediates formed in the aromatisation or dehydration reactions of the arene hydrates. The cyclohexadienyl ring is planar and the orientation of the substituent depends on the regioisomer studied. The *ipso* toluene cation (Fig 3.4-3(c)) shows the C-H bond of the methyl group perpendicular to the plane of the ring, whereas the *ortho* toluene cation has

the C-H bonds at 30° to the ring. The *meta* substituted carbocation (Fig 3.4-3(b)) has the substituent at 15° relative to the ring.

Figure 3.4-3: Structures of the carbocation intermediates calculated to the B3LYP/6-31g level of theory (a) benzene hydrate (b) biphenyl hydrate (c) *ipso* toluene hydrate and (d) *ortho* toluene hydrate**

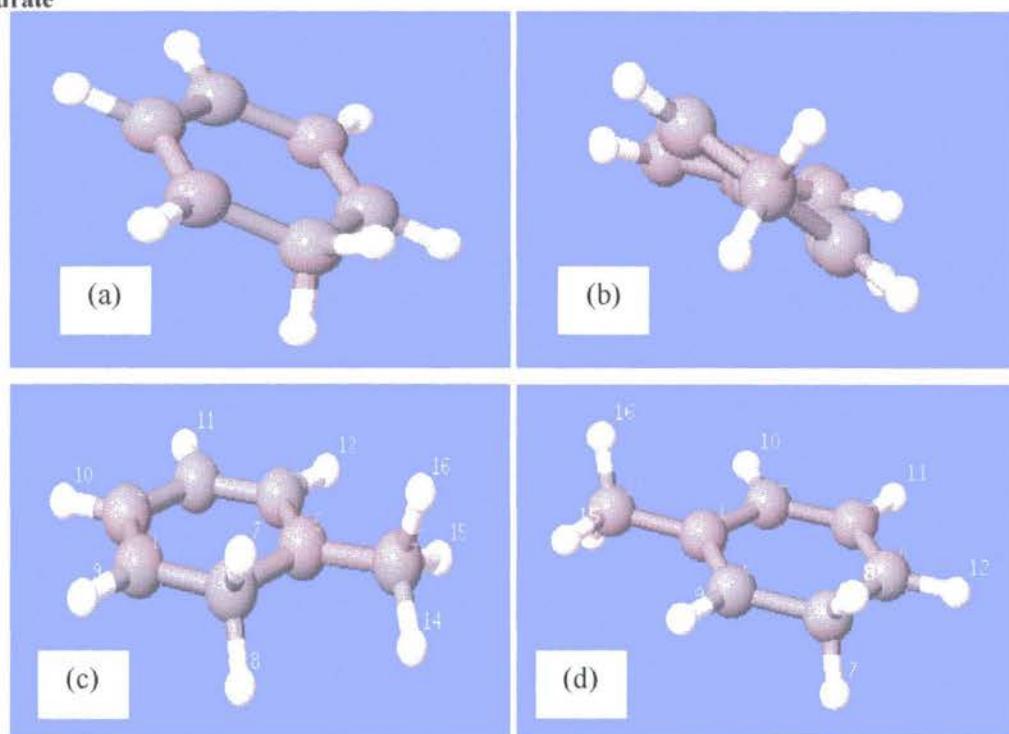


Figure 3.4-4 shows some examples of the minimum energy structures that we calculated for the substituted *cis*-dihydrodiols. These diols that were used for aromatisation kinetic studies were originally synthesised by Boyd et al. using a biosynthetic fermentation approach and so all show a common substitution pattern¹. The calculations show the hydrogen bonding between the two hydroxyl groups and, in the case of the methyl ester (Fig 3.4-4(a)) and methoxy (Fig 3.4-4 (b)) substituted diols, with the substituent also. The hydroxyl groups of the dihydrodiols are either equatorial or axial. The cyclohexadiene ring is puckered.

Figure 3.4-4: Structures of the *cis*-dihydrodiols calculated to the B3LYP/6-31g** level of theory: (a) Methylbenzoate and (b) anisole *cis*-dihydrodiol

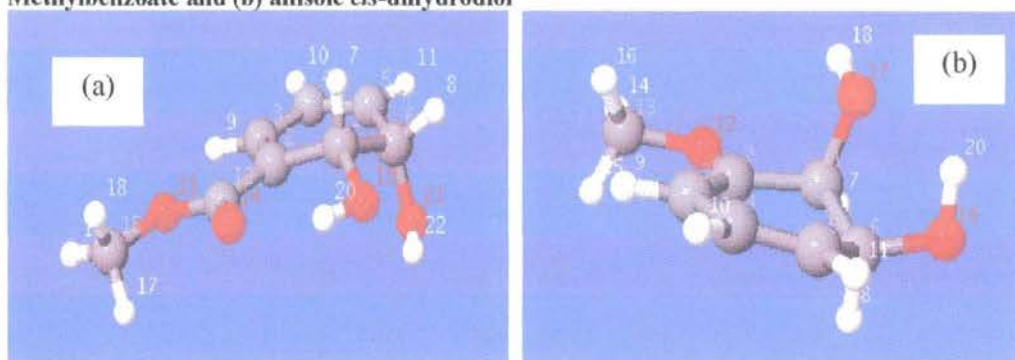
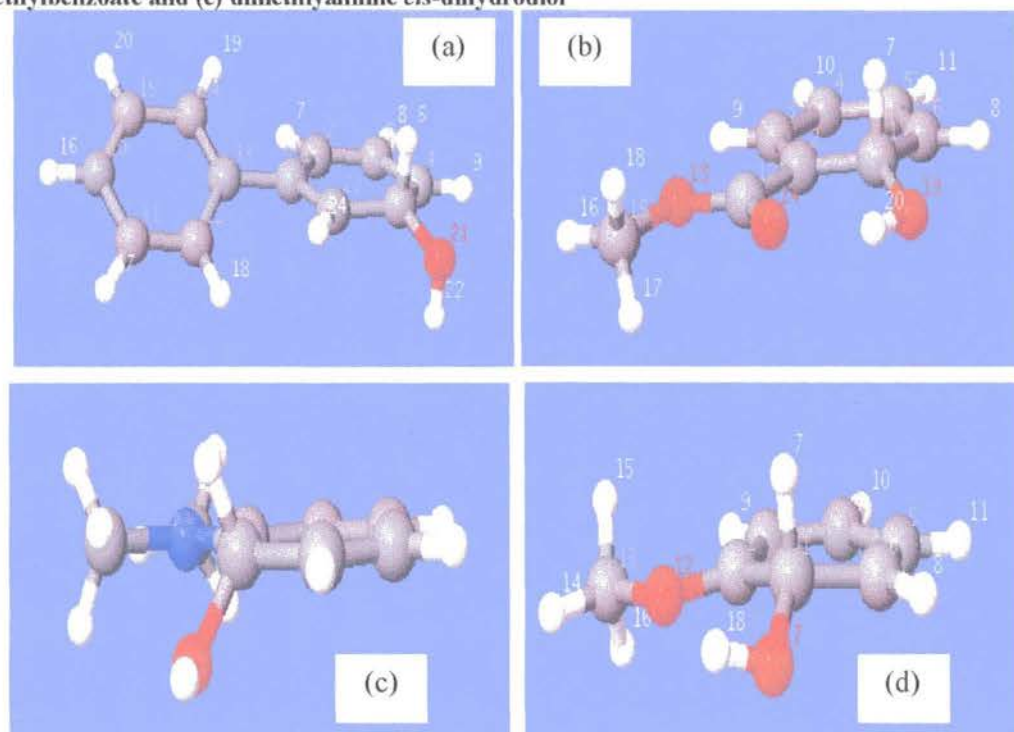


Figure 3.4-5 shows some examples of the carbocation intermediates formed in the dehydration of substituted *cis*-diols to give *ortho* phenols. The cyclohexadienyl rings are not planar, but are puckered at the carbon attached to the remaining hydroxyl group. The remaining hydroxyl group is in the equatorial position, as is shown for biphenyl (Fig 3.4-4(a)) and methyl benzoate (Fig 3.4-5(b)) *cis*-dihydrodiols. The carbocation in Figure 3.4-4(b) shows hydrogen bonding between the C=O of the ester and the remaining hydroxyl group. Interestingly, the only carbocation structure showing planarity is the dimethyl amino substituted dihydrodiol (Fig 3.4-5(c); this dihydrodiol has not been isolated¹). Also, there is no hydrogen bonding between the hydroxyl group and the nitrogen lone pair, which is seen in the precursor *cis*-dihydrodiol. The carbocation of the methoxy-substituted *cis*-dihydrodiol shows non-planarity (see Fig 3.4-5(d)), suggesting there may not be through-bond conjugation between the carbocation centre and the substituent, which corroborates the correlation with σ_p rather than σ^+ .

Figure 3.4-5: Carbocation structures calculated to the B3Lyp6-31g level of theory (a) biphenyl (b) methylbenzoate and (c) dimethylaniline *cis*-dihydrodiol**



The *cis*-dihydrodiols and the hydrates both show non-planarity in their structures. Due to the extra hydroxyl group, hydrogen bonding between the hydroxyl groups is available in the diols. For the hydrates with the substituent in the *meta* position relative to the hydroxyl, the substituent is forced to be coplanar with the dienyl system, similar to the diols. The alkyl hydrate structures are not directly comparable with the diols due to the different substituent patterns. It is in the carbocation structures where the major differences can be seen. The presence of the hydroxyl group in the diol carbocation results in puckering of the two saturated carbons relative to the dienyl part, whereas the hydrate carbocation intermediate is completely planar.

3.4.1 Calculated Energies of the arene hydrates, *cis*-dihydrodiols and corresponding carbocations

The calculated energies reflect both a gas phase calculation and a water sphere type calculation using the polarisable continuum model available. It must be stressed that the

energies reflect the absolute energies of the structures but do not take into account the leaving group.

Table 3.4-1 summarises the calculated values of the lowest energy conformers of the arene hydrates. The hydrates synthesised, and also the hydrates for which synthesis was unsuccessful, are included. The relative energies between the hydrates and carbocations in a water sphere are displayed from lowest to highest, i.e. from most stable to least stable. The final column shows the calculated natural logarithm of the ratio of rate constants for aromatisation of the substituted hydrate relative to benzene hydrate ($R = H$) based on equation 3.2, where ΔG_R^\ddagger and ΔG_H^\ddagger are the changes in the calculated free energies between the hydrate and its carbocation intermediate for the substituted (R) and unsubstituted (H) hydrates shown in Table 3.4-1 and the gas constant (R) used is $8.314 \text{ J K}^{-1} \text{ mol}^{-1}$ and temperature (T) is 298.15 K .

$$\ln\left(\frac{k^R}{k^H}\right) = \frac{1}{RT}(-\Delta G_R^\ddagger + \Delta G_H^\ddagger) \quad \text{Equation 3-2}$$

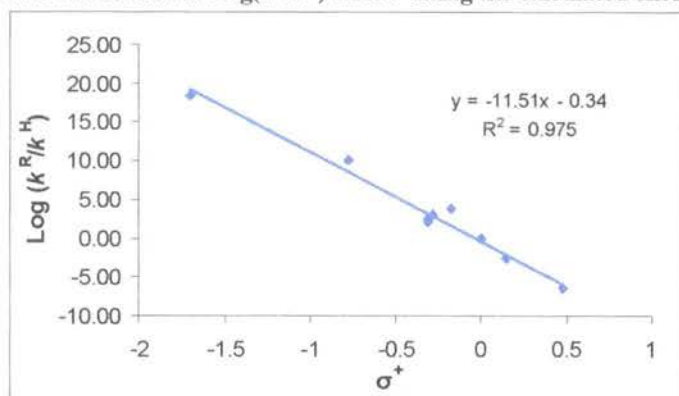
Table 3.4-1 shows that the dimethylamino substituted hydrate is predicted to be on the order of 2×10^{18} fold more reactive than benzene hydrate (and the ester substituted hydrate is 3×10^7 fold less reactive). The actual experimental value for dehydration of methylbenzoate hydrate relative to benzene hydrate $k^{\text{COOMe}}/k^H = 5 \times 10^{-4}$. For the bromo substituted hydrate, the predicted $k^{\text{Br}}/k^H = 2 \times 10^{-3}$, whereas the experimental value determined by O'Donoghue is 0.11.² The phenyl substituted hydrate has an experimental value of k^{Ph}/k^H of 11.6 whereas the calculated value is 7331.

Table 3.4-1: Summary of the arene hydrate energies and corresponding carbocation calculated to the B3Lyp6-31g level of theory**

R	hydrate (kJ/mol) ^(a)		carbocation (kJ/mol) ^(b)		$\Delta G^{(c)}$ (kJ/mol) pcm	$\ln(k^R/k^H)$ ^(d)
	Gas Phase	PCM (water)	Gas Phase	PCM (water)		
NMe ₂ (meta)	-1162099.81	-1162130.37	-962507.10	-962697.29	199433.08	42.55
OMe (meta)	-1111028.39	-1111063.14	-911375.45	-911582.24	199480.90	23.25
Ph (meta)	-1417008.69	-1417047.55	-1217330.44	-1217531.1	199516.44	8.91
<i>t</i> Bu (ipso)	-1223246.40	-1223270.71	-1023549.49	-1023751.6	199519.08	7.84
<i>i</i> Pr (ipso)	-1120031.52	-1120057.67	-920328.53	-920535.96	199521.71	6.78
Et (ipso)	-1016805.52	-1016834.16	-817099.1	-817311.27	199522.89	6.30
Me (ipso)	-913586.63	-913612.43	-713871.66	-714087.56	199524.87	5.50
Me (meta)	-913590.00	-913618.04	-713901.05	-714090.74	199527.30	4.52
H	-810344.18	-810375.71	-610605.30	-610837.21	199538.50	0.00
<i>i</i> Pr (ortho)	-1120039.41	-1120064.91	-920309.77	-920523.47	199541.44	-1.19
Et (ortho)	-1016816.25	-1016842.87	-817084.02	-817300.41	199542.45	-1.60
<i>t</i> Bu (ortho)	-1223257.38	-1223281.65	-1023531.06	-1023737.3	199544.32	-2.35
Me (ortho)	-913592.97	-913619.81	-713856.04	-714074.62	199545.08	-2.70
Br (meta)	-7560789.31	-7560823.19	-7361047.1	-7361270	199553.90	-5.92
Ester (meta)	-1408606.66	-1462130.37	-1208841.5	-1209082.5	199516.44	-14.96

(a) Calculated energies of the hydrate in the gas and aqueous phase. (b) Calculated energies of the carbocation intermediate in the gas and aqueous phase. (c) Change in calculated energy between the aqueous phase carbocation and hydrate. (d) Natural logarithm of the relative rate constants for dehydration, calculated using equation 3.2.

Figure 3.3-6 shows a Hammett correlation of the logarithm of the computed relative rates against σ^+ , which gives a ρ -value = -11.5. The sign of ρ is correct, however the magnitude is almost two-fold larger than the experimental value (-6.4). The alkyl-substituted hydrates have been excluded as the relevant kinetic data did not correlate with σ^+ . It must be emphasised that the relative rates used have been calculated assuming the change in the energy between the carbocation and the hydrate is the free energy and the effect of the hydroxyl leaving group is assumed to be constant. The values are purely qualitative and not quantitative.

Figure 3.4-6: Hammett correlation of $\text{Log}(k^R/k^H)$ with σ^+ using the calculated energies in Table 3.4-1

The calculated and experimental relative rate constants for dehydration of the different alkyl substituted hydrates to benzene hydrate are summarized together in Table 3.4-2. The calculated values are approximately 3-fold higher than the experimental values; however the correct order of reactivity is generally predicted.

Table 3.4-2: Calculated and experimental values for the rates of aromatisation of the *ipso* hydrate relative to the *ortho* for the alkyl hydrates

R	$\Delta G^{ipso(a)}$	$\Delta G^{ortho(a)}$	Calculated ^(b) $\ln(k^i/k^o)$	Experimental ^(c) $\ln(k^i/k^o)$
Me	199524.87	199545.19	8.2	2.9
Et	199522.85	199542.46	7.9	$\sim 2.9^{(d)}$
iPr	199521.71	199541.44	8.0	3.1
tBu	199519.08	199544.32	10.2	$\sim 3.1^{(d)}$

(a) Energy for carbocation – energy for hydrate calculated at the B3LYP6-31g** level of theory. (b) calculated using equation 3.2. (c) Using second-order rate constants from the relevant section in chapter 2. (d) Using estimation of the second-order rate constant for the *ipso* hydrate.

Table 3.4-3 (below) summarises the calculated energies of the substituted *cis*-dihydrodiols. As above for the hydrates, the table shows ΔG values calculated from the energies of the diol and the carbocation cation intermediate and also calculate $\ln(k^R/k^H)$. The calculated value of the ratio of k^{Me}/k^H is 237, whereas the experimental value is 13. For the phenyl substituent, k^{Ph}/k^H is equal to 0.41 and the calculated value is 6×10^{-3} . The calculations predict the correct order of reactivity for the *cis*-dihydrodiols i.e. a methyl substituent increases the rate of reaction compared to hydrogen and the phenyl substituent decreases the rate of reaction relative to hydrogen, however, the magnitudes

of the ratios disagree with experimental values. This is also noticeable in the Hammett correlations shown below.

Table 3.4-3: Energies of the substituted *cis*-dihydrodiols calculated to the B3LYP/6-31g level of theory.**

Substituent	Diol (kJ/mol) ^(a)		Carbocation (kJ/mol) ^(b)		$\Delta G^{(c)}$ (pcm)	$\ln(k^R/k^H)$ ^(d)
	GP	Aq	GP	Aq		
CO ₂ Me	-1606141.40	-1606179.56	-1406349.90	-1406582.51	199597	-11.12
Ph	-1614493.29	-1614542.43	-1414710.38	-1414960.40	199582	-5.06
H	-1007826.91	-1007868.15	-808033.70	-808299.45	199569	0.00
CH ₃	-1111069.36	-1111109.51	-911306.04	-911553.56	199556	5.47
OMe	-1308519.57	-1308561.70	-1108802.34	-1109036.95	199524	18.06
NMe ₂	-1359581.93	-1359625.83	-1159936.46	-1160153.81	199472	39.34

(a) Calculated energies of the hydrate in the gas and aqueous phase. (b) Calculated energies of the carbocation intermediate in the gas and aqueous phase. (c) Change in calculated energy between the aqueous phase carbocation and hydrate. (d) Natural logarithm of the relative rate constants for dehydration, calculated using equation 3.2.

Figure 3.4-7(a) shows a Hammett correlation of the calculated $\ln(k^R/k^H)$ values against σ^+ for the *cis*-dihydrodiols. Figure 3.4-7 (b) shows the correlation with σ_p . Both correlations are good however the correlation with σ^+ is slightly better. Boyd *et al.* report the ρ -value for the Hammett correlation of logarithm of the second-order rate constant for aromatisation (k_H) against σ_p as -8.2. The value of ρ^p from the calculated rate constants is -19.5. The value of ρ^+ from the calculated rate constants is -10.4, where the phenyl substituted *cis*-diol is the outlier. The calculations predict a better correlation with σ^+ , as would be expected for a carbocation forming reaction with through-bond conjugation.

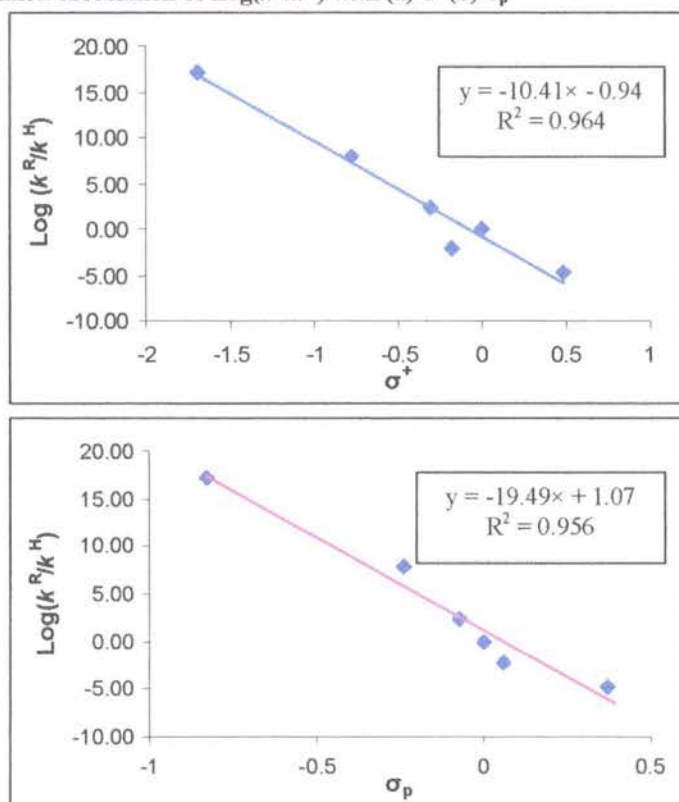
of the ratios disagree with experimental values. This is also noticeable in the Hammett correlations shown below.

Table 3.4-3: Energies of the substituted *cis*-dihydrodiols calculated to the B3LYP/6-31g level of theory.**

Substituent	Diol (kJ/mol) ^(a)		Carbocation (kJ/mol) ^(b)		$\Delta G^{(c)}$ (pcm)	$\ln(k^R/k^H)$ ^(d)
	GP	Aq	GP	Aq		
CO ₂ Me	-1606141.40	-1606179.56	-1406349.90	-1406582.51	199597	-11.12
Ph	-1614493.29	-1614542.43	-1414710.38	-1414960.40	199582	-5.06
H	-1007826.91	-1007868.15	-808033.70	-808299.45	199569	0.00
CH ₃	-1111069.36	-1111109.51	-911306.04	-911553.56	199556	5.47
OMe	-1308519.57	-1308561.70	-1108802.34	-1109036.95	199524	18.06
NMe ₂	-1359581.93	-1359625.83	-1159936.46	-1160153.81	199472	39.34

(a) Calculated energies of the hydrate in the gas and aqueous phase. (b) Calculated energies of the carbocation intermediate in the gas and aqueous phase. (c) Change in calculated energy between the aqueous phase carbocation and hydrate. (d) Natural logarithm of the relative rate constants for dehydration, calculated using equation 3.2.

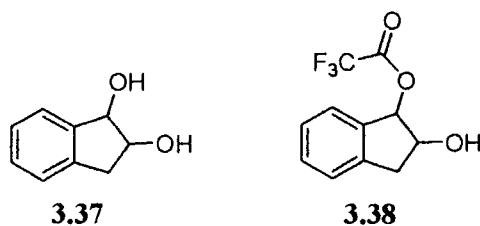
Figure 3.4-7(a) shows a Hammett correlation of the calculated $\ln(k^R/k^H)$ values against σ^+ for the *cis*-dihydrodiols. Figure 3.4-7 (b) shows the correlation with σ_p . Both correlations are good however the correlation with σ^+ is slightly better. Boyd *et al.* report the ρ -value for the Hammett correlation of logarithm of the second-order rate constant for aromatisation (k_H) against σ_p as -8.2. The value of ρ^p from the calculated rate constants is -19.5. The value of ρ^+ from the calculated rate constants is -10.4, where the phenyl substituted *cis*-diol is the outlier. The calculations predict a better correlation with σ^+ , as would be expected for a carbocation forming reaction with through-bond conjugation.

Figure 3.4-7: Hammett correlation of $\text{Log}(k^R/k^H)$ with (a) σ^+ (b) σ_p 

The Hammett plots generated from the calculated energies show a large difference between the experimental and calculated values for the magnitude of ρ . The calculations do, however, predict the correct order of reactivity. This is particularly interesting in the biphenyl hydrate and dihydrodiol case. The experimental results for biphenyl hydrate show the effect of the phenyl substituent is to increase the second-order rate constant for the aromatisation reaction. The phenyl substituent on the dihydrodiols decreases the second-order rate constant for aromatisation when compared to the unsubstituted case. The Gaussian calculations predict this.

3.5 pK_R of Indene dihydrodiol

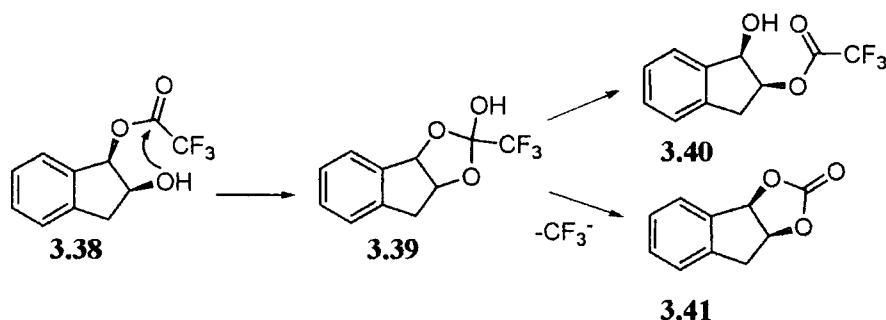
This section will discuss the results from the isomerisation and solvolysis studies of indene diols and its ester derivatives.



3.5.1 Synthesis of ester derivatives

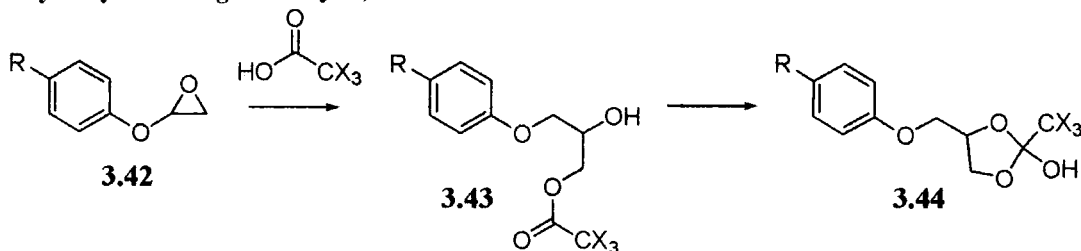
The ester derivatives were synthesised as described in section 2.9.1. As discussed the synthesis of the indene diol was straightforward, however the synthesis of the ester (trifluoroacetate) derivative was more difficult. The yields were low due to the formation of numerous side-products described in section 2.9.1. Side-product (3.40) is expected, as there is no reason to expect the trifluoroacetic anhydride to react exclusively at the 1-hydroxyl group. The formation of the side product (3.41) suggests that the trifluoroacetate group is migrating between the *cis*-hydroxyl groups. The third side-product has been assigned as (3.39) for reason discussed in section 2.9.3.

Scheme 3.5-1: Proposed mechanism for the synthesis of side-products 3.39, 3.40 and 3.49 from 2,3-dihydro-2-hydroxy-1H-inden-3-yl-trifluoroacetate (3.38)



Although the tetrahedral intermediate shown is expected to be unstable, there is evidence that similar compounds have been isolated and recrystallized⁹⁹. Kuliev *et al.* synthesised a range of halo orthoesters using the synthetic route outlined in the Scheme 3.5-2 (below). The adduct (3.44) formed after rearrangement of (3.43) is remarkably similar to structure (3.39). The *ortho*-ester (3.44) with X = F was considerably more stable than chlorine analogue.

Scheme 3.5-2: The addition of trihalogenoacetic acids to aryl glycide ethers forming 4-aroxyethyl-2-hydroxy-3-trihalogenomethyl-1,3-dioxolanes⁹⁹.



3.5.2 Determination of k_H – Isomerisation studies

The isomerisation reaction of (1R,2S)-2,3-dihydro-1H-indene-1,2-diol (3.37) was followed in deuterated perchloric acid solutions (0.1 to 3.13 M) as outlined in section 2.9.2. The measured second order rate constant is assumed to be equivalent to the rate of carbocation formation. A deuterium isotope effect is taken into account, as discussed in Section 2.9.6. The mechanism of racemisation is outlined below (see Scheme 3.5-3). Indene diol was sufficiently soluble in water at the concentrations required for NMR kinetics (10 mM) to enable the direct determination of a second order rate constant using only 5 % MeCN co-solvent.

Scheme 3.5-3: Isomerisation reaction of indene diol

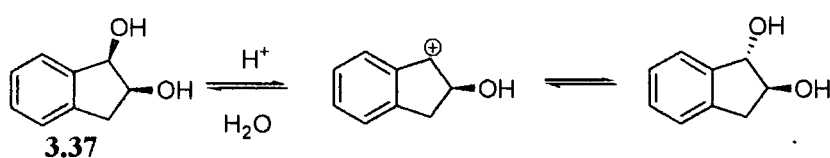
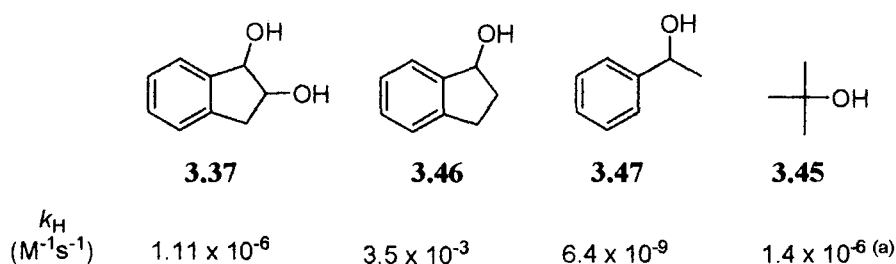


Chart 3.1 compares the second order rate constant for carbocation formation of indene diol (3.37) with the second order rate constants for carbocation formation of a number of other alcohols. The second-order rate constant for carbocation formation (k_H) was determined to be $1.11 \times 10^{-6} \text{ M}^{-1}\text{s}^{-1}$. This is comparable with *tert*-butanol (3.45) which has a rate of carbocation formation of $1.4 \times 10^{-6} \text{ M}^{-1}\text{s}^{-1}$. Indanol (3.46) has a rate of carbocation formation of $3.5 \times 10^{-3} \text{ M}^{-1}\text{s}^{-1}$ which is 1000-fold faster than indene diol (3.37). The racemisation of indanol requires dilute acids², whereas indene dihydrodiol

(3.47) requires concentration acids to induce ionisation and no elimination product was seen. The adjacent hydroxyl substituent disfavors carbocation formation and thus overall carbocation formation. The similar k_H values for *tert*butanol and indene dihydrodiol suggest the 2-hydroxyindanol carbocation is of similar stability to the *tert*butyl carbocation. Thus the 2-hydroxy substituent counteracts the stabilising effect of the benzylic substituent.

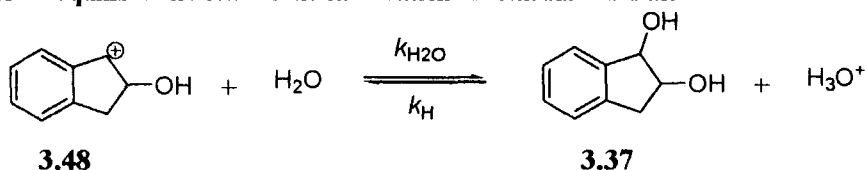
Chart 3.5-1: Comparison of benzylic, allylic and pro-aromatic alcohols



3.5.3 pK_R of indene dihydrodiol

Combining the rate constant for reaction of the carbocation with water (k_{H_2O}) which was determined by an azide-trapping experiment as described in section 2.9.3 and the rate constant for carbocation formation (k_H) described in section 2.9.3 the equilibrium shown in Scheme 2.9-6 can be calculated using Equation 2.19.

Scheme 3.5-4: Equilibrium between the carbocation intermediate and alcohol.

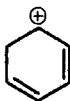
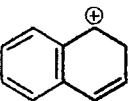

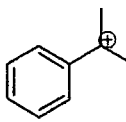
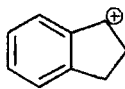
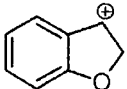
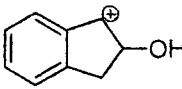
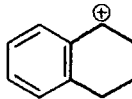
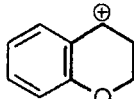
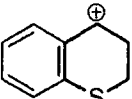


$$K_R = \frac{[\text{ROH}][\text{H}^+]}{[\text{R}^+]} = \frac{k_{H_2O}}{k_H} \quad \text{Equation 3-3}$$

A K_R value for cation (3.47) was determined, using Equation 2.19, as 4.3×10^{14} M, which corresponds to a pK_R of -14.6.

Chart 3.5-2 (below) shows a number of carbocation intermediates and their relevant pK_R values. The pK_R of the arene-forming carbocations (3.49 and 3.50) are considerably higher than the alkyl and benzylic carbocations. The β -hydroxyl group of indene diol substantially decreases the stability of the carbocation intermediate; pK_R of the indanol carbocation (3.51) is -11.7 versus -14.6 for indene dihydrodiol carbocation. The pK_R of the *tert*-butyl carbocation (3.52) is -16.4 which is less stable than carbocation (3.47).

Chart 3.5-2: Comparison of carbocation pK_R

				
	3.49	3.50	3.52	3.54
pK_R	-2.1	-7.6	-16.4 ^(a)	-12.3
				
	3.51	3.53	3.47	
pK_R	-11.7	-9.3	-14.6	
				
	3.55	3.56	3.57	
pK_R	-12.2	-12.0	-12.3	

The effect of resonance stabilisation is clearly demonstrated by the difference in pK_R between carbocation (3.47) and the benzofuran carbocation (3.53). Both carbocations have oxygen *ortho* to the carbocation centre, however, in the case of the benzofuran carbocation; the oxygen is positioned to allow for direct resonance through the aromatic ring with the carbocation centre. There is no equivalent resonance structure for the indene dihydrodiol carbocation. Oxygen is having a destabilising effect rather than a stabilising effect as shown in benzofuran.

The destabilising effect of the hydroxy group is also demonstrated by the difference in pK_R between cations (3.51), (3.52), and (3.54). The tertbutyl cation (3.51) is considerably less stable than the indanyl cation (3.51). One reason for the stability is the adjacent aromatic ring capable of stabilising the carbocation at the benzylic position; the other is the stabilising effect of the 5-membered ring versus an acyclic carbocation. This is shown by the difference in pK_R between (3.51) and (3.54). A pK_R of -14.6 for the indene dihydrodiol cation (3.47) suggests the adjacent hydroxyl group counteracts all the stabilising effects mentioned above. The results suggest the stability of the carbocation intermediate is closer to an acyclic carbocation rather than a benzylic stabilised carbocation.

Future Work

To further this work, there are a number of areas I would expand on. A Hammett plot for the *trans*-dihydrodiols should be generated for direct comparison with the arene hydrates and *cis*-dihydrodiols. Also a detailed computational study of the *trans*-dihydrodiols and their putative carbocation intermediate should be carried out and compared with the relevant *cis*-dihydrodiols.

I would also propose that a series of biphenyl hydrates and *cis*-dihydrodiols with substitution on the phenyl ring should be prepared so as to further explain the through-bond stabilisation which is present in the hydrates but not in the *cis*-dihydrodiols.

The pK_R of a series of analogous dihydrodiols should be calculated so as the indene dihydrodiol result can be compared with more similar compounds. This would also help in fully understanding the effect of the adjacent hydroxyl group.

Experimental

4.1 General Procedures (GP)

4.1.1 Birch Reduction

The relevant arene is added, via syringe, to a 500 mL three-neck flask fitted with a mechanical stirrer, cold-finger and gas inlet in a dry ice-acetone bath. Ethanol is then added and the mixture is allowed to equilibrate and then approximately 250 mL of ammonia is condensed. The solution is stirred while sodium is added giving usually a blue colour.

The reaction is left overnight to allow the ammonia to evaporate and then quenched cautiously with saturated ammonium chloride, water or sodium bicarbonate. The aqueous layer is extracted four times with diethyl ether. The organic layers are combined and washed with saturated salt solution and then dried over magnesium sulphate, filtered and the solvent removed *in vacuo*.

4.1.2 *m*CPBA Epoxidations

Dichloromethane is added to a 100 mL three neck flask fitted with a gas inlet, outlet and septum. To this the diene is added and stirred using a magnetic stirrer at 0 °C. A slight excess of *m*CPBA is added in portions over approximately 20 minutes. The white precipitate of the *m*-chlorobenzoic acid is seen as reaction proceeds.

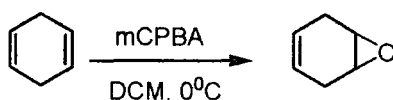
The reaction is followed by TLC and on completion quenched with 10 % sodium sulfite solution. The dichloromethane is washed four times with sodium hydroxide solution to remove the *m*-chlorobenzoic acid and then dried over magnesium sulphate, filtered and the solvent removed *in vacuo*.

4.1.3 Ring-opening

An excess of methyllithium (~1.6 M) solution is added to a solution of cyclohexene epoxide in dry diethyl ether at 0 °C, the reaction is left to stir on ice and followed by TLC. On completion the reaction is quenched with 10 mL of 10% sodium hydroxide solution. The aqueous layer is extracted with diethyl ether. The organic layers are combined and dried over magnesium sulphate and the solvent removed *in vacuo*.

4.2 Synthetic targets

4.2.1 7-oxa-bicyclo[4.1.0]hept-3-ene



mCPBA (4.66 g, 27.0 mmol) was added in portions to a solution of 1,4-cyclohexadiene (2.5 mL, 2.12 g, 26.6 mmol) in 50 cm³ dichloromethane cooled in an ice-bath and the reaction was left to stir overnight. TLC showed the reaction was completed. The reaction was quenched and the product extracted (see GP 1.2). The product was purified by column chromatography (silica gel, 10:90, hexane, diethyl ether) and then further purified by Kugel-Rohr distillation. The epoxide was isolated as a clear liquid with a yield of 80 % (2.05 g, 21.3 mmol).

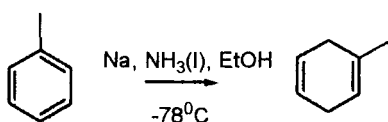
δ_{H} (CDCl₃, 400 MHz): 5.42(br s, 2H, HC=CH), 3.22 (br s, 2H, HCOCH), 2.48(m, 4H, 2 × CH₂).

δ_{C} (CDCl₃, 125 MHz) 121.2, 50.6, 24.7.

ν_{max} (cm⁻¹): 3000(C-H), 2893(C-H), 1682, 1423, 1213, 1010, 865, 792, 752, 659.

Consistent with literature reports^{100, 101}.

4.2.2 1-Methyl-1,4-cyclohexadiene



Ammonia was condensed into a solution of toluene (20 cm³, 0.19 mol) and ethanol (36 cm³, 0.63 mol) in 50 cm³ of dry diethyl ether (50 cm³). To this, sodium (13.1 g, 0.63 mol) was added to give the standard blue colour. The reaction was left overnight to allow

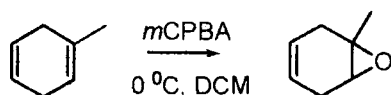
all ammonia to evaporate and then quenched cautiously with saturated ammonium chloride (10 mL). The aqueous layer was extracted four times with diethyl ether (4 × 100 mL). The organic layers were combined and washed with brine (50 mL) and then dried over magnesium sulphate, filtered and the solvent removed *in vacuo*. The product was isolated as a colourless liquid with a pungent odour (8.71 g, 49 %); percentage conversion to the diene of 95% (NMR integration).

δ_{H} (CDCl₃, 500 MHz) 5.71 (br m, 2H, HC=CH) 5.41 (br s, 1H, HC=C), 2.69-2.55 (m, 4H, 2 × CH₂) 1.67 (s, 3H, CH₃)

δ_{C} (CDCl₃, 125 MHz) 131.5 (C-1); 124.5 (C-4 or 5); 122.5 (C-4 or 5) 118.8 (C-2); 30.9 (C-3 or 6); 27.1 (C-3 or 6); 23.7 (C-7).

Consistent with literature reports^{100, 102, 103}.

4.2.3 1-Methyl-7-oxa-bicyclo[4.1.0]hept-3-ene



As per general procedure 4.1.2.

Solid *m*CPBA (10.17 g, 57.9 mmol) was added to a solution of 1-methyl-1,4-cyclohexadiene (4.91 g, 52.1 mmol) in dichloromethane (50 cm³) at 0 °C. The reaction was followed by TLC and on completion (4 hours) was quenched with 10 % sodium sulfite solution (10 mL). The organic layer was washed four times with sodium hydroxide solution to remove the *m*-chlorobenzoic acid and then dried over magnesium sulphate, filtered and the solvent removed *in vacuo*.

Purification was via column chromatography on silica gel (95:5, petroleum ether: ether) and the product (R_f = 0.4) was isolated as a colourless liquid (0.94 g, 8.6 mmol, 19 % yield).

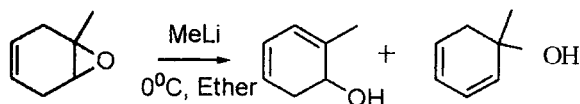
δ_{H} (CDCl₃, 500 MHz) 5.42 (t(br), 2H, HC=CH); 3.05 (s(br), 1H, HCOC), 2.4 – 2.3 (m, 4H, 2 × CH₂); 1.35 (s, 3H, CH₃).

δ_{C} (CDCl₃, 125 MHz) 122.66 (s, C-4 or 5); 121.56 (s, C-4 or 5); 50.27 (s, C-1 or 2); 49.48 (s, C-1 or 2); 30.50 (s, C-6); 28.39 (s, C-3); 26.32 (s, C-7).

m/z (EI⁺) 110.1 (M⁺)

All data consistent with the literature^{100, 104}.

4.2.4 2-Methylcyclohexa-2,4-dienol and 1-methylcyclohexa-2,4-dienol



As per general procedures 4.1.3

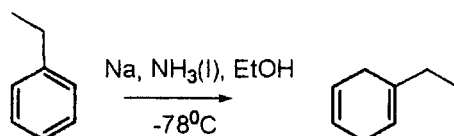
Methyl lithium (12 mL, 1.6 M, 20 mmol) was added slowly to a stirred solution of 1-methyl-7-oxa-bicyclo[4.1.0]hept-3-ene (1.98 g, 18.1 mmol) on ice. The reaction was allowed to stir overnight, warming to room temperature. The reaction was quenched with water (5 mL). The aqueous layer was extracted with diethyl ether (3 × 30 mL). The two hydrates were isolated together with a crude yield of 75 % (1.48g). From NMR integration of the C-2 proton of the *ortho*-hydrate relative to the CH₃ of the *ipso*-hydrate, the ratio of the hydrates *ortho* and *ipso* is 44:56.

Ortho-hydrate (2.13): $\delta_{\text{H}}(\text{D}_2\text{O}, 500 \text{ MHz})$: 6.0(m, 1H, HC=C); 5.9(m, 1H, HC=C); 5.8(m, 1H, HC=C); 4.0(m, 1H, CH-OH); 2.4(m, 2H, CH₂); 1.85(s, 3H, CH₃).

Ipsa-hydrate(2.14): $\delta_{\text{H}}(\text{CDCl}_3, 300 \text{ MHz})$ 6.0(m, 2H, HC=CH); 5.9(m, 1H, HC=C); 5.7(m, 1H, HC=C); 2.5(m, 2H, CH₂); 1.28(s, 3H, CH₃).

m/z (EI) Aromatised under the experimental conditions. Only the aromatic identified. (ES): Not detectable.

4.2.5 1-Ethyl-1,4-cyclohexadiene



As per general procedure 4.1.1

Ammonia (150 mL) was condensed to a solution of ethylbenzene (4.94 g, 46.6 mmol) and ethanol (10 mL, 170 mmol) in 50 cm³ of dry diethyl ether. To this, sodium (4.27 g, 190 mmol) was added to give the standard blue colour. The reaction was left overnight to allow all ammonia to evaporate and then quenched cautiously with saturated ammonium chloride (10 mL). The aqueous layer was extracted four times with diethyl ether (4 × 100 mL). The organic layers were combined and washed with brine (50 mL)

and then dried over magnesium sulphate, filtered and the solvent removed *in vacuo*. The diene was isolated as a colourless liquid (2.38 g, 48 % yield)

δ_{H} (CDCl₃, 500 MHz) 5.71(m, 2H, HC=CH); 5.41(br s, 1H, HC=C); 2.7-2.58(m, 4H, 2 × CH₂); 1.97(q, ³J_{HH} = 7.3 Hz, 2H, CH₂), 1.02(t, ³J_{HH} = 7.3 Hz, 3H, CH₃).

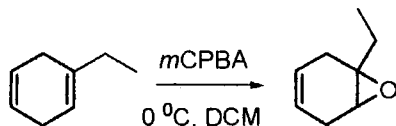
δ_{C} (CDCl₃, 500 MHz) 136.9(C-1); 124.65(C-4); 124.58(C-5); 117.13(C-2); 30.34(C-7); 29.21(C-6); 26.98(C-3); 12.22(C-8).

m/z (EI) 108.0 (M⁺, 24), 91 (44), 79 (100), 77 (66), 51(44), 41(30), 39(76), 27(42).

ν_{max} (cm⁻¹): 2990(C-H); 2965; 2877; 2775; 1454; 956; 758; 698; 660.

Spectroscopic data consistent with literature^{102, 103, 105}.

4.2.6 1-Ethyl-7-oxa-bicyclo[4.1.0]hept-3-ene



As per general procedures 4.1.2

mCPBA (0.68g, 3.9 mmol) was added to a solution of 1-ethylcyclohexa-1,4-diene (0.40 g, 3.7 mol) in chloroform (20 mL) on ice; the reaction was allowed to warm to room temperature and left to stir overnight. TLC indicated the reaction was complete and thus it was quenched as in GP 4.1.2.

The epoxide was isolated as a clear liquid with a crude yield of 0.56 g (81 %). The product was purified by column chromatography (silica gel, 99:1 petroleum ether: diethyl ether, R_f 0.6). The purified epoxide was isolated with a yield of 0.39 g (70%).

δ_{H} (CDCl₃, 400 MHz) 5.42(m, 2H, HC=CH); 3.05(br s, 1H, HCOC); 2.7-2.3(m, 4H, 2 × CH₂); 1.6(m, 2H, CH₂), 1.02(m, 3H, CH₃).

δ_{C} (CDCl₃, 100 MHz) 122.70(C-4); 121.66(C-5); 60.12(C-1); 57.22(C-2); 30.10(C-6); 28.19(C-3); 26.34(C-7); 9.06(C-8).

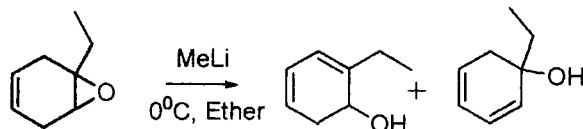
m/z (EI) 124.1 (M⁺, 4), 108.9(14), 94.9(46), 90.9(2), 81(40), 79(42), 76.9(50), 67(77), 64.9(50), 56.9(100).

ES- not detectable.

IR: 2972(C-H); 2895; 1452; 843; 662.

Elemental: calculated C:77.38 %, H: 9.74 %; found C:76.86 %; H: 9.54 %.

4.2.7 2-Ethylcyclohexa-2,4-dienol and 1-ethylcyclohexa-2,4-dienol



As per general procedures 4.1.3.

Methylolithium (1.2 mL, 1.6 M, 3.2 mmol) was added to a solution of 1-ethyl-7-oxabicyclo[4.1.0]hept-3-ene (0.27 g, 2.27 mmol) in dry diethyl ether. The reaction was left to stir overnight and worked up as in GP 1.3. The hydrates were isolated as a brown oil with a yield of 0.14 g (51 %).

(*ortho*-Hydrate) δ_{H} (CDCl₃ 400 MHz) 5.93(m, 1H, HC=C); 5.72(m, 1H, HC=C); 5.64(m, 1H, HC=C); 3.9(m, 1H, CHOH); 2.5(m, 2H, CH₂); 2.1(m, 2H, CH₂CH₃); 0.85(m, 3H, CH₂CH₃).

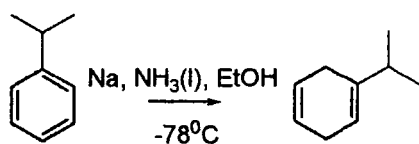
δ_{C} (CDCl₃ 100 MHz) 130(C-2); 122.3(C-4 or 5); 120.8(C-4 or 5); 117.7(C-3); 65(C-1); 32(C-6); 26 (C-7); 11(C-8).

(*ipso*-Hydrate) δ_{H} (CDCl₃ 400 MHz) Not isolated.

m/z EI: Aromatised under experimental conditions. ES: Not detectable

Elemental: calculated C:77.38 %, H: 9.74 %; found C:77.86 %; H: 9.84 %.

4.2.8 1-Isopropyl-1,4-cyclohexadiene



As per general procedures 4.1.1

Ammonia (150 mL) was condensed to a solution of cumene (5.02 g, 0.042 mol) and ethanol (10 mL, 0.2 mol) in dry diethyl ether (50 cm³). Sodium (5.2 g, 0.23 mol) was added and the solution turned blue. The reaction was left overnight to allow all ammonia to evaporate and then quenched cautiously with saturated ammonium chloride (10 mL). The aqueous layer was extracted four times with diethyl ether (4 × 100 mL). The organic

layers were combined and washed with brine (50 mL) and then dried over magnesium sulphate, filtered and the solvent removed *in vacuo*.

The diene was isolated as a colourless liquid with a yield of 2.03 g (42 %).

δ_{H} (CDCl₃, 400 MHz) 5.70(m, 2H, HC=CH); 5.43(br s, 1H, C=CH); 2.64(m, 4H, 2 × CH₂); 2.18(sept, 1H, ³J_{HH} 7.0 Hz, CH(CH₃)₂), 1.02(d, 6H, ³J_{HH} 7.0 Hz, CH(CH₃)₂).

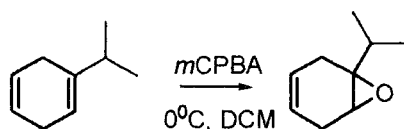
δ_{C} (CDCl₃, 100 MHz) 140.88(C-1); 124.83(C-5); 124.55(C-4); 116.22(C-2); 35.08(C-7); 26.98(C-3); 26.78(C-6); 21.37(C-8&9).

m/z (EI) 122.0 (M⁺, 40), 107(36), 80(22), 91(58), 79(100), 78(82), 51(22), 41(28), 39(30), 27 (18). ES: Not detectable.

ν_{max} (cm⁻¹): 3027(C=C-H); 2960 (C-H); 2872; 2822; 1462; 959; 759; 698; 665.

All characterization consistent with the literature^{102, 103, 105}.

4.2.9 1-Isopropyl-7-oxa-bicyclo[4.1.0]hept-3-ene



As per general procedures 4.1.2.

*m*CPBA (1.55 g, 8.98 mmol) was added to a stirred solution of 1-isopropyl-1,4-cyclohexadiene (0.96 g, 7.9 mmol) in dichloromethane (20 cm³) cooled in an ice-bath and the reaction was left to stir for 3.5 hours and quenched as in section 4.1.2. The epoxide was purified by column chromatography (silica gel, 99:1 petroleum ether, diethyl ether) and isolated as a yellow oil (0.54 g, 49 % yield).

δ_{H} (CDCl₃, 400 MHz) 5.45(m, 2H, HC=CH); 3.05(br s, 1H, COCH); 2.6-2.3(m, 4H, 2 × CH₂); 1.52 (sept, 1H, CH(CH₃)₂); 0.98(m, 6H, CH(CH₃)₂).

δ_{C} (CDCl₃, 100 MHz) 122.69(C-4 or 5); 121.63(C-4 or 5); 62.77(C-1); 57.27(C-2); 35.24(C-6); 26.35(C-3); 24.65(C-6); 18.76(C-8&9).

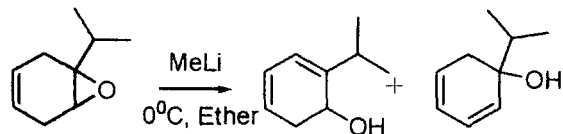
m/z(EI⁺) 138.1 (M⁺), 79(10), 77(11), 67(25), 65(15), 57(100), 55(18), 53(20), 51(15), 41(48), 39(66), 29(90), 27(34). ES: Not detectable

ν_{max} (cm⁻¹): 2962(C=C-H); 2893(C-H); 1667(C=C); 1453; 1365(iPr); 1034; 866(epoxide C-O); 855(epoxide C-O); 756; 661.

CHN calculated: C: 78.21 %, H: 10.21 %. Found: C 78.55 %, H: 10.03 %.

Data consistent with the literature¹⁰⁴.

4.2.10 1-Isopropylcyclohexa-2,4-dienol and 2-isopropylcyclohexa-2,4-dienol



As per general procedures 4.1.3.

Methylolithium (1.6 M, 2 mL, 3.2 mmol) was added to a stirred solution of 1-Isopropyl-7-oxa-bicyclo[4.1.0]hept-3-ene (0.15 g, 1.1 mmol) in dry diethyl ether (15 cm³). The crude hydrates were isolated as a brown oil (0.098 g, 67 % yield).

Ipsa-hydrate: $\delta_{\text{H}}(\text{D}_2\text{O}$ 500 MHz) 6.10(m, 1H, HC=CH-HC=CH); 6.06(m, 1H, HC=CH-HC=CH); 5.93(d, $J = 9$ Hz, 1H, HC=CH-HC=CH); 5.71(m, 1H, HC=CH-HC=CH); 2.3(m, 2H, CH₂); 1.76(sept, 1H, ³ $J_{\text{HH}} = 7$ Hz, CH(CH₃)₂); 0.90(d, ³ $J_{\text{HH}} = 7$ Hz, 3H, CH(CH₃)₂); 0.85(d, ³ $J_{\text{HH}} = 7$ Hz, 3H, CH(CH₃)₂).

$\delta_{\text{C}}(\text{CHCl}_3$ 500 MHz) 128(C-2); 126(C-5); 125(C-3 or 4); 120(C-3 or 4); 71(C-1); 40(C-7); 22(C-8 & 9).

Ortho-hydrate: $\delta_{\text{H}}(\text{D}_2\text{O}$ 500 MHz) 6.03(m, 1H, C=CH-HC=CH); 5.91(d, $J = 5.5$, C=CH-HC=CH); 5.75(m, 1H, C=CH-HC=CH); 4.18(m, 1H, CHOH); 2.43(m, 2H, CH₂); 1.06(d, ³ $J_{\text{HH}} = 5.9$, CH(CH₃)₂); 1.05 (d, ³ $J_{\text{HH}} = 5.9$, CH(CH₃)₂); 1.02(m, 1H, CH(CH₃)₂).

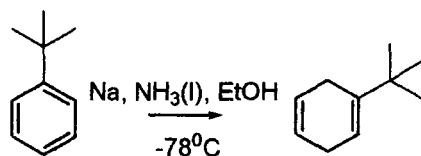
$\delta_{\text{C}}(\text{CHCl}_3$ 500 MHz) 131(C-2); 129(C-4or 5); 128(C-4 or 5); 118 (C-3); 65(C-1); 38(C-6); 26(C-7); 23(C-8 &9).

m/z (EI) M^+ (not observed), aromatised under experimental conditions – only arene detected. ES: not detectable.

ν_{max} (cm⁻¹): 2960(C=C-H); 1603(C=C); 1451, 1383; 1027, 760, 698.

CHN, calculated: C: 78.21 %, H:10.21 %. Found: C 78.79 %, H: 9.92 %.

4.2.11 1-Tertbutylcyclohexa-1,4-diene



As per general procedures 4.1.1

Ammonia (150 mL) was condensed to a stirred solution of tert-butyl benzene (5.04 g, 0.037 mol) and ethanol (10 mL, 0.2 mol) in dry diethyl ether (50 cm³). To this solution sodium (4.26 g, 0.19 mol) was added to give the standard blue colour. The reaction was left overnight to allow all ammonia to evaporate and then quenched cautiously with saturated ammonium chloride (10 mL). The aqueous layer was extracted four times with diethyl ether (4 × 100 mL). The organic layers were combined and washed with brine (50 mL) and then dried over magnesium sulphate, filtered and the solvent removed *in vacuo*. The diene was isolated as a colourless liquid with a crude yield of 2.88 g (57 %).

δ_{H} (CDCl₃, 500 MHz) 5.72(m, 2H, $\underline{\text{HC}}=\underline{\text{CH}}$); 5.50(br s, 1H, C= $\underline{\text{CH}}$); 2.69(m, 4H, 2 × $\underline{\text{CH}}_2$); 1.04(br s, 9H, C($\underline{\text{CH}}_3$)₃).

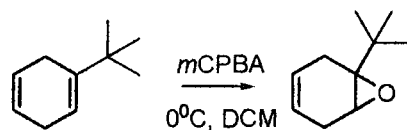
δ_{C} (CDCl₃, 125 MHz) 142.87(C-1); 125.31(C-4); 124.12(C-5); 115.53(C-2); 35.31(C-7); 29.26(C-8,9&10); 27.42(C-3 or 6); 25.18(C-3 or 6).

m/z(EI): 136(M⁺, 20), 121(42), 119(18), 105(20), 93(56), 91(42), 80(34), 79(100), 78(78), 77(42), 57(70), 41(56), 39(21), 28(16). (ES): Not detectable.

ν_{max} (cm⁻¹): 3025 (C=C-H); 2963 (C-C-H); 2869 (C-H), 1600, 1362 (tBu), 958, 752, 698, 668.

All data consistent with the literature^{102, 103}.

4.2.12 1-Tertbutyl-7-oxa-bicyclo[4.1.0]hept-3-ene



As per General Procedures 4.1.2

mCPBA (0.77 g, 4.48 mMol) was added to a stirred solution of 1-tertbutylcyclohexa-1,4-diene (0.52 g, 3.8 mMol) in DCM (30 cm³) at 0 °C. Reaction was left to stir overnight and warmed to room temperature. The reaction was quenched with a sodium sulfite (10 mL, 10 % w/v). The organic layer was separated and washed with sodium hydroxide solution (3 × 20 mL, 10 % w/v). The product was purified by column chromatography (silica gel, 99:1 petroleum ether: diethyl ether) and isolated as a colourless oil with a yield of 0.35 g (60 %).

δ_{H} (CDCl₃, 400 MHz) 5.45(m, 2H, HC=CH); 3.22(br s, 1H, COCH); 2.52–2.42(m, 4H, 2 × CH₂); 0.95(br s, 9H, C(CH₃)₃).

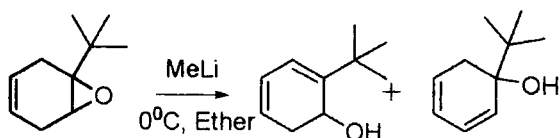
δ_{C} (CDCl₃, 100 MHz) 123(C-4 or 5); 121(C-4 or 5); 64(C-1); 54(C-2); 34(C-7); 27(C-3 or 6); 26(C-7, 8, 9); 24(C-3 or 6).

m/z (EI⁺) 152.0 (M⁺), 137(8), 109(14), 95(18), 91(16), 85(26), 67(28), 57(100), 41(60), 39(42), 29(20), 27(10). ES – not detectable.

ν_{max} (cm⁻¹): 2960 (C-H); 2905 (C-H), 1727, 1670, 1368 (tBu), 864, 756, 660.

CHN calculated: C: 78.50 %, H: 10.29 %. Found: C 78.00 %, H: 9.99 %.

4.2.13 1-*Tert*butylcyclohexa-2,4-dienol & 2-*tert*butylcyclohexa-2,4-dienol



As per general procedures 4.1.3.

Methylolithium (1.6 M, 3 mL, 4.8 mmol) was added to a stirred solution of 1-*tert*-butyl-7-oxa-bicyclo[4.1.0]hept-3-ene (0.10 g, 0.66 mmol) in dry diethyl ether (20 cm³). The reaction was quenched with water (1 cm³) which was quickly separated from the diethyl ether. The aqueous layer was washed with diethyl ether (3 × 20 mL) and the ether phases combined. The diethyl ether was removed *in vacuo*. The hydrates were isolated together in a 33 % yield. From the NMR integration, the ratio of hydrates is 4:1 with 20 % arene.

(*Ortho*-hydrate, 80 %) δ_{H} (CDCl₃ 400 MHz) 6.0 (m, 1H, C=CH-HC=CH); 5.85(m, 1H, C=CH-HC=CH); 5.4(m, C=CH-HC=CH); 4.2(m, 1H, CHOH); 2.5(m, 2H, CH₂) 1.09(m, 9H, C(CH₃)₃).

δ_{C} (CDCl₃ 100 MHz) 124.31(C-2), 122.64(C-4), 117.53(C-3), 62.87(C-1), 33.94(C-2), 29.5(C-7,8,9).

(*Ipso*-hydrate, 20 %) δ_{H} (CDCl₃ 400 MHz) 6.2 – 5.4 (m, 4H HC=CH-HC=CH); 2.5(m, 2H, CH₂); 0.9(m, 9H, C(CH₃)₃). δ_{C} (CDCl₃ 100 MHz) not distinguishable.

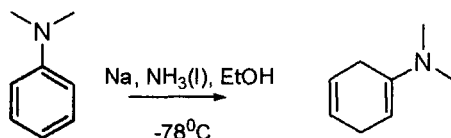
m/z (EI) M⁺ (not observed), aromatised under chromatographic conditions – only parent arene detected.

ES: Not detected.

ν_{\max} (cm⁻¹): 3406(O-H); 2960(C-H), 1463 (C-O), 1364(tBu); 1256; 1067; 802; 726.

CHN calculated: C: 78.90 %, H:10.59 %. Found: C 78.00 %, H: 9.99 %.

4.2.14 N,N-dimethylcyclohexa-1,4-dienamine



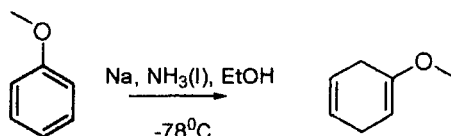
As per general procedures 4.1.1.

Ammonia (150 mL) was condensed into a stirred solution of N,N-dimethylaniline (4.934 g, 0.0407 mol) and ethanol (10 mL, 0.2 mol) in 35 cm³ dry THF. To this sodium (5.4 g, 0.23 mol) was added to give the standard blue colour. Conversion to the diene was observed with yield of 3.60 g (72 %).

The diene appears to be unstable due to isomerisation over time.

Crude δ_{H} (CDCl₃, 300 MHz) 5.95(m, 2H, HC=CH); 5.2(m, 1H, C=CH); 2.2-2.7(br m, 4H, 2 × CH₂); 2.02(m, 6H, N(CH₃)₂).

4.2.15 1-Methoxycyclohexa-1,4-diene



As per general procedures 4.1.1.

Ammonia (150 mL) was condensed into a stirred solution of anisole (5.04 g, 0.0465 mol) and ethanol (10 mL, 0.2 mol) in dry THF(35 cm³). To this, sodium (6.2 g, 0.27 mol) was added to give the standard blue colour. Conversion to the diene was observed with yield of 83 %(4.25 g).

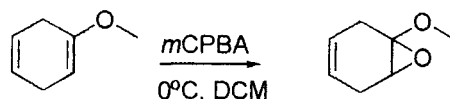
δ_{H} (CDCl₃, 400 MHz) 5.7(m, 2H, HC=CH); 4.6(s, 1H, C=CH); 3.54(s, 3H, OCH₃); 2.71(m, 4H, 2 × CH₂).

δ_{C} (CDCl₃, 100 MHz) 152.96 (s, C-1); 124.78(s, C-4 or 5); 124.42(s, C-4 or 5); 90.86(s,C-2); 53.92 (s, C-7) 28.67(s, C-3 or 6); 27.02(s, C-3 or 6).

m/z (EI^+) 111($M^+ + H$, 9), 110(M^+ , 100), 109(47), 95(35), 94(26), 79(39), 77(36), 67(78), 65(37), 51(24), 41(58), 39(58).

All data consistent with the literature¹⁰².

4.2.16 Attempted epoxidation of 1-methoxycyclohexa-1,4-diene



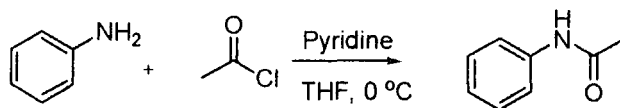
As per general procedures 4.1.2.

*m*CPBA (0.82 g, 4.8 mmol) was added to a stirred solution of 1-methoxycyclohexa-1,4-diene (0.52 g, 4.7 mmol) in DCM (30 cm³) at 0 °C. Reaction was left to stir overnight and warmed to room temperature. The reaction was quenched with sodium sulfite solution (10 mL, 10 % w/v). The organic layer was separated and washed with sodium hydroxide solution (3 × 20 mL, 10 % w/v).

The solvent was removed *in vacuo* and the isolated material was an unidentifiable mixture.

The *m*CPBA epoxidation was attempted with added sodium phosphate to buffer the reaction; as above, no identifiable product was isolated. The reaction was also attempted using dimethyldioxirane (DMD) as the oxidising agent and similarly an unidentifiable mixture was obtained.

4.2.17 N-Phenylacetamide (Acetanilide)



To a stirred solution of aniline (4.8 g, 0.052 mol) in dry THF (50 cm³) and dry pyridine (10 cm³, 0.12 mol), cooled on ice, acetyl chloride (4.5 mL, 0.055 mol) was added. The reaction was left to stir for two hours and then quenched with 5 % sodium bicarbonate. The product was extracted with ethyl acetate; the organic layers were combined and washed with sodium bicarbonate solution, dried over magnesium sulphate, filtered and

the solvent removed under reduced pressure. The product was isolated as a white powder.

δ_{H} (CDCl_3 , 400 MHz) 7.9(br s, 1H, NHC(O)CH_3); 7.5-7.1(br m, 5H, Ar- \underline{H}); 2.15(s, 3H, NHC(O)CH_3).

δ_{C} (CDCl_3 , 100 MHz) 169.06(s, NHC(O)CH_3); 138.22(C-1); 129.17(Ar-C); 124.53(Ar-C); 120.30(Ar-C); 24.73(NHC(O)CH_3).

All data consistent with the literature¹⁰⁶.

4.2.18 Attempted Birch reduction of N-phenylacetamide

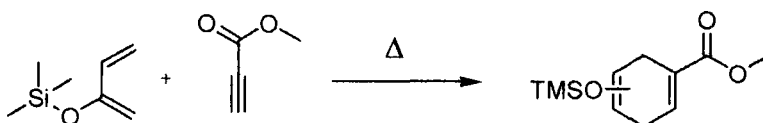


Adapted from procedures outlined in literature^{107, 108}.

Ammonia (150 mL) was condensed into a stirred solution of N-phenylacetamide (1.51 g, 0.010 mol) and ethanol (5 mL, 0.3 mol) in dry THF(40 mL). To this sodium (6.2 g, 0.27 mol) was added; the blue colour only appeared after vigorous stirring and disappeared after an hour. The ammonia was allowed to evaporate overnight, leaving a brown residue. Water (10 mL) was added slowly to the reaction vessel, followed by ethyl acetate (100 mL). The organic layer was washed with sodium bicarbonate (2 x 10 mL, 10 % (w/v)) and brine (2 x 10 mL) and then dried over magnesium sulphate, filtered and the solvent removed *in vacuo*

The isolated material was an unidentifiable complex mixture. The reaction was also attempted using NH_4Cl and *t*BuOH as the protonating agent, but neither reaction gave the desired product. The only identifiable product was a mono-substituted arene (either N-phenylacetamide or aniline).

4.2.19 Trimethylsiloxy-6-methylcarboxylate-cyclohexa-1,4-diene



The product was synthesised using the method outlined by Boyd and Berchtold¹⁰⁹.

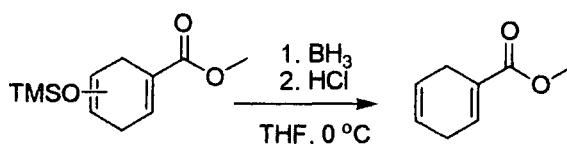
2-Trimethylsiloxy-1,3-butadiene (0.33 g, 2.3 mmol) and methyl propiolate (0.195 g, 2.3 mmol) were placed neat in a sealed container and heated for 1 hour at 150 °C under microwave conditions. Overall conversion to the cyclic product was 75% from NMR integration. Integration of the GC-MS trace showed the ratio of the 1,6 and 1,5 isomers formed to be 70:30.

The isomeric products were purified by column chromatography (silica gel, 95:5 petroleum ether, diethyl ether). The two isomeric products had an R_f of 0.65 with impurities at R_f equal to 0.95, 0.4, and 0.0. The cyclohexadienes were isolated with a yield of 43 % (1.2 g, 5.3 mmol).

δ_H (CDCl₃, 400 MHz) 6.9(br s, 1H, CH₃O₂C-C=CH); 4.9(br s, 1H, TMSO-C=CH); 3.75(s, 3H, CO₂CH₃); 3.1-2.8(m, 4H, 2 × CH₂) 0.20(m, 9H, OSi(CH₃)₃).

Characterisation consistent with literature^{109, 110}.

4.2.20 1-Methylcarboxylate-cyclohexa-1,4-diene



The product was synthesised using the method outlined by Boyd and Berchtold¹⁰⁹.

A solution of trimethylsiloxy-6-methylcarboxylate-cyclohexa-1,4-diene (0.70 g, 3.1 mmol) was added to dry THF (20 mL), under argon at 0 °C. To this, BH₃ in THF (2.2 mL, 1.0 M, 2.2 mmol) was added slowly. The reaction was stirred for 1 hour at room temperature. The hydride was then quenched slowly with water (0.5 mL). Then HCl solution (5 mL, 10 % (v/v)) was added and the reaction was left to reflux for 2.5 hours.

Diethyl ether (10 mL) was added to the worked reaction and the aqueous layer was extracted using diethyl ether (3 × 15 mL). The organic layer was washed with sodium bicarbonate (3 × 10 mL, 5 % (w/v)) and water (2 × 10 mL) and then dried over magnesium sulfate, filtered and the solvent removed under reduced pressure.

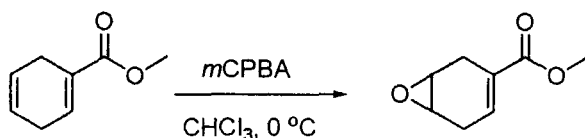
NMR showed removal of the trimethylsiloxy group from the Diels-Alder product. The product was purified by column chromatography (silica gel, 5:1 petroleum ether, diethyl ether) and isolated as a colourless liquid in a 51 % yield (0.22 g, 1.6 mmol).

δ_{H} (CDCl₃, 500 MHz) 6.99(s, 1H, CH₃CO₂C-C=CH); 5.72(m, 2H, HC=CH); 3.7(s, 3H, CO₂CH₃); 2.9(m, 4H, 2 × CH₂).

ν_{max} (cm⁻¹): 3034(C=C-H), 2950 (C-H), 1711(C=O), 1641, 1436, 1249, 1082, 652.

Data consistent with literature¹⁰⁹.

4.2.21 Methyl 7-oxa-bicyclo[4.1.0]hept-3-ene-3-carboxylate



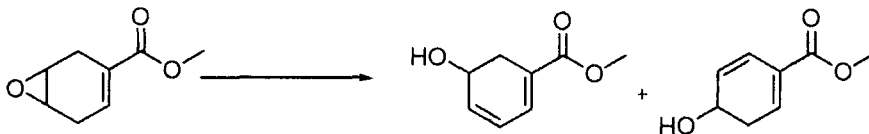
As per general procedure 4.1.2

*m*CPBA (0.13 g, 0.76 mmol) was added to a stirred solution of compound (0.084 g, 0.61 mmol) in chloroform (10 mL) at 0 °C. Reaction was left to stir overnight and warmed to room temperature. The white precipitate of the chloro-benzoic acid was filtered off and the product was purified by column chromatography (silica gel, 1:1 petroleum ether: diethyl ether) and isolated as a colourless oil (0.059 g, 63 %).

δ_{H} (CDCl₃, 500 MHz) 6.85(m, 1H, C=CH); 3.75(s, 3H, CO₂CH₃); 3.4(m, 1H, HCOCH); 3.2(m, 1H, HCOCH); 2.8(m, 2H, CH₂); 2.5(m, 2H, CH₂).

Characterisation consistent with the literature¹¹¹.

4.2.22 Attempted synthesis of methyl 5-hydroxycyclohexa-1,3-dienecarboxylate and methyl 4-hydroxycyclohexa-1,5-diene carboxylate

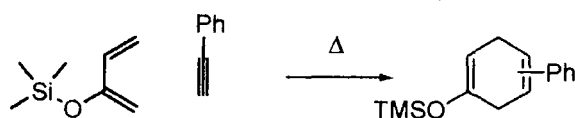


LDA(1.8 M, 0.8 mL, 1.44 mmol) was added to a stirred solution of methyl 7-oxa-bicyclo[4.1.0]hept-3-ene-3-carboxylate (0.10 g, 0.65 mmol) in diethyl ether (10 mL). The reaction was allowed to stir at -10 °C for four hours and then quenched with sodium hydroxide solution (2 mL, 10 % (w/v)) and water (2 mL). The aqueous phase was

washed with ether (3 × 20 mL), the organic layer was dried over magnesium sulphate, filtered and the solvent removed *in vacuo*.

The reaction mixture isolated was a complex mixture containing predominantly a mono-substituted arene. The hydrate was probably formed; however it appears to have aromatised under the reaction conditions. The reaction above was attempted using DBN as a base, outlined by McGowan and Berchtold¹¹¹; any future attempts should use a bulkier amine base.

4.2.23 (3 or 4-phenylcyclohexa-1,4-dienyloxy)trimethylsilane



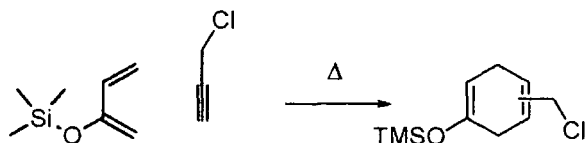
The reaction above was attempted using a similar procedure to that mentioned in section 4.2.21.

2-Trimethylsilyloxy-1,3-butadiene (1.42 g, 13.2 mmol) and phenylethyne (1.54 g, 15.0 mmol) were placed neat in a sealed container and heated for 2.5 hours at 125 °C at 100 watts under microwave conditions; however no reaction occurred.

The reaction was also attempted under reflux using acetic acid as a solvent. 2-Trimethylsilyloxy-1,3-butadiene (0.25 g, 1.7 mmol) and phenylethyne (0.19 g, 18.2 mmol) were added to acetic acid (6 mL) and the reaction mixture was heated at 78 °C for 24 hours. No reaction occurred.

The reaction was also attempted using a Lewis acid catalyst in dichloromethane. 2-trimethylsilyloxy-1,3-butadiene (0.25 g, 1.7 mmol) and phenylethyne (0.19 g, 18.2 mmol) were added to dry dichloromethane (15 mL). Aluminium chloride was added to this. The reaction was stirred at room temperature for two days. The reaction was quenched with sodium hydroxide (10 % (w/v), 5 mL), the aqueous layer was washed with dichloromethane (2 × 10 mL), the organic fractions were combined washed with water, dried over magnesium sulphate, filtered and the solvent removed *in vacuo*. No reaction occurred.

4.2.24 (3 or 4-(Chloromethyl)cyclohexa-1,4-dienyloxy)trimethylsilane

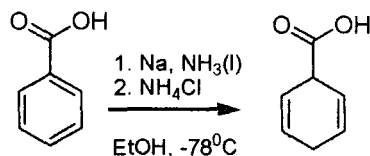


The above reaction was attempted using the procedure outlined in section 4.2.21 above. 2-trimethylsilyloxy-1,3-butadiene (0.089g, 1.2 mmol) and propargyl chloride (0.075 g, 1.2 mmol) were placed neat in a sealed container and heated for 1 hour at 125 °C at 100 watts under microwave conditions. No reaction occurred and only starting material was recovered.

The reaction was also attempted using a Lewis acid catalyst.

Aluminium chloride was added to a solution of 2-trimethylsilyloxy-1,3-butadiene (0.089g, 1.2 mmol) and propargyl chloride (0.075 g, 1.2 mmol) in dry dichloromethane. The reaction was left to stir at room temperature for two days. No reaction occurred.

4.2.25 Cyclohexa-2,5-dienecarboxylic acid



Procedure modified from general procedures 4.1.1 and literature.

Ammonia (200 mL) was condensed into a stirred solution of benzoic acid (5.24 g, 43 mmol) in ethanol (30 mL, 600 mmol, 14 equiv). To this, sodium (3.68 g, 160 mmol, 3.7 equiv) was added giving initially a green colour, followed by precipitation and some effervescence and then the formation of the standard blue colour. On disappearance of the blue colour ammonium chloride (8.2 g, 15.5 equiv) was added, the reaction was left to stir for one hour and then left overnight for the ammonia to evaporate. The reaction mixture was poured onto ice and acidified to approximately pH 1.5. The product was extracted with ether (4 × 100 mL). The ether was washed with brine and dried over magnesium sulphate, filtered and the solvent removed *in vacuo*. The product was used

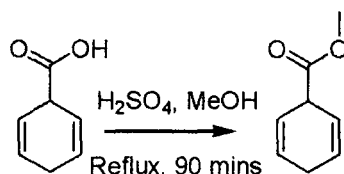
without any further purification. The product was isolated with a 90 % yield (4.72 g, 38 mmol).

δ_{H} (CDCl₃, 500 MHz) 5.85 (m, 4H, 2 × HC=CH); 3.80(br m, 1H, CHCO₂H); 2.71 (m, 2H, CH₂).

δ_{C} (CDCl₃, 125 MHz) 179.47(s, COOH); 127.61(s, C-2 & 6); 121.72(s, C-3 & 5); 41.74(s, C-1); 26.03(s, C-4).

All data consistent with literature^{108, 112, 113}.

4.2.26 Methyl cyclohexa-2,5-dienecarboxylate



The product was synthesised using the procedure outlined by Drew *et al*⁹¹.

Cyclohexa-2,5-dienecarboxylic acid (4.93 g, 0.040 mol) was heated under reflux in a solution of methanol (30 mL) and concentrated sulphuric acid (2.4 mL) for 90 minutes. The reaction mixture was diluted with deionised water and the product was extracted with diethyl ether (3 × 20 mL). The organic layer was washed with sodium bicarbonate (10 mL, 10 % (w/v)), water (10 mL) and brine (10 mL). The solvent was removed *in vacuo* to leave a yellow liquid. The product was purified by Kugel-Rohr was isolated as a colourless liquid in an 81 % yield (4.43 g, 0.032 mol).

δ_{H} (CDCl₃, 500 MHz) 5.81 (m, 4H, 2 × HC=CH); 3.70(br m, 1H, CHCO₂CH₃); 3.70 (s, 3H, COOCH₃); 2.68 (m, 2H, CH₂).

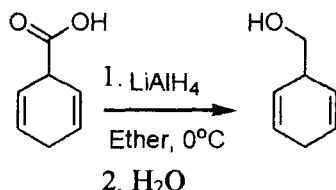
δ_{C} (CDCl₃, 125 MHz) 173.31 (COOCH₃); 126.68 (C-2 & 6); 122.32 (C-3 & 5); 52, 40 (COOCH₃); 41.91 (C-1); 26.02 (C-4).

m/z (EI⁺) 154 (M⁺, 25), 139(16), 105(16), 95(100), 93(24), 77(58), 67(28), 66(57), 65(59), 59(16), 51(41), 41(38), 39(52), 19(15).

ν_{max} (cm⁻¹): 2959(C-H), 1722(C=O), 1437, 1274, 1193, 1172, 1026, 940, 898, 788, 714, 674.

Characterization consistent with literature⁹¹.

4.2.27 2,5-Dihydrobenzoic Acid



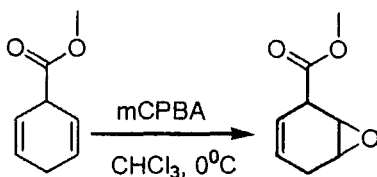
A solution of lithium aluminium hydride (5 mL, 2.4 M, 0.012 mol) in THF was added to a solution of cyclohexa-2,5-dienecarboxylic acid (2.08 g, mol) in dry ether (20 mL). The reaction was allowed to stir on ice for 1 hour and then quenched with water (2 mL). Diluted acid was added to dissolve the lithium salts and the product was extracted with diethyl ether (3 × 30 mL). The organic layer was washed with brine (1 × 20 mL), dried over magnesium sulphate, filtered and the solvent was removed *in vacuo* to leave a colourless liquid. The product was used without any further purification. The product was isolated in an 89 % yield (1.61 g, 0.015 mol).

δ_{H} (CDCl₃, 400 MHz) 5.82 (m, 2H, HC=CH-CH₂-HC=CH); 5.60(m, 2H, HC=CH-CH₂-HC=CH); 3.53 (d, 2H, CHCH₂OH); 2.92 (m, 1H, CHCH₂OH); 2.61(m, 2H,CH₂); 2.2-2.4 (br s, 1H, CH₂OH).

δ_{C} (CDCl₃, 100 MHz) 127 (C-2 & 6), 126 (C-3 & 5); 66 (C-7); 38 (C-1); 26 (C-4).

Data consistent with the literature¹¹⁴.

4.2.28 Methyl 7-oxa-bicyclo[4.1.0]hept-3-ene-2-carboxylate



The product was synthesised using a method outlined by Mah *et al*⁷⁵.

A solution of *m*CPBA(2.24 g, 0.013 mol) in chloroform was added slowly to a stirred solution of methyl cyclohexa-2,5-dienecarboxylate (1.81 g, 0.013 mol) in chloroform at 0 °C. The reaction mixture was allowed to warm to room temperature and left to stir for 15 hours. The solvent was concentrated under reduced pressure and the *meta*-chlorobenzoic

acid filtered off. The organic layer was washed with 10 % sodium sulphite, 10 % sodium bicarbonate and brine, dried over magnesium sulfate and the solvent was removed under reduced pressure leaving a yellow oil.

NMR analysis showed presence of two epoxide isomers and other impurities with a crude yield of 1.75 g (0.01 mol). The reaction mixture was purified by column chromatography (silica-gel, 25:75, petroleum ether; diethyl ether). The two epoxide diastereomers were isolated with a yield of only 31 % (0.61 g).

δ_{H} (CDCl₃, 500 MHz) 5.59 (m, 1H, HC=CH) 5.55 (m, 1H, HC=CH); 3.78 (s, 3H, CHCO₂CH₃); 3.65 (s, 1H, CHCO₂CH₃); 3.45 (1H, br s, HCOCH); 3.35 (1H, br s, HCOCH); 2.6-2.5 (m, 2H, CH₂).

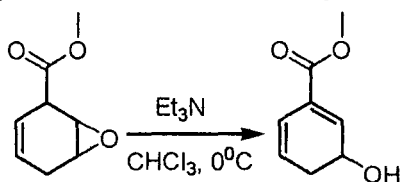
δ_{C} (CDCl₃, 500 MHz) 172 (C-7); 124 (C-5); 120 (C-6); 53 (C-8); 52 (C-2); 51 (C-3); 42 (C-1); 24 (C-4).

m/z (EI⁺) 154 (M⁺), 153(7), 139(7), 122(11), 111(10), 95(57), 94(49), 77(16), 68(20), 67.1(100), 66.1(60), 65(52), 59(30), 41.1(61), 39(61), 29(18), 27.1(12).

ν_{max} (cm⁻¹): 3500, (C=C-H); 2954 (C-C-H); 1732 (C=O), 1436(C=C); 1257 (C-OMe); 802.3 (epoxide C-O)

Characterisation consistent with the literature⁸⁶.

4.2.29 Methyl 3-hydroxycyclohexa-1,5-dienecarboxylate (2.1)



The procedure was adapted from the procedure outlined by Sirate et al⁷⁵.

Triethylamine (0.5 mL, 0.0036 mol) was added to a stirred solution of methyl 7-oxabicyclo[4.1.0]hept-3-ene-2-carboxylate (0.45 g, 0.0030 mol) in chloroform (20 mL). The reaction was allowed to stir for 40 minutes and then washed with copper sulphate (10 mL, 10 % (w/v) solution) to remove the triethylamine. The aqueous layer was washed twice with chloroform which in turn was washed with brine (10 mL). The solvent was

removed *in vacuo* and resulting purple liquid was purified by column chromatography (silica gel, 1:1 petroleum ether, diethyl ether). The product was isolated (0.403, 0.0026 mol, 90 %) as a yellow oil.

δ_{H} (CDCl₃, 500 MHz) 6.91 (m, 1H, HC=C); 6.45 (m, 1H, HC=H); 5.97(m, 1H, HC=CH); 4.46(m, 1H, CHOH); 3.78(s, 3H, CO₂CH₃); 2.5 (2H, m, CH₂); 2.03(m, 1H, OH).

δ_{C} (CDCl₃, 500 MHz) 166 (C-7); 135 (C-2); 129 (C-1); 126 (C-6); 121 (C-5), 64 (C-8); 52 (C-3); 31 (C-4).

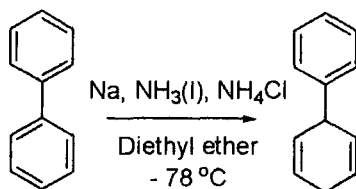
m/z (EI⁺) 154 (M⁺), 155(M⁺ + 1, 3), 153(10), 139(20), 123(18), 122(20), 121(16), 105(26), 95(100), 94(30), 93(26), 77(62), 67(40), 66(63), 65(54), 59(18), 51(22), 41(26), 39(30).

ν_{max} (cm⁻¹): 3416(O-H), 2952(C-H), 1711(C=O), 1437, 1250, 1083, 1025, 753, 714, 666.

λ_{max} = 228 nm ($\pi - \pi^*$)

Characterisation consistent with the literature⁷⁵.

4.2.30 1-(Cyclohexa-2,5-dienyl)benzene



Procedure adapted from literature.¹¹⁵

Ammonia (150 mL) was condensed into a stirred solution of biphenyl (2.69 g, 0.018 mol) in dry diethyl ether (30 mL). To this, sodium (1.46 g, 0.064 mol) was added giving initially a dark red colour, followed by a black colour. The reaction was allowed to stir for 20 minutes then ammonium chloride (3.60 g, 0.067 mol) was added. The reaction was left to stir for one hour and then left overnight to allow the ammonia to evaporate.

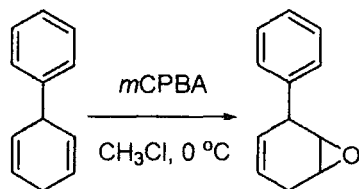
Magnesium sulphate was added to the reaction, the reaction mixture was filtered and the solvent removed *in vacuo*. The product was used without any further purification. The reaction mixture was isolated with a yield of 50 % (2.72 g, 0.02 mol).

δ_{H} (CDCl₃, 500 MHz) 7.34-7.36 (m, 2H, 2 × Ar-H); 7.22-7.29 (m, 3H, , 3 × Ar-H); 5.86(d *p*sext, ³J = 10.2 Hz, ⁴J = 2 Hz, 2H, HC=CH-CH₂-HC=CH); 5.77(d *p*quin, ³J = 10.2 Hz, ⁴J = 2 Hz, 2H, HC=CH-CH₂-HC=CH); 4.00 (1H, br m, CH-Ph); 2.85-2.7 (m, 2H, CH₂).

δ_{C} (CDCl₃, 125 MHz) 145.44(C-7); 128.81(C-2&6); 128.25(C-8&12); 127.52(C-9&11); 126.57(C-10); 124.00(C-3&5); 42.28(C-1); 26.10(C-4).

Data consistent with literature.^{77, 115, 116}

4.2.31 2-Phenyl-7-oxa-bicyclo[4.1.0]hept-3-ene



As per general procedures 4.1.2.

*m*CPBA (0.20 g, 1.13 mmol) was added to a stirred solution of 1-(cyclohexa-2,5-dienyl)benzene (2.62 g, 50 % aromatic, 8.39 mmol diene) in chloroform (100 mL) at 0 °C. Reaction was left to stir for two hours and quenched with sodium sulfite (10 mL, 10 % (w/v)). The organic layer was washed with sodium sulfite(3 × 10 mL) and brine (1 × 10 mL), dried over magnesium sulphate, filtered and the solvent removed *in vacuo*. The product was purified by column chromatography (silica gel, 4:1 petroleum ether: diethyl ether) and isolated as a colourless oil with a 79 % yield (1.14 g, 6.62 mmol).

δ_{H} (CDCl₃, 500 MHz): 7.31 (m, 5H, 5 × Ar-H); 5.64 (m, 2H, HC=CH); 3.90 (br s, 1H, CH-Ph); 3.37(br s, 1H, HCOCH); 3.24(br s, 1H, HCOCH); 2.7(m, 2H, CH₂).

δ_{C} (CDCl₃, 125 MHz): 140.8(C-7), 129.1(C-8 &12), 128.6(C-9 & 11), 127.4(C-10), 126(C-5), 121.8(C-4), 56.08 (C-1), 51.5(C-2), 42.4(C-6), 25.6(C-3).

m/z(EI): 172.1 (M⁺, 32), 171(17), 153(10), 144(42), 143(22), 142(12), 141(22), 129(30), 128(100), 115(56), 102(12), 91(28), 77(22), 65(22), 63(16), 51(24), 39(21).

ν_{max} (cm⁻¹): 3208, 2892, 1601, 1493, 1452, 885, 798, 749, 695.

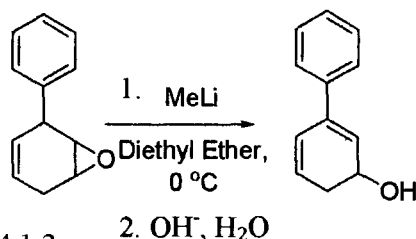
CHN: calculated: C: 83.69 % H:7.02 %. Found: C: 83.49 % H: 6.99 %.

Minor diastereomer:

δ_{H} (CDCl₃, 500 MHz): 7.39(5 ArH), 5.5 (m, 2H, C-4&5), 3.7(m, 1H, C-6), 3.4(m, 2H, C1 &2), 2.5(m, 2H, C-3).

δ_{C} (CDCl₃, 125 MHz): Distinguishable Carbons: 141(C-7), 129 (Ar C), 126(C-6), 122(C-5), 52(C-1), 41(C-2), 25(C-3).

4.2.32 3-Phenylcyclohexa-2,4-dienol (2.9)



As per general procedures 4.1.3.

Methyl lithium (1.5 mL, 1.6 M, 2.4 mmol) was added dropwise to a solution of 2-phenyl-7-oxa-bicyclo[4.1.0]hept-3-ene (0.10 g, 0.58 mmol) in dry diethyl ether (10 mL) on ice. The reaction was allowed to stir for 80 minutes and quenched with sodium hydroxide solution (2 mL, 10 % (w/v)). The aqueous layer was washed with diethyl ether (3 × 20 mL), the organic washings were dried over magnesium sulphate, filtered and the solvent removed *in vacuo*. The product was purified by rapid column chromatography (silica gel, 3:1 petroleum ether, diethyl ether) and isolated with a yield of 47 % (0.047 g, 0.27 mmol).

δ_{H} (CDCl₃, 500 MHz): 7.60(m, 1H, Ar-H (7)), 7.45(m, 2H, Ar-H (6 & 8)), 7.37(m, 2H, Ar-H (5 & 9)), 6.44(m, 1H, HC=CH), 6.21(m, 1H, HC=C-Ph), 6.08(m, 1H, HC=CH); 2.6(m, 2H, CH₂)

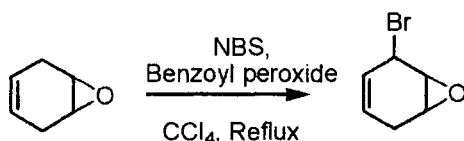
δ_{C} (CDCl₃, 125 MHz): 129.3(C-5 &9), 128.11(C-4), 127.3(C-7), 127.2(C-11), 126.3(C-6 & 8), 125.5(C-10), 123.7(C-2), 64.1(C-1), 32.6(C-12).

m/z: (EI): Aromatised under experimental conditions. (ES): Undetectable.

ν_{max} (cm⁻¹): 3351(O-H), 3034(C-H), 1597, 1478, 1430, 1307, 1202, 1007, 758, 737, 696.

CHN: calculated: C: 83.69 % H:7.02 %. Found: C: 83.29 % H: 6.96 %.

4.2.33 2-Bromo-7-oxa-bicyclo[4.1.0]hept-3-ene



N-Bromosuccinimide (NBS) (1.83 g, 10.3 mmol) was added slowly to a solution of 7-oxa-bicyclo[4.1.0]hept-3-ene (0.98 g, 10.2 mmol) in tetrachloromethane (20 mL). Benzoyl peroxide (0.010 g, 0.04 mmol) was added to initiate the reaction. The reaction mixture was left to stir under reflux overnight. The heavy yellow solid NBS was replaced by the lighter white precipitate of the succinimide. The reaction mixture was filtered, and the tetrachloromethane was distilled off under reduced pressure. The product was stored in freezer overnight to allow the dibrominated side product to crystallise out. The oil was removed from the crystals and further purified by column chromatography (silica gel, 1:1 petroleum ether, diethyl ether; then silica gel, 3:1 petroleum ether, diethyl ether). The product was isolated as a yellow liquid with a total yield of 50 % (0.865 g, 4.9 mmol).

Diastereomer 1:

δ_{H} (CDCl₃, 500 MHz): 5.75 (m, 1H, HC=CH), 5.52(m, 1H, HC=CH), 4.85(m, 1H, CH-Br), 3.56(br m, 1H, HCOCH), 3.41(br m, 1H, HCOCH), 2.65(dm, ²J_{HH} = 19 Hz, 1H, CH₂), 2.55(dm, ²J_{HH} = 19 Hz, 1H, CH₂').

δ_{C} (CDCl₃, 125 MHz): 124.8(C-6), 123.9(C-5), 53.9(C-1), 51.2(C-2), 42.7(C-3), 25.1(C-3).

m/z(EI): 176/174(M⁺, 22), 95(100), 67(90), 66(32), 65(60), 41(70), 39(68).

ν_{max} (cm⁻¹): 3000, 2362, 1722, 1650, 1426, 1346, 1254, 1213, 1150, 883, 794, 763, 731, 644.

Diastereomer 2:

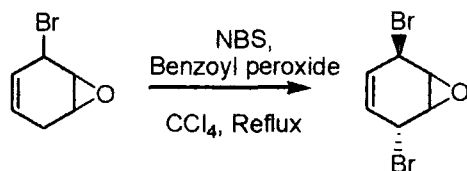
δ_{H} (CDCl₃, 500 MHz): 5.68(m, 1H, HC=CH), 5.55(m, 1H, HC=CH), 5.00(m, 1H, CH-Br), 3.60(br s, 1H, HCOCH), 3.54(m, 1H, HCOCH), 2.75(dm, ²J_{HH} = 20 Hz, 1H, CH₂), 2.40(dm, ²J_{HH} = 20 Hz, 1H, CH₂').

δ_{C} (CDCl₃, 125 MHz): 125.5(C-6), 125.0(C-5), 56.6(C-1), 54.7(C-2), 46.5(C-3), 25.8(C-3).

m/z (EI) 174/176(M^+ , 5), 119(10), 95(54), 81(20), 79(18), 67(92), 66(38), 65(58), 63(16), 51(21), 50(20), 41(54), 39(100), 38(28), 29(36), 27(20).

Characterisation consistent with the literature^{92, 93}.

4.2.34 2,5-Dibromo-7-oxa-bicyclo[4.1.0]hept-3-ene



This compound was isolated as the crystalline dibrominated side-product of the above reaction (see 4.2.34).

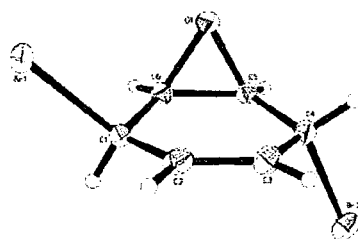
δ_H ($CDCl_3$, 500 MHz) 5.85(m, 1H, $\underline{H}C=CH$), 5.76(m, 1H, $HC=\underline{C}H$), 5.03(br s, 1H, $\underline{C}H$ -Br), 4.10(br d, 1H, $\underline{C}H$ -Br), 3.93(m, 1H, $\underline{H}COCH$), 3.71(m, 1H, $HCO\underline{C}H$).

δ_C ($CDCl_3$, 125 MHz) 126.38(C-5 or 6), 126.24(C-5 or 6), 59.11(C-1 or 4), 54.76(C-1 or 4), 43.29(C-2 or 3), 38.96(C-2 or 3).

m/z (EI): 256(2), 254(M^+ , 4), 252(2), 175(- Br, 74), 173(-Br, 72), 147(42), 145(43), 94(38), 66(82), 65(100), 63(16).

CHN: expected: C28.38 %, H2.38 %. Found: C28.68 %, H2.43 %.

Crystal structure (07srv009):

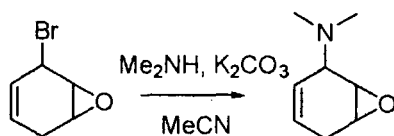


Crystal data and structure refinement for 07srv009.

Identification code	s009
Empirical formula	$C_6 H_6 Br_2 O$
Formula weight	253.93
Temperature	120(2) K

Wavelength	0.71073 Å	
Crystal system	Monoclinic	
Space group	P 2 ₁ /c	
Unit cell dimensions	a = 6.2301(2) Å	α = 90°.
	b = 8.3561(3) Å	β = 91.07(1)°.
	c = 14.0286(4) Å	γ = 90°.
Volume	730.19(4) Å ³	
Z	4	
Density (calculated)	2.310 Mg/m ³	
Absorption coefficient	11.014 mm ⁻¹	
F(000)	480	
Crystal size	0.26 x 0.10 x 0.08 mm ³	
Theta range for data collection	2.84 to 29.50°.	
Index ranges	-8 ≤ h ≤ 8, -11 ≤ k ≤ 10, -19 ≤ l ≤ 19	
Reflections collected	7183	
Independent reflections	2041 [R(int) = 0.0453]	
Completeness to theta = 29.50°	100.0 %	
Absorption correction	Numerical	
Max. and min. transmission	0.4383 and 0.1611	
Refinement method	Full-matrix least-squares on F ²	
Data / restraints / parameters	2041 / 0 / 107	
Goodness-of-fit on F ²	1.031	
Final R indices [I > 2σ(I)]	R ₁ = 0.0187, wR ₂ = 0.0450	
R indices (all data)	R ₁ = 0.0220, wR ₂ = 0.0456	
Extinction coefficient	0.0042(5)	
Largest diff. peak and hole	0.553 and -0.506 e.Å ⁻³	

4.2.35 N,N-Dimethyl-7-oxa-bicyclo[4.1.0]hept-3-en-2-amine



Adapted from procedure in literature¹¹⁷.

A solution of dimethylamine in THF (2M, 0.7 mL, 1.4 mmol) was added to a stirred solution of 2-bromo-7-oxa-bicyclo[4.1.0]hept-3-ene (0.057 g, 0.32 mmol) in acetonitrile

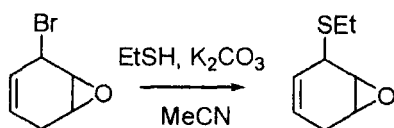
(5 mL). The solution was left to stir overnight at 0 °C and allowed to warm to room temperature. The product was purified by column chromatography (alumina, diethyl ether). The product was isolated as colourless oil with a yield of 0.032 g (73 %).

δ_{H} (CDCl₃, 500 MHz): 5.65(m, 1H, HC=CH), 5.5(m, 1H, HC=CH), 3.58(br s, 1H, CH-N(CH₃)₂), 3.27(br s, 1H, HCOCH), 3.21(br s, 1H, HCOCH), 2.57(dm, ²J_{HH} = 22 Hz, 1H, CH₂), 2.44(dm, ²J_{HH} = 22 Hz, 1H, CH₂). 2.34(s, 6H, N(CH₃)₂).

δ_{C} (CDCl₃, 125 MHz): 125.5(C-6), 121.0(C-5), 57.7(C-1), 52.8(C-2), 51.2(C-3), 41.6(C-7 & 8), 25.7(C-4).

m/z (EI): 139(22), 110(60), 94(37), 82(37), 71(24), 67(44), 65(21), 55(20), 44(27), 44, (28), 41.5(100), 39(35).

4.2.36 2-(Ethylthio)-7-oxa-bicyclo[4.1.0]hept-3-ene



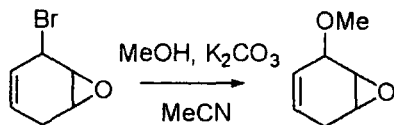
Ethanethiol (0.25 mL, 3.4 mmol) was added to a solution of 2-bromo-7-oxa-bicyclo[4.1.0]hept-3-ene in acetonitrile. Potassium carbonate (0.47 g, 3.4 mmol) was added quickly. The reaction was allowed to stir overnight. Magnesium sulphate was added and the reaction mixture was filtered. The solvent was removed *in vacuo*. Two regioisomers were formed and these were separated by column chromatography (Alumina, petroleum ether: ether 75:25 to 50:50). The compounds decomposed overtime to an unidentifiable mixture.

δ_{H} (CDCl₃, 500 MHz): 5.52 (m, 2H, HC=CH); 3.57(m, 1H, HCOCH); 3.48(m, 1H, HCSCH₂CH₃); 3.33(m, 1H, HCOCH); 2.74(m, 2H, HCSCH₂CH₃); 2.54(dm, 1H, ²J_{HH} = 20 Hz, HCH); 2.39(dm, 1H, ²J_{HH} = 20 Hz, HCH); 1.28(3H, m, HCSCH₂CH₃).

δ_{C} (CDCl₃, 125 MHz): 126(C-5 or 6), 124(C-5 or 6), 56(C-2), 53(C-3), 40(C-1), 24(C-4), 23(C-7), 15(C-8).

m/z; (EI): 156.1(M⁺, 4), 77(12), 67(100), 65(44), 51(12), 45(25), 41(48), 39(70), 29(35), 27(52).

4.2.37 2-Methoxy-7-oxa-bicyclo[4.1.0]hept-3-ene



A solution of 2-bromo-7-oxa-bicyclo[4.1.0]hept-3-ene (0.15 g, 0.88 mmol) in acetonitrile was added to a mixture K_2CO_3 (0.12 g, 0.88 mmol) in acetonitrile (5 mL). The mixture was allowed to stir for 2 minutes; then methanol (5 mL) was added. The reaction was allowed to warm to room temperature and left to stir for 100 hours. After 24 hours methanol (2.5 mL) was added. On completion, magnesium sulphate was added and the reaction mixture was filtered. The solvent was removed *in vacuo*. The product was purified by column chromatography (silica gel, 1:1 petroleum ether, diethyl ether). The product was isolated as a colourless liquid (0.072 g, 0.57 mol, 65 % yield). The product decomposed overtime.

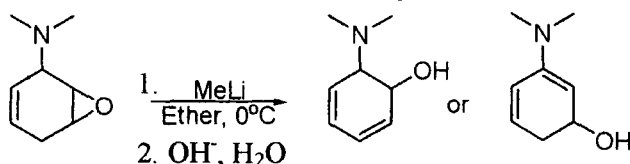
δ_H ($CDCl_3$, 500 MHz) 5.57 (m, 2H, $\underline{HC=CH}$); 4.17 (br s, 1H, $\underline{HC-OCH_3}$); 3.55 (br s, 1 H, \underline{HCOCH}); 3.50 (s, 3 H, \underline{HCOCH}); 3.40 (br s, 1 H, $\underline{HC-OCH_3}$);

δ_C ($CDCl_3$, 125 MHz) 124.5(C-6), 124.7(C-5), 73.2(C-1), 56.0(C-2), 52.9(C-3), 50.7(C-7), 25.4 (C-4).

m/z ; (EI): 126(M^+ , <1), 77(8), 67(20), 65(20), 55(18), 53(20), 50(16), 41(30), 39(86), 29(100), 27(34). (ES): 149.5 ($M^+ + Na$)

HRMS: ($M^+ + Na$) 149.05728

4.2.38 Attempted synthesis of dimethylaniline hydrate

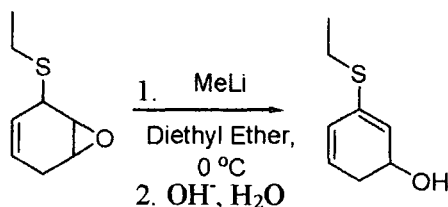


As per general procedures 4.1.3.

Methyl lithium (0.2 mL, 1.6 M, 0.3 mmol) was added dropwise to a solution of N,N-dimethyl-7-oxa-bicyclo[4.1.0]hept-3-en-2-amine (0.03 g, 0.2 mmol) in dry diethyl ether (10 mL) on ice. The reaction was allowed to stir for 80 minutes and quenched with sodium hydroxide solution (2 mL, 10 % (w/v)). The aqueous layer was washed with diethyl ether (3 × 10 mL), the organic washings were dried over magnesium sulphate,

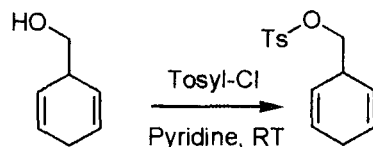
filtered and the solvent removed *in vacuo*. The only products isolated were phenol and dimethylaniline.

4.2.39 Attempted synthesis of ethylphenylsulfide hydrate



Methyl lithium (0.2 mL, 1.6 M, 0.3 mmol) was added dropwise to a solution of 2-(Ethylthio)-7-oxa-bicyclo[4.1.0]hept-3-ene (0.03 g, 0.2 mmol) in dry diethyl ether (10 mL) on ice. The reaction was allowed to stir for 80 minutes and quenched with sodium hydroxide solution (2 mL, 10 % (w/v)). The aqueous layer was washed with diethyl ether (3 × 10 mL), the organic washings were dried over magnesium sulphate, filtered and the solvent removed *in vacuo*. The reaction mixture was isolated as a brown oil and the only products that could be identified were phenol and ethyl phenyl sulfide.

4.2.40 (Cyclohexa-2,5-dienyl)methyl 4-methylbenzenesulfonate



Tosyl chloride (8.61 g, 45.3 mmol) was added to a solution of 2,5-dihydrobenzyl alcohol (4.51 g, 41 mmol) and pyridine (3 mL, 37.1 mmol) in dichloromethane (100 mL). The reaction was monitored by TLC and allowed to stir for 26 hours. The reaction was quenched with water (20 mL) and the organic layer was washed with sodium bicarbonate (3 × 20 mL) and brine (2 × 20 mL). The organic layer was dried over magnesium sulphate, filtered and the solvent removed *in vacuo*. The product was purified twice by column chromatography (silica gel), firstly with ether as the sole eluent, then secondly on silica with a gradient of petroleum ether: diethyl ether. The product was isolated as a colourless oil with a yield of 61 % (6.52 g, 24.7 mmol).

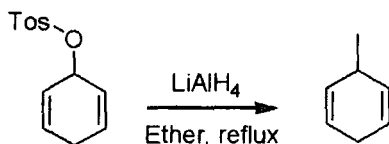
δ_{H} (CDCl₃, 500 MHz) 7.76(d, 2H, Ar-H(8 &9)); 7.32 (d, 2H, Ar-H (10&12)); 5.7(m, 2 H, HC=CH-CH₂-HC=CH); 5.5(m, 2H, C HC=CH-CH₂-HC=CH); 3.89(m, 2 H, CH-CH₂-OTs); 3.05 (br m, 1 H, CH-CH₂-OTs); 2.61(m, 2 H, HC=CH-CH₂-HC=CH); 2.42(s, 3H, Ar-CH₃).

δ_{C} (CDCl₃, 125 MHz) 145.04(C-11); 133.22(C-8); 129.99(C-12&10); 128.14(C-2&6); 127.30(C-9&13); 123.91(C-3&5); 73.66(C-7); 35.53(C-1); 26.49(C-4); 21.89(C-14).

ν_{max} (cm⁻¹): 3361(br), 1649(br), 1435, 1317, 1011, 950.

Data consistent with the literature¹¹⁴.

4.2.41 3-Methylcyclohexa-1,4-diene



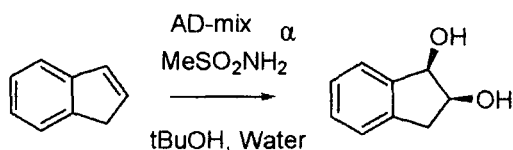
Procedure from literature¹¹⁸.

A solution of (cyclohexa-2,5-dienyl)methyl 4-methylbenzenesulfonate (3.65 g, 13.8 mmol) in THF was added slowly via cannula to a solution of lithium aluminium hydride (8 mL, 19.2 mmol) in THF at 0 °C. The reaction was allowed to warm to room temperature and left to stir for two days. The reaction was cooled and the 2 mL water was added slowly, then sodium hydroxide (2 mL, 30 % (w/v)) and then water (6 mL) and the mixture was filtered.

The residue was washed with diethyl ether (3 x 50 mL) and the solvent removed slowly at reduced pressure. The product was purified through a silica plug to remove any residual salts. The product was isolated with a yield of approximately 10 % (0.12 g, 1.27 mmol).

Scale-up was attempted; however none of these attempts proceeded with a high enough yield to continue with the proposed synthesis.

4.2.42 (1R,2S)-2,3-Dihydro-1H-indene-1,2-diol



AD-mix- α (12.02 g) and MeSO_2NH_2 (1.01g, 0.011 mol) were added to a stirred solvent system of *tert*-butanol (20 mL) and water (20 mL). The mixture was left to stir a room temperature until a yellow solution was seen. The solution was then cooled and the indene (1.20 g, 10.4 mmol) was added. The reaction was left to stir over 4 hours and monitored by TLC.

Sodium sulfite was added to quench the reaction and the reaction was allowed to warm to room temperature and stirred for 45 minutes. The product was extracted using dichloromethane, and this was washed with potassium hydroxide solution (10 mL, 2M). The organic layers were dried over magnesium sulfate and the solvent removed *in vacuo*.

The diol was purified by recrystallisation from a hexane/dichloromethane and filtered while still hot to remove impurities. The diol was isolated (1.09 g) with a 90 % yield.

δ_{H} (CDCl_3 , 500 MHz) 7.36(m, 1H, Ar-H (8)); 7.24(m, 3H, Ar-H (5,6 &7)); 4.87(m, 1H, CHOH (1)); 4.35(m, 1H, CHOH (2)); 3.03(dd, 1H, $^2J_{\text{HH}}=16.4$ Hz, 3J 5.75 CH₂); 2.88 (dd, 1H, $^2J_{\text{HH}}=16.4$ Hz, 3J = 3.6 Hz, CH₂).

δ_{C} (CDCl_3 , 125 MHz) 142.22(C-4); 140.43(C-9); 128.99(C-8); 127.37(C-5); 125.57(C-6); 125.32(C-7); 76.17(C-1); 73.68(C-2) 38.71(C-3).

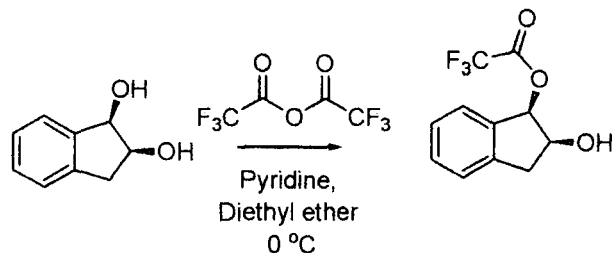
m/z (EI): 150(M^+ , 46), 132(90), 119(32), 107(52), 105(28), 103(100), 93(12), 91(48), 89(14), 79(38), 78(38), 77(52), 65(38), 63(18), 51(36), 50(14), 39(22).

ν_{max} (cm^{-1}): 3520 (O-H), 3436 (O-H), 3296, 2924, 1459, 1430, 1320, 1155, 1104, 1050, 987, 734, 635.

(ES): 173.1(M^+ + Na).

CHN Calculated, C: 71.98 %, H: 6.71 % found C: 71.65 %, H: 6.69 %.

4.2.43 2,3-Dihydro-2-hydroxy-1H-inden-3-yl-trifluoroacetate



Trifluoroacetic anhydride (50 μL , 0.4 mmol) was added slowly to a solution of (1R,2S)-2,3-dihydro-1H-indene-1,2-diol (0.05g, 0.3 mmol) and dry pyridine (50 μL , 0.6 mM) in dry diethyl ether (10 mL) at 0 $^{\circ}\text{C}$. The solution was allowed to stir for 40 minutes and then quenched with sodium carbonate (10 % (w/v), 2 mL). The organic layer was washed with copper sulphate solution (10 % w/v, 5 mL) and water. The organic layer was dried over magnesium sulphate, filtered and the solvent removed *in vacuo*.

The ester was purified by rapid column chromatography (silica gel, 9:1 chloroform petroleum ether then 100 % diethyl ether). The desired product eluted in the fourth fraction ($R_f = 0.8$). The product was isolated as a yellow oil in a 25 % yield (20 mg, 0.08 mMol.). A further fraction isolated ($R_f = 0.5$) showed 3 major side-products, detailed below.

Product (2,3-dihydro-2-hydroxy-1H-inden-3-yl-trifluoroacetate):

δ_{H} (CDCl_3 , 400 MHz) 7.40(m, 2H, Ar-H (6 & 7)); 7.30(m, 2H, Ar-H (5 & 8)); 6.36(d, $^3J_{\text{HH}} = 5.4$, CHOC(O)CF₃); 5.35(pq, $^3J_{\text{HH}} = 5.4$, CHOH); 3.35(m, 2H, CH₂).

δ_{C} (CDCl_3 , 100 MHz) 139(C(O)CF₃), 134.6(C-4 or 9), 134.5(C-4 or 9), 131(C-8), 128(C-5), 126(C-6 or 7), 125(C-6 or 7), 115(CF₃), 78(C-1), 76(C-2), 35(C-3).

δ_{F} (CDCl_3 , 376 MHz) – 75.4 (d, $^2J_{\text{CF}} = 12.3$ Hz).

m/z (EI): 246(M^+), 228(26), 132(100), 119 (14), 115(20), 105(20), 103(80), 91(35), 79(12), 78(26), 77(42), 69(28), 65(22), 63(12), 51(24), 39(12).

m/z (ES): Molecular ion not seen, 69 (CF_3^-), 113 (OCOCF_3).

Side-product 1: (2,3-dihydro-1-hydroxy-1H-inden-2-yl-trifluoroacetate)

δ_{H} (CDCl_3 , 500 MHz) 7.4 (m, 5H, Ar-H), 6.12 (d, $^3J = 5.2$, 1H, CHOH); 4.7(pq, 1H, $^3J = 5.2$, CHOC(O)CF₃); 3.2(m, 1H, CH₂); 3.0 (m, 1H, CH₂).

δ_{C} (CDCl₃, 125 MHz) 141.8(C-3), 136(C-8), 128(4C, C-4, 5, 6 & 7), 115.8(d, J = 8 Hz, CF₃), 81.5(C-2), 72.8(C-1), 38.6(C-9).

m/z(EI) 246(M⁺, 4), 228(34), 132(M⁺-OCOCF₃, 100), 119(21), 115(32), 105(28), 103(82), 91(40), 79(20), 78(30), 77(42), 69(CF₃, 32), 65(32), 63(18), 51(28), 39(18).

(ES): Molecular ion not seen, 69 (CF₃⁻), 113 (OCOCF₃).

Side-product 2: (*cis*-1,2-Dihydroxyindane Carbonate)

δ_{H} (CDCl₃, 500 MHz) 7.4 (m, 4H, Ar-H), 5.75(d, 1H, ³J_{HH} = 5.5 Hz, CHOC(O)OCH), 5.31(t, ³J_{HH} = 5.5, CHOC(O)OCH), 3.3(m, 2H, CH₂).

δ_{C} (CDCl₃, 125 MHz) 140.5, 139.5, indistinguishable carbons, 85.7 (C-2), 75.1 (C-10), 35.8 (C-9)

m/z(EI) 176 (M⁺, 10), 175(M⁺-H, 92), 133(M⁺-CO₂, 86), 131(30), 115(33), 104(42), 102(40), 91(12), 78(22), 77(42), 51(14), 43(CO₂, 100).

As per literature⁸⁵.

Side-product 3 (Unknown)

δ_{H} (CDCl₃, 500 MHz) 7.4(m, Ar-H), 5.6 (pq, J = 5.6, 1H), 5.3(d, J = 5.2 1H), 3.3(m, 2H).

δ_{C} (CDCl₃, 125 MHz) 140.9, 138, indistinguishable carbons, 113.5(d, J = 9 Hz, CF₃), 86.4, 79.8, 75.1, 37.7.

m/z (EI) 229(M⁺, 12), 228(64), 131(M⁺ - OCOCF₃, 100), 115(98), 103(64), 91(18), 77(22), 69(48).

13C: Unidentified double quartet: 157 ppm, J = 16, 40 Hz.

¹⁹F NMR: δ_{F} (CDCl₃, 376 MHz) -75.1(d, J = 23 Hz); -85.7(s); -85.9(s).

ν_{max} (cm⁻¹): ~3318 (O-H); ~2900 (C-H); 2359, 1782 (C=O); 1330, 1152, 1060, 1017, 987, 750. 634.

4.2.44 Preparation of lithium trichloroacetate

The solution was prepared as outlined by Amyes.¹¹⁹

Experimental

Trichloroacetic acid (52.5 g, 0.32 mol) was dissolved in ice-cold water. Lithium hydroxide monohydrate (12.4 g, 0.30 mol) was added slowly. The solution was allowed to stir for 10 minutes to ensure the salts had dissolved. The excess trichloroacetic acid was extracted with diethyl ether (5 x 50 mL). The aqueous solution was filtered through sintered glass and the water was removed *in vacuo* with the water bath at 70°. The salts were dried under vacuum over four days.

Elemental: expected C: 14.19, H: 0.00, Cl: 62.82. Found C 14.08, H: 0.00, Cl: 61.13.

4.3 General Information

4.3.1 Materials and preparation of solutions

Deuterium oxide (99.9 % D) was purchased from Apollo Scientific Ltd. Deuterated perchloric acid (60 %, 99.5 % D) and deuterated chloroform (99.8 % D) were purchased from Aldrich Chemical company. Acetonitrile-d₃ (99 % D), acetone-d₆ (99 % D) and sodium deuterioxide (40 wt % 98+ %D) were purchased from Cambridge Isotope Labs.

All commercially available reagents were used as received, from their respective suppliers. Solvents were dried using an appropriate drying agent when required: diethyl ether, THF and DCM were dried on the solvent purification system by literature techniques. Dry ethanol was prepared by refluxing over magnesium turnings and iodine followed by distillation. Water and H₂O refer to high purity water with conductivity of 18 mΩ obtained from the 'Milipore' purification system.

Thin-layer chromatography was carried out on neutral aluminium oxide plates (Merck Art 5550) or silica plates (Merck 5554), both visualised under UV irradiation (254 nm), potassium permanganate, or iodine staining. Preparative column chromatography was carried out using neutral aluminium oxide (Acros Aluminium Oxide 50-200 micron) or silica gel (Fluorochem silica gel, 40-63 micron).

Stock solutions of perchloric acid were prepared by dilution and titration of the commercial concentrated solutions. Stock solutions of sodium phosphate (Na₂HPO₄ and NaH₂PO₄) were prepared by dissolving dry commercial samples of Na₂HPO₄ and NaH₂PO₄ in distilled, deionised Millipore water to a final concentration of 1 M. Phosphate buffers were then prepared by mixing the stock solutions of Na₂HPO₄ and NaH₂PO₄ in water with addition of NaClO₄ to give solutions of buffer at various acid/base ratios and I = 0.5 (NaClO₄). Acetate buffers were prepared by dissolving suitable proportions of 1M sodium acetate and 1M acetic acid in distilled deionised Millipore water using NaClO₄ to maintain an ionic strength of 0.5. The buffer dilutions used were 0.2, 0.1, 0.05 and 0.025 M.

Stock solutions of sodium acetate were prepared by dissolving the dry commercial sample in distilled, deionised Millipore water to a final concentration of 1 M. Stock solutions of acetic acid were prepared by dilution and titration of the commercial concentrated solutions. Acetate buffers were then prepared by mixing the stock solutions of sodium acetate and perchloric acid in water with the addition of NaClO₄ to give solutions with 90 and 75 % free base (FB) and I = 0.5 (NaClO₄). Further acetate buffers were prepared by mixing the stock solution of sodium acetate with diluted acetic acid in water with the addition of NaClO₄ to give 0.5 M solutions with 50, 25 and 10 % FB and I = 0.5 (NaClO₄). The solutions were diluted to 0.2, 0.1, 0.05 and 0.025 M.

Stock solutions of sodium deuterioxide and deuterated perchloric acid were prepared by dilution and titration of the commercial concentrated solutions. Stock solutions of buffers, Na₂DPO₄ and NaD₂PO₄, were obtained from sodium phosphate monobasic and dibasic by exchanging the hydrogen atoms for deuterium. This was achieved by dissolving the salts in D₂O, followed by removal of solvent under reduced pressure. The process was repeated five times and the salts were freeze dried. Phosphate buffers were prepared by mixing stock solutions of Na₂DPO₄ and NaD₂PO₄ in D₂O with addition of NaClO₄ to give solutions of buffer at various acid/ base ratios and I = 0.5 (NaClO₄).

The internal standards for the ¹H NMR kinetics were prepared by accurately weighing either methanol or sodium 3-(trimethylsilyl)propanoate and accurately transferring sodium perchlorate solution (500 µL, 0.5 M in D₂O) to this by microlitre syringe to give a final concentration of 1 M.

The substrate solutions for the ¹H NMR kinetics were prepared by accurately weighing the substrate to be analysed and accurately transferring deuterated acetonitrile (500 µL) to this by microlitre syringe to give a final concentration of 100 mM. For the UV-Vis kinetics, the substrate solutions were prepared by accurately weighing the substrate to be analysed directly into a volumetric flask (5 mL) and acetonitrile was added to this to give

a final concentration of approximately 50 mM. The substrate stock solution was diluted as appropriate.

4.3.2 pH Measurement

The pH of buffered solutions was determined at 25 °C using a MeterLab™ PHM 290 pH-Stat Controller equipped with a radiometer (pH 4 - 7 - 10 @ 25 °C) combination electrode (type pHC4006) with a saturated calomel solution as reference, the filling solution used was a saturated solution of lithium trichloroacetate solution as described by Hershlag et al¹²⁰.

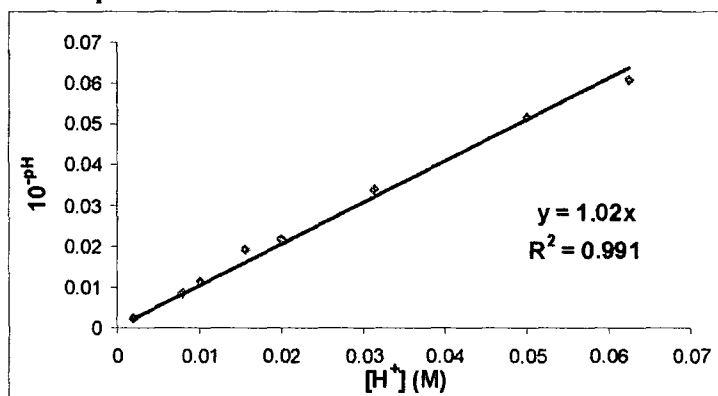
The filling solution of the pH electrode was exchanged from a saturated KCl solution to a saturated lithium trichloroacetate (LiTCA) solution. The LiTCA was prepared as described in section 4.2.44. A saturated solution (~5 M) was prepared using Millipore water. The saturated KCl was removed carefully from the probe and all traces of KCl were removed by careful washing using Millipore water. The saturated LiTCA solution was added and the probe was allowed to stand for 1 hour. This solution was replaced 5 times, allowing the probe to stand for 5 minutes between each washing. After the final solution of LiTCA was added the probe was allowed to stand in pH 1 buffer overnight and then calibrated as described below.

The pH meter was calibrated with standard buffer solutions of pH values 4.00 (phthalate buffer), 7.0 (phosphate buffer) and 10 (borate buffer). For calibration at lower pHs, a 0.1 M solution of HCl in KCl was freshly made and used, as described by Amyes¹¹⁹.

$$[\text{H}_3\text{O}^+] = 10^{-\text{pH}/\gamma_{\text{H}}} \quad \text{Equation 4-1}$$

The hydronium ion concentration at any pH was calculated using equation 4.1, where $\gamma_{\text{H}} = 1.0$ is the apparent activity coefficient of hydronium ion under our experimental conditions (see Figure 4.3-1). To determine a value for γ_{H} , a series of dilutions of standardised 1M HClO₄ were made to give a titrimetrically known series of HClO₄ solutions in the concentration range 0.001 – 0.1 M at ionic strength 0.5 (NaClO₄). The anti-logarithm of the pH was plotted against hydronium ion concentration. The slope of this plot is equal to the activity coefficient.

Figure 4.3-1: Plot of anti-log of pH against hydronium ion concentration where the slope is the activity coefficient of the pH electrode.



4.3.3 NMR spectroscopy

NMR samples were prepared in deuterated chloroform, deuterium oxide and d_6 -acetone. Tetramethylsilane (TMS) was used as an internal reference in deuterated chloroform. In University College Dublin, ^1H NMR and ^{13}C NMR spectra were recorded on Oxford Varian Unity Inova 300 MHz NMR spectrometers (^1H at 299.908 MHz, ^{13}C at 75.412 MHz). In the University of Durham, ^1H and ^{13}C NMR spectra were recorded on a Varian Mercury 200 (^1H at 199.975 MHz, ^{13}C at 50.289 MHz), Varian Unity 300 (^1H at 299.908 MHz, ^{13}C at 75.412 MHz), Varian Mercury 400 (^1H at 399.97 MHz, ^{13}C at 100.57 MHz), on a Bruker Advance 400 spectrometer (^1H at 400.13 MHz, ^{13}C at 100.61 MHz) and on an Oxford Varian Inova-500 (^1H at 499.78 MHz, ^{13}C at 125.67 MHz). ^1H and ^{13}C NMR chemical shifts in CDCl_3 are reported relative to CHCl_3 at 7.27 ppm and 77.0 ppm respectively. In D_2O ^1H NMR chemical shifts are reported relative to HOD at 4.67 ppm unless otherwise stated. In d_6 -acetone, ^1H NMR chemical shifts are reported relative to d^5 -acetone at 2.17 ppm respectively. All chemical shifts are given in ppm and coupling constants in Hz. Splitting patterns are described as singlet (s), doublet (d), double-doublet (dd), triplet (t), quartet (q), double multiplet (dm), pseudo quartet (pq) or multiplet (m).

4.3.4 HPLC

Reverse phase HPLC analysis were performed at 298 K on a Perkin Elmer System using a 4.6 x 250 mm 5μ Thermo ODS Hypersil analytical column at a flow rate of 1 mL/min

using a ratio of acetonitrile to water of 80:20. The reagents were detected using a diode array UV-Vis detector operating at 280 nm and 260 nm.

4.3.5 Mass spectrometry

Mass spectra were obtained from the Mass Spectroscopy Unit, Chemistry Department, Durham University. All electro ionisation (EI) spectra were run on a Thermo Finnegan Trace GC-MS with an injection temperature of 220 °C, a helium carrier gas, a Phenomenex Zebron column (5 % phenyl, 30 m × 0.25 mm) and a 0.25 µm filter. The program ran for 40 minutes with the temperature increasing by 10 °C per minute until a maximum temperature of 300 °C was reached. Low resolution electrospray (ES) mass spectra were run on a Thermo Finnegan LTQ and high resolution ES mass spectra were run on a Thermo Finnegan LTQ FT.

Elemental analyses were obtained from the Microanalytical Unit, Chemistry Department, UCD, and from the Microanalytical Unit, Chemistry Department, Durham University.

4.3.6 NMR Kinetics

The deuterated buffers were prepared as detailed above. A typical experiment involved accurately transferring by microlitre syringe buffer/dilute acid solution (890 µL) to a reaction vial. To this solution internal standard stock solution (10 µL) was added. Substrate stock solution (100 µL) was added to the buffered solution and mixed vigorously. An aliquot of the reaction mixture (750 µL) was transferred to an NMR tube and the reaction was followed by ¹H NMR spectroscopy *in situ*.

¹H NMR spectra of the solution dehydration reactions of cumene and toluene hydrates and the isomerisation of indene diol (3.13 M) were recorded on a Oxford Varian Inova 500 spectrometer with a relaxation delay of 18 s, sweep width of 7996.8 Hz, and acquisition time of 6 s, and a 90° pulse angle. Spectra were run with 32 transients with a total acquisition time of 12 minutes 32 seconds.

¹H NMR spectra of the dehydration reaction of methyl benzoate hydrate, the synthesis of benzene oxide and the racemisation of indene diol (0.1 and 1.0 M) were recorded on a Oxford Varian Inova 400 spectrometer with a relaxation delay of 18 s, sweep width of 7996.8 Hz, and acquisition time of 6 s, and a 90° pulse angle. Spectra were run with 32 transients with a total acquisition time of 12 minutes 32 seconds.

4.3.7 UV-Vis Spectroscopy

For UV-Vis spectrophotometric analyses both Cary 100 and Cary 50 spectrophotometers were used. Both operated in the 190 -800 nm range using deuterium and tungsten lamps as light sources and could work in single and multiple wavelength monitoring modes. Quartz cuvettes (1 cm, 3 mL) fitted with teflon caps were used and the temperature in the cell compartment was maintained at 25.0 ± 0.1 °C by circulating water from a thermostatted water bath.

A typical kinetics run was carried out by accurately pipetting 3 mL of buffer into a 3 mL cuvette, allowing it to equilibrate at 25 °C. The reaction was initiated by addition of the substrate stock solution (30 µL) by microlitre syringe. The reaction mixture was mixed by inverting the cuvette three times. The cuvette was then inserted into the spectrophotometer; which was equilibrated at 25.0 ± 0.1 °C, the collection of the absorbance versus time data was started at this point.

4.3.8 Data Analysis

The results obtained were analysed using the statistics software Sigma-plot (Version 8.02). The absorbance versus time data were fitted to a single exponential equation (Equation 6-2) and the double exponential equation (Equation 2-3).

$$y = y_0 + Ae^{-bx} \quad \text{Equation 4-2}$$

$$y = y_0 + Ae^{-bx} + Ce^{-dx} \quad \text{Equation 2.3}$$

The first order rate constants are b and d in the equations above. The accuracy of the estimate of k_{obs} was determined using three methods. The t-value is the ratio of the regression coefficient to its standard error, the independent variable. In this case, k_{obs} (b & d above) can be used to predict the dependent variable (i.e., that the coefficient is not zero) if t is large. The P-value is the probability of being wrong in concluding that the coefficient is not zero; the smaller the P-value, the greater the probability that the coefficient is not zero. The standard error of the estimate is a measure of the actual variability about the regression plane of the underlying population. The underlying population generally falls within about two standard errors of the observed sample.

The first order rate constant was also obtained from the slope of the semi-logarithmic plot of the change in absorbance against time ($\ln(A_t - A_\infty)$ against time). Reactions were typically followed for approximately 10 half-lives so as to accurately estimate A_∞ and the fit to a straight line.

The kinetic reactions were generally followed at the λ_{max} of the reactants and where possible the kinetic reactions were followed for both the appearance of products and the disappearance of the reactants.

The overall rate of the reaction at any particular pH was determined by the two methods; firstly the mean of the data was determined using Equation 4.4. Also, k_{int} was determined from the intercept of the plot of k_{obs} against buffer concentration at a fixed pH.

$$\bar{x} = \frac{1}{n} \sum_{i=1}^n x_i \quad \text{Equation 4-3}$$

The least squares analysis using equations 4.2 & 4.3 were compared with the results from the semi-logarithmic plot using paired and unpaired t-tests. A t-test determines if the mean values of two sets of data are significantly different by testing the hypothesis that the means of the data are equal. Sigma-Plot[®] uses the following equations to calculate t. Equation 4.5 is for the paired t-test

$$t = \frac{\bar{D}}{S_{\bar{D}}} \quad \text{Equation 4-4}$$

Where

$$\bar{D} = \bar{x} - \bar{y} \quad \text{Equation 4-5}$$

and

$$S_{\bar{D}} = \frac{\sqrt{\sum D_i^2 - \frac{(\sum D_i)^2}{n}}}{n(n-1)} \quad \text{Equation 4-6}$$

Where

$$D_i = x_i - y_i \quad \text{Equation 4-7}$$

Equation 6.10 is for the unpaired t-test:

$$t = \frac{\bar{D}}{\sqrt{\frac{1}{n_1} + \frac{1}{n_2}} \sqrt{\frac{\sum x_1^2 - n_1 \bar{x}^2 + \sum y_1^2 - n_2 \bar{y}^2}{n_1 + n_2 - 2}}} \quad \text{Equation 4-8}$$

Where

$$\bar{x} = \sum_{i=1}^{n_1} x_i \quad \& \quad \bar{y} = \sum_{i=1}^{n_2} y_i \quad \text{Equation 4-9}$$

The second-order rate constants were determined as the slopes of the plots of k_{obs} and k_{int} against acid concentration.

4.3.9 Measurements in Concentrated Acid Media

Rate constants for the isomerisation of indene diol were measured in concentrated perchloric acid solution. The second-order rate constant was obtained from the intercept of a plot of $\log(k_{\text{obs}})$ against the X-acidity function. Values for the X-acidity function at different perchloric acid concentrations were obtained using the method outlined by Kresge *et al*²³. H_0 refers to the Hammett acidity function and is related to the X-acidity function by equation 6-12 to 6-15. $\text{Log } C_{\text{H}^+}$ is the logarithm of the concentration of hydronium ion.

$$X_0 = \left(\frac{0.022 - H_R' - \text{Log } C_{\text{H}^+}}{2.854} \right) \quad \text{Equation 4-10}$$

Where H_R' is calculated using equation 6-13

$$-H_R' = \text{Log } C_{\text{H}^+} + 0.024 - 2.733(H_0 + \text{Log } C_{\text{H}^+}) \quad \text{Equation 4-11}$$

H_0 is calculated using equation 6-14.

$$H_0 = -4.397 \times 10^{-1} (\ln x) + 9.959 \times 10^{-1} - 2.262 \times 10^{-2} x - 3.680 \times 10^{-4} x^2 - 8.645 \times 10^{-6} x^3 + 6.961 \times 10^{-7} x^4 - 1.841 \times 10^{-8} x^5 + 1.169 \times 10^{-10} x^6 \quad \text{Equation 4-12}$$

Where x is the wt% HClO_4 and is calculated using equation 6-15

$$\text{Wt}\% = 1.008 \times 10^1 x - 5.698 \times 10^{-1} x^2 + 3.301 \times 10^{-2} x^3 - 2.473 \times 10^{-3} x^4 + 1.543 \times 10^{-4} x^5 - 3.854 \times 10^{-6} x^6 \quad \text{Equation 4-13}$$

Acknowledgements

Firstly I'd like to thank my supervisor Dr AnnMarie O'Donoghue for all her help, guidance and patience throughout the last three and a half years.

I would also like to thank all the academic staff in UCD and Durham University, particularly Rory More O'Ferrell for all his help and very useful discussions.

Thank you to all the technical staff in UCD and Durham. I would particularly like to thank Ian, Catherine and Alan in NMR in Durham for all there help with shimming and other life lessons.

Thank you to Team AMOD - Anita, Barry, Chucks, Eleanor and Terry and all the final year students who kept me entertained over the last few years. Thank you to the Fluorine for helping me settle-in so well.

A massive thanks to the tea group, I won't mention names... but you know who you are, you helped in so many ways, especially in welcoming me to a new department, University and city. All my housemates in Ferens Park, particularly Maud and Gaz, I miss the crazy cooking. Ed, thanks for the great chats in Habgood Drive. Ricky, your advice and friendship will always be cherished. Thanks to the science crowd, we may not see each other very much... but when we do... Caz and Dee; thank you so much for your friendship; I really miss not having you nearby but we shall relive those hang-over days!

Joe, thank you so much for being there, it's been a stress, without you I don't know what I'd have done!

Thank you to my brothers, Rob and Dara, my sisters Karen and Rachel, and my sister-in-law Fiona, I will always appreciate your help and advice and for being at the end of the phone whenever I needed a chat. My niece and nephew Kate and Dan, thank you for being so much fun and keeping me entertained when my world was just a pile of research papers.

I would especially like to thank my parents, Michael and Jacquie, for always being there for me.

References

1. Boyd, D. R.; Blacker, J.; Byrne, B.; Dalton, H.; Hand, M. V.; Kelly, S. C.; O'Ferrall, R. A. M.; Rao, N.; Sharma, N. D.; Sheldrake, G. N., *Journal of the Chemical Society - Chemical Communication* **1994**, 313.
2. O'Donoghue, A. *Ortho*-substituent effects on carbocation stability. University College Dublin, Dublin, 1999.
3. March, *Advanced Organic Chemistry*. 5th ed.; 2001; 'Vol.' p.
4. Olah, G. A., *Journal of Organic Chemistry* **2001**, 66, (18), 5943.
5. Mayr, H.; Ofial, A. R., *Angewandte Chemie* **2006**, 45, 1844.
6. Richard, J. P.; Yeary, P. E., *Journal of the American Chemical Society* **1993**, 115, 1739.
7. Tsuji, Y.; Mori, T.; Richard, J. P.; Amyes, T. L.; Fujio, M.; Tsuno, Y., *Organic Letters* **2001**, 3, (8), 1237.
8. Richard, J. P.; Jencks, W. P., *Journal Of The American Chemical Society* **1984**, 106, (5), 1383.
9. Richard, J. P.; Tsuji, Y., *Journal of the American Chemical Society* **2000**, 122, 3963.
10. Richard, J. P.; Jencks, W. P., *Journal Of The American Chemical Society* **1984**, 106, (5), 1373.
11. Richard, J. P.; Amyes, T. L.; Toteva, M. M., *Accounts Of Chemical Research* **2001**, 34, (12), 981.
12. Mayr, H.; Minegishi, S., *Angewandte Chemie* **2002**, 41, (23), 4493.
13. Toteva, M. M.; Moran, M.; Amyes, T. L.; Richard, J. P., *Journal of the American Chemical Society* **2003**, 125, 8814.
14. Richard, J. P.; Williams, K. B., *Journal of the American Chemical Society* **2007**, 129, 6952.
15. Richard, J. P.; Amyes, T. L.; Williams, K. B., *Pure & Applied Chemistry* **1998**, 70, (10), 2007.
16. McClelland, R. A., *Tetrahedron* **1996**, 52, (20), 6823.
17. Wang, Y.-T.; Wang, J.; Platz, M. S.; Novak, M., *Journal of the American Chemical Society* **2007**, 129, 14566.

18. Novak, M.; Poturalski, M. J.; Johnson, W. L.; Jones, M. P.; Wang, Y.; Glover, S. A., *Journal of Organic Chemistry* **2007**, 71, 3778.
19. Komatsu, K.; Akamatsu, H.; Aonuma, S.; Jinbu, Y.; Maekawa, N.; Takeuchi, K., *Tetrahedron* **1991**, 47, (34), 6951.
20. Ito, S.; Morita, N.; Asao, T., *Tetrahedron* **1994**, 35, (5), 751.
21. Erden, I.; Keefe, J. R.; Xu, F. P.; Zheng, J. B., *Journal of the American Chemical Society* **1993**, 115, 9834.
22. Cao, W.; Erden, I.; Keefe, J. R., *Angewandte Chemie* **1995**, 34, (10), 1091.
23. Kresge, A. J.; Chen, H. J.; Capen, G. L.; Powell, M. F., *Canadian Journal of Chemistry* **1983**, 61, 249.
24. Mathivanan, N.; McClelland, R. A.; Steenken, S., *Journal of the American Chemical Society* **1990**, 112, 8454.
25. McCormack, A. C.; McDonnell, C. M.; O'Ferrall, R. A. M.; O'Donoghue, A. C.; Rao, S. N., *Journal Of The American Chemical Society* **2002**, 124, (29), 8575.
26. Bronsted, J. N.; Kilpatrick, M.; Kilpatrick, M., *Journal of the American Chemical Society* **1929**, 51, 428.
27. Lundin, A.; Panas, I.; Ahlberg, E., *Journal of Physical Chemistry A* **2007**, 111, 9087.
28. Mohan, R. S.; Whalen, D. L., *Journal Of Organic Chemistry* **1993**, 58, (10), 2663.
29. Doan, L.; Bradley, K.; Gerdes, S.; Whalen, D. L., *Journal Of Organic Chemistry* **1999**, 64, (17), 6227.
30. Goering, H. L.; Vlazny, J. C., *Journal Of The American Chemical Society* **1979**, 101, (7), 1801.
31. Sayer, J. M.; Yagi, H.; Silverton, J. V.; Friedman, S. L.; Whalen, D. L.; Jerina, D. M., *Journal Of The American Chemical Society* **1982**, 104, 1972.
32. Doan, L. X.; Lin, B.; Yagi, H.; Jerina, D. M.; Whalen, D. L., *Journal Of The American Chemical Society* **2001**, 123, (28), 6785.
33. Doan, L.; Yagi, H.; Jerina, D. M.; Whalen, D. L., *Journal Of Organic Chemistry* **2004**, 69, (23), 8012.
34. Lin, B.; Doan, L. X.; Yagi, H.; Jerina, D. M.; Whalen, D. L., *Chemical Research In Toxicology* **1998**, 11, (6), 630.

35. Doan, L. X.; Yagi, H.; Jerina, D. M.; Whalen, D. H., *Journal Of The American Chemical Society* **2002**, 124, (48), 14382.
36. Sampson, K.; Paik, A.; Duvall, B.; Whalen, D. L., *Journal Of Organic Chemistry* **2004**, 69, (16), 5204.
37. Boyd, D. R.; Hamilton, J. T. G.; Sharma, N. D.; Harrison, J. S.; McRoberts, W. C.; Harper, D. B., *Chemical Communications* **2000**, (16), 1481.
38. Koerts, J.; Soffers, A.; Vervoort, J.; Jager, A. D.; Rietjens, I., *Chemical Research In Toxicology* **1998**, 11, 503.
39. Zhao, C. M.; Whalen, D. L., *Chemical Research In Toxicology* **2006**, 19, (2), 217.
40. Chao, H. S. I.; Berchtold, G. A., *Journal Of Organic Chemistry* **1981**, 46, 1948.
41. Kasperek, G. J.; Bruice, T. C., *Journal of the Chemical Society: Chemical Communications* **1972**, (784).
42. Bruice, P. Y.; Bruice, T. C.; Dansette, P. M.; Selander, H. G.; Yagi, H.; Jerinalb, D. M., *Journal Of The American Chemical Society* **1976**, 98, 2965.
43. Jeffrey, A. M.; Yeh, H. J. C.; Jerina, D. M.; DeMarinis, R. M.; Foster, C. H.; Piccolo, D. E.; Berchtold, G. A., *Journal Of The American Chemical Society* **1974**, 96, (22), 6929.
44. Staroscik, J.; Rickborn, B., *Journal Of The American Chemical Society* **1971**, 93, 3046.
45. Jeffrey, A. M.; Jerina, D. M., *Journal Of The American Chemical Society* **1972**, 94, 4048.
46. Boyd, D. R.; Austin, R.; McMordie, S.; Sharma, N. D.; Dalton, H.; Williams, P.; Jenkins, R. O., *Journal of the Chemical Society: Chemical Communications* **1989**, 339.
47. Boyd, D. R.; Sharma, N. D.; Agarwal, R.; McMordie, R. A. S.; MBessem, J. G.; Vanommen, B.; Vanbladeren, P. J., *Chemical Research In Toxicology* **1993**, 6, 808.
48. Bamberger, E.; Loder, W., *Justus Liebigs Ann. Chem* **1895**, 288, 100.
49. Boyd, D. R.; McMordie, R. A. S.; Sharma, N. D.; O'Ferrall, R. A. M.; Kelly, S. C., *Journal Of The American Chemical Society* **1990**, 112, 7822.
50. Rao, S. N.; O'Ferrall, R. A. M.; Kelly, S. C.; Boyd, D. R.; Agarwal, R., *Journal Of The American Chemical Society* **1993**, 115, (13), 5458.
51. O'Ferrall, R. A. M.; Rao, S. N., *Croatica Chemica Acta* **1992**, 65, (3), 593.

52. Lawlor, D. A.; O'Ferrall, R. A. M.; Rao, S. N., *Unpublished Results*.
53. Pirinccioglu, N.; Thibblin, A., *Journal Of The American Chemical Society* **1998**, 120, 6512.
54. Dey, J.; O'Donoghue, A. C.; O'Ferrall, R. A. M., *Journal Of The American Chemical Society* **2002**, 124, (29), 8561.
55. Cho, T. M.; Rose, R. L.; Hodgson, E., *Drug Metabolism and Disposition* **2006**, 34, (1), 176.
56. Jerina, D. M., *Polycyclic Aromatic Compounds* **2000**, 19, (1-4), 5.
57. Vannelli, T.; Hooper, A. B., *Biochemistry* **1995**, 34, 11743.
58. Kaubisch, N.; Daly, J. W.; Jerina, D. M., *Biochemistry* **1972**, 11, (16), 3080.
59. Auret, W. A.; Cruz, E. Z., *Tetrahedron Letters* **1993**, 34, 1589.
60. Resnick, S. M.; Lee, K.; Gibson, D. T., *Journal of Industrial Microbiology* **1996**, 17, 438.
61. Boyd, D. R.; Bugg, T. D. H., *Organic & Biomolecular Chemistry* **2005**, 4, 181.
62. Boyd, D. R.; Sharma, N. D.; Bowers, N. I.; Dalton, H.; Garrett, M. D.; Harrison, J. S.; Sheldrake, G. N., *Organic & Biomolecular Chemistry* **2006**, 4, 3343.
63. Boyd, D. R.; Sharma, N. D.; Coen, G. P.; Gray, P. J.; Malone, J. F.; Gawronski, J., *Chemistry: A European Journal* **2007**, 13, 5804.
64. Boyd, D. R.; Sheldrake, G. N., *Natural Product Reports* **1998**, 309.
65. Vitelio, C.; Bellomo, A.; Brovetto, M.; Seoane, G.; Gonzalezb, D., *Carbohydrate Research* **2004**, 339, 1773.
66. Hudlicky, T.; Rinner, U.; Gonzalez, D.; Akgun, H.; Schilling, S.; Siengalewicz, P.; Martinot, T. A.; Pettit, G. R., *Journal Of Organic Chemistry* **2002**, 67, 8726.
67. Franke, D.; Sprenger, G. A.; Muller, M., *Angewandte Chemie* **2001**, 40, (3), 555.
68. Troisi, G. M.; Bexton, S.; Robinson, I., *Environmental Science and Technology* **2006**, 40, (24), 7938.
69. Benedetti, M.; Martuccio, G.; Fattorini, D.; Canapa, A.; Barucca, M.; Nigro, M.; Regoli, F., *Aquatic Toxicology* **2007**, 85, 167.
70. Xue, W. L.; Warshawsky, D., *Toxicology And Applied Pharmacology* **2005**, 206, (1), 73.

71. Otero-Lobato, M. J.; Kaats-Richters, V. E. M.; Kopera, C.; Vlietstra, E. J.; Havenith, R. W. A.; Jenneskens, L. W.; Seinen, W., *Mutagenic Research* **2005**, 581, 115.
72. Rietjens, I. M. C. M.; Boersma, M. G.; Woude, H. v. d.; Jeurissen, S. M. F.; Schutte, M. E.; Alink, G. M., *Mutagenic Research* **2005**, 574, 124.
73. Phillips, D. H., *Mutagenic Research* **2005**, 577, 284.
74. Rodriguez, H.; Loechler, E. L., *Biochemistry* **1993**, 32, (7), 1759.
75. Sirate, H.; Thomas, E.; Tyrrell, N., *Journal of the Chemical Society Chemical Communications* **1979**, 36.
76. Frisch, M. J.; Trucks, G. W.; Schlegel, H. B.; Scuseria, G. E.; Robb, M. A.; Cheeseman, J. R.; Montgomery, J. A.; Vreven, T.; Kudin, K. N.; Burant, J. C.; Millam, J. M.; Iyengar, S. S.; Tomasi, J.; Barone, V.; Mennucci, B.; Cossi, M.; Scalmani, G.; Rega, N.; Petersson, G. A.; Nakatsuji, H.; Hada, M.; Ehara, M.; Toyota, K.; Fukuda, R.; Hasegawa, J.; Ishida, M.; Nakajima, T.; Honda, Y.; Kitao, O.; Nakai, H.; Klene, M.; Li, X.; Knox, J. E.; Hratchian, H. P.; Cross, J. B.; Bakken, V.; Adamo, C.; Jaramillo, J.; Gomperts, R.; Stratmann, R. E.; Yazyev, O.; Austin, A. J.; Cammi, R.; Pomelli, C.; Ochterski, J. W.; Ayala, P. Y.; Morokuma, K.; Voth, G. A.; Salvador, P.; Dannenberg, J. J.; Zakrzewski, V. G.; Dapprich, S.; Daniels, A. D.; Strain, M. C.; Farkas, O.; Malick, D. K.; Rabuck, A. D.; Raghavachari, K.; Foresman, J. B.; Ortiz, J. V.; Cui, Q.; Baboul, A. G.; Clifford, S.; Cioslowski, J.; Stefanov, B. B.; Liu, G.; Liashenko, A.; Piskorz, P.; Komaromi, I.; Martin, R. L.; Fox, D. J.; Keith, T.; Al-Laham, M. A.; Peng, C. Y.; Nanayakkara, A.; Challacombe, M.; Gill, P. M. W.; Johnson, B.; Chen, W.; Wong, M. W.; Gonzalez, C.; Pople, J. A. *Gaussian 03, Revision C.02*, Wallingford CT, 2004.
77. Huckel, W.; Schwen, R., *Chemie Berishte* **1956**, 89, (1), 150.
78. Mathis, J.; Gizir, A. M.; Yang, Y., *J. Chem. Eng. Data* **2004**, 49, (5), 1269.
79. Coyle, G. T.; Harmon, T. C.; Suffet, I. H., *Environmental Science & Technology* **1997**, 31, (2), 384.
80. Brett, C. L.; Gold, V., *Journal of the Chemical Society: Perkin Transactions* **1973**, 1437.
81. Kim, H.; Hemond, H. F.; Krumholz, L. R.; Cohen, B., *Environmental Science & Technology* **1995**, 29, (1), 108.

82. Dohanyosova, P.; Fenclova, D.; Vrbka, P.; Dohnal, V., *J. Chem. Eng. Data* **2001**, 46, (6), 1533.
83. Sutton, C.; Calder, J. A., *J. Chem. Eng. Data* **1975**, 20, (3), 320.
84. Hansch, C.; Leo, A.; Taft, R. W., *Chemical Reviews* **1991**, 91, 165.
85. White, R. C.; Drew, P.; Moorman, R., *Journal of Heterocyclic Chemistry* **1988**, 25, 1781.
86. Mah, T.; Sirat, H. M.; Thomas, E. J., *Journal of the Chemical society: Perkin Trans I* **1979**, 2255.
87. Vogel; Gunther, *Angewandte Chemie International Edition* **1967**, 6, 385.
88. Jia, Z. S.; Brandt, P.; Thibblin, A., *Journal of the American Chemical Society* **2001**, 123, (42), 10147.
89. Scagnolari, F.; Modelli, A.; Bottoni, A.; Jones, D.; Lazzari, D., *Journal of the Chemical Society: Faraday Transactions* **1996**, 92, (9), 1447.
90. Rigby, J. H.; Bazin, B.; Meyer, J. H.; Mohammadi, F., *Organic Letters* **2002**, 4, (5), 799.
91. Drew, M. G. B.; Regan, C. M.; Nelson, S. M., *Journal of the Chemical society: Dalton Transactions* **1981**, 1034.
92. Meinwald, J.; Nozaki, H., *J. Am. Chem. Soc.* **1958**, 80, (12), 3132.
93. Kuehlmeier, R.; Keller, R.; Schwesinger, R.; Netscher, T.; Fritz, H.; Prinzbach, H., *Chemische Berishte* **1984**, 117, (5), 1765.
94. Boyd, D. R.; Berchtold, G. A., *Journal of the American Chemical Society* **1979**, 101, (9), 2470.
95. Taft, R. W., *Journal of the American Chemical Society* **1952**, 74, 2729.
96. Popeney, C.; Guan, Z., *Organometallics* **2005**, 24, 1145.
97. Tavaresa, L. C.; Amaralb, A. T. d., *Bioorganic & Medicinal Chemistry* **2004**, 12, 1377.
98. Schneider, H.-J.; Hoppen, V., *Journal of Organic Chemistry* **1978**, 43, (20), 3866.
99. Kuliev, A. M.; Zeinalova, G. A.; Kuliev, A. B.; Nurieva, T. Z.; Damirova, F. G., *Journal of Organic Chemistry of the USSR (English Edition)* **1971**, 7, (3), 469.
100. Staroscik, J. A.; Rickborn, B., *Journal of Organic Chemistry* **1972**, 37, (5), 738.
101. Costero, A. M.; Rodriguez, S., *Tetrahedron* **1992**, 48, (30), 6265.

102. Benkeser, R. A.; Burrous, M. L.; Hazdra, J. J.; Kaiser, E. M., *Journal of Organic Chemistry* **1962**, 28, 1094.
103. Krapcho, A. P.; Bothner-By, A. A., *Journal of the American Chemical Society* **1958**, 81, (3658-3666).
104. Huckel, W.; Graf, B.; Munkner, D., *Chemice Berishte* **1958**, 91, 47.
105. Benkeser, R. A.; L.Burrous, M.; Hazdra, J. J.; Kaiser, E. M., *Journal of Organic Chemistry* **1963**, 28, 1094.
106. Kita, Y.; Akai, S.; Ajimura, N.; Yoshigi, M.; Tsugoshi, T.; Yasuda, H.; Tamura, Y., *Journal of the American Chemical Society* **1986**, 51, (22), 4150.
107. Schultz, A. G., *Chemical Communications* **1999**, 1263.
108. Dickenson, L.; Matuszak, C. A.; Qazi, A. H., *Journal of Organic Chemistry* **1978**, 43, (5), 1007.
109. Boyd, D. R.; Berchtold, G. A., *Journal of the American Chemical Society* **1978**, 101, (9), 2470.
110. Ackland, D. J.; Pinhey, J. T.,
Journal of the Chemical society: Perkin Trans 1 **1987**, 2689.
111. McGowan, D. A.; Berchtold, G. A., *Journal of the American Chemical Society* **1982**, 104, (25), 7036.
112. Kuehne, M. E.; Lambert, B. F., *Journal of the American Chemical Society* **1958**, 81, 4278.
113. Marshall, J. L.; Erickson, K. C.; Folsom, T. K., *J. Org. Chem.* **1970**, 35, (6), 2038.
114. Nelson, N. A.; Fassnacht, J. H.; Piper, J. U., *Journal of the American Chemical Society* **1960**, 83, 206.
115. Lindow, D. F.; Cortez, C. N.; Harvey, R. G., *Journal of the American Chemical Society* **1972**, 94, (15), 5406.
116. Grisdale, P. J.; Regan, T. H.; Doty, J. C.; Figueras, J.; Williams, J. L., *Journal of Organic Chemistry* **1968**, 33, 1116.
117. Baasov, T.; Sheves, M., *Journal of the American Chemical Society* **1985**, 107, (25), 7525.
118. Paquette, L. A.; Kuhla, D. E.; Barrett, J. H.; Haluska, R. J., *Journal of Organic Chemistry* **1969**, 34, (10), 2866.

References

119. Amyes, T., Correspondance.
120. Herschlag, D.; Jencks, W. P., *Journal of the American Chemical Society* **1986**, 108, (25), 7938.

